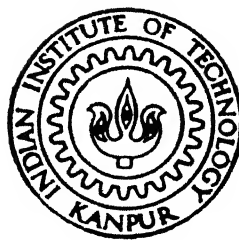


DYNAMIC RESPONSE OF FLEXIBLE AIRCRAFT IN GROUND RUNS OVER NONHOMOGENEOUSLY PROFILED FLEXIBLE RUNWAY

By
SUDIP TALUKDAR



AE
1997
D
TAL
DYN

DEPARTMENT OF AEROSPACE ENGINEERING
INDIAN INSTITUTE OF TECHNOLOGY KANPUR
JULY, 1997

DYNAMIC RESPONSE OF FLEXIBLE AIRCRAFT IN GROUND RUNS OVER NONHOMOGENEOUSLY PROFILED FLEXIBLE RUNWAY

A Thesis Submitted

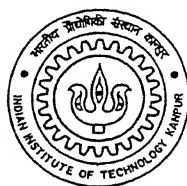
in Partial Fulfilment of the Requirements

for the Degree of

Doctor of Philosophy

by

Sudip Talukdar



to the

DEPARTMENT OF AEROSPACE ENGINEERING

INDIAN INSTITUTE OF TECHNOLOGY KANPUR

July, 1997

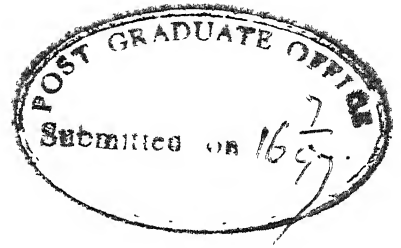
10 JUL 1998

CENTRAL LIBRARY
I. I. T., KANPUR

IN No. A125696

Entered in system

CERTIFICATE



This is to certify that the work contained in the thesis entitled **Dynamic Response of Flexible Aircraft in Ground Runs over Nonhomogeneously Profiled Flexible Runway** by Sudip Talukdar is a record of bonafied research work carried out under our supervision and that this work has not been submitted elsewhere for a degree.

A handwritten signature in cursive script, appearing to read "S. Kamle".

Dr. S. Kamle

Associate Professor

Dept. of Aerospace Engineering

I. I. T. Kanpur

A handwritten signature in cursive script, appearing to read "D. Yadav".

Dr. D. Yadav

Professor

Dept. of Aerospace Engineering

I. I. T. Kanpur

July, 1997.

ACKNOWLEDGEMENT

I would like this opportunity to express my sincere gratitude to my thesis supervisors Dr. D. Yadav and Dr. S. Kamle for their sincere help, fruitful suggestions and inspiration during the entire course of this work. I am extremely thankful to them for giving me complete freedom of work, thus helping me to gain confidence and to work independently. I feel most privileged to have been associated with them for a number of years which has been the most enlightening phase of my academic career.

I sincerely thank the Principal, Regional Engineering College, Silchar (India), for sponsoring me in Ph.D. course at I. I. T. Kanpur under Quality Improvement Programme. My thanks are also to Prof. B. U. A. Barbhuiya, Head and other faculty colleagues of the Civil Engineering Department, Regional Engineering College, Silchar, who inspite of their busy and tight schedule, shared my teaching load, thus enabling me to complete the programme.

Sincere thanks are due to Shri V. N. Pandey, Shri J. Prasad and Shri H. C. Bhattacharya, the technical staffs of Aerospace Engineering Department, I. I. T. Kanpur for their valuable suggestions and help in conducting the experiments. Thanks are also due to Shri A. K. Ganguli of Aerospace Engineering Department, I. I. T. Kanpur for preparing nice drawings.

I am also very much thankful to my friends Shri U. Dixit, Shri K. Sivakumar, Shri K. D. Kumar and Shri N. Verma for their allround support, encouragement and suggestions.

I wish to express my indebtedness to my parents in laws, my mother, brothers and sisters whose deep affection and silent inspiration have always guided me towards success and helped me in facing various problems encountered in my life.

Lastly, I appreciate the immense sense of tolerance and compromising attitude of my wife, Aparna during the course of this study. To my daughters Chandni and Sanju, I can now shower more smiles than frowns.

Sudip Talukdar

PAPERS EMERGED OUT FROM THE STUDIES

1. TALUKDAR, S., KAMLE, S. and YADAV, D., 'Track induced heave-pitch dynamics of vehicles with variable section flexible attachment', *Vehicle System Dynamics* (to appear in vol 28, 1997)
2. YADAV, D., KAMLE, S. and TALUKDAR, S., 'Transverse vibration of multi mass loaded variable section beam under random excitation' *Journal of Sound and Vibration* (under review - first revision communicated)
3. YADAV, D., KAMLE, S. and TALUKDAR, S., 'Nonstationary response of aircraft with tapered flexible wing over uneven and elastic track', *Journal of Sound and Vibration* (under review)
4. YADAV, D., KAMLE, S. and TALUKDAR, S., 'Nonstationary response of flexible vehicle in variable velocity run', *Mechanics of Machines and Structures* (communicated)
5. YADAV, D., KAMLE, S. and TALUKDAR, S., 'Heave - pitch - roll dynamics of flexible vehicle in variable velocity run', *Vehicle System Dynamics* (communicated)
6. YADAV, D., KAMLE, S. and TALUKDAR, S., 'Nonstationary response of nonlinear vehicle - An instantaneously linear approach', *Probabilistic Engineering Mechanics* (communicated)

Dedicated
to
MY LATE FATHER

CONTENTS

	LIST OF SYMBOLS	xiv
	LIST OF TABLES	xix
	LIST OF FIGURES	xx
	SYNOPSIS	xxv
CHAPTER 1	INTRODUCTION	1
1.1	Track Induced Vehicle Dynamics	1
1.2	Literature Review	3
1.3	Present Work	20
CHAPTER 2	SYSTEM DESCRIPTION	24
2.1	Vehicle Forward Motion	24
2.2	Track Roughness	25
2.3	Vehicle-Track Dynamic Model	29
2.3.1	Single Point Input Heave Model	30
2.3.2	Two Point Input Heave-Pitch Model	32
2.3.3	Three Point Input Heave-Pitch-Roll Model	34
2.4	System Equations	37
2.4.1	Heave Model	37
2.4.2	Heave-Pitch Model	41
2.4.3	Heave-Pitch-Roll Model	47
CHAPTER 3	SOLUTION TECHNIQUE FOR LINEAR MODEL	53
3.1	Model Analysis of Flexible Structures	53
3.2	Natural Frequencies and Mode Shapes	54
3.2.1	Bending Vibration	54

3.2.2	Coupled Bending-Torsion Vibration	59
3.3	Orthogonality of Modes	64
3.4	Discretization Procedure of Equation of Motion of Continuous Element	68
3.4.1	Bending Vibration	68
3.4.2	Coupled Bending-Torsion Vibration	69
3.5	Discretized Equations for Continuous Elements of Vehicle Models	72
3.5.1	Heave-Model	72
3.5.2	Heave-Pitch Model	74
3.5.3	Heave-Pitch-Roll Model	76
3.6	Decoupling of System Equations	78
3.7	Response Statistics	80
3.7.1	Mean Response	80
3.7.2	Response Covariance	90
CHAPTER 4	NONLINEAR VEHICLE MODEL	101
4.1	Brief Discussion on the Available Methods	101
4.2	Vehicle-Track Model	103
4.3	System Equations	103
4.4	Discretised Equations for Continuous System	107
4.5	Solution Approach	108
4.5.1	Response Statistics	111
CHAPTER 5	RESULTS AND DISCUSSIONS	115

5.1	Free Vibration of Nonuniform Section Beam	116
5.1.1	Natural Frequencies in Bending Vibration	116
5.1.2	Experimental Evaluation of Natural Frequencies in Bending Vibration	117
5.1.3	Effect of Parameter Variation on Natural Frequencies in Bending Vibration	123
5.1.3.1	Effect of taper ratio on natural frequencies	124
5.1.3.2	Effect of mass location on natural frequencies	126
5.1.4	Natural Frequencies in Coupled Bending - Torsion Vibration	130
5.1.4.1	Uniform beam	130
5.1.4.2	Nonuniform beam	132
5.2	Response Statistics of Linear Vehicle Model	134
5.2.1	Heave Model	137
5.2.1.1	Taxi run	137
5.2.1.2	Takeoff run	139
5.2.1.3	Landing run	141
5.2.2	Heave - Pitch Model with Rigid Fuselage	142
5.2.2.1	Taxi run	142
5.2.2.2	Takeoff run	155

5.2.2.3	Landing run	156
5.2.3	Heave-Pitch Model with Fuselage Flexible in bending	157
5.2.3.1	Taxi run	171
5.2.3.2	Takeoff run	172
5.2.3.3	Landing run	173
5.2.4	Heave- Pitch -Roll Model (Flexible Fuselage in Bending with Rigid Roll)	174
5.2.4.1	Taxi run	174
5.2.4.2	Takeoff run	194
5.2.4.3	Landing run	196
5.2.5	Heave -Pitch-Roll Model (Flexible Fuselage in Bending and Torsion)	197
5.2.5.1	Taxirun	222
5.2.5.2	Takeoff run	224
5.2.5.3	Landing run	225
5.2.6	Comparison of Some Linear Models Behaviour	226
5.3	Nonlinear Model Response Statistics	259
5.3.1	Taxi run	266
5.3.2	Takeoff run	266
5.3.3	Landing run	267
CHAPTER 6	CONCLUSIONS	278
6.1	Nonuniform Beam Vibration	278
6.2	Response Statistics of Linear Vehicle Models	279

6.3	Nonlinear Aircraft Model	280
6.4	Suggestions for Future Works	282
	REFERENCES	283

LIST OF SYMBOLS

A	State matrix
A	Area
A_r	Roughness constant
A_T	Aspect ratio
a_k	Coefficients of polynomial
B	Characteristic matrix
b_k	Coefficients of power series for bending mode
C	System damping matrix
C_L, C_{mac}	Lift and aerodynamic moment coefficients
C	Viscous damping
C_d	Coefficient of discharge
c	Viscous damping per unit length
c_k	Coefficients of power series for torsional mode
c_h	Mean chord length
D	Modal damping coefficient
E	Young's modulus of elasticity
e	Shear center offset
F	Generalised force vector
F_a	Pneumatic force in aircraft suspension
F_f	Frictional force
F_h	Hydraulic force in aircraft suspension
f	Distributed applied loading

G	Shear modulus
g	Distance measured perpendicular to vehicle longitudinal axis
H	Frequency response function
h	Track elevation
h_m	Mean track unevenness
h_R	Random track roughness
I	Polar moment of inertia (MI) of the concentrated mass about the shear center; Wing MI; Track cross section MI
I_s	Aircraft pitch MI about c.g.
I_r	Aircraft roll MI about c.g.
$I_{w\alpha}$	Wing mass polar MI about elastic axis
J	Torsional constant
j	Imaginary unit
K	Covariance, Spring constant
K	System stiffness matrix
k	Distributed spring stiffness, counting index
k_r	Track roughness correlation index
L	Length
l_0, l_1, l_2	Wing elastic axis and axle distance from the vehicle c.g
M	System mass matrix
M	Distributed bending moment
m	Mass per unit length, counting index
N	Number of term in a series

n	Dimensions of the system matrices, number of normal modes, polytropic index
Q	Generalised force
q	Response vector
r	Space coordinate of the fuselage, counting index
S	Surface area
s	Space coordinate
T	Torsional mode shape
t	Time instant
U	Modal matrix
u	Eigen vector
V	Vehicle forward velocity
V_w	Lift force per unit length on the wing
W	Bending mode shape function
w	Transverse displacement
X_0	Integration constant
x	Distance along the track
x_c	Location of vehicle c.g along the track
y	Track transverse displacement
z	Unsprung mass vertical displacement
α	Eigen values
δ	Dirac delta function; Kronecker delta
Γ	Distributed torque
η	Generalised coordinates
θ	Angle of twist, Fuselage roll

ϑ	Distributed rotational damping
μ, σ	Mean and standard deviation
ρ	Mass density
Φ	Power spectral density
ϕ	Torsional displacement functions
ψ	Track displacement function in the i th mode
φ	Random phase angle
Ω	Spatial frequency of the track input
ω	Temporal frequency of the track input; natural frequency

Subscripts

L	Left
R	Right
1	Front axle, Center wheel
2	Rear axle, Left wheel
3	Right wheel
f	Foundation
i	i th mode
p	Track
r	Rigid body roll
s	Suspension
u	Tyre
b	Vehicle body bending
t	Vehicle body torsion
w	Wing

k kth concentrated mass

Superscript

g Generalised quantity

L Left wing

R Right wing

LIST OF TABLES

5.1 Nondimensional Natural Frequency $(\omega^2 m_0 L^4 / EI_0)^{1/2}$ of linearly tapered beams with no concentrated mass loading	118
5.2 Nondimensional Natural Frequency $(\omega^2 m_0 L^4 / EI_0)^{1/2}$ of cantilever beams with concentrated mass loadings	119
5.3 Experimental Validation of Natural Frequency	122
5.4 Natural Frequencies of Thin walled Open Section Beams in Coupled Bending-Torsion (Hz)	131
5.5 Natural Frequencies of a Uniform Section Wing Beam in Coupled Bending-Torsion (ω rad/s)	132
5.6 Comparison of Theoretical and Experimental Values of Natural Frequency (Hz)	134

LIST OF FIGURES

2.1	Heave Model	31
2.2	Heave-Pitch Model (Rigid fuselage)	33
2.3	Heave-Pitch Model (Flexible fuselage)	35
2.3	Heave-Pitch-Roll Model	36
4.1	Nonlinear Aircraft Model	104
5.1	Block diagram of experimental set-up	121
5.2	Effect of taper on natural frequencies (a) width taper (b) height taper (c) width and height taper	127
5.3	Effect of mass location on natural frequencies (a) width taper (b) height taper (c) width and height taper	129
5.4	Polynomial fit of wing cross sectional properties	133
5.5	Heave Model-Mean response in taxi run	143
5.6	Heave Model-Response variance in taxi run	145
5.7	Heave Model-Mean response in takeoff run	147
5.8	Heave Model-Response variance in takeoff run	149
5.9	Heave Model-Mean response in landing run	151
5.10	Heave Model-Response variance in landing run	153
5.11	Heave-Pitch Model (Rigid fuselage)-Mean response in taxi run	158
5.12	Heave-Pitch Model (Rigid fuselage)-Response variance in taxi run	160

5.13 Heave-Pitch Model (Rigid fuselage)-Mean response in takeoff run	162
5.14 Heave-Pitch Model (Rigid fuselage)-Response variance in takeoff run	164
5.15 Heave-Pitch Model (Rigid fuselage)-Mean response in landing run	166
5.16 Heave-Pitch Model (Rigid fuselage)-Response variance in landing run	168
5.17 Bending-torsion displacement ratio of the wing	170
5.18 Heave-Pitch Model (Flexible fuselage in bending)-Mean response in taxi run	175
5.19 Heave-Pitch Model (Flexible fuselage in bending)-Response variance in taxi run	178
5.20 Heave-Pitch Model (Flexible fuselage in bending)-Mean response in takeoff run	181
5.21 Heave-Pitch Model (Flexible fuselage in bending)-Response variance in takeoff run	184
5.22 Heave-Pitch Model (Flexible fuselage in bending)-Mean response in landing run	187
5.23 Heave-Pitch Model (Flexible fuselage in bending)-Response variance in landing run	190
5.24 Heave-Pitch-Roll Model (Flexible fuselage in bending with rigid roll)- Mean response in taxi run	198
5.25 Heave-Pitch-Roll Model (Flexible fuselage in bending with rigid roll)-Response variance in taxi run	202

5.26	Heave-Pitch-Roll Model (Flexible fuselage in bending with rigid roll)- Mean response in takeoff run	206
5.27	Heave-Pitch-Roll Model (Flexible fuselage in bending with rigid roll)-Response variance in takeoff run	210
5.28	Heave-Pitch-Roll Model (Flexible fuselage in bending with rigid roll)- Mean response in landing run	214
5.29	Heave-Pitch Model (Flexible fuselage in bending with rigid roll)-Response variance in landing run	218
5.30	Heave-Pitch-Roll Model (Flexible fuselage in bending and torsion)-Mean response in taxi run	227
5.31	Heave-Pitch-Roll Model (Flexible fuselage in bending and torsion)-Response variance in taxi run	232
5.32	Heave-Pitch-Roll Model (Flexible fuselage in bending and torsion)-Mean response in takeoff run	237
5.33	Heave-Pitch-Roll Model (Flexible fuselage in bending and torsion)-Response variance in takeoff run	242
5.34	Heave-Pitch-Roll Model (Flexible fuselage in bending and torsion)-Mean response in landing run	247
5.35	Heave-Pitch-Roll Model (Flexible fuselage in bending and torsion)-Response variance in landing run	252
5.36	Comparison of mean and variance of displacement in taxi run	260
5.37	Comparison of mean and variance of displacement in takeoff run	262

5.38	Comparison of mean and variance of displacement in landing run	264
5.39	Nonlinear Aircraft Model - Mean and variance of displacement in taxi run	269
5.40	Nonlinear Aircraft Model - Mean and variance of velocity in taxi run	270
5.41	Nonlinear Aircraft Model - Mean and variance of acceleration in taxi run	271
5.42	Nonlinear Aircraft Model - Mean and variance of displacement in takeoff run	272
5.43	Nonlinear Aircraft Model - Mean and variance of velocity in takeoff run	273
5.44	Nonlinear Aircraft Model - Mean and variance of acceleration in takeoff run	274
5.45	Nonlinear Aircraft Model - Mean and variance of displacement in landing run	275
5.46	Nonlinear Aircraft Model - Mean and variance of velocity in landing run	276
5.47	Nonlinear Aircraft Model - Mean and variance of acceleration in landing run	277

SYNOPSIS

Unevenness in the track induces vibrations in moving vehicles. Aircraft ground maneuvers over uneven runway induce dynamics in the air frame. Excessive level of vibration causes discomfort among passengers and crews, produces undesirable movement of the cargo and may undermine the vehicle instrumentations and control mechanism. The dynamics may lead to fatigue and failure of structural components. The pavement also experiences dynamic loading, undergoes deflection and stress cycling and the associated wear and tear.

Rapid growth of traffic and high speed transportation has brought a significant change in the design of vehicles and their component parts. To allow for more passengers and pay loads, vehicle size has increased. More advanced materials and construction techniques have evolved causing greater flexibility in the vehicles. Modern aircraft with its less rigid structures and higher takeoff and landing speeds presents the best example. Under these conditions, analysis of vehicle dynamic behaviour has assumed greater importance for assessing ride quality, design of vehicle structures, control of vibration and optimization of suspension systems.

Moving vehicles exert fluctuating forces on the track pavement caused by its vibration. The track may undergo deformation of varying degree depending on the type of its construction. This is

particularly important for ropeways, other types of guideways and aircraft operations from carrier decks.

In the present study, analytical methods have been developed to study the vehicle-track system dynamics induced by track unevenness. The track unevenness is assumed to be a nonhomogeneous random process specified by a generalised power spectral density function. The mean track profile may be variable to model defects like slope, bumps, dips, uneven and differential settlements, craters, repair patches, etc. The track is assumed to deflect vertically under vehicle imposed loads. It is modelled as a beam of uniform mass and flexural rigidity supported by elastic and dissipative subgrade.

Aircraft takeoff is an accelerating while landing is a decelerating run. Variable ground motion pattern of the vehicle has been modelled by a power series with finite terms. Coefficients of the polynomials can be selected to depict any ground run pattern of the vehicle. Consequent to the variable vehicle velocity and nonhomogeneous characteristics of the track, input sensed by the vehicle wheels become nonstationary in time.

The vehicle has been modelled as a combination of discrete and continuous elements with different wheel arrangements. Vehicle wheels, tyres and part of the suspension systems are lumped as unsprung masses. Aircraft fuselage and wings are modelled as beam elements with variable mass, stiffness and damping distributions. The wings may carry arbitrary numbers of concentrated masses at arbitrary locations.

The variation of the sectional properties of the nonuniform beam has been modelled by power series. This representation is general and any type of variation can be accommodated with desired accuracy. A method has been outlined to find the exact solution for nonuniform beam vibration. Natural frequencies and mode shape functions have been obtained in closed form for bending, torsion and bending-torsion coupled dynamics of variable section beams.

The proposed theory has been validated by comparison with experimental values and available published results. Experiments have been conducted to obtain resonant frequencies in bending for mass loaded tapered beams with different support conditions.

Coupled bending-torsion free vibration of a wing of a small military aircraft has been studied. Available data for wing sectional properties at discrete span locations have been fitted to the polynomial series and natural frequencies are obtained by the present theoretical approach. Available experimental results on the natural frequencies of the same wing are compared with the theoretical results.

Vehicle-track dynamic equations have been developed. The continuous elements of the model involve partial differential equations with space variable coefficients. Equations of motion corresponding to lumped elements are ordinary differential equations. In the present approach, the equations of motion of the continuous systems are first reduced to a set of linear ordinary differential equations in time dependent generalised coordinates using normal mode expansion techniques. The set of ordinary

differential equations together with the equations of lumped masses are then recast into first order state space form. These equations are completely uncoupled using modal analysis.

Analytical solution for the response has been obtained and expressions for second order statistics have been developed. The following models, in order of increasing complexity, have been considered:

- (1) Single Point Input Heave Model
- (2) Two Points Input Heave-Pitch Model
 - (a) Rigid Fuselage.
 - (b) Flexible Fuselage in Bending.
- (3) Three Point Input Heave-Pitch-Roll Model
 - (a) Flexible Fuselage in Bending and Rigid Roll,
 - (b) Flexible Fuselage in Bending and Torsion.

In the next part of the study, nonlinear behaviour of the suspension parameters is included in the analysis. Combination of air spring, orifice and coulomb damping have been treated with single point input heave model including tapered flexible wings. An instantaneous linear approach has been proposed. The method derives the benefit of linear theory while at the same time retains the original nonlinear behaviour.

System equations for the nonlinear model have been developed wherein the suspensions forces are nonlinear functions of instantaneous shock strut stroke and velocity. The system equations are integrated numerically with simulated track profile samples. Suspension forces are determined at discrete time steps

from known response of original nonlinear systems. Derivatives of the forces evaluated at discrete time steps are utilized to represent ``instantaneous spring and damping constant''. With these instantaneous suspension parameters, step by step application of the analogous linear model has been carried out to obtain second order response statistics. Reliability of the solution has been assessed by comparison with Monte Carlo simulated results.

A passenger aircraft has been selected in the study for generating numerical results. Response statistics have been obtained for constant velocity taxi, accelerating takeoff and decelerating landing runs. Some major conclusions drawn from the studies are

- (1) Mean response are primarily dependent on the track mean profile while response covariance are primarily influenced by track second order statistics.
- (2) Vehicle and track response are sensitive to the vehicle forward speed. For the vehicle, track and subgrade parameters selected in the study, the evaluated track deformation is smaller in magnitude.
- (3) Unsymmetrical distribution of roughness across the track causes a significant system response not only in the roll mode but also in the heave and pitch modes due to strong coupling in the system.
- (4) Response magnitude of aircraft, in general, is found to be more at landing touch down compared to taxi and takeoff runs.

xxx

- (5) The modelling predicts higher response magnitudes for rigid vehicles as compared to flexible vehicles.
- (6) Bending flexibility of aircraft type of vehicle is important for accurate description of the response behaviour. The low tread makes the torsional flexibility less significant for the prediction of vehicle response.
- (7) Consideration of rigid vehicle model may be adequate for preliminary design of undercarriages and vehicle structural components.
- (8) General response behaviours in instantaneously linearised model and Monte Carlo simulation show close similarity.
- (9) The proposed instantaneously linearised scheme uses much less computer processing time and storage space as compared to Monte Carlo simulation.

The analytical methods presented can handle the coupled vehicle-track dynamics problem with any general description of vehicle forward motion. Spatial nonhomogeneity of the track roughness can be included in the analysis. The method uses linear suspension and track behaviour. Flexible vehicle body along with slender attachments can be incorporated in the system model. A general variation of cross sectional properties of flexible systems modelled as a beam can be handled by the analytical approach developed for the variable section beam. The results of the nonuniform beam vibrations are in good agreement with the experimental and other published results.

A general combination of spring and damping nonlinearity in

vehicle suspension can be tackled by the proposed instantaneously linear approach. The present approach differs from other linearised schemes in the way that instead of finding equivalent set of linear parameters at one time, it introduces 'instantaneous spring and damping coefficients' evaluated from the response of the original nonlinear system at discrete time instants close to each other. The proposed instant to instant linearisation scheme may be useful to other nonlinear systems where conventional methods are difficult to apply.

CHAPTER 1

INTRODUCTION

1.1 TRACK INDUCED VEHICLE DYNAMICS

All tracked vehicles in motion receive dynamic excitation from the track and are induced to oscillate. The primary cause of vehicle excitation is the surface unevenness of the track. Track surfaces have some irregularities however carefully they are prepared. There are several causes of track unevenness: traffic loading, environmental effects, construction materials and built in construction irregularities. Newly constructed tracks may be poorly finished or may have many design features such as construction joints, thermal expansion joints etc. Tracks that have been in service for sometime often form localised distresses due to the application of heavy wheel load and environmental changes. These normally include cracks, bumps, potholes, and other defects. Tracks are supported by prepared subgrade/foundation system. Poor drainage, swelling soils, freeze-thaw cycles and nonuniform consolidation of subgrade may all contribute to surface roughness.

Vehicles are complex structural systems with combinations of wheels and body connected by suspension elements. The shock and vibration caused by track unevenness are transmitted from wheels to the superstructure of the vehicle through the suspension system. The vertical irregularities due to variations in the track level in longitudinal and transverse directions induce in the

vehicle heave, pitch, roll, yaw, side sway and axial motions. The result is a time varying stress in the structural components. These may, at times, reach levels to cause structural failures. However, in general, stress levels are much lower than the critical value. The cumulative effects of the repeated stress cycling may be significant to bring about metal fatigue damage. The excessive level of vibration causes discomfort among passengers and crews, produce undesirable movement of the cargo and may undermine the vehicle instrumentations and the control mechanism.

Suspension system has a major role in absorbing the shock and vibration effects on the vehicle. Different types of shock absorbers are used in the suspension systems to meet the requirements. Most ground vehicles and aircraft landing gear suspensions use oleopneumatic type absorbers. The oleopneumatic absorber, commonly termed as oleostrut, is a member composed of two telescopic cylinders. When the strut compresses or expands, oil inside the air tight cylinder is forced through an orifice from one cylinder to the other. This provides a damping effect while compression and expansion of air inside the air chamber produces spring action.

A moving vehicle exerts a fluctuating component of force on the track due to vibratory motion induced by the surface unevenness. For a given track, the magnitude of the wheel-track force variation is a function of the track roughness, vehicle speed and suspension characteristics. The fluctuating nature of the dynamic wheel load, with increase in number of load repetitions, may cause track degradation and fatigue damage.

For guided ground vehicles, the track is formed with slender members while for non guided vehicles the track is generally a paved surface. The track is supported by proper foundation systems whose construction techniques are different for different types of tracks. Nonguided vehicles such as automobiles and airplanes use roads and airport pavements in their ground maneuvers. These pavements are constructed with one or more layers of processed or unprocessed materials placed on the prepared subgrade. There are two categories of road and airport pavements- flexible and rigid. Flexible pavements typically consist of bituminous surface course, a base course of crushed or uncrushed aggregate and subbase course of lower quality material than in base course. Rigid pavements consist a of slab of cement concrete that rests on a prepared subgrade or subbase. This is reinforced with steel to control and minimise harmful effects of cracking. Concrete pavements are provided with longitudinal and transverse joints between the slabs.

Rapid growth of traffic and high speed transportation has enhanced the importance of track induced vehicle dynamics. Analysis of vehicle dynamic behaviour is essential for assessing ride quality, design of vehicle structures, control of vibration and optimisation of suspension parameters. This has brought about improved vehicle-track design, lower maintenance costs and greater ride comfort.

1.2 LITERATURE REVIEW

Study of track induced dynamics of vehicle has assumed greater significance from the view point of passengers comfort,

cargo safety, fatigue damage analysis and controllability of the system. A review of earlier works on different aspects of the problem is being presented in this section.

In early attempts to investigate vehicle dynamics, excitation from the ground has been modelled as sinusoidal waves, triangular waves or step functions. Response have been obtained for a single degree freedom vehicle model with linear suspension at constant velocity run with step input by Houbolt [1] and with sinusoidal input by Wong [2].

While these studies could provide a basis for various designs, they could not reflect the actual ride behaviour since surface profiles are rarely of simple forms. Soon it was realised that ground surface profiles should be more realistically described as a random process. The concept of the track profile being a random process, has induced many studies for the characterisation of input process in probabilistic sense. Walls et al. [3] carried out spectral analysis from the measured data of actual runway surface. Power Spectral Density (PSD) function of runway elevations have been determined in order to permit a description of the frequency characteristics of the runway roughness.

Dodds and Robson [4] have shown that typical road surfaces may be considered as realisation of homogeneous and isotropic two dimensional Gaussian random process. The complete description of the roughness is provided by single autocorrelation function evaluated from any longitudinal profile.

Different track roughness models have been proposed by Sussman [5], Kamesh and Robson [6] and Honda et al. [7]. Their

relationships cater for a wider frequency range. It has been shown that PSD is related to parameters called roughness and waviness index. These parameters can shift the roughness level up and down and thus a guideline for classification of roads in terms of roughness has been framed.

Heath [8] developed cross-spectrum between heights of parallel profiles on a homogeneous and isotropic random surface. Formulae involving single integration have been derived which express the cross-spectrum in terms of PSD of single track. Limit behaviour of the cross-spectrum at small and large wave numbers have been found and discussed.

Marcondes et al. [9] have shown that some modification of PSD of track profiles are necessary when road section contains concentrated roughness like pothole, discrete bump, rail road crossing and other inhomogeneities. From profile survey report of several road and airport pavements, they suggested different fits for different section of the pavement incorporating a discontinuity in frequency.

Later Marcondes et al. [10] proposed a model of relationship between pavement PSD and parameter called International Roughness Index (IRI). In order to establish the relationship, spectral analysis of different measured profiles was carried out whereas IRI was computed using mathematical model of quarter car simulation.

A recent study by Iyengar and Jaiswal [11] has shown that train track irregularity can be modelled as stationary Gaussian process which can be defined in terms of the PSD function. PSD function obtained can be used to extract further information on

level crossing and peak statistics of unevenness data.

Stochastic description of track input in terms of mean and correlation or PSD function expedited the research on vehicle dynamics using random vibration theory. Silsby [12] studied the effect of various landing gear parameters on the airplane response on runway roughness with a rigid mass vehicle model. Tung et al. [13] used a heave-pitch model of aircraft to study the response of aircraft to runway roughness while including landing gear nonlinear behaviour. Numerical integration scheme has been employed for deterministic input while statistical linearisation and perturbation method was used for stationary input.

Kirk and Perry [14] studied the taxiing induced vibration in aircraft by the PSD method with two degrees of freedom heave model. This work has been extended to heave-pitch degrees of freedom model [15]. The aircraft fuselage has been idealised as a rigid beam. Suspension parameters have been linearised by equivalent linearisation technique.

Prediction of vehicle response at constant velocity run is not always appropriate as it can be appreciated that vehicle velocity is commonly variable in time. Specifically to aircraft, landing and takeoff run take place in decelerating and accelerating conditions. This renders the track input experienced by the vehicle nonstationary.

Virchis and Robson [16] conducted an analytical study on a simple vehicle model at accelerating runs. They concluded that nonstationary effects are not large and can be neglected as a first approximation. Sobczyk and Macvean [17] developed a method for analysing the response of linear vehicle travelling with

variable velocity. Both deterministic and random variation of the vehicle forward velocity have been considered. Numerical integration of system equations in time domain with track correlation as input yields the second order response statistics.

Yadav and Nigam [18] investigated the response of lumped mass model of vehicle to nonstationary ground input using a formulation of the system equation in space domain. This results in the governing differential equations to have space dependent coefficients while the input process remains homogeneous in space domain. The evolutionary spectral approach is then used to determine the response statistics of vehicles in constant and variable velocity runs.

More complicated ground velocity variations are incorporated in the study of vehicle dynamics with the concept of filter theory in order to simplify stochastic ground inputs. Kotb et al. [19] used a frequency domain formulation with modelling of the spectral density function as the output of a second order shaping filter under white noise input. Hammond and Harrison [20] have employed time domain solution for single degree of freedom linear vehicle model. State space form has been employed to represent the vehicle dynamic equations. Track excitation utilised a spatial shaping filter model.

In another study by Harrison and Hammond [21], a nonlinear model excited by nonstationary random process has been considered. The method is based on the technique of modelling the input process as a spatial shaping filter which may be linked to vehicle dynamic equations through velocity functions. The nonlinear problem was overcome by statistical linearisation.

Ground profiles are usually nonhomogeneous in practice. This non homogeneity may be due to variable mean in presence of slope or defects like dip, bumps, fault or uneven settlement of subgrade and repair patches etc., even when the random part of the track unevenness is homogeneous in space. Yadav [22] obtained the response of two degrees of freedom heave vehicle model for nonhomogeneous track input by direct solution of the system equations. Yadav and Kapadia [23] and Yadav and Ramamoorthy [24] have used Monte Carlo simulation technique for the evaluation of response statistics of heave and heave-pitch models of aircraft. The effect of linkage dynamics and nonlinearity of the suspension characteristics have been considered. Track inputs were simulated in time domain with known statistics of input and ground velocity history. Response has been found by numerically integrating the system equations. Averaging across a large number of response samples yields the vehicle response statistics.

Vehicle suspension system may be passive with spring and dashpot elements which do not require any external power source to operate. On the other way, active system generates suspension forces using servomechanism with external power source. Dahelberg [25] studied the response of a single degree of freedom vehicle model and developed an optimisation procedure to compare the behaviour under passive and active systems. The suspension parameters have been optimised under the constraint of ride comfort, road holding and suspension working space. The scheme has been extended to two degrees of freedom system [26]. The random road input was considered as zero mean random process.

Narayanan and Raju developed stochastic optimal control

theory of nonstationary response of a single degree freedom [27] and two degree freedom vehicle model [28]. Vehicle has been idealised as rigid lumped mass/masses, suspension behaviour being linear. Effect of nonlinearity on active system performance has been examined in extension of the work [29]. Velocity squared quadratic damping and hysteresis type of stiffness nonlinearities have been considered in the analysis. Constant acceleration run and random road profiles have been assumed.

Aircraft landing response with decelerating run on the uneven runway depends to a great extent on the geometric layout of the shock strut. Venketeshan [30] carried out a comparative study of the landing response of aircraft employing telescopic gear with linear and nonlinear characteristics. Relative merits of landing gears have been shown comparing their merits under optimum conditions. Study has been carried out with lumped aircraft model with zero aircraft forward velocity. It was found that performance of nonlinear gear is better than the linear one.

Reddy et al. have analysed levered [31] and semilevered [32] suspension type landing gears by including kinematics of the linkage in the formulation. They have examined two degrees of freedom heave model while incorporating shock strut and tyre nonlinearities.

Yadav and Ramamoorthy [33] have studied nonlinear landing gear behaviour at touchdown. A heave pitch model of aircraft with oleopneumatic shock strut in the articulated nose and the telescopic main gear has been considered. The system equations have been integrated numerically to obtain response in the duration of impact. Sensitivity of the system response to

variations in some shock strut parameters has been investigated to bring out improvements in the performance.

Yadav and Singh [34] have studied the braked landing response of aircraft. Optimal landing run without any skidding has been obtained with a one-step prediction of variable braking force with a linear two degrees of freedom aircraft model. Performance has been studied with different mean shapes for the random runway profile.

Increasing traffic demand and operational speed of ground vehicles have brought a significant change in the design of vehicle. The vehicles have increased in size and load carrying capacity while at the same time becoming lighter and flexible due to use of advanced materials in their construction. Effects of structural flexibility necessitated the change in modelling considerations.

Flexible models of guided ground vehicles have been analysed for response by Wilson and Biggers [35]. In their analysis, the vehicle model was considered to be a slender beam of uniform mass and stiffness property. Interaction of the first few flexural modes of the vehicle along with the rigid body modes have been considered. Track irregularity has been modelled as a stationary random process.

Cherchas [36] studied the combined effects of vehicle and guideway flexibility in a mathematical model of magnetically levitated guided ground vehicle. The study also included the effects of vehicle suspension and propulsion pad translation and multiple guideway spans. He concluded that vehicle flexibility is significant in certain frequency ranges..

Hac [37] considered a discrete - continuous vibratory system at constant forward speed. The model used was to represent a model of vehicle with active suspension. The road irregularity has been assumed to be a stationary Gaussian zero mean process. He evaluated the effect of body elasticity on system dynamics and proposed a stochastic optimal control theory for vibration isolation in the system.

Hac et al. [38] modified the control strategies for active vehicle suspensions with the goal of reducing high frequency vibration. Vehicle elasticity has been taken into account in the modelling and vehicle forward velocity has been assumed constant. The authors also considered the vibration control problem of flexible model with semiactive suspension [39]. They used adjustable dampers as force actuator in which the rate of energy dissipation can be varied either between two distinct levels or continuously within a given range of damping. Flexible vehicle model has been idealised as uniform beam with few flexural modes.

In the study of flexible vehicles, many authors have modelled the vehicle body as uniform section beam for which modal parameters can be easily derived. However, in many practical situations, beam geometry varies along the span. This becomes sometimes necessary to cut the cost of the material or for structural and architectural reasons. The dynamics of nonuniform beam element is complex as the governing differential equation contains space dependent coefficients. Analytical solutions of nonuniform bending vibrations have been attempted by Conway and Dubil[40], Sanger [41] and Gorman [42] with the help of Bessel functions. Natural frequency and mode shapes have been obtained

for wedge and cone beams and linearly tapered beams with simple boundary conditions. Bessel function solutions for the normal mode function are restricted to a class of tapered beam and thus can not handle general situation.

Wang [43] introduced hypergeometric series solution for nonuniform beam vibration. The method imposes less restriction on the type of taper but is too complicated for general use. Naguleswaran has applied Frobenious method for a beam with constant depth and linearly varying breadth [44] and wedge and cone section beams [45]. Natural frequencies for different support conditions and wide range of taper ratios have been obtained.

Recently Abrate [46] has shown that for some nonuniform beams, differential equation of motion can be transformed into the equation of motion of a uniform beam. The eigen values then become same as for the uniform beam or rod. However, the method has serious restriction on the beam's taper and boundary conditions.

A uniform section cantilever beam with tip mass has been analysed for free and forced vibration response by To [47]. Closed form solution for the response has been obtained for deterministic base excitation.

The many analytical methods available are unable to handle the general variation of cross sectional property in a complex structural model of vehicle. Chehil and Jategaonkar [48] applied Galerkin technique for the solution of natural frequency of beam with variable section.

Bapat et al. [49] have applied transfer matrix method to determine natural frequencies of uniform beams carrying several concentrated masses. Classical and nonclassical boundary

conditions have been considered in the study. Kim and Dickinson [50] employed Rayleigh Ritz method for the solution of nonuniform beam with linear and parabolic taper. An orthogonal polynomial shape function has been assumed. Effect of concentrated masses and different boundary conditions on the natural frequency have been studied.

Karabolis and Beskos [51] introduced finite element method (FEM) in the static and dynamic analysis of tapered beams. Beskos also applied the boundary element method [52] to the problem. Use of transfer matrix has been made by Chu and Pilkey [53] for the solution of nonuniform beam vibration. Wu and Lin [54] suggested combined numerical and analytical method for free vibration solution of a beam carrying several concentrated masses. However only uniform section beam has been treated.

Variation of cross sectional properties of a vehicle body has been considered in its modelling by Gibson [55]. He used FEM for the flat car body idealising it as an assemblage of uniform beam elements connected at the nodes. Response of the vehicle has been obtained in sinusoidal environment to establish resonance frequency and decay rate.

Khulief and Sun [56] presented an analysis of long wheel base vehicles such as buses, rail cars and truck trailers. Vehicle's elastic chassis has been represented by finite beam elements. The track irregularity has been modelled by discrete bumps and constant vehicle speed has been assumed. Semiactive control technique has been used for the suppression of vehicle vibration. FEM technique used in flexible vehicle vibration problem is essentially a lumped parameter approach; wherein the distributed

physical properties of a structure are represented by a finite number of idealised substructures interconnected at finite number of grid points. Although the method can handle most of the practical cases, it requires refined discretization of vehicle domain for accurate results leading to a costly computation.

Apetaur and Opicka [57] developed an analytical method for the study of the vehicle response. Vehicle body has been treated as a combination of rigid and elastic bodies. Nonlinearity in the suspension behaviour has been taken into account. Road input was modelled by stationary random process. Results indicated that structural flexibility may play an important role in the deformation characteristics of the system above certain frequency range.

Valk and Pacejka [58] proposed a mathematical model of landing gear taking into account the lateral bending and torsional motion of the shock strut. They neglected the randomness in runway profiles. The model was applied to test the stability of the landing gears in a civil aircraft.

Vibration of most of the vehicle and their components are characterised by a combination of bending deflections and torsional rotations. The motions usually remain coupled whenever shear center and mass center do not coincide. Aircraft wings, control surfaces and many sections in ships and other ground vehicles fall under this category. The practical importance of the coupled bending-torsion vibrations of the beam element has induced many approaches for evaluation of the normal modes. Gonaldd [59], Timoshenko [60], and Dokumaci [61] have obtained exact modal solutions for uniform section beams with simple boundary

conditions. The methods have been applied to thin walled beams, aircraft wings and turbine blades.

Bishop and Price [62] developed an exact solution of coupled-bending torsion of a beam including the effect of rotary inertia and shear deformation. Orthogonality condition for the coupled normal modes have been derived and used to express the equation of motion in terms of normal coordinates. Bishop [63] extended the study on coupled bending - torsion of beam including warping.

Different numerical and approximate methods have been tried for the solution of coupled bending-torsion modes of beams. Anderson and Houbolt [64] used Rayleigh's energy principle for the vibration of aircraft wings. Both unswept and swept wing's natural frequency and mode shape have been determined. Rao and Carnegie [65] used Galerkin technique for bladeing vibration in turbine. Mei [66] and Klausbruckner et al. [67] introduced FEM technique for coupled bending torsion vibration of beams. Klausbruckner in his formulation has taken the effect of warping. The theoretical results have been compared with the experimental results for channel section beams. Hallaur and Liu [68] and Banerjee [69] have developed dynamic stiffness matrix for coupled bending-torsion of beam elements. Dynamic stiffness matrix has been obtained by directly solving the governing differential equations. The theory developed for an individual member has been applied to multiple span beams and more general planar assemblage of beams.

Eslimy-Isfahany et al. [70] developed an analytical theory for the response of a cantilever aircraft wing coupled in bending and torsion. Normal mode theory has been applied for the response

solution. Both deterministic and stationary random excitations have been compared.

Moving vehicle exerts fluctuating force on the track which vary both in space and time. The structure undergoes deformation of varying degree depending on its construction. Track design is identified as a critical area of potential capital savings in any transport system. As track becomes lighter and more flexible, material cost is reduced though it causes complex vehicle-track interaction and affect ride quality.

Blejwas [71] developed a procedure for simulating the dynamic interaction between traversing vehicle and support structure. Lagrange multipliers have been used to satisfy constraint relations between the interacting systems. Response has been obtained with a point mass and spring-mass-damper system over smooth and sinusoidal track at constant vehicle speed.

Duff [72] considered the vibration analysis of infinite rail road track due to moving vibratory load passing over it. The rail road track has been modelled as infinite beam resting on Winkler foundation. Laplace and Fourier transform have been used to obtain the response.

Yadav and Upadhayay [73] carried out analytical study on nonstationary dynamics of rigid heave model of train and flexible track over inertial foundation during variable velocity runs. Track has been assumed to be a finite length beam resting on elastic foundation. Track mean line was considered variable in vertical plane superimposed by random roughness. The above model was then extended to heave-pitch, heave-roll [74] and heave-pitch-roll models [75]. Comparison of model behaviour has

revealed strong influence of pitch and roll modes on the bounce motion of the vehicles while track response was sensitive to the types of sleepers used.

Hardy and Cebon [76] have analysed the response of continuous road pavement to moving vehicle load. Response have been obtained in time domain for linear two degrees of freedom heave model using convolution theory. Road has been idealised as slender beam resting on Winkler foundation having distributed spring and damping. Road unevenness has been assumed to have a deterministic form represented by discrete steps.

Hiltunen and Bush [77] developed a testing and analysis technique to determine airfield pavement deflection under moving aircraft loads. Deflections have been obtained both on the surface and at depths below the surface. Geophones were employed in actual field measurements to gather information of the propagated waves caused by dynamic effects of moving aircraft loads.

Anant et al. [78] presented a dynamic analysis of rigid airport pavement with discontinuous joints. Aircraft model was assumed to be single degree of freedom mass, spring and dashpot system. Runway pavement has been idealised as thin elastic plates resting on a Winkler foundation. FEM technique was used to obtain vehicle and pavement dynamic behaviour. Peak dynamic deflection of the pavement has been found to depend significantly on the mass inertia of the aircraft.

Cai et al. [79] studied the dynamic interaction between the vehicle and guideways of high speed transportation system. Flexible guideway has been modelled as a Bernouli Euler beam and the dynamic model of the vehicle consisted of a single mass

yielding a two degrees of freedom heave model with primary and secondary linear suspensions. Modal analysis technique has been used for the response calculation. It was shown that for a certain range of vehicle-guideway parameters, the interaction between guideway and vehicle can be ignored. In this, situation representation of vehicle model by single moving mass has been found to be adequate.

In another study, Cai et al. [80] considered the model of multi-car and multi-load vehicle travelling at constant speed over randomly profiled double span guideway. Coupled effects of vehicle-guideway interactions over a wide range of vehicle speed and various guideway parameters have been investigated. Multicar vehicles have been found to provide better ride comfort than single car because of inter car constraints. The analytical techniques developed are suitable for analysis of vehicle/guideway interactions in maglev systems.

Dynamic tyre force applied to road surface by heavy vehicles can cause premature road failure. Potter and Cole et al. [81] devised a measuring system of dynamic tyre force of commercial vehicles. Measured dynamic wheel load of instrumented vehicles has been used to investigate the effects of vehicle configurations, vehicle vibration and road strength on the prediction of road damage potential.

Laib [82] investigated the dynamics of off-road vehicles on deformable soil. Here the original ground profile is altered significantly by the vehicle passing over the rough terrain. The vehicle transfer function has been used to compute effective ground profile which generates the actual vibratory motion in the

vehicle. The method has been illustrated for several soil type and for number of vehicles.

Although technical literatures contain substantial amount of studies relating to various aspects of vehicle dynamics to track irregularities, the following have not been adequately covered or not completely addressed -

- (1) Nonstationary excitation due to variable velocity run have been studied mostly on lumped mass rigid vehicle models. Analytical formulation for the flexible vehicle-track system response with a general case of vehicle ground motion including spatially nonhomogeneous track roughness do not appear in the literatures.
- (2) In most flexible system, vehicle body has been modelled as an elastic beam with constant cross sectional properties. In many vehicles flexible attachments are also present, one example being aircraft wings. These may undergo appreciable dynamics induced by their support motion. The dynamics of flexible attachment of the vehicles has been ignored in earlier studies.
- (3) The flexible structures are distributed parameter systems. Their cross sectional properties and damping characteristics may be nonuniform. In the solution of linear flexible vehicle model, mode superposition technique has been tried from time to time. Accurate knowledge of natural frequency and mode shape functions are essential requirements of the method. In many studies, FEM and other numerical techniques have been used to obtain the vehicle modal parameters when cross sectional geometry is variable in space. Analytical techniques

for general variable section beams are not fully addressed in literatures

- (4) Flexible vehicle models with multi-axle - multi-wheeled configurations including combined effect of rigid body heave-pitch-roll motion and coupled bending-torsional elastic modes have not been tackled for nonstationary track excitations.
- (5) Nonlinear suspension characteristics have been handled mostly by statistical linearisation and perturbation techniques for lower degrees of freedom model under stationary excitation and in more general case by Monte Carlo simulation. Statistical linearisation method may induce appreciable error when response probability function is different than the form assumed, which may happen in most practical cases of nonstationary input. Perturbation technique, on the other hand, has been applied with expansion of suspension forces in polynomial form. Nonlinear terms of the series are scaled by small parameters. Though theoretically valid, this brings out a restriction during application on its use to only weakly nonlinear systems. Monte Carlo simulation can take care of all the complexities involved in the problem. However, it becomes less attractive in terms of computer processing time and storage.

1.3 PRESENT WORK

In the present study an attempt has been made to fill some of the gaps mentioned above. Analytical methods have been developed to obtain response statistics of vehicle-track system induced by

track unevenness. The track unevenness is assumed to be a nonhomogeneous random process specified by a generalised PSD function. A variable mean of the track profile superimposed over zero mean random process has been considered. Track is assumed to deflect vertically under the vehicle imposed loads. It is modelled as a beam of uniform mass and flexural rigidity supported by elastic and dissipative subgrade.

Vehicle forward velocity has been assumed to be variable with time. Vehicle ground motion is modelled by a polynomial series with finite terms. Coefficients of the polynomial can be properly adjusted to depict any condition of the vehicle run. With the help of vehicle forward motion history, track input to vehicle can be obtained as a function of time.

Vehicle has been modelled as a combination of discrete and continuous elements. Vehicle wheels, tyres and part of the suspension systems are lumped as unsprung masses. Vehicle body contains slender attachments. Flexible vehicle body and slender attachments are modelled as beam elements with variable mass, stiffness and damping distributions. The attachments are allowed to carry arbitrary number of concentrated masses at arbitrary locations.

Sectional properties of the nonuniform beam has been modelled by power series. This representation is most general and any type of variation can be accommodated with desired accuracy. A method is outlined to find exact solution of nonuniform beam vibration. Natural frequencies and mode shape functions have been obtained in closed form for bending, torsion and bending-torsion coupled dynamics of variable section beam.

As the natural frequencies and mode shapes are very important to understand the system behaviour, validation of the proposed theory has been sought by comparison with available published results and by conducting experiments.

Governing differential equations for the vehicle-track systems have been developed. Continuous elements of the model involve partial differential equations with space variable coefficients. Equations of motion corresponding to lumped elements are ordinary differential equations.

In the present analysis, the equations of motion of the continuous systems are first reduced to a set of linear ordinary differential equations in time dependent generalised coordinates using normal mode expansion techniques. The set of ordinary differential equations together with the equations of lumped masses are then recast into first order state space form. These equations are completely uncoupled using modal analysis.

Analytical solution for response is obtained and expressions for second order statistics have been developed. The approach presented does not put any restriction on the nature of damping. The present method is applied to obtain the response statistics of transport aircraft with linear suspension parameters. Following models in order of increasing complexity have been tried:

- (1) Single Point Input Heave Model
- (2) Two Points Input Heave-Pitch Model
 - (a) Rigid fuselage
 - (b) Flexible fuselage in bending
- (3) Three Point Input Heave-Pitch-Roll Model
 - (a) Flexible fuselage in bending with rigid roll

(b) Flexible fuselage in bending and torsion

In the next part of the study, nonlinear behaviour of the suspension parameters is included in the analysis. Combination of air spring, orifice and coulomb damping has been treated with single point input heave model including tapered flexible wings. An instantaneous linear approach has been proposed. The method derives the benefit of linear theory while at the same time retains original nonlinear behaviour by incorporating instantaneous change in slope of the suspension forces at discrete operating points in time.

System equations for the nonlinear model have been developed wherein the suspensions forces are nonlinear functions of instantaneous stroke length and velocity. The system equations are integrated numerically with digitally simulated track profile samples using Shinozuka's algorithm [83]. Suspension forces are determined at discrete time steps from known response of original nonlinear systems. Derivatives of the forces at discrete time steps are evaluated which are used to represent 'instantaneous spring and damping constant'. With these instantaneous suspension parameters, step by step application of the analogous linear model has been carried out to obtain second order response statistics. Reliability of the solution has been assessed by comparison with Monte Carlo simulated results.

CHAPTER 2

SYSTEM DESCRIPTION

The system consists of a vehicle travelling over an uneven track supported by elastic and dissipative subgrade. Models have been developed for the system elements to study the coupled vehicle-track dynamics. These are being described below.

2.1 VEHICLE FORWARD MOTION

Any general forward velocity pattern of vehicle may be described by the position of its center of gravity (c.g.) along the track with reference to a fixed datum. Let the position of the vehicle c.g. x_c from the origin at time t be given by a polynomial of degree m as

$$x_c(t) = \sum_{k=0}^m a_k t^k \quad (2.1)$$

This form can easily be used, as mentioned above, to represent different conditions of vehicle forward motions with suitable selection of the coefficients of the polynomial. For example, a constant velocity travel requires $a_2 = a_3 = \dots = a_m = 0$ with a_0 and a_1 having non zero values. The vehicle with uniform acceleration or deceleration, can be represented with $a_3 = a_4 = \dots = a_m = 0$ with a_0 , a_1 and a_2 being non zero. In a situation where acceleration or deceleration is variable, the coefficients a_3 , a_4 , etc. are retained.

A vehicle has, in general, front and rear axles. Location of the front and rear axle from the vehicle c.g can be obtained when

wheel base length is known. Thus one has

$$x_1(t) = x_c(t) + l_1 = \sum_{k=0}^m a_{1k} t^k \quad (2.2)$$

$$x_2(t) = x_c(t) - l_2 = \sum_{k=0}^m a_{2k} t^k \quad (2.3)$$

$$\text{where } a_{10} = a_0 + l_1 ; a_{20} = a_0 - l_2 \quad (2.4)$$

$$\text{and } a_{1k} = a_{2k} = a_k, \quad k=1,2,\dots,m \quad (2.5)$$

where x_1 and x_2 are the instantaneous location of the front and rear axles measured from a reference point, l_1 and l_2 are the distances of the front and rear axles from the vehicle c.g. and wheel base length is the summation of l_1 and l_2

2.2 TRACK ROUGHNESS

The vertical height of the track along the longitudinal axis measured with respect to a flat datum at a distance x from the reference station can be represented by

$$h(x) = h_m(x) + h_R(x) \quad (2.6)$$

where $h_m(x)$ is a deterministic function describing the track mean and $h_R(x)$ is a zero mean random process. The mathematical representation of $h_R(x)$ using Stieltje's form is

$$h_R(x) = \int_{-\infty}^{\infty} dS_{h_R}(\Omega) \exp(j\Omega x) \quad (2.7)$$

where j is the imaginary unit equal to $\sqrt{-1}$, Ω is the spatial frequency and $dS_{h_R}(\Omega)$ is an orthogonal function with the

properties

$$E [dS_{h_R}(\Omega)] = \mu_{h_R}(\Omega) d\Omega = 0 \quad (2.8)$$

$$\text{and } E \left[| dS_{h_R}(\Omega_1) dS_{h_R}^*(\Omega_2) | \right] = \Phi_{h_R h_R}(\Omega_1, \Omega_2) d\Omega_1 d\Omega_2 \quad (2.9)$$

where $\Phi_{h_R h_R}(\Omega_1, \Omega_2)$ is the generalised PSD function of the track random unevenness. Asterisk denotes complex conjugate.

The Fourier transform of the track random roughness can be expressed as

$$\bar{h}_R(\Omega) = \frac{1}{2\pi} \int_{-\infty}^{\infty} h_R'(x) \exp(-j\Omega x) dx \quad (2.10)$$

Using eq.(2.7) in eq.(2.10)

$$\bar{h}_R(\Omega) = \frac{1}{2\pi} \int_{-\infty}^{\infty} \left\{ \int_{-\infty}^{\infty} dS_{h_R}(\Omega_1) \exp(j\Omega_1 x) \right\} \exp(-j\Omega x) dx$$

Interchanging the order of integration and using the definition of Dirac delta function, it can be shown that

$$\bar{h}_R(\Omega) = \int_{-\infty}^{\infty} dS_{h_R}(\Omega_1) \delta(\Omega - \Omega_1) \quad (2.11)$$

where $\delta(.)$ is the Dirac delta function

During variable velocity run the vehicle senses a nonstationary track input. The transformation of frequency from space to time domain would be governed by the relation

$$\omega = \Omega V(t) \quad (2.12)$$

where ω is the temporal frequency and $V(t)$ is the vehicle forward velocity at time t . This gives a nonlinear mapping of the temporal frequency ω into the wave number Ω .

Let the relation between the frequency and wave number for the track PSD be

$$\omega_1 = \Omega_1 V_1 \quad \text{and} \quad \omega_2 = \Omega_2 V_2 \quad (2.13)$$

where V_1 and V_2 are the vehicle forward velocities at time instants t_1 and t_2 respectively. Now from the definition of generalised PSD, one has

$$\begin{aligned} \Phi_{h_R h_R}(\Omega_1, \Omega_2) &= E \left[| \bar{h}_R(\Omega_1) \bar{h}_R^*(\Omega_2) | \right] \\ &= E \left[\left| \left\{ \int_{-\infty}^{\infty} dS_{h_R}(r_1) \delta(r_1 - \Omega_1) \right\} \left\{ \int_{-\infty}^{\infty} dS_{h_R}(r_2) \delta(r_2 - \Omega_2) \right\} \right| \right] \\ &= \int_{-\infty}^{\infty} \int_{-\infty}^{\infty} E \left[dS_{h_R}(r_1) dS_{h_R}^*(r_2) \right] \delta(r_1 - \Omega_1) \delta(r_2 - \Omega_2) \\ &= \int_{-\infty}^{\infty} \int_{-\infty}^{\infty} \Phi_{h_R h_R}(r_1, r_2) \delta(r_1 - \omega_1 / V_1) \delta(r_2 - \omega_2 / V_2) dr_1 dr_2 \\ &= \Phi_{h_R h_R}(\omega_1 / V_1, \omega_2 / V_2) \end{aligned} \quad (2.14)$$

The function $h_m(x)$ describing the variable mean track is assumed as a power series

$$h_m(x) = \sum_{i=1}^{\ell} h_i x^i \quad (2.15)$$

This representation is general and many shapes can be represented with this form accurately. Making use of eq.(2.1) in eq.(2.15), one has the mean track height experienced by the vehicle wheel at instant t

$$h_m(t) = \sum_{i=0}^{\ell} h_i \left(\sum_{k=0}^m a_k t^k \right)^i \quad (2.16)$$

Noting that, a polynomial of degree m raised to a power i, is a polynomial of degree m x i, eq.(2.16) can be expressed as [84],

$$h_m(t) = \sum_{i=0}^{\ell} h_i \sum_{r=0}^k c_{i,r} t^r \quad (2.17)$$

where $k = mi$

$$\begin{aligned} c_{i,0} &= a_0^i \\ c_{i,r} &= \frac{1}{r} a_0 \sum_{k=1}^r (ki - r + k) a_k c_{i,r-k} \quad \text{for } r \geq 1 \end{aligned} \quad (2.18)$$

The time derivative of $h_m(t)$ can be written as

$$\dot{h}_m(t) = \sum_{i=1}^{\ell} h_i \sum_{r=0}^{k-1} c_{i,r+1} (r+1) t^r \quad (2.19)$$

In case of vehicles with two axle and three wheel configurations, mean track levels at the various wheel locations would be

$$h_{m11} = \sum_{i=0}^{\ell} (h_i)_{11} \sum_{r=0}^k (c_{i,r})_{11} t^r \quad (2.20)$$

$$h_{m2p} = \sum_{i=0}^{\ell} (h_i)_{2p} \sum_{r=0}^k (c_{i,r})_{2p} t^r, \quad p=2,3 \quad (2.21)$$

where $(c_{i,0})_{11} = (a_{10})^i$ and

$$(c_{i,r})_{11} = \frac{1}{a_{10}^r} \sum_{k=1}^r (ki-r+k) a_{1k} (c_{i,r-k})_{11}; \quad r \geq 1 \quad (2.22)$$

The expression for coefficients $(c_{i,r})_{2p}$ are as eq. (2.22) with a_{1k} ($k=0,1,\dots$) replaced by a_{pk} where

$$\begin{aligned} a_{30} &= a_{20} \\ a_{1k} &= a_{2k} = a_{3k} = a_k, \quad k=1,2,\dots,m \end{aligned}$$

The two numerals in the suffixes are used to denote the axle and the wheel locations. The first numeral is 1 for the front and 2 for the rear axle. The second numeral becomes 1, 2 and 3 for centre, left and right wheels on a particular axle.

The above track roughness model with the mean level and random parts, may be used with homogeneous as well as nonhomogeneous tracks. The analysis has been developed for the general nonhomogeneous unevenness, the homogeneous form being a particular case.

2.3 VEHICLE-TRACK DYNAMIC MODEL

Vehicle structural elements are elastic members. These are usually modelled as rigid masses to reduce the mathematical complexity of the analysis. However, idealising some slender

components as rigid masses may induce unacceptable errors. The present study attempts to use a combination of rigid and continuous idealisations of the vehicle.

As mentioned in chapter 1, in the present study, the following linear suspension vehicle models with increasing order of details are considered :-

- (a) Heave Model
- (b) Heave-Pitch Model
 - (i) Rigid fuselage
 - (ii) Flexible fuselage in bending
- (c) Heave-Pitch-Roll Model
 - (i) Flexible fuselage in bending with rigid roll
 - (ii) Flexible fuselage in bending and torsion

These linear models are being described below.

2.3.1 Single Point Input Heave model

A model of the vehicle and the track is shown in Fig.2.1. The wheel track contact is assumed to be at one point only. The aircraft fuselage is modelled as a rigid lumped sprung mass onto which are attached flexible left and right wings, designated by superscript / subscript L and R respectively. Each wing is considered to act as a cantilever beam having distributed mass, flexural rigidity and damping, that are variable along the span. Various stores and attachments carried by the wings are modelled as concentrated mass loadings. The landing gear assembly is idealised as a lumped unsprung mass with linear spring and viscous damper. Tyre stiffness and damping are also assumed linear. The runway track elastic behaviour is accounted for by

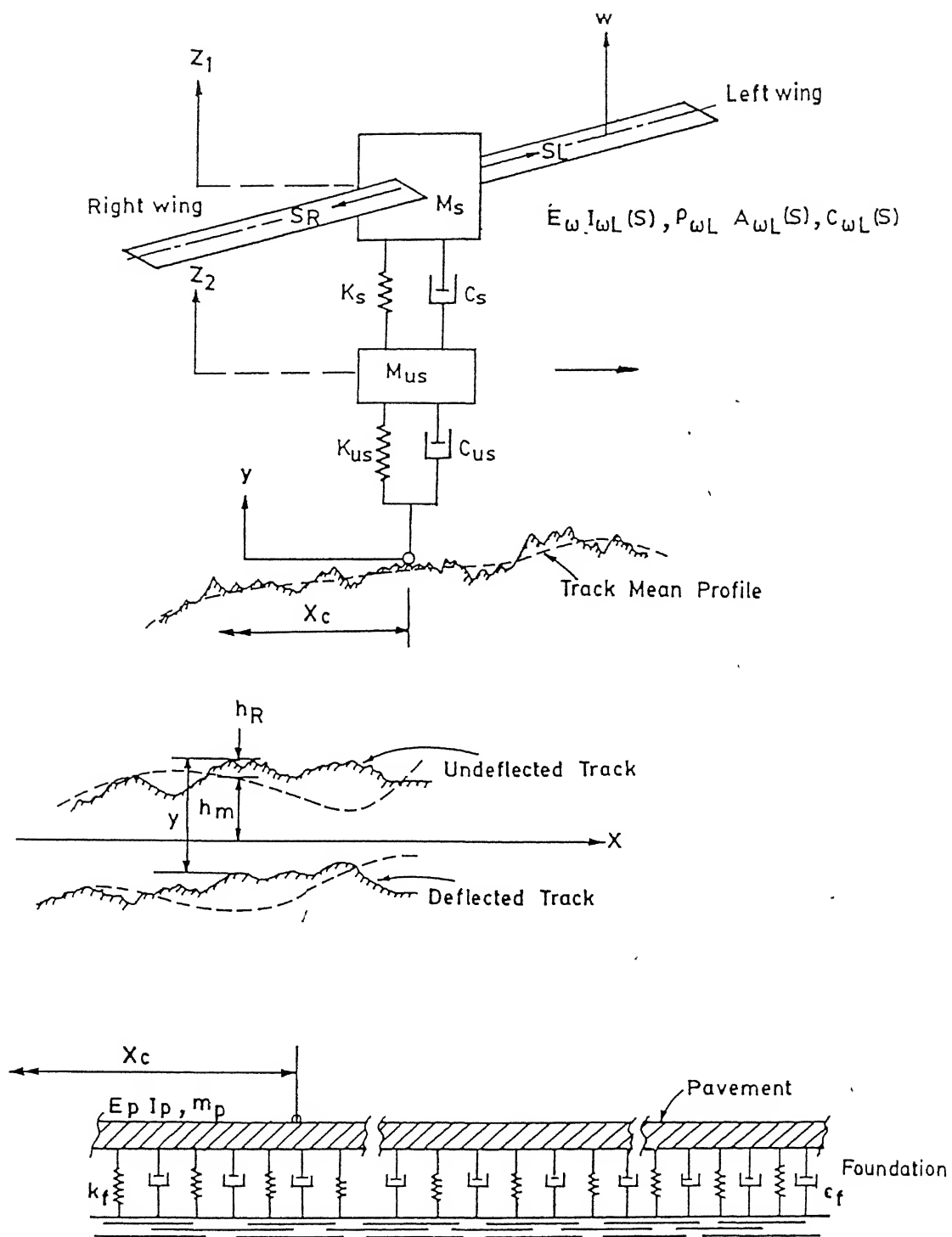


Fig.2.1. Heave Model

modelling the pavement as a Euler Bernouli beam with distributed flexural rigidity and mass taken constant along the span. The track is supported over elastic subgrade foundation having distributed stiffness and damping. These are assumed to be constant along the length of the track. The mass of the foundation is considered to incorporate the inertia effects under dynamic conditions.

2.3.2 Two Point Input, Heave-Pitch Model

(a) Rigid Fuselage:-

The aircraft fuselage is idealised as a rigid beam and wings as the flexible attachments. The vehicle and track models for the present analysis are illustrated in Fig.2.2 The track input through the wheel contacts are assumed to be at two points only. The vehicle body (fuselage) has pitching along with vertical bounce or heave motions. The two undercarriage shock absorbers and wheels are modelled as lumped masses with linear springs and dampers having only heave degrees of freedom. The wings are considered as variable taper cantilevered beams oscillating in coupled bending- torsion modes relative to fuselage. The wings may carry a number of concentrated masses placed at various locations along the span. The track is idealised as a continuous member supported by elastic and dissipative subgrade.

(b) Bending Flexible Fuselage:-

The model of the vehicle and the track adopted is shown in Fig.2.3. The c.g of the aircraft is taken as the body fixed

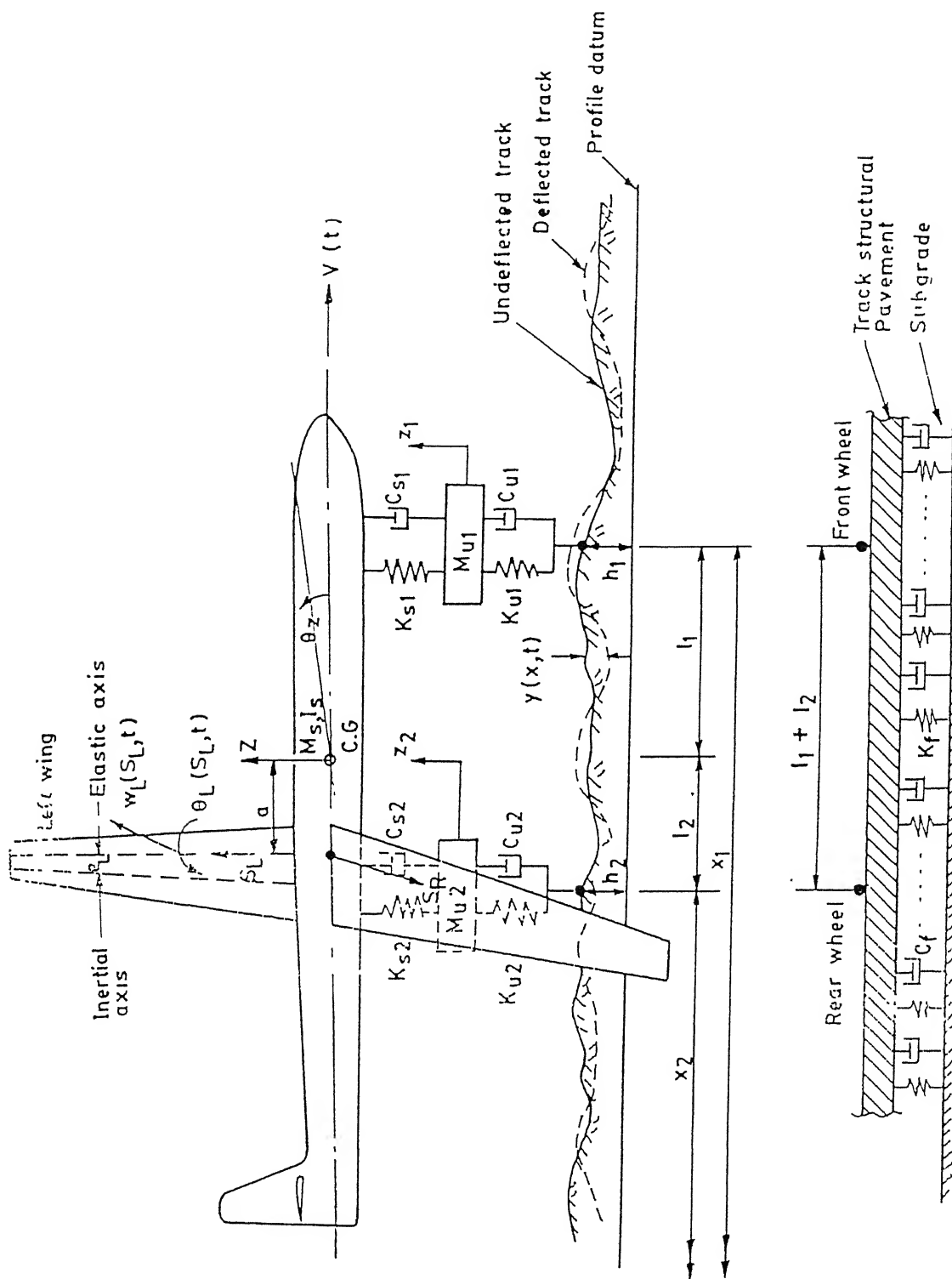


Fig.2.2. Heave-Pitch Model (Rigid fuselage)

origin. The fuselage is treated as a flexible continuous beam in bending with variable sectional properties. The absolute transverse displacement of the fuselage is composed of rigid body heave translation, pitch rotation of the longitudinal axis and elastic bending deformation relative to the rigid body displacement. The wings are modelled as cantilever beams of non uniform section having coupled bending - torsional motions. The front and rear undercarriage systems are modelled with linear shock strut springs and dampers. Tyre stiffness and dampings are treated as linear. The undercarriage masses are taken as lumped masses having only vertical heave motions.

2.3.3 Three Point Input Heave-Pitch-Roll Model

(a) Bending flexible fuselage with rigid roll:-

Aircraft model with tricycle landing gear arrangement is used (Fig.2.4). The front wheel follows the centre line profile while two main wheels follow the left and right profile of the track. The wheels of the vehicle in motion experience different track levels in the longitudinal and transverse direction. As a result, the vehicle is set to combined heave, pitch and roll motion.

Vehicle body is considered to be flexible in bending but rigid in torsional deformations. Flexible wings are considered as cantilever beams with roots attached to the vehicle body. The root motion of the beam induces dynamic loading on the span. Two main wheels are located under the wings. Wheels are treated as lumped masses, having only vertical degrees of freedom.

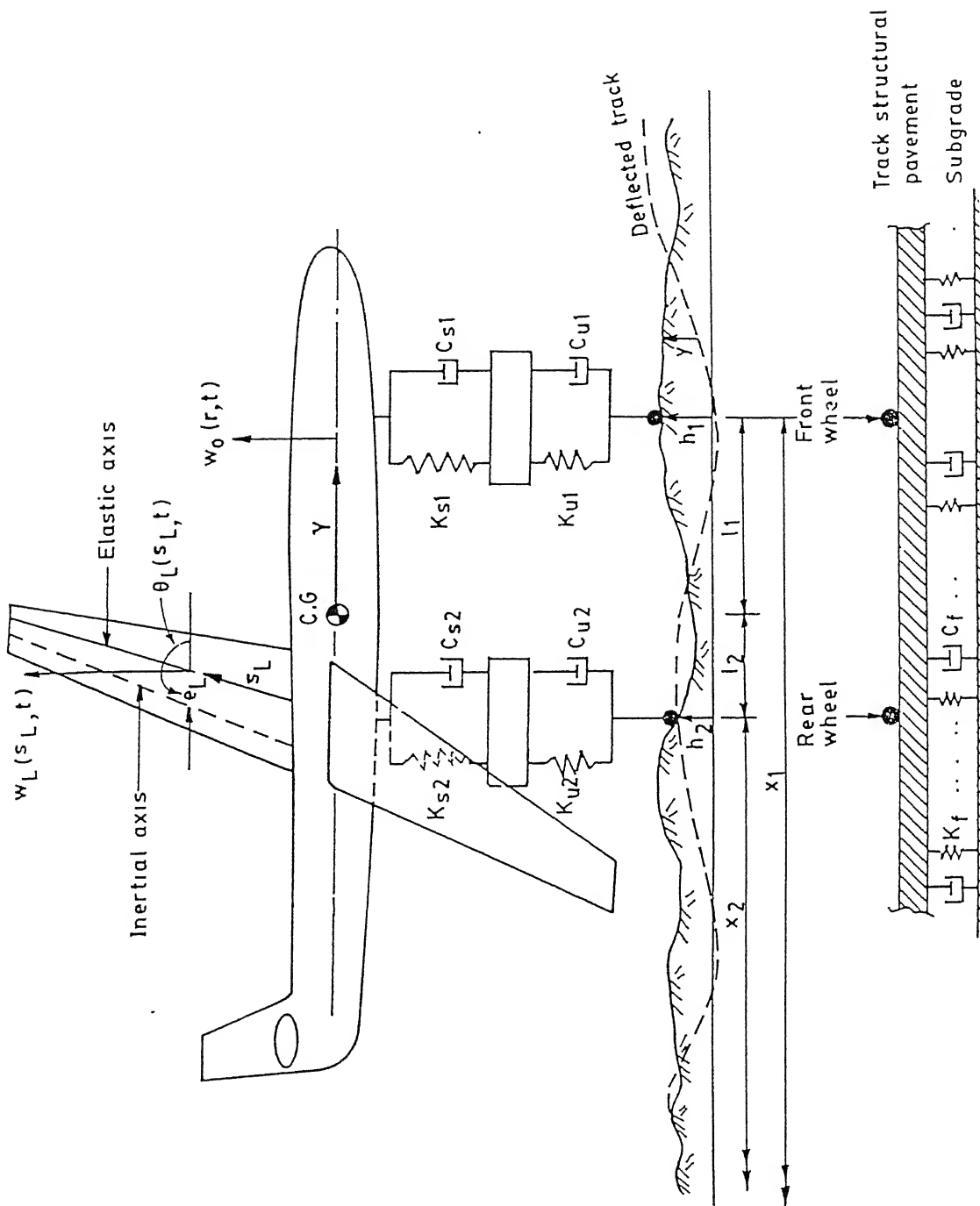


Fig.2.3. Heave-Pitch Model (Flexible fuselage)

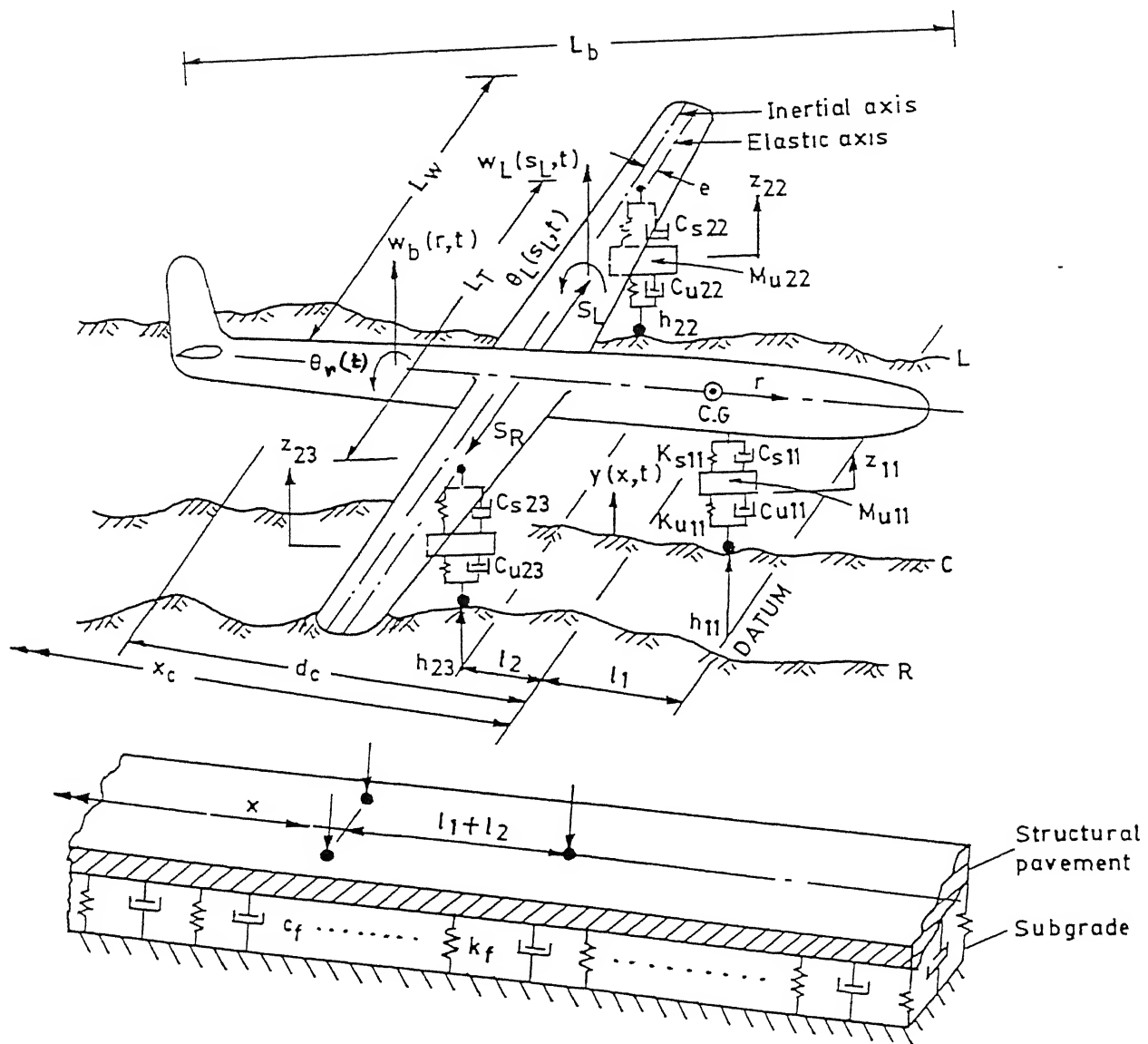


Fig.2.4. Heave-Pitch-Roll Model

(b) Bending and torsionally flexible fuselage:-

The above three points input model is further improved by considering elastic torsional deformation of the vehicle body. Interactions of flexural and torsional modes of the vehicle body along with rigid body heave-pitch-roll motions have been considered.

2.4 SYSTEM EQUATIONS

2.4.1. Heave Model

The system displacements are considered only in the vertical plane and are designated positive upward (Fig.2.1). The displacements z_1 and z_2 of the sprung and unsprung masses are measured from their respective static equilibrium positions. The transverse displacements of left and right wing w_L and w_R are measured off their respective bending axes drawn from the roots. Deflection of the track mean line y at any instant t is taken transverse to its longitudinal axis.

The equations of motion of two lumped masses are

$$M_S \ddot{z}_1 + C_S (\dot{z}_1 - \dot{z}_2) + K_S (z_1 - z_2) =$$

$$- \frac{\partial}{\partial s_L} \left[E_{wL} I_{wL} (s_L) \frac{\partial^2 w_L}{\partial s_L^2} \right]_{s_L=0} - \frac{\partial}{\partial s_R} \left[E_{wR} I_{wR} (s_R) \frac{\partial^2 w_R}{\partial s_R^2} \right]_{s_R=0}$$

(2.23)

$$\begin{aligned}
& M_{us} \ddot{z}_2 + C_{us} \left\{ \dot{z}_2 - \dot{y}(x_c, t) - \dot{h}(x_c) \right\} \\
& + K_{us} \left\{ z_2 - y(x_c, t) - h(x_c) \right\} - C_s (\dot{z}_1 - \dot{z}_2) - K_s (z_1 - z_2) = 0 \quad (2.24)
\end{aligned}$$

where M_s and M_{us} are the sprung and unsprung masses, K_s and C_s are the linearised spring and damping constant of the shock absorber. K_{us} and C_{us} are tyre stiffness and tyre damping coefficients. $E_w I_w$ are the wing's flexural rigidity. w is the transverse bending displacement of the cantilever wing. Subscript L or R is used for left and right wing. x_c is the distance of the vehicle along the track and gives the wheel track contact location.

The wings act like cantilever beams with base excitation as these are clamped at the fuselage and excited by the fuselage vertical displacement. The distributed aerodynamic lift as well as concentrated mass loadings at discrete locations are considered to act on the wing. The equations of motion of the left and right wing are,

$$\begin{aligned}
\frac{\partial^2}{\partial s_L^2} \left[E_{wL} I_{wL} (s_L) \frac{\partial^2 w_L}{\partial s_L^2} \right] + m_{wL}(s_L) \frac{\partial^2 w_L}{\partial t^2} + c_{wL}(s_L) \frac{\partial w_L}{\partial t} \\
= f_w^L(s_L, t) \quad (2.25)
\end{aligned}$$

$$\frac{\partial^2}{\partial s_R^2} \left[E_{wR} I_{wR} (s_R) \frac{\partial^2 w_R}{\partial s_R^2} \right] + m_{wR}(s_R) \frac{\partial^2 w_R}{\partial t^2} + c_{wR}(s_R) \frac{\partial w_R}{\partial t} = f_w^R(s_R, t) \quad (2.26)$$

where m_w and c_w are mass and viscous damping per unit span. The distributed applied force on the left wing beam is given by

$$f_w^L(s, t) = - \left\{ m_{wL}(s_L) \ddot{z}_1 + c_{wL}(s_L) \dot{z}_1 \right\} - \sum_{k=1}^{p_L} M_k^L \{ \ddot{w}_L(s, t) + \ddot{z}_1 \} \delta(s_L - s_k) + V_w^L(s, t) \quad (2.27)$$

where M_k is k th concentrated mass loading on the wing at span location s_k and $V_w(s, t)$ is the aerodynamic lift force per unit length of the wing. These quantities can be particularised for the right wing by using proper subscript/superscript.

There exists a similar expression for the impressed force on the right wing which can be obtained from eq. (2.27) by using subscript/superscript R.

Assuming an elliptical distribution, lift on either wing can be expressed as [85]

$$V_w(s, t) = L_0 V(t)^2 \left[1 - (s / L_w)^2 \right]^{1/2} \quad (2.28)$$

$$\text{where } L_0 = \frac{\rho_a C_L S_w}{2 \pi L_w} \quad (2.29)$$

in which ρ_a is the air density, C_L is the lift coefficient, S_w is the wing surface area, and L_w is the semi wing span.

The quantity $V(t)$ is the aircraft forward velocity and we have from eq.(2.1),

$$V^2(t) = \left\{ \dot{x}_c(t) \right\}^2 = \sum_{r=0}^{2(m-1)} c'_r t^r \quad (2.30)$$

where $c'_0 = (a'_0)^2$

$$\text{and } c'_r = \frac{1}{r a_0} \sum_{k=1}^r (3k - r) a'_k c'_{r-k}, \quad r \geq 1 \quad (2.31)$$

$$a'_k = (k+1) a_{k+1}$$

For vehicles where aerodynamic lift is not significant, the lift terms may be dropped from eq.(2.27).

The track is assumed to behave like a beam with continuous elastic support along its length. The wheel reaction acts as a moving dynamic excitation for the track beam. Its differential equation of motion for a single point input is given by

$$E_p I_p \frac{\partial^4 y}{\partial x^4} + m_p \frac{\partial^2 y}{\partial t^2} + c_f \frac{\partial y}{\partial t} + k_f y = f_p(x, t) \quad (2.32)$$

where $E_p I_p$, m_p are the track flexural rigidity and distributed mass; c_f and k_f are distributed viscous damping and spring constant for the foundation. These are assumed uniform along the track length. The applied force per unit length for one point input model is given by

$$\begin{aligned}
f_p(x,t) = & - \left[C_{us} \left\{ \dot{z}_2 - \dot{y}(x,t) - \dot{h}(x) \right\} \right. \\
& \left. + K_{us} \left\{ z_2 - y(x,t) - h(x) \right\} \right] \delta(x - x_c)
\end{aligned} \tag{2.33}$$

2.4.2 Heave-Pitch Model

(a) Rigid Model

The fuselage beam undergoes rigid body heave motion z and pitch rotation of the longitudinal axis θ_z . Front and rear unsprung masses have only vertical degrees of freedom z_1 and z_2 measured from their static equilibrium positions. The wings attached to fuselage are assumed to have variable cross sections where the shear centre does not coincide with the centroid. The coupled bending -torsion oscillation of the wings is induced by fuselage heave-pitch motion. The transverse displacement and twist of the wings relative to the fuselage motion are denoted by w and θ . All rotational displacements are assumed leading end up positive and linear displacements are assumed positive upward as indicated in Fig. 2.2

The governing differential equations for the heave-pitch motions of the rigid fuselage are

$$\begin{aligned}
M_s \ddot{z} + C_{s1}(\dot{z} + l_1 \dot{\theta}_z - \dot{z}_1) + K_{s1}(z + l_1 \theta_z - z_1) + C_{s2}(\dot{z} - l_2 \dot{\theta}_z - \dot{z}_2) \\
+ K_{s2}(z - l_2 \theta_z - z_2) = - \frac{\partial}{\partial s_L} \left\{ E_{wL} I_{wL}(s_L) \frac{\partial^2 w_L}{\partial s_L^2} \right\}_{s_L=0} \\
- \frac{\partial}{\partial s_R} \left\{ E_{wR} I_{wR}(s_R) \frac{\partial^2 w_R}{\partial s_R^2} \right\}_{s_R=0}
\end{aligned} \tag{2.34}$$

$$\begin{aligned}
& I_s \ddot{\theta}_z + \left\{ C_{s1} (\dot{z} + l_1 \dot{\theta}_z - \dot{z}_1) + K_{s1} (z + l_1 \theta_z - z_1) \right\} l_1 - \left\{ C_{s2} (\dot{z} - \right. \\
& \left. l_2 \dot{\theta}_z - \dot{z}_2) + K_{s2} (z - l_2 \theta_z - z_2) \right\} l_2 = \\
& l_0 \left[\frac{\partial}{\partial s_L} \left\{ E_{wL} I_{wL}(s_L) \frac{\partial^2 w_L}{\partial s_L^2} \right\}_{s_L=0} + \frac{\partial}{\partial s_R} \left\{ E_{wR} I_{wR}(s_R) \frac{\partial^2 w_R}{\partial s_R^2} \right\}_{s_R=0} \right] \\
& - \left\{ G_{wL} J_{wL}(s_L) \frac{\partial \theta_L}{\partial s_L} \right\}_{s_L=0} - \left\{ G_{wR} J_{wR}(s_R) \frac{\partial \theta_R}{\partial s_R} \right\}_{s_R=0} \quad (2.35)
\end{aligned}$$

where C_{s1} , K_{s1} ; C_{s2} , K_{s2} are nose and main gear suspension damping and spring constants respectively, I_s is the mass moment of inertia of the fuselage, $E_w I_w(s)$, $G_w J_w(s)$ are flexural and torsional rigidities of the wing beam. Here l_0 is the distance of the wing's shear center at root measured parallel to longitudinal axis from the aircraft c.g.

Equations of motion for the two unsprung masses are

$$\begin{aligned}
& M_{ui} \ddot{z}_i + C_{si} \left\{ \dot{z}_i - \dot{z} - l_i \dot{\theta}_z \right\} + K_{si} \left\{ z_i - z - l_i \theta_z \right\} \\
& + C_{ui} \left\{ \dot{z}_i - \dot{h}(x_i) - \dot{y}(x_i, t) \right\} + K_{ui} \left\{ z_i - h(x_i) - y(x_i, t) \right\} = 0 \quad (2.36) \\
& \quad \quad \quad i=1,2
\end{aligned}$$

i is equal to 1 for the nose wheel and 2 for the main wheel.

The wing beam gets disturbance from the fuselage vertical motion and rotation at its support location. The equations of motion describing the coupled bending - torsion forced vibration of the wing beams are

$$\frac{\partial^2}{\partial s^2} \left\{ E_w I_w(s) \frac{\partial^2 w}{\partial s^2} \right\} + m_w(s) \frac{\partial^2 w}{\partial t^2} - m_w(s) e_w(s) \frac{\partial^2 \theta}{\partial t^2} + c_w(s) \frac{\partial w}{\partial t} - e_w(s) c_w(s) \frac{\partial \theta}{\partial t} = f_w(s, t) \quad (2.37)$$

$$\frac{\partial}{\partial s} \left\{ G_w J_w(s) \frac{\partial \theta}{\partial s} \right\} - I_{w\alpha}(s) \frac{\partial^2 \theta}{\partial t^2} + m_w(s) e_w(s) \frac{\partial^2 w}{\partial t^2} - \left\{ \vartheta_w(s) + e_w^2(s) c(s) \right\} \frac{\partial \theta}{\partial t} + c_w(s) e_w(s) \frac{\partial w}{\partial t} = e_w(s) f_w(s, t) - \Gamma_w(s, t) \quad (2.38)$$

where $I_{w\alpha}(s)$ is the polar mass moment of inertia of the wing cross section about the shear center, $m_w(s)$ is the distributed mass along the span, $e_w(s)$ is the off set of shear center from the elastic axis, $c_w(s)$ is the distributed viscous damping to translational motion and $\vartheta_w(s)$ is the distributed damping to rotational motion. The impressed force f_w and torque Γ_w per unit span are

$$f_w(s, t) = - m_w(s) (\ddot{z} - l_0 \ddot{\theta}_z) - c_w(s) (\dot{z} - l_0 \dot{\theta}_z) + m_w(s) e_w(s) \ddot{\theta}_z + e_w(s) c_w(s) \dot{\theta}_z - \sum_{k=1}^p M_k \left\{ \ddot{z} - l_0 \ddot{\theta}_z + \ddot{w}(s, t) \right\} \delta(s - s_k) + \sum_{k=1}^p M_k e_w(s) \left\{ \ddot{\theta}_z + \ddot{\theta}(s, t) \right\} \delta(s - s_k) + V_w(s, t) \quad (2.39)$$

$$\begin{aligned}
\Gamma_w(s,t) = & - I_{w\alpha}(s) \ddot{\theta}_z + m_w(s) e_w(s) (\ddot{z} - l_0 \ddot{\theta}_z) - \left\{ v_w(s) + \right. \\
& \left. e_w^2(s) c_w(s) \right\} \dot{\theta}_z + c_w(s) e_w(s) (\dot{z} - l_0 \dot{\theta}_z) - \sum_{k=1}^p I_k \left\{ \ddot{\theta}_z + \ddot{\theta}(s,t) \right\} \\
& \delta(s - s_k) + \sum_{k=1}^p M_k e_w(s) \left\{ \ddot{z} - l_0 \ddot{\theta}_z + w(s,t) \right\} \delta(s - s_k) + M_{ac}(s,t)
\end{aligned}
\tag{2.40}$$

where p is the number of concentrated masses, M_k and I_k are the magnitudes of the k th concentrated mass and its moment of inertia about the shear center, V_w and M_{ac} are the distributed lift force and aerodynamic center moment per unit span of the wing. The left and right wing equations of motion are designated by placing appropriate subscripts L or R for the variables in eqs. (2.37) - (2.40).

The vertical lift distribution on the $V_w(s,t)$ is given by eq. (2.28) while aerodynamic center moment $M_{ac}(s,t)$ may be expressed as

$$M_{ac}(s,t) = M_0 c_h^2(s) V^2(t) \tag{2.41}$$

$$\text{where } M_0 = \frac{\rho_a C_{mac}}{2}$$

' C_{mac} ' being the aerodynamic centre moment coefficient and c_h is the mean chord.

The equation of motion of the track beam with foundation reaction taken into account is given by eq. (2.32). The track beam

is subject to two point loads and the applied loading per unit length can be written as

$$f_p(x,t) = - \sum_{i=1}^2 \{ C_{ui} (\dot{z}_i - \dot{h}(x) - \dot{y}(x,t)) + K_{ui} (z_i - h(x) - y(x,t)) \} \delta(x - x_i) \quad (2.42)$$

(b) Flexible Vehicle body:-

The vehicle body is treated as beam with variable cross section. The transverse displacement $w_b(r,t)$ at any station r is given by

$$\frac{\partial^2}{\partial r^2} \left\{ E_b I_b(r) \frac{\partial^2 w_b}{\partial r^2} \right\} + m_b(r) \frac{\partial^2 w_b}{\partial t^2} + c_b(r) \frac{\partial w_b}{\partial t} = f_b(r,t) + \frac{\partial}{\partial r} M_b(r,t) \quad (2.43)$$

where $E_b I_b$ is the flexural stiffness, m_b is the mass and c_b is the viscous damping per unit length of the vehicle body. The impressed force f_b and moment M_b per unit length are

$$f_b(r,t) = - \sum_{i=1}^2 \left[K_{si} \{ w_b(r,t) - z_i \} + C_{si} \{ \dot{w}_b(r,t) - \dot{z}_i \} \right] \delta(r-l_i) - \left[\frac{\partial}{\partial s_L} \left\{ E_{wL} I_{wL}(s_L) \frac{\partial^2 w_L}{\partial s_L^2} \right\}_{s_L=0} + \frac{\partial}{\partial s_R} \left\{ E_{wR} I_{wR}(s_R) \frac{\partial^2 w_R}{\partial s_R^2} \right\}_{s_R=0} \right] \delta(r-l_0) \quad (2.44)$$

and

$$M_b(r,t) = - \left[\left\{ G_{wL} J_{wL}(s_L) \frac{\partial \theta_L}{\partial s_L} \right\}_{s_L=0} + \left\{ G_{wR} J_{wR}(s_R) \frac{\partial \theta_R}{\partial s_R} \right\}_{s_R=0} \right] \delta(r-l_0) \quad (2.45)$$

The equations of motion of the two unsprung masses can be written as

$$M_{ui} \ddot{z}_i + C_{ui} \left\{ \dot{z}_i - \dot{h}(x_i) - \dot{y}(x_i, t) \right\} + K_{ui} \left\{ z_i - h(x_i) - y(x_i, t) \right\} + C_{si} \left\{ \dot{z}_i - \dot{w}_b(l_i, t) \right\} + K_{si} \left\{ z_i - w_b(l_i, t) \right\} = 0 \quad (2.46)$$

(i=1,2)

The equations of motion of the non uniform flexible attachment in coupled bending - torsion are same as eqs. (2.37) and (2.38). The induced forces are however modified in view of the interaction of flexural modes of the fuselage. These are given as

$$f_w(s,t) = - m_w(s) \ddot{w}_b(l_0, t) - c_w(s) \dot{w}_b(l_0, t) + m_w(s) e_w(s) \frac{\partial^2}{\partial t^2} w'_b(l_0, t) + e_w(s) c_w(s) \frac{\partial}{\partial t} w'_b(l_0, t) - \left[\sum_{k=1}^p M_k \left\{ \ddot{w}_b(l_0, t) + \ddot{w}(s, t) \right\} - \sum_{k=1}^p M_k e_w(s) \left\{ \frac{\partial^2}{\partial t^2} w'_b(l_0, t) + \ddot{\theta}(s, t) \right\} \right] \delta(s-s_k) + V_w(s, t) \quad (2.47)$$

and

$$\begin{aligned}
\Gamma_w(s, t) = & - I_{w\alpha}(s) \frac{\partial^2}{\partial t^2} w'_b(l_0, t) + m_w(s) e_w(s) \ddot{w}_b(l_0, t) \\
& - \left\{ \vartheta(s) + e_w^2(s) c_w(s) \right\} \frac{\partial}{\partial t} w'_b(l_0, t) + c_w(s) e_w(s) \frac{\partial}{\partial t} w'_b(l_0, t) \\
& - \left[\sum_{k=1}^p I_k \left\{ \frac{\partial^2}{\partial t^2} w'_b(l_0, t) + \ddot{\theta}(s, t) \right\} - \sum_{k=1}^p M_k e_w(s) \left\{ \ddot{w}_b(l_0, t) \right. \right. \\
& \left. \left. + \ddot{w}(s, t) \right\} \right] \delta(s-s_k) + M_{ac}(s, t)
\end{aligned} \tag{2.48}$$

The equation of motion for transverse oscillation of the track beam has the form same as in eq.(2.32) with the vertical force imposed on the track at the location of front and rear wheel is given by the expression (2.42)

2.4.3 Heave-Pitch-Roll Model

(a) Bending flexible fuselage with rigid roll:-

Transverse oscillation of the vehicle body can be described by eq.(2.43). However, the vertical force and bending moment per unit length induced in the vehicle body taking account of the rigid body rolling and interactions of the landing gear suspensions are given as

$$\begin{aligned}
f_b(r, t) = & - \left[C_{s11} \left\{ \dot{w}_b(r, t) - \dot{z}_{11} \right\} + K_{s11} \left\{ w_b(r, t) - z_{11} \right\} \right] \delta(r-l_1) \\
& - \sum_{i=2}^3 \left[C_{s2i} \left\{ \dot{w}_0(r, t) - \dot{z}_{2i} \right\} + K_{s2i} \left\{ w_0(r, t) - z_{2i} \right\} \right] \delta(r-l_i)
\end{aligned}$$

$$- \left[\frac{\partial}{\partial s_L} \left\{ E_{wL} I_{wL}(s_L) \frac{\partial^2 w_L}{\partial s_L^2} \right\} + \frac{\partial}{\partial s_R} \left\{ E_{wR} I_{wR}(s_R) \frac{\partial^2 w_R}{\partial s_R^2} \right\} \right]_{s_L=0} \delta(r-l_0) \quad (2.49)$$

and

$$M_b(r,t) = - \left[\left\{ G_{wL} J_{wL}(s_L) \frac{\partial \theta_L}{\partial s_L} \right\}_{s_L=0} + \left\{ G_{wR} J_{wR}(s_R) \frac{\partial \theta_R}{\partial s_R} \right\}_{s_R=0} \right] \delta(r-l_0) \quad (2.50)$$

where C_s and K_s are the suspension damping and stiffness. As mentioned earlier, two numerals in the suffixes are used to denote axle location and wheel location on the axle. The first numeral is 1 for front and 2 for rear axle. Second numeral becomes 1, 2 and 3 for centre, left and right wheel respectively on the particular axle. The quantity w_0 is the total deflection of the vehicle body at any transverse location from its longitudinal axis and is given by

$$w_0(r,t) = w_b(r,t) + g_b(r) \theta_r(t) \quad (2.51)$$

where $g_b(r)$ is the distance of the point on the vehicle body at station r , measured transverse to the longitudinal axis. θ_r is the rigid body roll motion. The equation of motion governing the rigid body roll of the vehicle can be written as

$$I_r \ddot{\theta}_r + \sum_{i=2}^3 \left[C_{s2i} \left\{ \dot{w}_0(l_2,t) - \dot{z}_{2i} \right\} + K_{s2i} \left\{ w_0(l_2,t) - z_{2i} \right\} \right] e_i$$

$$= - \left\{ E_{wL} I_{wL}(s_L) \frac{\partial^2 w_L}{\partial s_L^2} \right\}_{s_L=0} + \left\{ E_{wR} I_{wR}(s_R) \frac{\partial^2 w_R}{\partial s_R^2} \right\} \quad (2.52)$$

where e_2 and e_3 are the distance of the wheels on the rear axle from the longitudinal axis of the vehicle body and are given by

$$e_2 = g_b(l_2) + s_{gL}; \quad e_3 = -\{g_b(l_2) + s_{gR}\}$$

The equations of motion for the front and the rear wheels are

$$\begin{aligned} & M_{u11} \ddot{z}_{11} + C_{u11} \left\{ \dot{z}_{11} - \dot{h}_{11}(x_1) - \dot{y}(x_1, t) \right\} \\ & + K_{u11} \left\{ z_{11} - h_{11}(x_1) - y(x_1, t) \right\} + C_{s11} \left\{ \dot{z}_{11} - \dot{w}_b(l_1, t) \right\} + \\ & K_{s11} \left\{ z_{11} - w_b(l_1, t) \right\} = 0 \end{aligned} \quad (2.53)$$

and

$$\begin{aligned} & M_{u2i} \ddot{z}_{2i} + C_{u2i} \left\{ \dot{z}_{2i} - \dot{h}_{2i}(x_2) - \dot{y}(x_2, t) \right\} \\ & + K_{u2i} \left\{ z_{2i} - h_{2i}(x_2) - y(x_2, t) \right\} + C_{s2i} \left\{ \dot{z}_{2i} - \dot{w}_0(l_i, t) - \dot{w}_i(s_{gi}, t) \right\} \\ & + K_{s2i} \left\{ z_{2i} - w_0(l_i, t) - w_i(s_{gi}, t) \right\} = 0 \end{aligned} \quad (2.54)$$

$$(i=2, 3 ; w_2=w_L ; w_3 = w_R ; s_{g2} = s_{gL}; s_{g3} = s_{gR})$$

The coupled bending -torsional oscillation of the flexible attachment have the same form as eq.(2.37) and eq.(2.38) except that the applied vertical force and torque induced by fuselage motions and landing gear reaction are modified as

$$\begin{aligned}
 f_w(s,t) = & -m_w(s)\ddot{w}_0(l_0,t) - c_w(s)\dot{w}_0(l_0,t) + m_w(s)e_w(s)\frac{\partial^2}{\partial t^2} w'_0(l_0,t) \\
 & + e_w(s)c_w(s)\frac{\partial}{\partial t} w'_0(l_0,t) - \sum_{k=1}^p \left[M_k \{ \ddot{w}_0(l_0,t) + \ddot{w}(s,t) \} - M_k e_w(s) \right. \\
 & \left. \{ \frac{\partial^2}{\partial t^2} w'_0(l_0,t) + \ddot{\theta}(s,t) \} \right] \delta(s-s_k) - \left[C_{s2i} \{ \dot{w}_0(l_0,t) + \right. \\
 & \left. \dot{w}(s,t) - \dot{z}_{2i} \} + K_{s2i} \{ w_0(l_0,t) + w(s,t) - z_{2i} \} \right] \delta(s-s_{gi}) + V_w(s,t) \quad ,
 \end{aligned}
 \tag{2.55}$$

and

$$\begin{aligned}
 \Gamma_w(s,t) = & M_{ac}(s,t) - I_{w\alpha}(s) \frac{\partial^2}{\partial t^2} w'_0(l_0,t) + m_w(s)e_w(s)\ddot{w}_0(l_0,t) \\
 & - \{ \vartheta_w(s) + e_w^2(s)c_w(s) \} \frac{\partial}{\partial t} w'_0(l_0,t) + c_w(s)e_w(s)\dot{w}_0(l_0,t) \\
 & - \left[\sum_{k=1}^p I_k \{ \frac{\partial^2}{\partial t^2} w'_0(l_0,t) + \ddot{\theta}(s,t) \} - \right. \\
 & \left. \sum_{k=1}^p M_k \{ e_w(s) \ddot{w}_0(l_0,t) + \ddot{w}(s,t) \} \right] \delta(s-s_k)
 \end{aligned}
 \tag{2.56}$$

The forces on the left and right wing can simply be written by placing subscript L and i=2 for left attachment; R and i=3 for right attachment in eqs.(2.55) and (2.56).

It is assumed that the track beam deforms in the vertical

direction and amount of torsion on the track because of eccentricity of the wheels is small. The equation of motion for the transverse oscillation of beam is same as eq. (2.32) with impressed force given by

$$f_p(x,t) = - \left[C_{u11} \{ \dot{z}_{11} - \dot{h}_{11}(x) - \dot{y}(x,t) \} + K_{u11} \{ z_{11} - h_{11}(x) - y(x,t) \} \right] \delta(x-x_1) - \sum_{i=2}^3 \left[C_{u2i} \{ \dot{z}_{2i} - \dot{h}_{2i}(x) - \dot{y}(x,t) \} + K_{u2i} \{ z_{2i} - h_{2i}(x) - y(x,t) \} \right] \delta(x-x_i) \quad (2.57)$$

(b) Bending and torsionally flexible fuselage:-

In this model, the vehicle body is assumed to have elastic bending and torsional deformation induced by track roughness input. Total deflection of the vehicle body $w_0(r,t)$ at any transverse location from its longitudinal axis is given by

$$w_0(r,t) = w_b(r,t) + g_b(r) \theta_b(r,t) \quad (2.58)$$

where $\theta_b(r,t)$ is the torsional deformation of the vehicle body measured positive counterclockwise from untwisted configuration.

The transverse displacement in bending can be represented by eq.(2.43) where the expression for the impressed force f_b has to be modified for the interactions of elastic torsional modes and thus w_0 from eq.(2.58) needs to be substituted in the expression for f_b .

The torsional deformation of the vehicle body is governed by the differential equation

CENTRAL LIBRARY
I. I. T., KANPUR

Ms. A 125696

$$\frac{\partial}{\partial r} \left\{ G_b J_b(r) \frac{\partial \theta_b}{\partial r} \right\} - I_{br}(r) \frac{\partial^2 \theta_b}{\partial t^2} - \vartheta_b(r) \frac{\partial \theta_b}{\partial t} = -\Gamma_b(r, t) \quad (2.59)$$

where $G_b J_b$, I_{br} and ϑ_b are torsional stiffness, mass moment of inertia and rotational viscous damping per unit length of the beam. The applied torque Γ_b per unit length is given by,

$$\Gamma_b(r, t) = \sum_{i=2}^3 \left[C_{s2i} \left\{ \dot{w}_0(r, t) - \dot{z}_{2i} \right\} + K_{s2i} \left\{ w_0(r, t) - z_{2i} \right\} \right] e_i(r)$$

$$\delta(r-l_2) + \left[\left\{ E_{wL} I_{wL}(s_L) \frac{\partial^2 w_L}{\partial s_L^2} \right\}_{s_L=0} - \left\{ E_{wR} I_{wR}(s_R) \frac{\partial^2 w_R}{\partial s_R^2} \right\}_{s_R=0} \right]$$

$$\delta(r-l_2) \quad (2.60)$$

The equations of motion for the front and rear wheels can be obtained from eq.(2.53) and (2.54) after substituting w_0 from eq.(2.58).

The coupled bending -torsional oscillation of the flexible attachment are induced by transverse displacement and rolling of the fuselage including the elastic modes. The governing equations of motion can be represented by eq.(2.37) and (2.38). Induced dynamic loading will be modified on account of elastic bending and twist and thus w_0 from eq.(2.58) has to be used in forcing terms.

Transverse oscillation of the track beam is given by eq.(2.32) with forcing term as in eq.(2.57)

CHAPTER 3

SOLUTION TECHNIQUE FOR LINEAR MODELS

The system equations consist of a set of ordinary and partial differential equations. These can be solved with known initial and boundary conditions and input statistics. The linear models employed in describing the system yield coupled equations of motion. The present approach first reduces the partial differential equations of motion of continuous elements into a set of ordinary differential equations employing modal expansion technique. Subsequently, the complete set of system equations (including lumped mass equations of motion) are decoupled using complex modal analysis which are further processed to obtain response statistics.

3.1 MODAL ANALYSIS OF FLEXIBLE STRUCTURES

Flexible structures are characterised by parameters, such as mass, stiffness and damping that are functions of spatial variables. Continuous structures represent distributed parameter systems. The motion of a given structure is governed by partial differential equations to be satisfied over the domain of the structure and boundary conditions to be satisfied at the boundaries of the domain. The response of a flexible structure may be obtained by modal analysis which requires the solution of the eigenvalue problem. For distributed parameter systems, there exists an infinite set of eigenvalues and corresponding eigen

functions. The displacement may be assumed in the form of a series of space-dependent eigenfunctions multiplied by time dependent generalised coordinates. This helps in transforming the partial differential equations into a set of independent ordinary differential equations.

For most of the cases, the physical parameters of the flexible structures are not uniform in the domain of the structures. For an arbitrary variation of cross sectional properties, the closed form solution of the partial differential equations are not always feasible. The alternative is to use approximate solutions. This, however, may produce appreciable error in predicting natural frequency and displacement shape function specially in higher mode excitation. In the present study, a method has been outlined to obtain exact solution for the natural frequencies and mode shapes for a beam with arbitrary variation of cross section. This has been utilized for the modal analysis of the continuous elements in different vehicle models. The different steps involved in modal analysis are, solution of free vibration problem, development of orthogonality condition and discretization of the equations of motion of flexible structures in time dependent generalised coordinates.

3.2 NATURAL FREQUENCIES AND MODE SHAPES

3.2.1 Bending Vibration

In absence of external disturbance, the free vibration equation of non uniform beam can be written as

$$\frac{\partial^2}{\partial s^2} \left[EI(s) \frac{\partial^2 w}{\partial s^2} \right] + m(s) \frac{\partial^2 w}{\partial t^2} + c(s) \frac{\partial w}{\partial t} = 0 \quad (3.1)$$

Let the beam deflection be given by

$$w(s,t) = W(s) \exp (\zeta + j\omega)t \quad (3.2)$$

where $W(s)$ is the mode shape function, ω is the damped natural frequency and ζ is a factor related to the damping.

Substitution of eq.(3.2) in the eq.(3.1) yields

$$\frac{d^2}{ds^2} \left[EI(s) \frac{d^2 W}{ds^2} \right] + m(s) (\zeta + j\omega)^2 W(s) + c(s) (\zeta + j\omega) W(s) = 0 \quad (3.3)$$

Let the variation of moment of inertia, cross sectional area and distributed damping be expressed as general polynomials whose coefficients can be matched to represent any desired variations. It is assumed that distributed damping is proportional to the distribution of cross sectional area and hence to the mass. Thus we have

$$\begin{aligned} I(s) &= I(0) f_1(s) : f_1(s) = \sum_{i=0}^{\infty} p_i s^i \\ A(s) &= A(0) f_2(s) : f_2(s) = \sum_{i=0}^{\infty} q_i s^i \end{aligned} \quad (3.4)$$

$$c(s) = c(0) f_2(s)$$

where $I(0)$, $A(0)$, $c(0)$ are the moment of inertia, cross sectional area and damping at the reference section.

Substitution of eq.(3.4) in eq.(3.3), yields

$$f_1(s) \frac{d^4 W}{ds^4} + 2 \frac{df_1}{ds} \frac{d^3 W}{ds^3} + \frac{d^2 f_1}{ds^2} \frac{d^2 W}{ds^2} - \lambda^4 f_2(s) W(s) = 0 \quad (3.5)$$

$$\text{where } \lambda^4 = \frac{\rho A(0)}{EI(0)} \left[(\omega^2 - \zeta^2 - D\zeta) - j\omega(2\zeta + D) \right] \quad (3.6)$$

$$\text{with } D = c(0) / \rho A(0)$$

Introducing a new independent variable $z = \lambda s$ in eq.(3.5) transforms it to

$$\bar{f}_1(z) \frac{d^4 W}{dz^4} + 2 \frac{d\bar{f}_1}{dz} \frac{d^3 W}{dz^3} + \frac{d^2 \bar{f}_1}{dz^2} \frac{d^2 W}{dz^2} - \bar{f}_2(z) W = 0 \quad (3.7)$$

$$\text{where } \bar{f}_1(z) = \sum_{k=0}^{\infty} \bar{p}_k z^k ; \quad \bar{f}_2(z) = \sum_{k=0}^{\infty} \bar{q}_k z^k \quad (3.8)$$

$$\text{with } \bar{p}_k = p_k / \lambda^k \quad \text{and} \quad \bar{q}_k = q_k / \lambda^k \quad (3.9)$$

Let a series solution of the equation (3.7) be of the form

$$W(z) = \sum_{i=0}^{\infty} \bar{c}_i z^i \quad (3.10)$$

Using W and its derivatives from eq.(3.10) along with eq.(3.8) in eq.(3.7) and following the product rule of two series [84], one has

$$\sum_{n=0}^{\infty} (P_n + Q_n + R_n - S_n) z^n = 0 \quad (3.11)$$

where

$$P_n = \sum_{k=0}^n (n-k+1) (n-k+2) (n-k+3) (n-k+4) \bar{p}_k \bar{c}_{n-k+4} \quad (3.12)$$

$$Q_n = \sum_{k=0}^n 2(k+1) (n-k+1) (n-k+2) (n-k+3) \bar{p}_{k+1} \bar{c}_{n-k+3} \quad (3.13)$$

$$R_n = \sum_{k=0}^n (k+1) (k+2) (n-k+1) (n-k+2) \bar{p}_{k+2} \bar{c}_{n-k+2} \quad (3.14)$$

$$S_n = \sum_{k=0}^n \bar{q}_k \bar{c}_{n-k} \quad (3.15)$$

Since eq.(3.11) must be satisfied for every value of z , it implies that coefficient of each power of z must vanish. Thus we have

$$\begin{aligned} \bar{c}_{n+4} = & \frac{1}{(n+1) (n+2) (n+3) (n+4) \bar{p}_0} \left[\sum_{k=0}^n \bar{q}_k \bar{c}_{n-k} \right. \\ & - \sum_{k=1}^n (n-k+1) (n-k+2) (n-k+3) (n-k+4) \bar{p}_k \bar{c}_{n-k+4} \\ & - \sum_{k=0}^n 2(k+1) (n-k+1) (n-k+2) (n-k+3) \bar{p}_{k+1} \bar{c}_{n-k+3} \\ & \left. - \sum_{k=0}^n (k+1) (k+2) (n-k+1) (n-k+2) \bar{p}_{k+2} \bar{c}_{n-k+2} \right] \quad (3.16) \\ & (n = 0, 1, 2, \dots) \end{aligned}$$

Equation (3.16) above gives a recurrence relationship which can be used to determine the unknown coefficients of the series W except the first four coefficients \bar{c}_0 , \bar{c}_1 , \bar{c}_2 and \bar{c}_3 . These have to be determined with the help of the beam boundary conditions.

After expanding eq.(3.16), it can be shown that all other coefficients \bar{c}_i ($i = 4, 5, \dots$) are linearly dependent on the first four coefficients $\bar{c}_0, \bar{c}_1, \bar{c}_2, \bar{c}_3$. Thus one can write

$$\bar{c}_i = \sum_{k=0}^3 L_{ik} \bar{c}_k \quad (3.17)$$

where $L_{ik} = f_i(p_r, q_r, \lambda)$, $i=4, 5, \dots$; $r=1, 2, \dots$

Expressing all coefficients of the series in terms of first four coefficients, it is now possible to have the solution in the form

$$W(s) = \bar{c}_0 + \bar{c}_1 \lambda s + \bar{c}_2 \lambda^2 s^2 + \bar{c}_3 \lambda^3 s^3 + \sum_{i=4}^{\infty} \sum_{k=0}^3 L_{ik} \bar{c}_k \lambda^i s^i \quad (3.18)$$

The above equation may be re expressed,

$$W(s) = \sum_{i=0}^3 g_i(p_k, q_k, \lambda, s) \quad (3.19)$$

The application of appropriate boundary conditions of the beam in eq.(3.19) results in the homogeneous equation

$$\mathbf{B} \mathbf{c} = \mathbf{0} \quad (3.20)$$

where the elements b_{ik} of the matrix \mathbf{B} contain W and its derivatives evaluated at beam boundaries. The element \bar{c}_i of vector \mathbf{c} contains unknown coefficients $\bar{c}_0, \bar{c}_1, \bar{c}_2, \bar{c}_3$. For non trivial solution of eq.(3.20), the determinant of the matrix \mathbf{B} needs to be equated to zero. The roots of the characteristic determinant gives multiple values of λ which upon substitution in eq.(3.20), yields the vector \mathbf{c} , which can be utilized for evaluation of the

mode shape function W . The damped natural frequencies are obtained from eq.(3.6)

3.2.2 Coupled Bending-Torsion Vibration

The method developed for pure bending vibration is being now extended for a variable section beam in coupled bending-torsion mode.

Assuming free undamped harmonic vibration in the normal modes one has

$$w(s,t) = W(s) \exp(j\omega t) \quad (3.21)$$

$$\theta(s,t) = \phi(s) \exp(j\omega t)$$

where $W(s)$ and $\phi(s)$ are mode shape functions for the bending and torsional displacements and ω is the undamped natural frequency of the beam in its natural mode.

Substitution of eqs.(3.21) in coupled differential equations of motion for the beam in free vibration, yields

$$\frac{d^2}{ds^2} \left\{ EI(s) \frac{d^2 W}{ds^2} \right\} - \omega^2 \left\{ m(s)W(s) - e(s)m(s)\phi(s) \right\} = 0 \quad (3.22)$$

$$\frac{d}{ds} \left\{ GJ(s) \frac{d\phi}{ds} \right\} + \omega^2 \left\{ I_\alpha(s)\phi(s) - e(s)m(s)W(s) \right\} = 0 \quad (3.23)$$

As in eq.(3.4), variation of the sectional properties may be expressed as polynomial functions whose coefficients can be selected to match a given variation. Let

$$\begin{aligned}
I(s) &= I(0) \quad f_1(s) = I(0) \sum_{i=0}^{\infty} p_i s^i \\
m(s) &= \rho A(0) \quad f_2(s) = \rho A(0) \sum_{i=0}^{\infty} q_i s^i \\
J(s) &= J(0) \quad f_3(s) = J(0) \sum_{i=0}^{\infty} r_i s^i \\
I_{\alpha}(s) &= I_{\alpha}(0) \quad f_4(s) = I_{\alpha}(0) \sum_{i=0}^{\infty} u_i s^i \\
e(s) &= e(0) \quad f_5(s) = e(0) \sum_{i=0}^{\infty} g_i s^i
\end{aligned} \tag{3.24}$$

Substitution of equations (3.24) in eqs.(3.22) and (3.23) yields

$$\frac{d^2}{ds^2} \left\{ f_1(s) \frac{d^2 W}{ds^2} \right\} - \lambda^4 \left\{ f_2(s) W(s) - e(0) f_2(s) f_5(s) \phi(s) \right\} = 0 \tag{3.25}$$

$$\frac{d}{ds} \left\{ f_3(s) \frac{d\phi}{ds} \right\} + \lambda^4 \beta \left\{ k_{\alpha 0}^2 f_4(s) \phi(s) - e(0) f_2(s) W(s) f_5(s) \right\} = 0 \tag{3.26}$$

$$\text{where } \lambda^4 = \frac{\omega^2 \rho A(0)}{EI(0)} ; \quad \beta = \frac{EI(0)}{GJ(0)} ; \quad k_{\alpha 0}^2 = \frac{I_{\alpha}(0)}{\rho A(0)} \tag{3.27}$$

Again transforming from s to z coordinate, where $z = \lambda s$, eqs.(3.25) and (3.26) transform to

$$\begin{aligned}
\bar{f}_1(z) \frac{d^4 \bar{W}}{dz^4} + 2 \frac{d\bar{f}_1}{dz} \frac{d^3 \bar{W}}{dz^3} + \frac{d^2 \bar{f}_1}{dz^2} \frac{d^2 \bar{W}}{dz^2} - \left\{ \bar{W}(z) \bar{f}_2(z) - \right. \\
\left. e(0) \bar{f}_2(z) \bar{f}_5(z) \bar{\phi}(z) \right\} = 0
\end{aligned} \tag{3.28}$$

$$\bar{f}_3(z) \frac{d^2 \bar{\phi}}{dz^2} + \frac{d\bar{f}_3}{dz} \frac{d\bar{\phi}}{dz} + \lambda^2 \beta \left\{ K_{\alpha 0}^2 \bar{f}_4(z) \bar{\phi}(z) - e(0) \bar{f}_2(z) \bar{f}_5(z) \bar{W}(z) \right\} = 0 \quad (3.29)$$

where

$$\bar{W}(z) = W(\lambda s) \text{ and } \bar{\phi}(z) = \phi(\lambda s)$$

and

$$\begin{aligned} \bar{f}_1(z) &= \sum_{i=0}^{\infty} \bar{p}_i z^i, \quad \bar{p}_i = p_i / \lambda^i; \quad \bar{f}_2(z) = \sum_{i=0}^{\infty} \bar{q}_i z^i, \quad \bar{q}_i = q_i / \lambda^i \\ \bar{f}_3(z) &= \sum_{i=0}^{\infty} \bar{r}_i z^i, \quad \bar{r}_i = r_i / \lambda^i; \quad \bar{f}_4(z) = \sum_{i=0}^{\infty} \bar{u}_i z^i, \quad \bar{u}_i = u_i / \lambda^i \\ \bar{f}_5(z) &= \sum_{i=0}^{\infty} \bar{g}_i z^i; \quad \bar{g}_i = g_i / \lambda^i \end{aligned} \quad (3.30)$$

Assume the shape functions in the polynomial form

$$\bar{W}(z) = \sum_{i=0}^{\infty} \bar{b}_i z^i; \quad \bar{\Phi}(z) = \sum_{i=0}^{\infty} \bar{c}_i z^i \quad (3.31)$$

Substituting \bar{W} , $\bar{\phi}$ and their derivatives along with eqs. (3.30) in eqs. (3.28) and (3.29) and following the series product rules [84], one has

$$\begin{aligned} \sum_{n=0}^{\infty} \left\{ \sum_{k=0}^n \bar{p}_k (n-k+1) (n-k+2) (n-k+3) (n-k+4) \bar{b}_{n-k+4} + 2 \sum_{k=0}^n \bar{p}_{k+1} (k+1) \right. \\ \left. (n-k+1) (n-k+2) (n-k+3) \bar{b}_{n-k+3} + \sum_{k=0}^n \bar{p}_{k+2} (k+1) (k+2) (n-k+1) \right. \\ \left. (n-k+2) \bar{b}_{n-k+2} - \sum_{k=0}^n \bar{q}_k \bar{b}_{n-k} + e(0) \sum_{k=0}^n \sum_{l=0}^k \bar{q}_l \bar{g}_{k-l} \bar{c}_{n-k} \right\} z^n = 0 \end{aligned} \quad (3.32)$$

$$\sum_{n=0}^{\infty} \left\{ \sum_{k=0}^n \bar{r}_k (n-k+1) (n-k+2) \bar{c}_{n-k+2} + \sum_{k=0}^n (k+1) \bar{r}_{k+1} (n-k+1) \bar{c}_{n-k+1} \right. \\ \left. + \lambda^2 \beta k_{\alpha 0}^2 \sum_{k=0}^n \bar{u}_k \bar{c}_{n-k} - \lambda^2 \beta e(0) \sum_{k=0}^n \sum_{l=0}^k \bar{q}_l \bar{g}_{k-l} \bar{b}_{n-k} \right\} z^n = 0 \quad (3.33)$$

Since eqs.(3.32) and (3.33) must be satisfied for every value of z , it implies that coefficients of each power of z must vanish. Thus one has

$$\bar{b}_{n+4} = \frac{n!}{(n+4)! \bar{p}_0} \left[\sum_{k=0}^n \bar{q}_k \bar{b}_{n-k} - e(0) \sum_{k=0}^n \sum_{l=0}^k \bar{q}_l \bar{g}_{k-l} \bar{c}_{n-k} \right. \\ - \sum_{k=1}^n \bar{p}_k (n-k+1) (n-k+2) (n-k+3) (n-k+4) \bar{b}_{n-k+4} \\ - 2 \sum_{k=0}^n \bar{p}_{k+1} (k+1) (n-k+1) (n-k+2) (n-k+3) \bar{b}_{n-k+3} \\ \left. - \sum_{k=0}^n \bar{p}_{k+2} (k+1) (k+2) (n-k+1) (n-k+2) \bar{b}_{n-k+2} \right] \quad (3.34)$$

$$\bar{c}_{n+2} = \frac{n!}{(n+2)! \bar{r}_0} \left[\lambda^2 \beta e(0) \sum_{k=0}^n \sum_{l=0}^k \bar{q}_l \bar{g}_{k-l} \bar{b}_{n-k} \right. \\ - k_{\alpha 0}^2 \lambda^2 \beta \sum_{k=0}^n \bar{u}_k \bar{c}_{n-k} - \sum_{k=1}^n \bar{r}_k (n-k+1) (n-k+2) \bar{c}_{n-k+2} \\ \left. - \sum_{k=0}^n (k+1) \bar{r}_{k+1} (n-k+1) \bar{c}_{n-k+1} \right] \quad (3.35)$$

$$(n = 0, 1, 2, \dots)$$

Equations (3.34) and (3.35) give recurrence relationships for the coefficients \bar{b}_i and \bar{c}_i ($i=0,1,2,\dots$). After expanding these two, it can be shown that coefficients \bar{b}_i ($i=4,5,\dots$) can be expressed in terms of the four basic coefficients $\bar{b}_0, \bar{b}_1, \bar{b}_2$ and \bar{b}_3 of the series \bar{W} and two basic coefficients \bar{c}_0, \bar{c}_1 of the series $\bar{\phi}$. Similarly, \bar{c}_i ($i=2,3,\dots$) can be expressed in terms of $\bar{b}_0, \bar{b}_1, \bar{b}_2, \bar{b}_3, \bar{c}_0$ and \bar{c}_1 . Thus one can write

$$\begin{aligned}\bar{b}_i &= \sum_{k=0}^3 L_{ik} \bar{b}_k + \sum_{k=0}^1 M_{ik} \bar{c}_k \quad ; i=4,5,\dots \\ \bar{c}_i &= \sum_{k=0}^3 L'_{ik} \bar{b}_k + \sum_{k=0}^1 M'_{ik} \bar{c}_k \quad ; i=2,3,\dots\end{aligned}\tag{3.36}$$

The terms L_{ik}, M_{ik} and L'_{ik}, M'_{ik} are to be obtained from eqs.(3.34) and (3.35) in terms of known parameters $p_k, q_k, r_k, u_k, g_k, k_{\alpha 0}, \beta, e_w(0)$ and the unknown frequency parameter λ . From expressions (3.34) and (3.35), it can be seen when $e(s) = 0$, the coefficients \bar{b}_i and \bar{c}_i are independent of each other. This signifies uncoupling of the equations of motions.

Solution for the free vibration in coupled bending torsion can now be expressed as

$$\begin{aligned}W(s) &= \bar{b}_0 + \bar{b}_1(\lambda s) + \bar{b}_2(\lambda s)^2 + \bar{b}_3(\lambda s)^3 + \sum_{i=4}^{\infty} \left(\sum_{k=0}^3 L_{ik} \bar{b}_k + \right. \\ &\quad \left. \sum_{k=0}^1 M_{ik} \bar{c}_k \right) (\lambda s)^i\end{aligned}\tag{3.37}$$

$$\phi(s) = \bar{c}_0 + \bar{c}_1(\lambda s) + \sum_{i=2}^{\infty} \left(\sum_{k=0}^3 L'_{ik} \bar{b}_k + \sum_{k=0}^1 M'_{ik} \bar{c}_k \right) (\lambda s)^i \quad (3.38)$$

The six independent constants of integration can be found using six boundary conditions - four on W and two on ϕ . Use of the boundary conditions yields homogeneous equations of the form

$$B u = 0 \quad (3.39)$$

where the elements of the characteristic matrix B contain W , ϕ and their derivatives evaluated at beam boundaries. The vector u contains the unknown constants of integration \bar{b}_i ($i=0,1,2,3$) and \bar{c}_i ($i=0,1$).

As mentioned in case of bending vibration, the nontrivial solutions of the eq.(3.39) yields eigenvalues and eigenvectors that can be utilised to obtain natural frequencies and mode shapes from eqs.(3.27), (3.37) and (3.38)

3.3 ORTHOGONALITY OF THE MODES

Given a set of eigenfunctions, the orthogonality of the normal modes can be proved. Let us consider the more general case as in the coupled bending - torsion vibration.

Assuming the solutions of the eigen value problem in two distinct modes i and k as $W_i(s)$; $\phi_i(s)$ (corresponding to natural frequency ω_i) and $W_k(s)$; $\phi_k(s)$ (corresponding to natural frequency ω_k) one has from eqs.(3.22) and (3.23) for the i th mode

$$\frac{d^2}{ds^2} \left[EI(s) \frac{d^2 W_i}{ds^2} \right] = \omega_i^2 \left[m(s) W_i(s) - e(s) m(s) \phi_i(s) \right] \quad (3.40)$$

$$\frac{d}{ds} \left[GJ(s) \frac{d\phi_i}{ds} \right] = \omega_i^2 \left[e(s)m(s)W_i(s) - I_\alpha(s)\phi_i(s) \right] \quad (3.41)$$

Multiplying eq.(3.40) by W_k and eq.(3.41) by ϕ_k and integrating over the beam length, for any combination of clamped, hinged and free ends yields

$$\int_0^L EI(s) \frac{d^2 W_i}{ds^2} \frac{d^2 W_k}{ds^2} ds = \omega_i^2 \int_0^L \left\{ m(s)W_i(s)W_k(s) - e(s)m(s)\phi_i(s)W_k(s) \right\} ds \quad (3.42)$$

and

$$\int_0^L GJ(s) \frac{d\phi_i}{ds} \frac{d\phi_k}{ds} ds = \omega_i^2 \int_0^L \left\{ I_\alpha(s)\phi_i(s)\phi_k(s) - m(s)e(s)W_i(s)\phi_k(s) \right\} ds \quad (3.43)$$

Similarly for the k th mode of vibration, replacing i by k in eqs.(3.40) and (3.41), multiplying eq.(3.40) by W_i and eq.(3.41) by ϕ_i and performing integrations over the length of the beam, one has

$$\int_0^L EI(s) \frac{d^2 W_i}{ds^2} \frac{d^2 W_k}{ds^2} ds = \omega_k^2 \int_0^L \left\{ m(s)W_k(s)W_i(s) - e(s)m(s)\phi_k(s)W_i(s) \right\} ds \quad (3.44)$$

and

$$\int_0^L GJ(s) \frac{d\phi_i}{ds} \frac{d\phi_k}{ds} ds = \omega_k^2 \int_0^L \left\{ I_\alpha(s) \phi_k(s) \phi_i(s) - m(s) e(s) W_k(s) \phi_i(s) \right\} ds \quad (3.45)$$

Subtracting eq.(3.44) from eq.(3.42) and eq.(3.45) from eq.(3.43), yield

$$\begin{aligned} (\omega_i^2 - \omega_k^2) \int_0^L m(s) W_k(s) W_i(s) ds - \omega_i^2 \int_0^L e(s) m(s) \phi_i(s) W_k(s) ds \\ + \omega_k^2 \int_0^L e(s) m(s) \phi_k(s) W_i(s) ds = 0 \end{aligned} \quad (3.46)$$

and

$$\begin{aligned} (\omega_i^2 - \omega_k^2) \int_0^L I_\alpha(s) \phi_k(s) \phi_i(s) ds - \omega_i^2 \int_0^L e(s) m(s) W_i(s) \phi_k(s) ds \\ + \omega_k^2 \int_0^L e(s) m(s) W_k(s) \phi_i(s) ds = 0 \end{aligned} \quad (3.47)$$

Combining eqs.(3.46) and (3.47), yields

$$\begin{aligned} (\omega_i^2 - \omega_k^2) \int_0^L \left\{ m(s) W_k(s) W_i(s) + I_\alpha(s) \phi_i(s) \phi_k(s) \right. \\ \left. - e(s) m(s) \left(\phi_i(s) W_k(s) + \phi_k(s) W_i(s) \right) \right\} ds = 0 \end{aligned} \quad (3.48)$$

For $\omega_k \neq \omega_i$, it follows

$$\int_0^L \left\{ m(s) W_k(s) W_i(s) + I_\alpha(s) \phi_i(s) \phi_k(s) - e(s) m(s) \left(\phi_i(s) W_k(s) + \phi_k(s) W_i(s) \right) \right\} ds = 0 \quad (3.49)$$

Equation (3.49) provides a combined orthogonality condition of normal modes in coupled bending - torsion vibration. Orthogonality conditions for independent bending and torsional modes can be obtained from eq.(3.49) as a special case of coupled modes for which $e(s)=0$.

Thus for only bending of beam with $\phi(s)=0$, the orthogonality conditions may be stated as

$$\int_0^L m(s) W_i(s) W_k(s) ds = 0 \quad \text{if } i \neq k \quad (3.50)$$

and for only torsion with $W(s)=0$, the orthogonality condition becomes

$$\int_0^L I_\alpha(s) \phi_i(s) \phi_k(s) ds = 0 \quad \text{for } i \neq k \quad (3.51)$$

The relations given by eqs.(3.50) and (3.51) agree with the results derived for independent bending and torsional vibrations in ref. [86].

3.4 DISCRETIZATION PROCEDURE OF EQUATION OF MOTION OF CONTINUOUS ELEMENT

3.4.1 Bending Vibration

Assuming transverse displacement of the beam as

$$w(s,t) = \sum_{i=1}^{\infty} W_i(s) \eta_i(t) \quad (3.52)$$

where $W_i(s)$ and $\eta_i(t)$ are the mode shape function and generalised coordinate associated with the i th normal mode. Substituting this in eq.(2.26) for general forced vibration equation of beam in bending and multiplying both side of the equation by W_k one has

$$\sum_{i=1}^{\infty} \left[\frac{d^2}{ds^2} \left\{ EI(s) \frac{d^2 W_i}{ds^2} \right\} W_k(s) \eta_i(t) + m(s) W_i(s) W_k(s) \ddot{\eta}_i(t) + c(s) W_i(s) W_k(s) \dot{\eta}_i(t) \right] = f(s,t) W_k(s) \quad (3.53)$$

Assuming damping proportional to the mass distribution, one has from eq.(3.3)

$$\frac{d^2}{ds^2} \left\{ EI(s) \frac{d^2 W_i}{ds^2} \right\} = \left\{ (\omega_i^2 - \zeta_i^2 - D\zeta_i) - j\omega_i(2\zeta_i + D) \right\} m(s) W_i(s) \quad (3.54)$$

Introducing eq.(3.54) in eq.(3.53), integrating in the beam domain and invoking the orthogonality property of the normal modes from eq.(3.50), one has

$$\ddot{\eta}_i(t) + D\dot{\eta}_i(t) + \left\{ (\omega_i^2 - \zeta_i^2 - D\zeta_i) - j\omega_i(2\zeta_i + D) \right\} \eta_i(t) = Q_i(t) \quad (3.55)$$

$i=1, 2, \dots$

where $Q_i(t)$ is the generalised force given by

$$Q_i(t) = (1/M_{gi}) \int_0^L f(s,t) W_i(s) ds \quad (3.56)$$

M_{gi} is the generalised mass associated with the i th normal mode and is given by

$$M_{gi} = \int_0^L m(s) W_i^2(s) ds \quad (3.57)$$

Here the damping term is decoupled as damping is assumed to be proportional to the mass. Considering the case of general damping and using undamped modes of free vibration, the discretized equations have coupled damping terms. The discretized equations for this case becomes

$$\ddot{\eta}_i(t) + \sum_{k=1}^{\infty} D_{ik} \dot{\eta}_k(t) + \omega_i^2 \eta_i(t) = Q_i(t) \quad (3.58)$$

$i=1, 2, \dots$

$$\text{where } D_{ik} = (1/M_{gi}) \int_0^L c(s) W_i(s) W_k(s) ds \quad (3.59)$$

3.4.2 Coupled-Bending Torsion Vibrations

Let the transverse bending deformation and twist of the beam be expressed as

$$\begin{aligned}
w(s,t) &= \sum_{i=1}^{\infty} W_i(s) \eta_i(t) \\
\theta(s,t) &= \sum_{i=1}^{\infty} \phi_i(s) \eta_i(t)
\end{aligned} \tag{3.60}$$

Substituting eqs.(3.60) in eq.(2.37) for the general forced vibration equation of coupled bending -torsion of the beam , multiplying both sides by W_k and integrating with respect to s from 0 to L

$$\begin{aligned}
&\sum_{i=1}^{\infty} \int_0^L \left[\frac{d^2}{ds^2} \left\{ EI(s) \frac{d^2 W_i}{ds^2} \right\} W_k(s) \eta_i + m(s) W_i(s) W_k(s) \ddot{\eta}_i(t) - \right. \\
&- m(s) e(s) \phi_i(s) W_k(s) \ddot{\eta}_i(t) + c(s) W_i(s) W_k(s) \dot{\eta}_i(t) \\
&\left. - e(s) c(s) \phi_i(s) W_k(s) \dot{\eta}_i(t) \right] ds = \int_0^L f(s,t) W_k(s) ds
\end{aligned} \tag{3.61}$$

Again substituting eqs.(3.60) in eq.(2.38), multiplying both side by ϕ_k and integrating in beam domain

$$\begin{aligned}
&\sum_{i=1}^{\infty} \left[\int_0^L \frac{d}{ds} \left\{ GJ(s) \frac{d\phi_i}{ds} \right\} \phi_k(s) \eta_i(t) - I_\alpha(s) \phi_i(s) \phi_k(s) \ddot{\eta}_i(t) + \right. \\
&m(s) e(s) W_i(s) \phi_k(s) \ddot{\eta}_i(t) - \left\{ \vartheta(s) + e^2(s) c(s) \right\} \phi_i(s) \phi_k(s) \dot{\eta}_i(t) \\
&\left. + e(s) c(s) W_i(s) \phi_k(s) \dot{\eta}_i(t) \right] ds
\end{aligned}$$

$$= \int_0^L \left\{ f(s,t) e(s) \phi_k(s) - \Gamma(s,t) \phi_k(s) \right\} ds \quad (3.62)$$

Using eqs (3.22) and (3.23) in eqs.(3.61) and (3.62), one has

$$\begin{aligned} \sum_{i=1}^{\infty} \int_0^L \left[\omega_i^2 \left\{ m(s) W_i(s) - e(s) m(s) \phi_i(s) \right\} W_k(s) \eta_i(t) + m(s) W_i(s) W_k(s) \ddot{\eta}_i \right. \\ \left. - m(s) e(s) \phi_i(s) W_k(s) \ddot{\eta}_i + c(s) W_i(s) W_k(s) \dot{\eta}_i - e(s) c(s) \phi_i(s) W_k(s) \dot{\eta}_i \right] ds \\ = \int_0^L f(s,t) W_k(s) ds \end{aligned} \quad (3.63)$$

$$\begin{aligned} \sum_{i=1}^{\infty} \int_0^L \left[\omega_i^2 \left\{ I_{\alpha}(s) \phi_i(s) - e(s) m(s) W_i(s) \right\} \phi_k(s) \eta_i(t) \right. \\ \left. + I_{\alpha}(s) \phi_i(s) \phi_k(s) \ddot{\eta}_i(t) - m(s) e(s) W_i(s) \phi_k(s) \ddot{\eta}_i(t) + \phi_i(s) \phi_k(s) \right. \\ \left. \left\{ \psi(s) + c(s) e^2(s) \right\} \dot{\eta}_i(t) - e(s) c(s) \phi_k(s) W_i(s) \dot{\eta}_i(t) \right] ds \\ = \int_0^L \left\{ \Gamma(s,t) \phi_k(s) - f(s,t) e(s) \phi_k(s) \right\} ds \end{aligned} \quad (3.64)$$

Combining eqs.(3.63) and (3.64) and invoking the orthogonality property of the coupled modes eq.(3.49), yields after simplification

$$\ddot{\eta}_i(t) + \sum_{k=1}^{\infty} D_{ik} \dot{\eta}_k(t) + \omega_i^2 \eta_i(t) = Q_i(t) \quad (3.65)$$

$i=1,2,\dots$

where the modal damping coefficients .D, generalised force Q

associated in i th mode are given by

$$D_{ik} = \frac{1}{M_{gi}} \int_0^L \left[c(s) W_i(s) W_k(s) + \left\{ \vartheta(s) + e^2(s) c(s) \right\} \phi_i(s) \phi_k(s) - e(s) c(s) \left\{ \phi_i(s) W_k(s) + W_i(s) \phi_k(s) \right\} \right] ds \quad (3.66)$$

$$Q_i(t) = \frac{1}{M_{gi}} \int_0^L \left[f(s, t) \left\{ W_i(s) - e(s) \phi_i(s) \right\} + \Gamma(s, t) \phi_i(s) \right] ds \quad (3.67)$$

where generalised mass M_{gi} is given as

$$M_{gi} = \int_0^L \left\{ m(s) W_i^2(s) + I_\alpha(s) \phi_i^2(s) - 2m(s) e(s) \phi_i(s) W_i(s) \right\} ds \quad (3.68)$$

3.5 DISCRETIZED EQUATIONS FOR CONTINUOUS ELEMENTS OF VEHICLE MODELS

Following the procedure discussed in the previous section, the discretized equations for the continuous elements in each model can be obtained.

3.5.1 Heave Model

In this model, the continuous elements tapered wings and track are represented by distributed parameter beam element.

Let η_{wi} represent the i th normal coordinate for the wing. The discretized equations for the left and right wing are (from eq.3.55)

$$\ddot{\eta}_{wi}^L(t) + D\dot{\eta}_{wi}^L(t) + \left\{ (\omega_{Li}^2 - \zeta_{Li}^2 - D\zeta_{Li}) - j\omega_{Li}(2\zeta_{Li} + D) \right\} \eta_{wi}^L(t) = Q_{wi}^L(t) \quad (3.69)$$

and

$$\ddot{\eta}_{wi}^R(t) + D\dot{\eta}_{wi}^R(t) + \left\{ (\omega_{Ri}^2 - \zeta_{Ri}^2 - D\zeta_{Ri}) - j\omega_{Ri}(2\zeta_{Ri} + D) \right\} \eta_{wi}^R(t) = Q_{wi}^R(t) \quad (3.70)$$

where ω_i is the damped natural frequency of the wing and Q_{wi} is the generalised force associated with the i th mode. The generalised force and generalised mass can be obtained for the wing beam from eqs.(3.56) and (3.57) with proper substitution of left and right wing quantities.

The track equation of motion (2.32) can be discretised in terms of the normal coordinates η_{pi} as

$$\ddot{\eta}_{pi}(t) + B\dot{\eta}_{pi}(t) + \left\{ (\omega_{pi}^2 - \xi_i^2 - B\xi_i) - j\omega_{pi}(2\xi_i + B) \right\} \eta_{pi}(t) = Q_{pi}(t) \quad (3.71)$$

where ω_p is the track damped natural frequency; ξ is a factor related to the foundation damping and the constant B is c_f/m_p . The displacement function is given by [86]

$$\psi_i(x) = Y_1 \sin \gamma_i x + Y_2 \cos \gamma_i x + Y_3 \sinh \gamma_i x + Y_4 \cosh \gamma_i x \quad (3.72)$$

in which Y_1 , Y_2 , Y_3 and Y_4 are constants of integration and the

parameter γ is expressed by

$$\gamma^4 = \frac{m_p}{E_p I_p} \left\{ (\omega_p^2 - \omega_f^2 - \xi^2 - B\xi) - j\omega_p(2\xi + B) \right\} \quad (3.73)$$

where $\omega_f^2 = k_f/m_p$

The eigen parameter γ and constants of integration Y_1, Y_2, Y_3 and Y_4 can be found with the appropriate end conditions of the track beam. The generalised parameters for the track beam can be obtained from eqs.(3.56) and (3.57) by using track-subgrade quantities.

3.5.2 Heave -Pitch Model

(a) Rigid Vehicle Body:-

In this model, the partial differential equations of motion representing the coupled bending torsional motion are discretized to their time dependent generalised coordinates. The equations for left and right wing, thus become (from eq.3.65)

$$\ddot{\eta}_{Li}(t) + \sum_{k=1}^{\infty} D_{ik}^L \dot{\eta}_{Lk}(t) + \omega_{Li}^2 \eta_{Li}(t) = Q_{wi}^L(t) \quad (3.74)$$

and

$$\ddot{\eta}_{Ri}(t) + \sum_{k=1}^{\infty} D_{ik}^R \dot{\eta}_{Rk}(t) + \omega_{Ri}^2 \eta_{Ri}(t) = Q_{wi}^R(t) \quad (3.75)$$

where the modal damping coefficients D , generalised force Q and generalised M_g for each wing can be evaluated using eqs.(3.66) - (3.68).

The track discretized equations would be same as in heave model

except generalised forces are to be evaluated with the expression for impressed force given for a two point input model in eq.(2.42)

(b) Flexible Fuselage in bending:-

The equation of motion for the i th normal coordinate of the flexible fuselage in bending can be written as

$$\ddot{\eta}_{bi}(t) + \sum_{k=1}^{\infty} D_{ik} \dot{\eta}_{bk}(t) + \omega_{bi}^2 \eta_{bi}(t) = Q_{bi}(t) \quad (3.76)$$

where η_{bi} represents normal coordinates in the i th mode.

Here ω_{bi} is the undamped natural frequency corresponding to the i th normal mode. D_{ik} is the modal damping coefficient and Q_{bi} is the generalised force. The damping term is allowed to remain coupled as no assumption has been made regarding the nature of damping.

It may be mentioned that vehicle body performs two rigid body motions in heave and pitch which correspond to zero natural frequencies. Other finite non zero frequencies are associated with elastic bending modes. The natural frequencies and mode shape functions for bending displacement have been found analytically for a variable section beam. The displacement shape can be obtained from eq.(3.18) with $(r+d_c)$ substituted for s for the vehicle domain $-d_c \leq r \leq (L_b - d_c)$ where L_b is the length of the fuselage and d_c denotes the aircraft c.g distance from the tail end.

Modal parameters for generalised force, mass and damping can be obtained from eqs.(3.56), (3.57) and (3.59) using fuselage

quantities.

The modal equations for the left and right wing remain same as rigid model. However, the generalised forces should be calculated with inclusion of fuselage flexural modes in the induced force and torque given in eqs.(2.47) and (2.48).

3.5.3 Heave-Pitch-Roll Model

(a) Flexible fuselage in bending with rigid roll:-

The fuselage of the aircraft undergoes rigid body heave, pitch and roll motions along with elastic bending. The partial differential equation of motion representing transverse bending will have discretized form same as eq.(3.76). The generalised forcing term has to be evaluated on account of the rigid body rolling which effect the vertical motions of the two rear wheels.

Similarly, the discretized equations of the left and right wing have the same form as in eqs.(3.74) and (3.75) except the generalised force calculation will be different for rolling of the airplane inducing different reactions in two main landing gears carried under the wings. The generalised forces are to be calculated using f and Γ in eqs.(2.55) and (2.56).

In track discretized equations, the generalised forcing term has to be evaluated for the dynamic load transfered on the track by three wheels in eq.(2.57)

(b) Flexible fuselage in bending and torsion:-

The discretized equations for the bending of fuselage body is given by eq.(3.76) with generalised force evaluated after

substituting the expression for vertical applied force to take torsional deformation into account. The equation for torsion is

$$\ddot{\eta}_{ti}(t) + \sum_{k=1}^{\infty} D'_{ik} \dot{\eta}_{tk}(t) + \omega_{ti}^2 \eta_{ti}(t) = Q_{ti}(t) \quad (3.77)$$

$i=1,2,\dots$

where the η_{ti} are the generalised coordinates, ω_{ti} torsional natural frequencies, D'_{ik} and Q_{ti} are modal damping coefficients in torsional modes of the vehicle body. The vehicle body performs rigid body heave - pitch - roll motion and thus first two modes in bending represent heave and pitch motion as mentioned earlier where as first mode in torsion represent rigid roll. Rigid body modes correspond to zero natural frequencies of the flexible modes. For the vehicle body modelled as variable section beam the torsional mode T_b can be found as

$$T_b(r) = T_0 + T_1 \lambda_t (r+d_c) + \sum_{i=2}^{\infty} \frac{1}{\sum_{k=0} M_{ik} T_k} \lambda_t^i (r+d_c)^i \quad (3.78)$$

for $-d_c \leq r \leq (L_b - d_c)$

where torsional frequency parameters λ_t defined as

$$\lambda_t^2 = \omega_t^2 I_{br}(0) / G_b J_b(0) \quad (3.79)$$

The integration constants T_0 and T_1 appearing in torsional mode shape function can be obtained with application of two boundary conditions for torsional motion in eq. (3.78). The generalised modal quantities for force, mass and damping may be obtained from eqs. (3.56), (3.57) and (3.59) by substituting

appropriate rotational quantities.

The discretized equations for the wing will remain same, except the generalised forces are to be re evaluated using the expression for f and Γ from eqs.(2.55) and (2.56) with w_0 substituted from eq.(2.58). The track modal equations in normal coordinates are same as that used in rigid heave-pitch-roll model.

3.6 DECOUPLING OF SYSTEM EQUATIONS

The system equations include the equations of motion for lumped mass elements and modal equations for flexible elements in the vehicle models. Theoretically, continuous elements have infinite number of normal modes. However, the higher modes do not contribute as much to the response as the lower modes. The number of significant modes can, therefore, be truncated to a finite size. Let there be n_b number of significant modes in transverse bending of vehicle body (including rigid body bounce and pitch motion), n_t number of twisting modes of the vehicle body (including rigid body rolling), n_r vertical degrees of freedom for unsprung masses, n_w and n_p elastic modes of the flexible wing and track. Then total degrees of freedom of the system would be $n = n_b + n_t + n_r + 2n_w + n_p$. The system equations then can be represented using matrices as

$$M \ddot{\mathbf{q}}(t) + C \dot{\mathbf{q}}(t) + K \mathbf{q}(t) = \mathbf{F}(t) \quad (3.80)$$

where $\mathbf{q}(t)$ is the response vector, $\mathbf{F}(t)$ is the generalised force vector ($n \times 1$) and M , C , and K are system mass, damping and

stiffness matrices (nxn) respectively.

Premultiplying both sides of the eq.(3.80) by M^{-1} and using an identity $\dot{\bar{q}}(t) - \dot{q}(t) = 0$, the eq.(3.80) can be cast into 2n form as

$$\dot{p}(t) + A p(t) = P(t) \quad (3.81)$$

$$\text{where } p(t) = \begin{Bmatrix} \dot{q}(t) \\ q(t) \end{Bmatrix} ; \quad P(t) = \begin{Bmatrix} M^{-1} F(t) \\ 0 \end{Bmatrix} \quad \text{and}$$

$$\text{and } A = \begin{bmatrix} -M^{-1}C & -M^{-1}K \\ -I & 0 \end{bmatrix} \quad (3.82)$$

I being an identity matrix and 0 a null vector/matrix.

Let α_i be the eigen values and u_i the eigen vectors for the matrix A. Consider a linear transformation of the response vectors

$$v(t) = U^{-1}p(t) \quad (3.83)$$

in which U is the modal matrix with eigen vectors u_i arranged as its columns. It is now possible to uncouple [87] the system equations (3.81) as

$$\dot{v}_i(t) + \alpha_i v_i(t) = R_i(t) ; \quad i=1,2,\dots,2n \quad (3.84)$$

where

$$R_i(t) = \sum_{r=1}^n \bar{u}_{ir} P_r(t) = \sum_{r=1}^n \bar{u}_{ir} \sum_{k=1}^n \bar{m}_{rk} F_k \quad (3.85)$$

here \bar{u}_{ir} are elements of the inverse of matrix U and \bar{m}_{rk} are the elements of the inverse of matrix M.

The general solution of eq.(3.84) may be written as

$$v_i(t) = X_{oi} \exp(-\alpha_i t) + \int_{-\infty}^{\infty} H_i(\omega, t) dS(R_i(\omega)) \quad (3.86)$$

where X_{oi} are the constants of integration to be determined from the initial condition, and $H_i(\omega, t)$ are the transient frequency response functions given by [87]

$$H_i(\omega, t) = \frac{1}{j\omega + \alpha_i} \left[\exp(j\omega t) - \exp\{-\alpha_i(t-t_0)\} \right] \quad (3.87)$$

It can be seen that as $t_0 \rightarrow -\infty$, for positive real part of α_i , H_i approaches a limiting value of $\frac{1}{j\omega + \alpha_i} \exp(j\omega t)$

The response in generalised coordinates now can be expressed by substituting eqs. (3.85) in eq.(3.86) and using eq.(3.82)

$$q_m(t) = \sum_{i=1}^{2n} X_{oi} u_{m_1 i} \exp(-\alpha_i t) + \sum_{i=1}^{2n} u_{m_1 i} \sum_{r=1}^n \bar{u}_{ir} \sum_{k=1}^n m_{rk} \int_{-\infty}^{\infty} H_i(\omega, t) dS(F_k(\omega)) \quad (3.88)$$

$m=1, 2, \dots, n; m_1 = m + n$

3.7 RESPONSE STATISTICS

3.7.1 Mean Response

Considering the expectation of eq.(3.88) the mean response

becomes

$$\begin{aligned}
\mu_{q_m}(t) &= E \left[q_m(t) \right] \\
\mu_{q_m}(t) &= \sum_{i=1}^{2n} X_{oi} u_{m1i} \exp(-\alpha_i t) \\
&+ \sum_{i=1}^{2n} u_{m1i} \sum_{r=1}^n \bar{u}_{ir} \sum_{k=1}^n m_{rk} \int_{-\infty}^{\infty} H_i(\omega, t) E \left[dS(F_k(\omega)) \right] \\
&\quad m=1, 2, \dots, n
\end{aligned} \tag{3.89}$$

$$\text{where} \quad E \left[dS(F_k(\omega)) \right] = \mu_{F_k}^*(\omega) \tag{3.90}$$

in which $\mu_{F_k}^*(\omega)$ is the Fourier transform of the mean generalised force process μ_F and defined by the integral

$$\mu_{F_k}^*(\omega) = \frac{1}{2\pi} \int_{-\infty}^{\infty} \mu_{F_k}(\tau) \exp(-j\omega\tau) d\tau \tag{3.91}$$

The mean generalised force depends on the track profile characteristics as well as aerodynamic force and moments. The k th element of the mean generalised forcing vector can be expressed as

$$\mu_{F_k}(t) = \sum_{p=1}^2 \sum_{s=1}^3 \left\{ A_{kps} h_{mps}(t) + B_{kps} \dot{h}_{mps}(t) \right\} + C_k V(t)^2 \tag{3.92}$$

in which $h_{mps}(t)$, $\dot{h}_{mps}(t)$ and $V(t)$ can be obtained from eqs.(2.20), (2.21) and (2.30). The coefficients A_k , B_k and C_k would be different for each model. Substituting for $H_i(\omega, t)$ and

using eqs. (3.90)- (3.92) in eq.(3.89) and performing the integration over ω , yields

$$\mu_{q_m}(t) = \sum_{i=1}^{2n} X_{oi} u_{m_1 i} \exp(-\alpha_i t) + \sum_{i=1}^{2n} u_{m_1 i} \sum_{r=1}^n \bar{u}_{ir} \sum_{k=1}^n m_{rk} I_{ik}(t) \quad m=1,2,\dots,n \quad (3.93)$$

where

$$I_{ik}(t) = \left[\sum_{p=1}^2 \sum_{s=1}^3 \left(A_{kps} \tau_{1ps}(t) + B_{kps} \tau_{2ps}(t) \right) \right] + C_k \tau_3(t) \quad (3.94)$$

The coefficients A_k , B_k and C_k and the components τ_1 , τ_2 and τ_3 of the integral I_{ik} for different models are given below

Heave Model

In this model, input from the track is at single point for which $p=s=1$. Hence these two subscripts are omitted in the expression.

Coefficients A_k are given as

$$A_k = \begin{cases} 0 & \text{for } k = 1, 3, 4, \dots, n_1 \\ K_{us} & \text{for } k = 2 \\ \frac{\psi_{k-n_1}(x_c)}{M_{k-n_1}^p} K_{us} & \text{for } k = n_1+1, n_1+2, \dots, n \end{cases} \quad (3.95)$$

where $n_1 = 2n_w + 2$

The expression for B_k is obtained from the expression of A_k by replacing K_{us} with C_{us} .

$$C_k = \begin{cases} 0, & \text{for } k = 1, 2, n_1+1, n_1+2, \dots, n ; \\ \frac{L_0}{M g_{k-2}^L} \int_0^{L_{wL}} w_{k-2}^L(s_L) \left(1 - (s_L / L_{wL})^2 \right)^{1/2} ds_L & \text{for } k = 3, 4, \dots, n_w+2 ; \\ \frac{L_0}{M g_{k-r}^R} \int_0^{L_{wR}} w_{k-(n_w+2)}^R(s_R) \left(1 - (s_R / L_{wR})^2 \right)^{1/2} ds_R, & \text{for } k = (n_w+3), (n_w+4), \dots, n_1; r=n_w+2, n_1=2n_w+2 \end{cases} \quad (3.96)$$

The components \mathcal{T}_1 , \mathcal{T}_2 and \mathcal{T}_3 are

$$\begin{aligned} \mathcal{T}_1(t) &= \int_0^t h_m(\tau) \exp(-\alpha_i(t-\tau)) d\tau \\ &= \left(h_0 + \sum_{i=1}^{\ell} h_i c_{i,0} \right) J_1 + \sum_{i=1}^{\ell} h_i \sum_{r=1}^{mi} c_{i,r} J_2 \end{aligned} \quad (3.97)$$

$$\begin{aligned} \mathcal{T}_2(t) &= \int_0^t \dot{h}_m(\tau) \exp(-\alpha_i(t-\tau)) d\tau \\ &= \sum_{i=1}^{\ell} h_i c_{i,1} J_1 + \sum_{i=1}^{\ell} h_i \sum_{r=1}^{k-1} c_{i,r+1}^{(r+1)} J_2 \end{aligned} \quad (3.98)$$

$$\mathcal{T}_3(t) = \int_0^t v(\tau)^2 \exp(-\alpha_i(t-\tau)) d\tau = c'_0 J_1 + \sum_{r=1}^{2(m-1)} c'_r J_2 \quad (3.99)$$

$$\text{with } J_1 = \frac{1}{\alpha_i} \left\{ 1 - \exp(-\alpha_i t) \right\}, \quad \text{and} \quad (3.100)$$

$$J_2 = \frac{t^r}{\alpha_i} + \sum_{k=1}^r \frac{(-1)^k r!}{(r-k)!} \frac{t^{r-k}}{\alpha_i^{k+1}} - (-1)^r \frac{r!}{\alpha_i^{r+1}} \exp(-\alpha_i t)$$

The infinite limits of the integrals \mathcal{T}_1 , \mathcal{T}_2 and \mathcal{T}_3 are considered finite as $\mu_{F_k}(\tau)$ is zero for $\tau < 0$ and available only up to $\tau \leq t$

Heave-Pitch-Model

In this model, there are two wheels. Each of them is located on the centre of front and rear axle. Both wheels follow the same profile along the centre line of the track although input to one wheel is time delayed version of the other. The expressions for the coefficients of the mean force and integrals are given separately for the models with rigid and flexible fuselage.

(a) Rigid Fuselage

The coefficients A_{kp} are

$$A_{kp} = \left\{ \begin{array}{ll} 0 \text{ for } k=1,2,5,\dots,n_1 \text{ and } p=1,2; \text{ } k=3 \text{ and } p=2; \\ \quad k=4 \text{ and } p=1 \\ K_{u1} \text{ for } k=3, p=1 \\ k_{u2} \text{ for } k=4, p=2 \\ \frac{\psi_{k-n_1}(x_1)}{M_{k-n_1}^p} K_{u1} \text{ for } k = n_1+1, \dots, n \text{ and } p = 1 \\ \frac{\psi_{k-n_1}(x_2)}{M_{k-n_1}^p} K_{u2} \text{ for } k=n_1+1, \dots, n \text{ and } p = 2 \end{array} \right. \quad (n_1 = 4 + 2n_w) \quad (3.101)$$

The coefficients B_{kp} are exactly similar to A_{kp} , except K_{u1} and K_{u2} are to be replaced by C_{u1} and C_{u2} respectively. The coefficient C_k is given by

$$C_k = \begin{cases} 0 & \text{for } k = 1, \dots, 4, n_1+1, \dots, n \\ (L_0 / M_{k-4}^{gL}) \left[\int_0^{L_{wL}} \left\{ W_{k-4}^L(s_L) - e_{wL}(s_L) \phi_{k-4}^L(s_L) \right\} \right. \\ \left. \left\{ 1 - s_L^2 / L_{wL}^2 \right\}^{1/2} ds_L \right] + (M_0 / M_{k-4}^{gL}) \int_0^{L_{wL}} c_h^2(s_L) \phi_{k-4}^L(s_L) ds_L \\ & \text{for } k = 5, 6, \dots, m_1 \quad (m_1 = 4 + n_w) \\ (L_0 / M_{k-m_1}^{gR}) \left[\int_0^{L_{wR}} \left\{ W_{k-m_1}^R(s_R) - e_{wR}(s_R) \phi_{k-m_1}^R(s_R) \right\} \right. \\ \left. \left\{ 1 - s_R^2 / L_{wR}^2 \right\}^{1/2} ds_R \right] + (M_0 / M_{k-m_1}^{gR}) \int_0^{L_{wR}} c_h^2(s_R) \phi_{k-m_1}^R(s_R) ds_R \\ & \text{for } k = m_1+1, \dots, n_1 \end{cases} \quad (3.102)$$

The integral components \mathcal{T}_{1p} , \mathcal{T}_{2p} and \mathcal{T}_3 are

$$\mathcal{T}_{1p}(t) = \left(h_0 + \sum_{i=1}^{\ell} h_i (c_{i,0})_p \right) J_1 + \sum_{i=1}^{\ell} h_i \sum_{r=1}^k (c_{i,r})_p J_2 \quad (3.103)$$

$$\mathcal{T}_{2p}(t) = \sum_{i=1}^{\ell} h_i (c_{i,1})_p J_1 + \sum_{i=1}^{\ell} h_i \sum_{r=1}^{k-1} (c_{i,r+1})_p (r+1) J_2 \quad (3.104)$$

\mathcal{T}_3 , J_1 and J_2 are given by eqs. (3.99) and (3.100)

(b) Flexible fuselage

The coefficients A_{kp} , B_{kp} and C_k are as

$$A_{kp} = \begin{cases} 0 & \text{for } k=1,2,\dots,n_b, n_b+3,\dots,n_b+2+2n_w \text{ and } p=1,2; \\ & k = n_b+1 \text{ and } p=2; k=n_b+2 \text{ and } p=1 \\ K_{up} & \text{for } k=n_b+1 \text{ and } p=1; k=n_b+2 \text{ and } p=2 \\ \psi_{k-n_1}(x_p) K_{up} / M_{k-n_1} & \text{for } k = n_1+1,\dots,n \text{ and } p=1,2 \\ & (n_1 = n_b + 2 + 2n_w) \end{cases} \quad (3.105)$$

The coefficients B_{kp} are exactly similar to A_{kp} except the stiffness term K is to be replaced by damping term C . The coefficients C_k are

$$C_k = \begin{cases} 0 & \text{for } k = 1, 2, \dots, n_b+2 ; n_1+1, \dots, n \\ (L_0 / M_{k-r}^{gL}) \left[\int_0^{L_{wL}} \left\{ w_{k-r}^L(s_L) - e_{wL}(s_L) \phi_{k-r}^L(s_L) \right\} \left\{ 1 - s_L^2 / L_w^2 \right\}^{1/2} ds_L \right. \\ & \quad \left. + (M_0 / M_{k-r}^{gL}) \int_0^{L_{wL}} c_h^2(s_L) \phi_{k-r}^L(s_L) ds_L \right] \\ & \text{for } k = n_b+3, \dots, (n_b+2+n_w) \text{ and } r = n_b+2 \\ (L_0 / M_{k-r}^{gR}) \left[\int_0^{L_{wR}} \left\{ w_{k-r}^R(s_R) - e_{wR}(s_R) \phi_{k-r}^R(s_R) \right\} \left\{ 1 - s_R^2 / L_w^2 \right\}^{1/2} ds_R \right. \\ & \quad \left. + (M_0 / M_{k-r}^{gR}) \int_0^{L_{wR}} c_h^2(s_R) \phi_{k-r}^R(s_R) ds_R \right] \\ & \text{for } k = (n_b+n_w+3), \dots, n_1 \text{ and } r = n_b + n_w+2 \end{cases} \quad (3.106)$$

The integral \mathcal{T}_1 , \mathcal{T}_2 and \mathcal{T}_3 are same as eqs (3.103), (3.104) and (3.99)

Heave-Pitch-Roll Model

In this model, each wheel follows different path along the track. Due to variation of longitudinal and transverse roughness, input to each wheel is different. Coefficients of mean forcing function and the integral for the mean response for two types of models are given below.

(a) Bending of fuselage with rigid body roll

$$A_{kps} = \begin{cases} 0 & \text{for } k=1,2,\dots,n_b+1,n_b+5,\dots,n_b+4+2n_w \text{ for all } p,s \\ K_{ups} & \text{for } k=n_b+2 \text{ and } p=1, s=1; k=n_b+3 \text{ and } p=2, s=2; \\ & k=n_b+4 \text{ and } p=2, s=3 \\ \psi_{k-j} (x_p) K_{ups} / M_{k-j} & \text{for } k = n_b+5+2n_w, \dots, n \text{ and either} \\ & p=s=1 \text{ or } p=2, s=2 \text{ or } p=2, s=3 \end{cases} \quad (j=n_b+4+2n_w) \quad (3.107)$$

The coefficients B_{kps} are exactly similar to A_{kps} except the stiffness term \tilde{K} is to be replaced by damping term C . The coefficients C_k are

$$\begin{aligned}
C_k = & \left\{ \begin{aligned}
& 0 \text{ for } k = 1, 2, \dots, n_b + 1, n_b + 5 + 2n_w, \dots, n \\
& (L_0 / M_{k-j}^{gL}) \left[\int_0^{L_{wL}} \left\{ W_{k-j}^L(s_L) - e_{wL}(s_L) \phi_{k-j}^L(s_L) \right\} \left\{ 1 - s_L^2 / L_{wL}^2 \right\}^{1/2} ds_L \right. \\
& \quad \left. + (M_0 / M_{k-j}^{gL}) \int_0^{L_{wL}} c_h^2(s_L) \phi_{k-j}^L(s_L) ds_L \right. \\
& \quad \text{for } k = n_b + 5, \dots, n_b + 4 + n_w; j = n_b + 4 \\
& (L_0 / M_{k-j}^{gR}) \left[\int_0^{L_{wR}} \left\{ W_{k-j}^R(s_R) - e_{wR}(s_R) \phi_{k-j}^R(s_R) \right\} \left\{ 1 - s_R^2 / L_w^2 \right\}^{1/2} ds_R \right. \\
& \quad \left. + (M_0 / M_{k-j}^{gR}) \int_0^{L_{wR}} c_h^2(s_R) \phi_{k-j}^R(s_R) ds_R \right. \\
& \quad \text{for } k = n_b + n_w + 5, \dots, n_b + 4 + 2n_w; j = n_b + 4 + n_w
\end{aligned} \right.
\end{aligned} \tag{3.108}$$

The components of integral I_{ik} for the mean response are given as

$$\mathcal{T}_{1ps} = \left[(h_0)_{ps} + \sum_{i=1}^{\ell} (h_i)_{ps} (c_{i,0})_{ps} \right] J_1 + \sum_{i=1}^{\ell} (h_i)_{ps} \sum_{r=1}^k (c_{i,r})_{ps} J_2 \tag{3.109}$$

$$\mathcal{T}_{2ps} = \sum_{i=1}^{\ell} (h_i)_{ps} (c_{i,1})_{ps} J_1 + \sum_{i=1}^{\ell} (h_i)_{ps} \sum_{r=1}^{k-1} (c_{i,r+1})_{ps} J_2$$

where \mathcal{T}_3 and J_1 and J_2 are same as other models.

(b) Bending and torsionally flexible fuselage

$$A_{kps} = \begin{cases} 0 & \text{for } k=1,2,\dots,n_b+n_t, n_b+n_t+4,\dots,n_b+n_t+3+2n_w \text{ for all } p,s \\ K_{ups} & \text{for } k=n_b+n_t+1 \text{ and } p=1, s=1; k=n_b+n_t+2 \text{ and } p=2, s=2; \\ & k=n_b+n_t+3 \text{ and } p=2, s=3 \\ \psi_{k-j}(x_p) K_{ups} / M_{k-j} & \text{for } k = n_b+n_t+4+2n_w, \dots, n \text{ and} \\ & \text{either } p=s=1 \text{ or } p=2, s=2 \text{ or } p=2, s=3 \\ & j=n_b+n_t+3+2n_w \end{cases} \quad (3.110)$$

The coefficients B_{kps} can be obtained from eqs.(3.110) simply by replacing the stiffness term K by damping term C . The coefficients C_k are

$$C_k = \begin{cases} 0 & \text{for } k = 1, 2, \dots, n_b+n_t+3, n_b+n_t+4+2n_w, \dots, n \\ (L_0 / M_{k-j}^{gL}) \left[\int_0^{L_{wL}} \left\{ w_{k-j}^L(s_L) - e_{wL}(s_L) \phi_{k-j}^L(s_L) \right\} \left\{ 1 - s_L^2 / L_w^2 \right\}^{1/2} ds_L \right. \\ \quad \left. + (M_0 / M_{k-j}^{gL}) \int_0^{L_{wL}} c_h^2(s_L) \phi_{k-j}^L(s_L) ds_L \right] \\ & \text{for } k = n_b+n_t+4, \dots, n_b+n_t+3+n_w; j=n_b+n_t+3 \\ (L_0 / M_{k-j}^{gR}) \left[\int_0^{L_{wR}} \left\{ w_{k-j}^R(s_R) - e_{wR}(s_R) \phi_{k-j}^R(s_R) \right\} \left\{ 1 - s_R^2 / L_w^2 \right\}^{1/2} ds_R \right. \\ \quad \left. + (M_0 / M_{k-j}^{gR}) \int_0^{L_{wR}} c_h^2(s_R) \phi_{k-j}^R(s_R) ds_R \right] \\ & \text{for } k = n_b+n_t+4+n_w, \dots, n_b+n_t+3+2n_w; j=n_b+n_t+3+n_w \end{cases} \quad (3.111)$$

The components of integral I_{ik} for the mean response are given by eqs. (3.109)

3.7.2 Response Covariance

Covariance of the response for the system generalised coordinates can be written as

$$K_{q_i q_k}(t_1, t_2) = E \left[\left\{ q_i(t_1) - \mu_{q_i}(t_1) \right\} \left\{ q_k(t_2) - \mu_{q_k}(t_2) \right\}^* \right] \quad (3.112)$$

Upon substitution of eqs. (3.88) and (3.89) in eq.(3.112) and after simplification yields

$$K_{q_i q_k}(t_1, t_2) = \sum_{\ell=1}^{2n} \sum_{r=1}^n \sum_{p=1}^{2n} \sum_{s=1}^n \sum_{g=1}^n \sum_{w=1}^n u_{i_n \ell} \bar{u}_{\ell r} \bar{m}_{rs} u_{k_n} \bar{u}_{pg} \bar{m}_{gw} \times \left\{ I_{s,g}(t_1, t_2) - I_{\ell s}(t_1) I_{pg}(t_2) \right\} \quad (3.113)$$

where $i_n = i+n$, $k_n = k+n$, $I_{\ell s}$ and I_{pg} are defined in eq.(3.94) and integral $I_{s,g}$ is given by

$$\begin{aligned} I_{s,g}(t_1, t_2) &= \int_{-\infty}^{\infty} \int_{-\infty}^{\infty} H_{\ell}(\omega_1, t_1) H_p^*(\omega_2, t_2) E \left[dS(F_s(\omega_1)) dS^*(F_g(\omega_2)) \right] \\ &= \int_{-\infty}^{\infty} \int_{-\infty}^{\infty} H_{\ell}(\omega_1, t_1) H_p^*(\omega_2, t_2) \Phi_{F_s F_g}(\omega_1, \omega_2) d\omega_1 d\omega_2 \end{aligned} \quad (3.114)$$

The evaluation of the above integral requires the description of the generalised PSD $\Phi(\omega_1, \omega_2)$ of the input process F . It is assumed that aerodynamic forces are uncorrelated with the track unevenness. Thus input PSD can be expressed in terms of track profile PSD only.

Various expressions for track PSD have been used in literatures and most of them are close to the measured value in the range of interest of the spatial frequency. To illustrate the present approach, the track roughness is assumed as a homogeneous process in space domain with the PSD [73]

$$\Phi_{h_R}(\Omega) = A_r \exp(-k_r \Omega^2) \quad (3.115)$$

where A_r and k_r are roughness and correlation constants for a particular class of track. The corresponding generalised PSD can be put as

$$\Phi_{h_R h_R}(\Omega_1, \Omega_2) = \Phi_{h_R}(\Omega_1) \delta(\Omega_1 - \Omega_2) \quad (3.116)$$

With the description of input PSD in terms of track characteristics, the integral $I_{s,g}$ can be evaluated in complex domain using Cauchy's residue theorem. The input PSD and integral $I_{s,g}$ for different models are given below

Heave Model

The input PSD are

$$\Phi_{F_s F_g} = \begin{cases} 0 & \text{for } s, g = 1, 3, 4, \dots, 2n_w + 2 \\ \phi_{F_2 F_2}(\omega_1, \omega_2) & \text{for } s = g = 2 \\ \frac{\psi_{s-n_1}(x_c)}{M_{s-n_1}^p} \frac{\psi_{g-n_1}(x_c)}{M_{g-n_1}^p} \phi_{F_2 F_2}(\omega_1, \omega_2) & \text{for } s = g = 2n_w + 3, \dots, n; n_1 = 2n_w + 2 \end{cases} \quad (3.117)$$

with

$$\Phi_{F_2 F_2}(\omega_1, \omega_2) = \left\{ C_{us}^2 \omega_1 \omega_2 + j C_{us} K_{us}(\omega_1 - \omega_2) + K_{us}^2 \right\} \times \Phi_{h_R h_R}(\omega_1, \omega_2) \quad (3.118)$$

The value of the integral $I_{s,g}$ for the base value $s = g = 2$ becomes

$$I_{2,2}(t_1, t_2) = \frac{2\pi A_r V_1}{v_r} \left[\exp \left\{ - \frac{\alpha_\ell}{v_r} |v_r t_1 - t_2| \right\} - \exp(-\alpha_\ell t_1 - \alpha_p t_2) \right] \exp \left(\frac{k_r \alpha_\ell^2}{v_1^2} \right) \cdot \left\{ \frac{v_r K_{us}^2 + (1 - v_r) C_{us} K_{us} \alpha_\ell - C_{us}^2 \alpha_\ell^2}{(\alpha_\ell + v_r \alpha_p)} \right\} \quad (3.119)$$

The integrals for base values other than 2 can be obtained from equations (3.117) and (3.119)

Heave-Pitch Model

(a) Rigid fuselage

The input PSD for the two point input rigid model are given as

$$\Phi_{F_s F_g} = \left\{ \begin{array}{l} 0 \quad ; \text{ for } s \text{ or } g = 1, 2 \text{ and } s \neq g \\ \\ \left\{ C_{u1}^2 \omega_1 \omega_2 + j C_{u1} K_{u1} (\omega_1 - \omega_2) + K_{u1}^2 \right\} \Phi_{h_1 h_1} (\omega_1, \omega_2) \\ \quad \text{for } s = g = 3 . \\ \\ \left\{ C_{u1} C_{u2} \omega_1 \omega_2 + j (C_{u1} K_{u2} \omega_1 - K_{u1} C_{u2} \omega_2) \right. \\ \quad \left. + K_{u1} K_{u2} \right\} \Phi_{h_1 h_2} (\omega_1, \omega_2) ; \text{ for } s=3, g=4 \\ \\ \left\{ C_{u2}^2 \omega_1 \omega_2 + j C_{u2} K_{u2} (\omega_1 - \omega_2) + K_{u2}^2 \right\} \Phi_{h_2 h_2} (\omega_1, \omega_2) ; \\ \quad \text{for } s = g = 4 . \\ \\ (1/M_{p, g-n_1}) \left\{ \psi_{g-n_1} (x_1) \Phi_{F_3 F_3} (\omega_1, \omega_2) + \right. \\ \quad \left. \psi_{g-n_1} (x_2) \Phi_{F_3 F_4} (\omega_1, \omega_2) \right\} \text{ for } s=3, g= n_1+1, \dots, n \\ \quad \quad \quad n_1 = 4 + 2n_w \\ \\ (1/M_{p, g-n_1}) \left\{ \psi_{g-n_1} (x_1) \Phi_{F_3 F_4} (\omega_1, \omega_2) + \right. \\ \quad \left. \psi_{g-n_1} (x_2) \Phi_{F_4 F_4} (\omega_1, \omega_2) \right\} \text{ for } s=4, g= n_1+1, \dots, n \\ \\ \frac{1}{M_{p, s-n_1} M_{p, g-n_1}} \left[\psi_{s-n_1} (x_1) \psi_{g-n_1} (x_1) \Phi_{F_3 F_3} (\omega_1, \omega_2) + \right. \\ \quad \left\{ \psi_{s-n_1} (x_1) \psi_{g-n_1} (x_2) + \psi_{s-n_1} (x_2) \psi_{g-n_1} (x_1) \right\} \Phi_{F_3 F_4} (\omega_1, \omega_2) \\ \quad \left. + \psi_{s-n_1} (x_2) \psi_{g-n_1} (x_1) \Phi_{F_4 F_4} (\omega_1, \omega_2) \right] \text{ for } s = n_1+1, \dots, n \\ \quad \quad \quad \text{and } g = n_1+1, \dots, n \quad (3.120) \end{array} \right.$$

Since in the heave pitch model, two wheels follow the same path along the centre line of the track surface and h_1 and h_2 are representatives of the same process, it can be tacitly assumed that

$$\Phi_{h_1 h_1}(\omega_1, \omega_2) = \Phi_{h_1 h_2}(\omega_1, \omega_2) = \Phi_{h_2 h_2}(\omega_1, \omega_2) = \Phi_{h_R h_R}(\omega_1, \omega_2)$$

.g

With the PSD of the input process known, the integral $I_{s,g}^n$ can be evaluated in complex domain using Cauchy's Residue theorem. The integral for the base value $s = 3, g = 4$ is given as

$$I_{3,4}(t_1, t_2) = \frac{2\pi A_r V_1}{v_r} \left[\exp \left\{ -\frac{\alpha_\ell}{v_r} |v_r t_1 - t_2| \right\} - \exp(-\alpha_\ell t_1 - \alpha_p t_2) \right] \exp \left(-\frac{k_r \alpha_\ell^2}{v_1^2} \right) \left\{ \frac{v_r K_{u1} K_{u2} + \alpha_\ell (K_{u1} C_{u2} - v_r C_{u1} K_{u2}) - C_{u1} C_{u2} \alpha_\ell^2}{\alpha_\ell + v_r \alpha_p} \right\} \quad (3.121)$$

ly

The other two basic terms $I_{3,3}$ and $I_{4,4}$ have forms closely related to $I_{3,4}$ and can be obtained by simply changing subscripts of the damping and stiffness coefficients. $I_{3,3}$ is obtained from eq.(3.121) by replacing the subscripts 2 of K_u and C_u with 1 everywhere, while $I_{4,4}$ is given by replacing subscripts 1 of K_u and C_u

with 2.

(b) Flexible Fuselage

The input PSD for this model are expressed as

$$\Phi_{F_s F_g} = \left\{ \begin{array}{l} 0 \quad \text{for } s, g = 1, 2, \dots, n_b, n_b+3, \dots, n_b+2+2n_w \\ \quad \text{and } s \neq g \\ \left\{ C_{ur} C_{uk} \omega_1 \omega_2 + j C_{ur} K_{ur} (\omega_1 - \omega_2) + K_{ur} K_{uk} \right\} \Phi_{h_r h_k}(\omega_1, \omega_2) \\ \text{for } s=g; s=n_b+1, r=k=1; s=g, s=n_b+2, r=k=2; \\ \quad s=n_b+1, g=n_b+2, r=1, k=2 \\ \\ (1/M_{p, g-n_1}) \left\{ \psi_{g-n_1}(x_1) \Phi_{F_s F_{j+1}}(\omega_1, \omega_2) + \psi_{g-n_1}(x_2) \Phi_{F_s F_{j+1}}(\omega_1, \omega_2) \right\} \\ \\ \text{for } s = n_b+1, n_b+2 \text{ and } g=n_1+1, \dots, n \\ \\ (1/M_{p, s-n_1} M_{p, g-n_1}) \left[\psi_{s-n_1}(x_1) \psi_{g-n_1}(x_1) \Phi_{F_j F_j}(\omega_1, \omega_2) \right. \\ + \left\{ \psi_{s-n_1}(x_1) \psi_{g-n_1}(x_2) + \psi_{s-n_1}(x_2) \psi_{g-n_1}(x_1) \right\} \Phi_{F_j F_{j+1}}(\omega_1, \omega_2) \\ + \left. \psi_{s-n_1}(x_2) \psi_{g-n_1}(x_2) \Phi_{F_{j+1} F_{j+1}}(\omega_1, \omega_2) \right] \\ \\ \text{for } s = n_1+1, n_1+2, \dots, n \\ \text{and } g=n_1+1, n_1+2, \dots, n; j = n_b+1 \end{array} \right. \quad (3.122)$$

The integral $I_{s,g}$ is evaluated in complex domain using Cauchy's residue theorem. The basic terms needed for covariance evaluation are

$$\begin{aligned}
 I_{s,g}(t_1, t_2) = & (2\pi A_r V_1 / v_r) \left[\exp \left\{ - \frac{\alpha}{v_r} \ell |v_r t_1 - t_2| \right\} \right. \\
 & \left. - \exp \left(-\alpha_\ell t_1 - \alpha_p t_2 \right) \right] \exp \left(k_r \alpha_\ell^2 / v_1^2 \right) \left\{ v_r K_{ur} K_{uk} \right. \\
 & \left. + \alpha_\ell \left(K_{ur} C_{uk} - v_r C_{ur} K_{uk} \right) - C_{ur} C_{uk} \alpha_\ell^2 \right\} / (\alpha_\ell + v_r \alpha_p) \quad (3.123)
 \end{aligned}$$

for $s=g$, $s=n_b+1$, $r=k=1$; and $s=g$, $s=n_b+2$, $r=k=2$;

$$s=n_b+1, \quad g=n_b+2, \quad r=1, \quad k=2$$

The integral for other base values can be found with the help of eqs.(3.122) and (3.123).

Heave-Pitch-Roll Model

(a) Bending of fuselage with rigid roll

The input PSD for this model are

$$\phi_{F_s F_g}(\omega_1, \omega_2) = 0 \quad \text{for } s, g = 1, 2, \dots, n_b+1; n_b+5, \dots, n_b+4+2n_w$$

$$= \left[C_{urk} C_{ur'k'} \omega_1 \omega_2 + j \left\{ \omega_1 C_{urk} K_{ur'k'} - \omega_2 K_{urk} C_{ur'k'} \right\} + K_{urk} K_{ur'k'} \right]$$

$$\Phi_{h_{rk} h_{r'k'}}(\omega_1, \omega_2)$$

$$\text{for } s = g = n_b+2, \dots, n_b+4$$

$$s = n_b+2, r = r' = k = k' = 1; s = n_b+3, r = r' = k = k' = 2 \text{ and}$$

$$s = n_b+4, r = r' = 2, k = k' = 3$$

$$\text{for } s \neq g, s = n_b+2, g = s+1, r = k = 1, r' = k' = 2; s = n_b+2,$$

$$g = s+2, r = k = 1, r' = 2, k' = 3; s = n_b+3, g = s+2, r = k = 2,$$

$$r' = 2, k' = 3$$

$$= (1/M_{p, g-k}) \left[\psi_{g-k}(x_1) \Phi_{F_s F_j}(\omega_1, \omega_2) + \psi_{g-k}(x_2) \left\{ \Phi_{F_s F_{j+1}}(\omega_1, \omega_2) \right. \right.$$

$$\left. \left. + \Phi_{F_s F_{j+2}}(\omega_1, \omega_2) \right\} \right]$$

$$\text{for } s = n_b+2, \dots, n_b+4; g = n_b+5+2n_w, \dots, n; k = n_b+4+2n_w; j = n_b+2$$

$$= (1/M_{p, s-k} M_{p, g-k}) \left[\psi_{s-k}(x_1) \psi_{g-k}(x_1) \Phi_{F_j F_j}(\omega_1, \omega_2) \right.$$

$$+ \left\{ \psi_{s-k}(x_1) \psi_{g-k}(x_2) + \psi_{s-k}(x_2) \psi_{g-k}(x_1) \right\} \left\{ \Phi_{F_j F_{j+1}}(\omega_1, \omega_2) \right.$$

$$+ \Phi_{F_j F_{j+2}}(\omega_1, \omega_2) \left. \right\} + \Phi_{s-k}(x_2) \psi_{g-k}(x_2) \left\{ \Phi_{F_{j+1} F_{j+1}}(\omega_1, \omega_2) \right.$$

$$+ 2 \Phi_{F_{j+1} F_{j+2}}(\omega_1, \omega_2) + \Phi_{F_{j+2} F_{j+2}}(\omega_1, \omega_2) \left. \right\}]$$

$$\text{for } s, g = n_b+5+2n_w, \dots, n \quad (3.124)$$

The integral $I_{s,g}$ has the following basic terms needed for covariance calculations

$$\begin{aligned}
 I_{s,g}(t_1, t_2) = & (2\pi A_r V_1 / v_r) \left[\exp \left\{ - \frac{\alpha_\ell}{v_r} |v_r t_1 - t_2| \right\} \right. \\
 & - \exp \left(-\alpha_\ell t_1 - \alpha_p t_2 \right) \left. \right] \exp \left(k_r \alpha_\ell^2 / v_1^2 \right) \left\{ v_r K_{urk} K_{ur'k'} \right. \\
 & + \alpha_\ell \left(K_{urk} C_{ur'k'} - v_r C_{urk} K_{ur'k'} \right) - C_{urk} C_{ur'k'} \alpha_\ell^2 \left. \right\} / (\alpha_\ell + v_r \alpha_p)
 \end{aligned}
 \tag{3.125}$$

for $s=g, s=n_b+2, \dots, n_b+4$

$s=n_b+2, r=k=r'=k'=1; s=n_b+3, r=k=r'=k'=2$ and

$s=n_b+4, r=r'=2, k=k'=3$

The integral for other base values can be found with the help of eqs.(3.124) and (3.125)

(b) Fuselage with bending and torsional flexibility

Input PSD in terms of track characteristics are

$$\phi_{F_s F_g}(\omega_1, \omega_2) = 0 \quad \text{for } s, g = 1, 2, \dots, n_b + n_t; n_b + n_t + 4, \dots, n_b + n_t + 3 + 2n_w$$

$$= \left[C_{urk} C_{ur'k'} \omega_1 \omega_2 + j \left\{ \omega_1 C_{urk} K_{ur'k'} - \omega_2 K_{urk} C_{ur'k'} \right\} + K_{urk} K_{ur'k'} \right]$$

$$\Phi_{h_{rk} h_{r'k'}}(\omega_1, \omega_2)$$

$$\text{for } s = g = n_b + n_t + 1, \dots, n_b + n_t + 3$$

$$s = n_b + n_t + 1, r = r' = k = k' = 1; s = n_b + n_t + 2, r = r' = k = k' = 2 \text{ and}$$

$$s = n_b + n_t + 3, r = r' = 2, k = k' = 3$$

$$\text{for } s \neq g, s = n_b + n_t + 1, g = s + 1, r = k = 1, r' = k' = 2; s = n_b + n_t + 1,$$

$$g = s + 2, r = k = 1, r' = 2, k' = 3; s = n_b + n_t + 2, g = s + 2, r = k = 2,$$

$$r' = 2, k' = 3$$

$$= (1/M_{p, g-k}) \left[\psi_{g-k}(x_1) \Phi_{F_s F_j}(\omega_1, \omega_2) + \psi_{g-k}(x_2) \left\{ \Phi_{F_s F_{j+1}}(\omega_1, \omega_2) \right. \right.$$

$$\left. + \Phi_{F_s F_{j+2}}(\omega_1, \omega_2) \right\} \left. \right]$$

$$\text{for } s = n_b + n_t + 1, \dots, n_b + n_t + 3; g = n_b + n_t + 4 + 2n_w, \dots, n;$$

$$k = n_b + n_t + 3 + 2n_w; j = n_b + n_t + 1$$

$$= (1/M_{p, s-k} M_{p, g-k}) \left[\psi_{s-k}(x_1) \psi_{g-k}(x_1) \Phi_{F_j F_j}(\omega_1, \omega_2) \right.$$

$$+ \left\{ \psi_{s-k}(x_1) \psi_{g-k}(x_2) + \psi_{s-k}(x_2) \psi_{g-k}(x_1) \right\} \left\{ \Phi_{F_j F_{j+1}}(\omega_1, \omega_2) \right.$$

$$+ \Phi_{F_j F_{j+2}}(\omega_1, \omega_2) \left. \right\} + \Phi_{s-k}(x_2) \psi_{g-k}(x_2) \left\{ \Phi_{F_{j+1} F_{j+1}}(\omega_1, \omega_2) + \right.$$

$$\left. 2 \Phi_{F_{j+1} F_{j+2}}(\omega_1, \omega_2) + \Phi_{F_{j+2} F_{j+2}}(\omega_1, \omega_2) \right\} \left. \right]$$

$$\text{for } s, g = n_b + n_t + 4 + 2n_w, \dots, n \quad (3.126)$$

The basic terms of the integral $I_{s,g}$ needed for covariance calculations are

$$\begin{aligned}
 I_{s,g}(t_1, t_2) = & (2\pi A_r V_1 / v_r) \left[\exp \left\{ - \frac{\alpha}{v_r} |v_r t_1 - t_2| \right\} \right. \\
 & \left. - \exp \left(-\alpha_\ell t_1 - \alpha_p t_2 \right) \right] \exp \left(k_r \alpha_\ell^2 / v_1^2 \right) \left\{ v_r K_{urk} K_{ur'k'} \right. \\
 & \left. + \alpha_\ell \left(K_{urk} C_{ur'k'} - v_r C_{urk} K_{ur'k'} \right) - C_{urk} C_{ur'k'} \alpha_\ell^2 \right\} / (\alpha_\ell + v_r \alpha_p)
 \end{aligned}
 \tag{3.127}$$

for $s=g$, $s=n_b+n_t+1, \dots, n_b+n_t+3$

$s=n_b+n_t+1$, $r=k=r'=k'=1$; $s=n_b+n_t+2$, $r=k=r'=k'=2$ and

$s=n_b+n_t+3$, $r=r'=2$, $k=k'=3$

The integral for other base values can be found with the help of eqs.(3.126) and (3.127)

Using expressions for the coefficients for mean forcing function and integral I_{ik} and input PSD function with integral $I_{s,g}$ for covariance function, displacement mean and covariance of the system generalised coordinates can be evaluated in different vehicle models. In these two expressions only lower half of the matrix U are used. Utilisation of the upper half of the matrix U would yield the velocity response mean and covariance. The acceleration mean and covariance are to be determined by time differentiation of the corresponding velocity characteristics.

CHAPTER 4

NONLINEAR VEHICLE MODEL

All mechanical and structural systems have some nonlinearities that arise in various forms. In vehicle systems these may be due to suspension, structural stiffness and damping nonlinearities as well as due to friction in the suspension.

4.1 BRIEF DISCUSSION ON THE AVAILABLE METHODS

Exact solution of randomly excited nonlinear systems, is not always possible except for some cases modelled by a Fokker-Plank equation with specific conditions. To handle practical problems, various approximate methods have been developed. These may be broadly grouped as equivalent linearisation, perturbation and Monte Carlo simulation

In the equivalent approach a linear model is developed for the nonlinear system based on some performance criterion. Energy dissipation per harmonic cycle between nonlinear system and an equivalent linear system may be balanced to obtain linearised parameters. The linearised parameters can be used in the linear model for response evaluation. This method is suitable for systems subjected to stationary input.

In statistical linearisation, the nonlinear system is replaced by an auxiliary equivalent linear system. The replacement is made so as to minimize the response error between the original and the auxiliary systems. Although statistical linearisation has

high degree of flexibility in its application to stationary and nonstationary excitations, it has some basic limitations. In this approach, the probability density function of the response has to be assumed a priori. In most applications, it is taken to be Gaussian to simplify the mathematics. When the response is not having the assumed probability structure, it becomes ineffective in providing the correct estimates of the response statistics.

The perturbation technique needs a power series expansion of structural forces with nonlinear terms scaled by small parameters. It works well in first order application to small degrees of freedom. The technique becomes extremely tedious for system with larger degrees of freedom and for orders higher than one.

An alternative approach for estimating the response statistics of randomly excited nonlinear systems is based on random digital experiments, popularly known as Monte Carlo simulation. The theoretical basis of the approach is that the stochastic environment of the system can be interpreted as a sufficiently large set of samples confirming to the known statistical description. Random environment may consist of randomness in the input or system parameters. During experiment, the input sample environment is used in deterministic form and corresponding response is obtained by structural analysis to give a response function. Repeating the experiment generates an ensemble which is analysed to provide the response statistics.

Monte Carlo simulation, in general can tackle the practical problems in many real situations. However, it becomes less attractive in terms of computer storage and processing time.

4.2 VEHICLE-TRACK MODEL

A single point input model of the aircraft is considered (see Fig.4.1). Vehicle mass is assumed to be a sprung mass lumped at its centre of gravity. A part of the landing gear mass, wheel and tyre is modelled as lumped unsprung mass. Shock absorber characteristics are treated as nonlinear with combination of air spring, orifice and Columb friction damper. Tyre stiffness and damping are assumed linear. Two wings are modelled as cantilever beams clamped to the fuselage. The mass, stiffness and damping of the wings are function of spatial coordinate along the span. Runway pavement is modelled by a uniform beam with surface unevenness and supported by elastic and dissipative subgrade along its length as in the linear model.

4.3 SYSTEM EQUATIONS

All displacements are constrained to be in the vertical direction and assumed positive upward. Sprung and unsprung mass vertical displacements z_1 and z_2 are measured from their respective static equilibrium positions. Deflection of wing relative to sprung mass displacement along the span is $w(s,t)$. Track centre line deflection along the longitudinal axis x at any time instant t is denoted by $y(x,t)$.

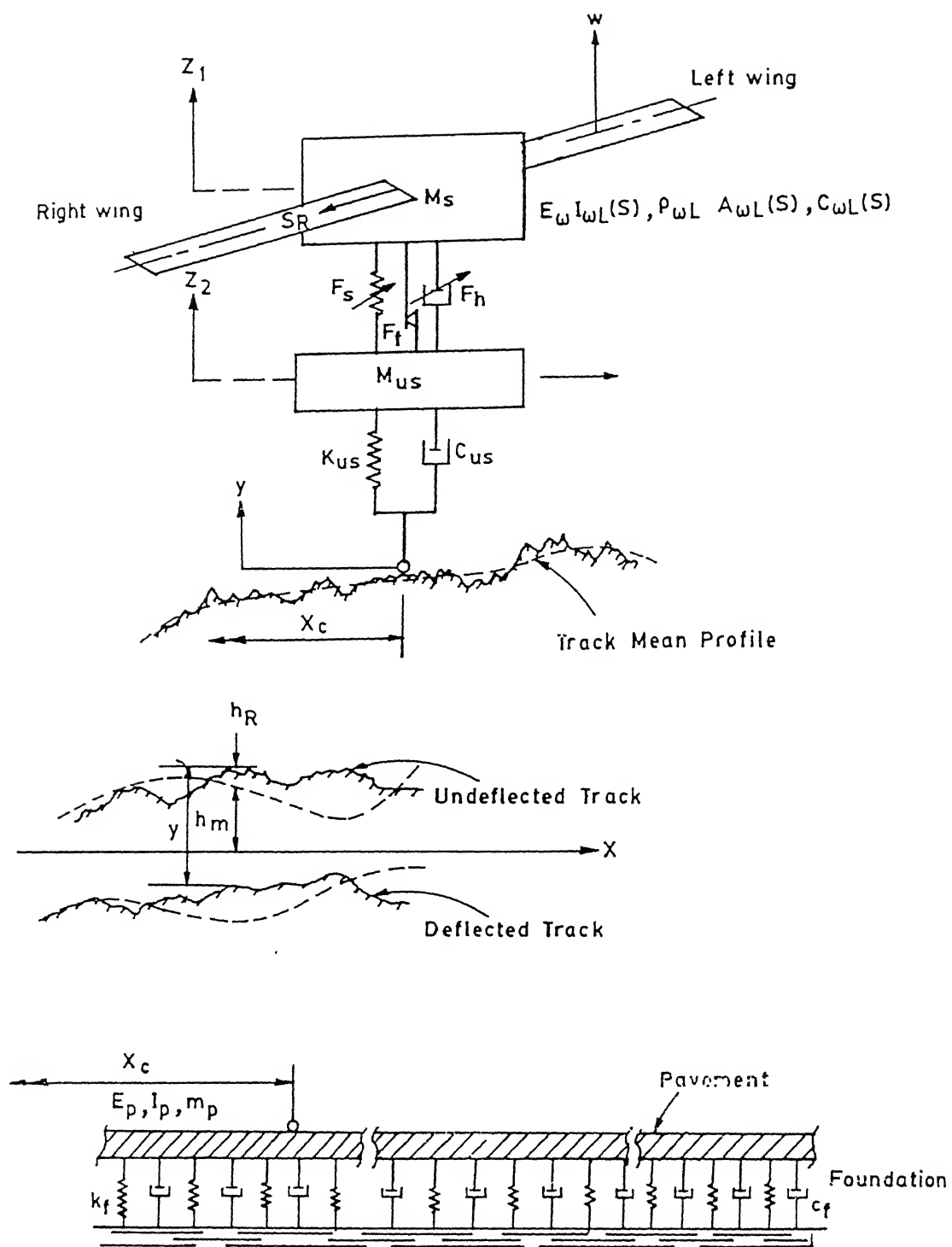


Fig.4.1. Nonlinear Aircraft Model

The equations of motion of the sprung and unsprung masses are

$$M_s \ddot{z}_1 + F_s(z_1, z_2, \dot{z}_1, \dot{z}_2) = - \frac{\partial}{\partial s_L} \left[E_{wL} I_{wL}(s_L) \frac{\partial^2 w_L}{\partial s_L^2} \right]_{s_L=0} - \frac{\partial}{\partial s_R} \left[E_{wR} I_{wR}(s_R) \frac{\partial^2 w_R}{\partial s_R^2} \right]_{s_R=0} \quad (4.1)$$

$$M_{us} \ddot{z}_2 - F_s(z_1, z_2, \dot{z}_1, \dot{z}_2) + C_{us} \{ \dot{z}_2 - \dot{y}(x_c, t) - \dot{h}(x_c) \} + K_{us} \{ z_2 - y(x_c, t) - h(x_c) \} = 0 \quad (4.2)$$

where F_s is the shock strut force. This force is due to the compression of enclosed air in the pneumatic chamber of shock strut providing a spring effect (F_a), discharge of compressed oil from hydraulic chamber through an orifice (F_h) and friction between sliding parts (F_f) producing damping. Thus

$$F_s = F_a + F_d$$

$$\text{where } F_a = P_{ao} A_{ao} \left(\frac{V_{ao}}{V_{ao} - A_{ao} s} \right)^n \quad (4.3)$$

$$F_d = C_{nL} | \dot{s} | \dot{s} + \frac{\dot{s}}{|\dot{s}|} \mu_s F_a \quad (4.4)$$

where $s = z_1 - z_2$ is the shock strut stroke, \dot{s} is the stroke velocity, A_a is the pneumatic area, P_a is pneumatic pressure, V_a

is the air volume (o refers to initial condition for the fully extended strut), n is polytropic exponent for air compression, μ_s is the coefficient of seal friction and C_{nL} is the hydraulic damping coefficient which is given by

$$C_{nL} = \rho A_h^3 / 2 C_d^2 A_n^2 \quad (4.5)$$

where ρ is the specific mass of the fluid, A_h is the hydraulic area, A_n is the orifice area and C_d is the coefficient of discharge.

The oscillation of the flexible tapered wing can be represented by partial differential equation as

$$\frac{\partial^2}{\partial s^2} \left\{ E_w I_w(s) \frac{\partial^2 w}{\partial s^2} \right\} + m_w(s) \frac{\partial^2 w}{\partial t^2} + c_w(s) \frac{\partial w}{\partial t} = f_w(s, t) \quad (4.6)$$

where the impressed force per unit length of the span is given by

$$f_w(s, t) = -m_w(s) \ddot{z}_1 - c_w(s) \dot{z}_1 - \sum_{k=1}^p M_k (\ddot{w}(s, t) + \ddot{z}_1) \delta(s - s_k) + V_w(s, t) \quad (4.7)$$

where M_k is the kth concentrated mass at span location s_k and V_{ac} is the aerodynamic lift force. The aerodynamic lift force can be expressed as a function of vehicle forward velocity, exposed surface characteristics and aerodynamic coefficient as discussed in chapter 2.

The track is subjected to wheel load that varies with space and time. The equation of motion of the track beam elastically supported by dissipative subgrade is given by

$$E_p I_p \frac{\partial^4 y}{\partial x^4} + m_p \frac{\partial^2 y}{\partial t^2} + c_f \frac{\partial y}{\partial t} + k_f y = f_p(x, t) \quad (4.8)$$

where the impressed load per unit length is given by

$$f_p(x, t) = - \left[C_{us} \left\{ \dot{z}_2 - \dot{y}(x, t) - \dot{h}(x) \right\} + K_{us} \left\{ z_2 - y(x, t) - h(x) \right\} \right] \delta(x - x_c) \quad (4.9)$$

4.4 DISCRETISED EQUATIONS FOR CONTINUOUS SYSTEM

The wings and tracks are continuous members with distributed parameters. The partial differential equations of motion can be discretized in terms of normal coordinates by adopting mode superposition technique described in chapter 3.

Assuming wing response as a superimposition of the normal modes

$$w(s, t) = \sum_{i=1}^{\infty} W_i(s) \eta_i(t) \quad (4.10)$$

where $W_i(s)$ is the i th bending mode shape and $\eta_i(t)$ is the corresponding generalised coordinates.

Using eq.(4.10) in eq.(4.6) and invoking the orthogonality property of the normal mode, yields the modal equations for the left and right wing as given in eq.(3.69) and (3.70).

Following a similar procedure, the discretised equation of

the track is found and is given in eq.(3.71) for the linear heave model with single point input.

4.5 SOLUTION APPROACH

The set of coupled ordinary differential equations (4.1), (4.2), (3.69), (3.70) and (3.71) have nonlinearities and can be solved by some numerical integration scheme. Of the continuous members only first n_w bending modes of each wing and n_p for the track have been retained in order to limit the size of modal equations. The integration of the system equations requires the track input.

The random track profile is generated following Shinozuka's algorithm [83]. The track unevenness is homogeneous process in space. The zero mean random process is simulated in space using its statistical description as

$$h_R(x) = \sigma (2/N)^{1/2} \sum_{k=1}^N \cos (\Omega_k x + \varphi_k) \quad (4.11)$$

where σ is the standard deviation of the track roughness $h_R(x)$, Ω_k are independent random variables identically distributed with the density function $g(\Omega) \equiv g(\Omega_k)$ obtained by normalising $\Phi_h(\Omega)$. The φ_k are identically distributed independent random variables with uniform density $1/2\pi$ between 0 and 2π . N , the number of terms selected for the series has to be large.

The deterministic part is then superimposed on this to obtain complete profile. The track height experienced by the wheel as it moves along the track is known against time parameter with the

help of eq.(2.1)

Integration of the nonlinear equations of motions in time domain yields system response and the shock absorber stroke and velocity at each discrete time step. These are used in eqs.(4.3) and (4.4) to obtain the shock strut force F_a and F_d . At each time step t_k , differentiation of eq.(4.3) yields instantaneous spring constant as

$$K_s(t_k) = \partial F_a / \partial s \quad (4.12)$$

The expression for the damping force in equation (4.4) is not analytically differentiable in the form used. However, being a real process its derivative should exist at all times. To obtain a usable derivative with velocity a limited order polynomial is fitted locally in the force- velocity relation and instantaneous damping constant is determined as

$$C_s(t_k) = (\partial F'_d / \partial t) (\partial t / \partial \dot{s}) \quad (4.13)$$

where F'_d is the damping force obtained by a polynomial fit.

The system is then assumed to have a instantaneously linear behaviour at instant t_k that sustains in the interval $t=t_k$ to $t=t_{k+1}$. This assumption is accurate if the time interval used is small. The system then can be represented by a set of coupled linear differential equations in the small time interval as

$$M \ddot{q}(t) + C(t) \dot{q}(t) + K(t) q(t) = F(t) \quad (4.14)$$

$$(t_k \leq t \leq t_{k+1})$$

where M , C and K is the mass, damping and stiffness matrices of the system at the instant t_k . The dimension of the matrix is n , where

$$n = 2 + 2 n_w + n_p$$

Instantaneous response of the linear system can be determined after decoupling of the system equation (4.14) by modal approach. Response of the system generalised coordinates may be expressed as

$$q_m(t) = \sum_{i=1}^{2n} X_{oi}(t_k) u_{m_1 i}(t_k) \exp(-\alpha_i(t_k)(t - t_k)) + \sum_{i=1}^{2n} u_{m_1 i}(t_k) \sum_{r=1}^n \bar{u}_{ir}(t_k) \sum_{g=1}^n \bar{m}_{rg} \int_{-\infty}^{\infty} H_i(\omega, t) dS(F_g(\omega)) \quad (4.15)$$

$m=1, 2, \dots, n; m_1 = m+n$

where $X_{oi}(t_k)$ are the constants of integration to be determined at each time step to match the response at the end of the previous time step. $\alpha_i(t_k)$ and $u_i(t_k)$ are the eigenvalues and eigenvectors of the instantaneous state matrix A

$$A(t_k) = \begin{bmatrix} M^{-1}C(t_k) & \vdots & M^{-1}K(t_k) \\ -I & & 0 \end{bmatrix} \quad (4.16)$$

Further, \bar{u}_{ir} are the elements of the inverted modal matrix U formed by eigenvectors u_i arranged as columns. $H_i(\omega, t)$ are the transient frequency response functions for the linear system in the time interval, given as

$$H_i(\omega, t) = \frac{1}{j\omega + \alpha_i(t_k)} \left\{ \exp(j\omega t) - \exp(-\alpha_i(t_k)(t - t_k)) \right\} \quad (4.17)$$

4.5.1 Response Statistics

The mean and covariance of the response can be found by considering the expectations of equation (4.15). Mean response may be expressed as

$$\begin{aligned} \mu_{q_m}(t) = & \sum_{i=1}^{2n} X_{oi}(t_k) u_{m_i}(t_k) \exp(-\alpha_i(t_k)(t-t_k)) \\ & + \sum_{i=1}^{2n} u_{m_i}(t_k) \sum_{r=1}^n \bar{u}_{ir}(t_k) \sum_{g=1}^n \bar{m}_{rg} I_{ig}(t) \end{aligned} \quad (4.18)$$

$$\text{where } I_{ig}(t) = A_g I_1(t) + B_g I_2(t) + C_g I_3(t) \quad (4.19)$$

Expressions for the coefficients A_g , B_g and C_g have been given in eqs.(3.95) and (3.96). Components of the mean response integral I_1 , I_2 and I_3 are given as

$$\begin{aligned} I_1(t_k) &= (h_0 + \sum_{i=1}^{\ell} h_i c_{i,0}) J_1 + \sum_{i=1}^{\ell} h_i \sum_{r=1}^k c_{i,r} J_2 \\ I_2(t_k) &= \sum_{i=1}^{\ell} h_i c_{i,1} J_1 + \sum_{i=1}^{\ell} h_i \sum_{r=1}^{k-1} c_{i,r+1}^{(r+1)} J_2 \\ I_3(t_k) &= c'_0 J_1 + \sum_{r=1}^{2(m-1)} c'_r J_2 \end{aligned} \quad (4.20)$$

$$\text{where } J_1 = \frac{1}{\alpha_i(t_k)} \left\{ 1 - \exp(-\alpha_i(t_k)(t-t_k)) \right\} \quad (4.21)$$

$$J_2 = \frac{t^r}{\alpha_i} + \sum_{p=1}^r (-1)^p \frac{r!}{(r-p)!} \frac{1}{\alpha_i^{p+1}} t^{r-p} - \left\{ \frac{t_k^r}{\alpha_i} + \right.$$

$$\left. \sum_{p=1}^r (-1)^p \frac{r!}{(r-p)!} \frac{1}{\alpha_i^{p+1}} t_k^{r-p} \right\} \exp(-\alpha_i(t-t_k)) \quad (4.22)$$

and

$$c_{i,0} = a_0^i; \quad c_{i,r} = (1/ra_0) \sum_{k=1}^r (ki-r+k) a_k c_{i,r-k} \quad \text{for } r \geq 1, i=0,1,\dots,\ell$$

$$c'_0 = (a'_0)^2; \quad c'_r = (1/ra_0) \sum_{k=1}^r (3k-r) a'_k c'_{r-k}; \quad a'_k = (k+1) a_{k+1}$$

$$r \geq 1 \text{ and } k=0,1,\dots,m$$

The covariance response of the system generalised coordinates may be expressed as

$$K_{q_r q_s}(t_1, t_2) = \sum_{j=1}^{2n} \sum_{\ell=1}^n \sum_{p=1}^{2n} \sum_{g=1}^n \sum_{b=1}^n \sum_{w=1}^n u_{r_n j} \bar{u}_{j\ell} \bar{m}_{\ell g} u_{s_n p} \bar{u}_{pb} \bar{m}_{bw}$$

$$\left\{ I_{g,b}(t_1, t_2) - I_{jg}(t_1) I_{pb}(t_2) \right\} \quad (4.23)$$

$$t_k \leq t_1, t_2 \leq t_{k+1}$$

where $r_n = r+n$, $s_n = s+n$; $r, s=1, 2, \dots, n$

The integral $I_{g,b}$ is

$$I_{g,b}(t_1, t_2) = \int_{-\infty}^{\infty} \int_{-\infty}^{\infty} H_j(\omega_1, t_1) H_p^*(\omega_2, t_2) \Phi_{R_g F_b}(\omega_1, \omega_2) d\omega_1 d\omega_2 \quad (4.24)$$

Description of the input PSD are required to evaluate the

above integrals. These can be expressed in terms of the track PSD and are given by eqs.(3.117) and (3.118). Using the track generalised PSD in eq.(3.116), the integral $I_{g,b}$ can be evaluated in complex domain with Cauchys' residue theorem. For base value $g=b=2$, the integral becomes

$$\begin{aligned}
 I_{2,2}(t_1, t_2) = & \frac{2\pi A_r V_1 \exp(k_r \alpha_j^2 / V_1^2)}{v_r (\alpha_j + v_r \alpha_p)} \left[\left\{ \exp(-\alpha_j |v_r t_1 - t_2| / v_r) \right. \right. \\
 & - \exp(-\alpha_j t_1 - \alpha_p (t_2 - t_k)) \left. \right\} \left\{ K_{us}^2 v_r + C_{us} K_{us} \alpha_j (1 - v_r) - C_u^2 \alpha_j^2 \right\} + \\
 & v_r \exp(k_r (v_r^2 \alpha_p^2 - \alpha_j^2) / V_1^2) \left\{ \exp(-\alpha_j (t_1 - t_k) - \alpha_p t_2) - \exp(-\alpha_j (t_1 - t_k) \right. \\
 & \left. \left. - \alpha_p (t_2 - t_k)) \right\} \left\{ C_{us}^2 v_r \alpha_p^2 + C_{us} K_{us} \alpha_p (1 - v_r) - K_{us}^2 \right\} \right] \quad (4.25)
 \end{aligned}$$

in which $v_r = V_1/V_2$ where V_1 and V_2 are vehicle forward velocities at the two time instants t_1 and t_2 defined in small interval $t_{k+1} - t_k$. The integral for other base values can be obtained with the help of $I_{2,2}$ in eq.(4.25) and expression for input PSD in eqs.(3.117) and (3.118).

It may be noted that only the lower half of the matrix U has been utilised in equations (4.18) and (4.23) to obtain the mean and the covariance of the displacement response. Utilisation of the upper half yields the mean and the variance of the velocity response. Acceleration characteristics have to be obtained by differentiation of the velocity characteristics.

The above sequence of operations from instantaneous linearisation to evaluation of response characteristics are repeated from step to step to cover the required time range.

CHAPTER 5

RESULTS AND DISCUSSIONS

The present study aims at analytically obtaining the response statistics of aircrafts to track induced excitations. In different aircraft models considered, slender flexible members like wings and fuselage have been idealised as continuous elements with nonuniformly distributed parameters. Their natural frequencies and mode shapes have been obtained with the application of the approach developed in Chapter 3. The natural frequencies and mode shapes are used in response analysis of different vehicle models with linear shock absorber by adopting modal superposition technique. Nonlinearities in the shock absorber behaviour have been handled by "instantaneous linearisation" of the shock strut behaviour.

Results have been presented in three sections in this chapter. Section 1 contains the theoretical and experimental natural frequencies for nonuniform beam and comparison with results available in literature. This also serves as a validation study for the approach developed. Section 2 presents the vehicle-track response statistics for different linear models. In section 3, the response statistics of the nonlinear vehicle model obtained by instantaneous linear approach of Chapter 4 have been presented. Monte Carlo simulation studies have also been carried out for the same nonlinear models and results are compared with that obtained the by instantaneous linear approach.

5.1 FREE VIBRATION OF NONUNIFORM SECTION BEAM

This section presents results for natural frequencies of nonuniform slender members in bending and coupled bending-torsion mode of oscillations.

Results are presented for bending vibration using the analytical approach proposed in the present study. These are also compared with results available in literature. Experiments have been conducted with variable section beams having classical end conditions. The experimental results have been compared with those predicted by the analytical approach as further validation of the proposed theory. To give insight into the behaviour of variable section beams, a study is conducted on the sensitivity of its natural frequency to changes in beam taper and externally added mass.

Results are also presented for natural frequencies in coupled bending-torsion mode for uniform and variable section beams and compared with numerical and experimental results available in literature.

5.1.1 Natural Frequencies in Bending Vibration

The analytical results obtained by using the present approach have been compared with published results and are presented in Tables 5.1 and 5.2. The natural frequency is nondimensionalised to frequency number as $(\omega^2 m_0 L^4 / EI_0)^{1/2}$, where m_0 and I_0 refer to $s=0$ end. The larger end is mentioned first in describing the beam end conditions. The ratios of the end widths $b(L)/b(0)$ and end heights $h(L)/h(0)$ are termed as taper ratios and denoted by t_b and t_h respectively. The ratio of the concentrated mass to the beam mass

is denoted by m_r and the concentrated mass location as a fraction of the beam length is denoted by s_r .

Table 5.1 presents the comparison of nondimensional frequencies (frequency numbers) of beams with no concentrated mass loading and various end conditions. Table 5.2 is for beams with one or more concentrated masses. Published results are shown from various references indicated in the tables.

Comparison indicates good agreement between the analytical values obtained and published results. The agreement is better in lower modes. This may be so because most of the references have used approximate methods and the system becomes more sensitive to errors in modelling with the increase in modal sequence.

5.1.2 Experimental Evaluation of Natural Frequencies in Bending Vibration

Experiments have been conducted on variable section beams with three classical support conditions clamped-free (Cl-Fr), pinned-pinned (Pn-Pn) and clamped-clamped (Cl-Cl). A schematic diagram for the experimental set up is shown in Fig.5.1

The clamped end condition has been simulated by bolting the wider end of the beam between two M.S. plates by six bolts of 6mm size. The base plate was 100mmx100mmx10mm in size and was welded to a heavy frame. The cover plate was 100mmx100mmx6mm in size. The pinned end condition has been simulated with the help of a fixture carrying two shafts one vertically above the another. Each shaft has been mounted with three sets of ball bearings. The lower shaft is held in position while the upper shaft can be raised or lowered with the help of a screw arrangement. The beam end was accommodated between the upper and the lower ball bearings. The

Table. 5.1

*Nondimensional Natural Frequency $(\omega^2 m_0 L^4 / EI_0)^{1/2}$ of
linearly tapered beams with no concentrated mass loadings*

End Cond.	Taper t_b, t_h	Result Source	1	2	3	4	5
Cl-Fr	0.2, 1.0	*	5.3973	25.6555	65.7473	125.2584	204.3782
		[43]	5.3969	25.656	-	-	-
		[44]	5.3976	25.6558	65.7470	-	-
		[50]	5.3976	25.6560	65.7470	125.2600	204.5500
	1.0, 0.2	*	4.2920	15.7425	36.8848	68.1160	109.9079
		[43]	4.2926	15.7420	-	-	-
		[44]	4.2925	15.743	36.886	68.144	110.06
	0.2, 0.2	*	6.1965	18.3852	39.8335	71.2413	112.8328
		[43]	6.1972	18.384	-	-	-
		[50]	6.1964	18.386	39.8370	71.2880	113.3300
	Fr-Cl	*	2.1709	18.9589	58.5574	117.5956	196.5318
		[44]	2.1709	18.9589	58.5574	-	-
Cl-Cl	0.2, 1.0	*	21.4707	60.3316	119.3342	198.1076	295.2434
		[44]	21.4707	60.3321	119.3396	-	-
	1.0, 1.2	*	24.5634	67.7044	132.7371	219.2361	324.8328
		[46]	24.5634	67.7048	132.7240	-	-
Cl-Pn	0.2, 1.0	*	16.5075	51.0248	105.4035	179.0118	272.0306
		[44]	16.5074	51.0250	105.4009	-	-
	1.0, 1.2	*	16.5029	54.4611	114.0600	195.1918	296.6478
		[46]	16.5029	54.4614	114.0516	-	-
Pn-Cl	0.2, 1.0	*	13.4846	47.7671	101.8402	175.7147	268.8754
		[44]	13.4845	47.7672	101.8389	-	-
Pn-Pn	0.2, 1.0	*	9.6722	39.5851	89.0714	158.2421	246.7976
		[44]	9.6721	39.5851	89.0704	-	-
	1.0, 1.2	*	10.8267	43.3565	97.5357	173.3681	271.4061
		[50]	10.8270	43.357	97.535	173.38	271.41

Note: * represents the results from the present work.

Table. 5.2

Nondimensional Natural Frequency $(\omega^2 m_0 L^4 / EI_0)^{1/2}$ of cantilever
beams with concentrated mass loadings

Taper t_b, t_h	Result Source	1	2	Mode Sequence 3	4	5
(a) Single Concentrated Mass						
$m_r=0.5, s_r=0.3$						
1.0, 1.0	*	3.4513	17.4415	47.3072	113.8837	196.6725
	[50]	3.4512	17.430	47.302	113.83	196.35
$m_r=0.5, s_r=1.0$						
	*	2.0156	16.9036	51.7071	106.1008	180.2362
	[50]	2.0163	16.901	51.701	106.06	180.18
	[47]	2.0163	16.901	51.701	106.06	180.12
(b) Three equal Concentrated Masses						
$m_r=0.01; s_r=1/3, 2/3, 1.0$						
	*	3.4256	21.3949	59.4744	118.5629	194.3881
	[49]	3.4262	21.3943	59.4734	118.5838	194.4162
$m_r=0.1; s_r=1/3, 2/3, 1.0$						
	*	2.8406	17.5515	47.7382	109.3044	171.7031
	[49]	2.8406	17.5502	47.7528	109.2080	171.6661
$m_r=0.2; s_r=1/3, 2/3, 1.0$						
	*	2.4460	15.1708	41.1835	105.3713	162.1602
	[49]	2.4460	15.1688	41.1555	105.3552	162.1501

Note: * represents the results from the present work.

upper shaft was lowered to just make bearing contact with the top of the beam surface. This allowed freedom of rotation to the beam end with no vertical displacement. The arrangement was housed in a rigid frame constructed with 150mmx75mmx10mm M.S. channel section.

The beam was excited harmonically by an electromagnetic shaker (capacity 62.5 Kg) through a power amplifier. The power amplifier had a built in sinusoidal waveform generator which provided a variable amplitude, variable frequency, sine wave out put. The frequency of the wave could be adjusted from 1 Hz to 20 KHz in seven over lapping ranges. In the experiment, driving frequency was monitored through the power amplifier and was varied to match the resonant frequency. Accelerometers weighing 0.0296 kg were mounted at planned locations on the beam and were treated as concentrated masses. The output signals from the accelerometers were passed through a signal conditioner and observed on a dual-trace oscilloscope to identify the event of resonance and the corresponding frequency was recorded.

Two different beam specimens made of Aluminum ($\rho = 2744 \text{ kg/m}^3$, $E = 70 \text{ GPa}$) have been tested. The beams have linearly varying width with constant height. Details of the specimens and their support conditions are listed below.

Specimen B1:

$L = 0.3 \text{ m}$, $b(0) = 0.05 \text{ m}$, $h(0) = 0.00325 \text{ m}$, $b(L) = 0.02 \text{ m}$. End conditions: clamped- free and pinned- pinned. Concentrated mass: $m_1 = 0.31$, $s_1 = 0.5 L$.

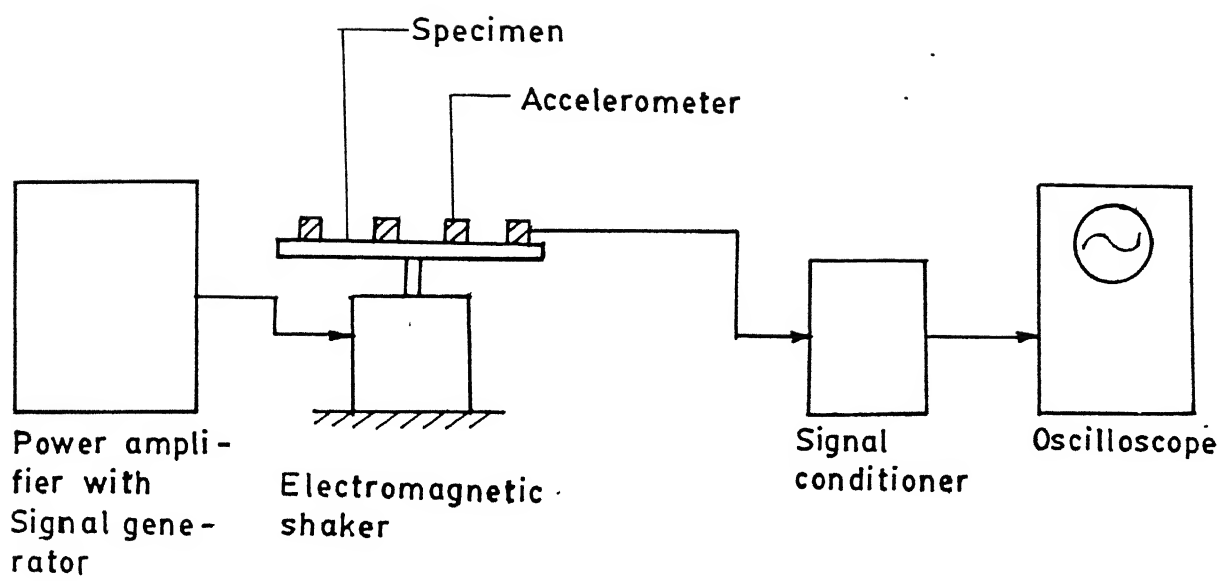


Fig.5.1. Block diagram of experimental set-up

Specimen B2 :

$L = 0.60$ m, $b(0) = 0.1$ m, $h(0) = 0.00385$ m, $b(L) = 0.04$ m. End conditions: clamped- clamped; Concentrated masses: $m_1 = m_2 = m_3 = m_4 = 0.067$, $s_1 = 0.225$ L, $s_2 = 0.492$ L, $s_3 = 0.710$ L, $s_4 = 0.980$ L.

The experimental values of the first three natural frequencies are given along with the theoretical values in Table 5.3. These show that first three natural frequencies match within acceptable limits for clamped-free and clamped-clamped conditions. However, for the simply supported condition the matching is not so good as in the other cases. The discrepancies may be due to the limitations of the experimental set up not being able to provide a ideal clamped and pinned end supports used in analysis. The disagreement is greater in the pinned ends case as the restraint against rotation at the ends was not completely eliminated by the fixtures.

Table 5.3
Experimental validation of Natural frequency
($t_b = 0.4$, $t_h = 1.0$)

Specimen No.	Support condition	Source of Result	Natural Frequencies (Hz)		
			f_1	f_2	f_3
B1	Cl-Fr	Theory	27.62	187.79	444.69
		Experiment	27.00	190.00	451.00
	Pn-Pn	Theory	103.33	325.00	770.00
		Experiment	107.00	337.00	790.00
B2	Cl-Cl	Theory	46.74	130.05	250.18
		Experiment	43.00	125.00	241.00

5.1.3 Effect of parameter variation on natural frequencies in bending vibration.

The sensitivity of the bending vibration to beam taper and mass location have been studied by varying these parameters. The proposed analytical approach is used to obtain the natural frequencies and mode shapes for variable section cantilevered beams. Numerical results have been generated with the following data:

$$\rho = 2744 \text{ kg/m}^3, E = 70.0 \text{ GPa}, L = 0.60 \text{ m}, b(0) = 0.10 \text{ m}, h(0) = 0.00385 \text{ m}, c(0)/\rho A(0) = 0.56 \text{ s}^{-1}$$

The boundary conditions of the beam are assumed as clamped at $s = 0$, and free at $s = L$. Two cases of variation of beam width and depth have been considered. These variations are chosen to represent a linear and nonlinear convex (parabolic) taper. The width $b(s)$ at a distance s from the origin, can be written as

$$\begin{aligned} b(s) &= b(0) \left[1 - w_1(s/L) \right] && \text{(linear)} \\ b(s) &= b(0) \left[1 - w_1(s/L)^2 \right] && \text{(parabolic)} \end{aligned} \tag{5.1}$$

in which $w_1 = 1 - b(L)/b(0)$.

Similarly the thickness of the beam can be expressed by appropriately replacing $b(s)$ by $h(s)$, $b(0)$ by $h(0)$, $b(L)$ by $h(L)$ and w_1 by w_2 where $w_2 = 1 - h(L)/h(0)$.

The polynomial functions $f_1(s)$ and $f_2(s)$ for the stiffness and mass and damping variation along the span are expressed as

(i) Linear

$$f_1(s) = 1 - (w_1 + 3w_2) (s/L) + 3(w_2^2 + w_1w_2) (s/L)^2 - (w_2^3 + 3w_1w_2^2) (s/L)^3 + w_1w_2^3 (s/L)^4 \quad (5.2)$$

$$f_2(s) = 1 - (w_1 + w_2) (s/L) + w_1w_2 (s/L)^2$$

(ii) Parabolic

$$f_1(s) = 1 - (w_1 + 3w_2) (s/L)^2 + 3(w_2^2 + w_1w_2) (s/L)^4 - (w_2^3 + 3w_1w_2^2) (s/L)^6 + w_1w_2^3 (s/L)^8 \quad (5.3)$$

$$f_2(s) = 1 - (w_1 + w_2) (s/L)^2 + w_1w_2 (s/L)^4$$

The natural frequencies are obtained for the following forms of tapered cross sections - width varying with thickness constant, thickness varying with width constant and width and thickness varying simultaneously. The effect of these three forms of taper on natural frequencies have been studied without any external mass loading as well as with one concentrated mass at different locations. The eigen values α_i are complex in presence of damping and appear in complex conjugate pairs. The real part of α_i gives a decaying factor associated with each mode and the imaginary part gives the corresponding damped natural frequency.

5.1.3.1 Effect of taper ratio on natural frequencies

Nondimensional damped natural frequencies of cantilevered beam in first five modes for different combinations of taper are plotted against taper ratios and shown in Fig. 5.2

(a) Width taper, height constant

Fig.5.2(a) presents the variation of the first five frequency numbers with the two types of taper in width only. The fundamental frequency of the beam is seen to decrease with the increase in taper ratio for linear as well as parabolic shapes. At lower taper ratio, parabolically tapered beam has slightly lower natural frequency compared to a linearly tapered beam. In the second mode, the frequency number gradually falls with the increase in taper ratio. The two types of tapered beams show similar behaviour. Third and fourth frequency numbers of the beams show decreasing values with taper ratios for both linear and parabolically tapered beams. Out of the two, the parabolically tapered beam has slightly higher values with the difference decreasing with increase in taper ratio. The fifth bending mode frequency for the linearly tapered beam has a pattern similar to the third and the fourth bending modes. Parabolically, tapered beam, however, has a smaller frequency number compared to the linearly tapered beam at low values of taper ratios. It has a more moderate decrease in frequency with change in taper ratio.

(b) Height taper, width constant

The variation of first five frequency numbers for the cantilever beam with height tapering and constant width is shown in Fig.5.2(b). In case of the first mode, the fundamental frequency for tapered beams decreases with increase in value of the taper ratio. Second, third, fourth and fifth frequency numbers increase with increase in taper ratio. The natural frequency for the parabolic tapered beam is seen to be higher than the linearly

tapered beam for all the modes considered.

(c) Height and width taper

The variation of frequency numbers when both width and height taper simultaneously in the same proportion, are presented in Fig.5.2(c). The first mode frequency is seen to decrease with increase in taper ratio for both types of beams showing nonlinear trends. The second, third, fourth and fifth frequency numbers for linearly tapered beam are seen to increase with taper ratios. This is also observed for parabolically tapered beams in the third, fourth and fifth modes. However, in the second mode, the parabolically tapered beam has reduction in frequency with increase in taper ratio for small values of taper ratios. With the increase in taper ratio beyond 0.4, the change in natural frequency is very small for the parabolically tapered beams.

5.1.3.2 *Effect of mass location on natural frequencies*

The effect of location of single concentrated mass ($m_1 = 0.27$) on the nondimensional natural frequency number of the tapered beam has been shown in Fig. 5.3 for different combinations of taper. Only one taper ratio is considered to illustrate the results.

In Fig. 5.3 (a), the first five frequency numbers of the beam tapered in width only are shown for linearly and parabolically tapered beams with taper ratio $t_b = 0.4$. In the first mode, for both types of taper, frequency increases as the point mass moves from tip towards the support. In the second, third, fourth and fifth modes, frequency shows a strong dependence on the position of mass, but no regular pattern can be observed. Both types of

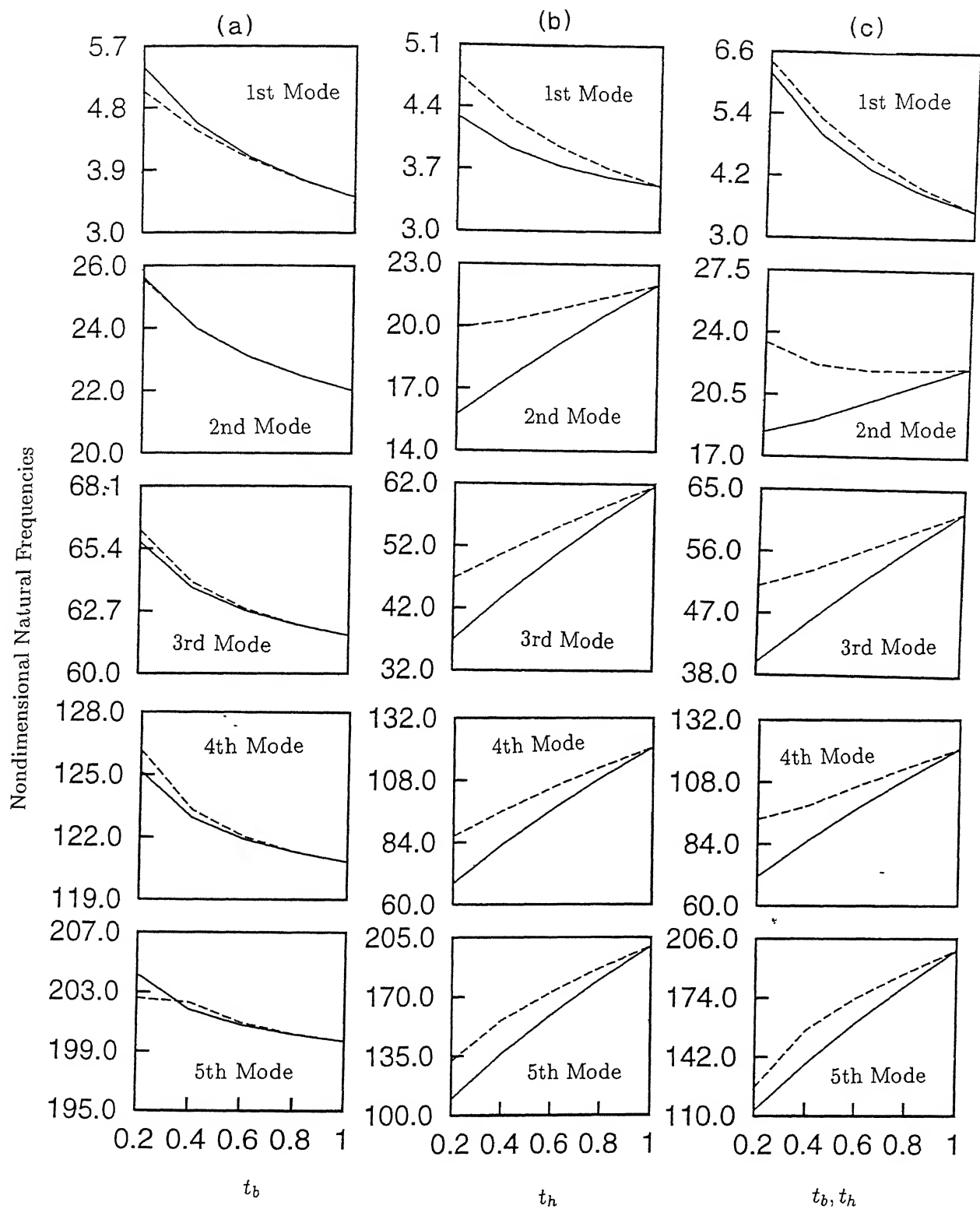


Fig.5.2. Effect of taper on natural frequencies. (a) Width taper (b) height taper (c) width and height taper.
Key: Linear taper —————, parabolic taper - - - - -

taper, in general show a similarity in frequency behaviour. In the first mode, the natural frequency of parabolically tapered beam is higher than the linearly tapered beam when the mass is near the tip and is lower with the mass closer to the root. In all other cases, for most of the location of concentrated mass, the natural frequency of parabolically tapered beam seems to be higher than the linearly tapered beam.

Fig.5.3(b) presents the variation of frequency numbers for the beam tapered in height only with width constant. The first mode frequency decreases as the location of the mass shifts towards the tip. Second, third, fourth and fifth mode frequency numbers in linearly tapered beam do not reveal any regular pattern of variation. The parabolically tapered beam follows similar pattern in all the higher modes except in fifth mode. In the fifth mode, frequency number of the parabolically tapered beam decreases only marginally as the mass is moved towards the tip. For every location of concentrated mass, the parabolically tapered beam shows higher value of natural frequency in the first five modes considered.

The variation of frequency number of the beam tapered in width and height simultaneously in the same proportion is shown in Fig. 5.3(c) for various locations of single concentrated mass. Linear as well as parabolically tapered beams show decreasing values of the fundamental frequency with the shifting of mass towards free end. Second, third, fourth and fifth frequency numbers do not show any predictable pattern of variation with location of mass for the linearly tapered beam. Parabolically tapered beam shows more or less similar behaviour in second, third and fourth modes. However,

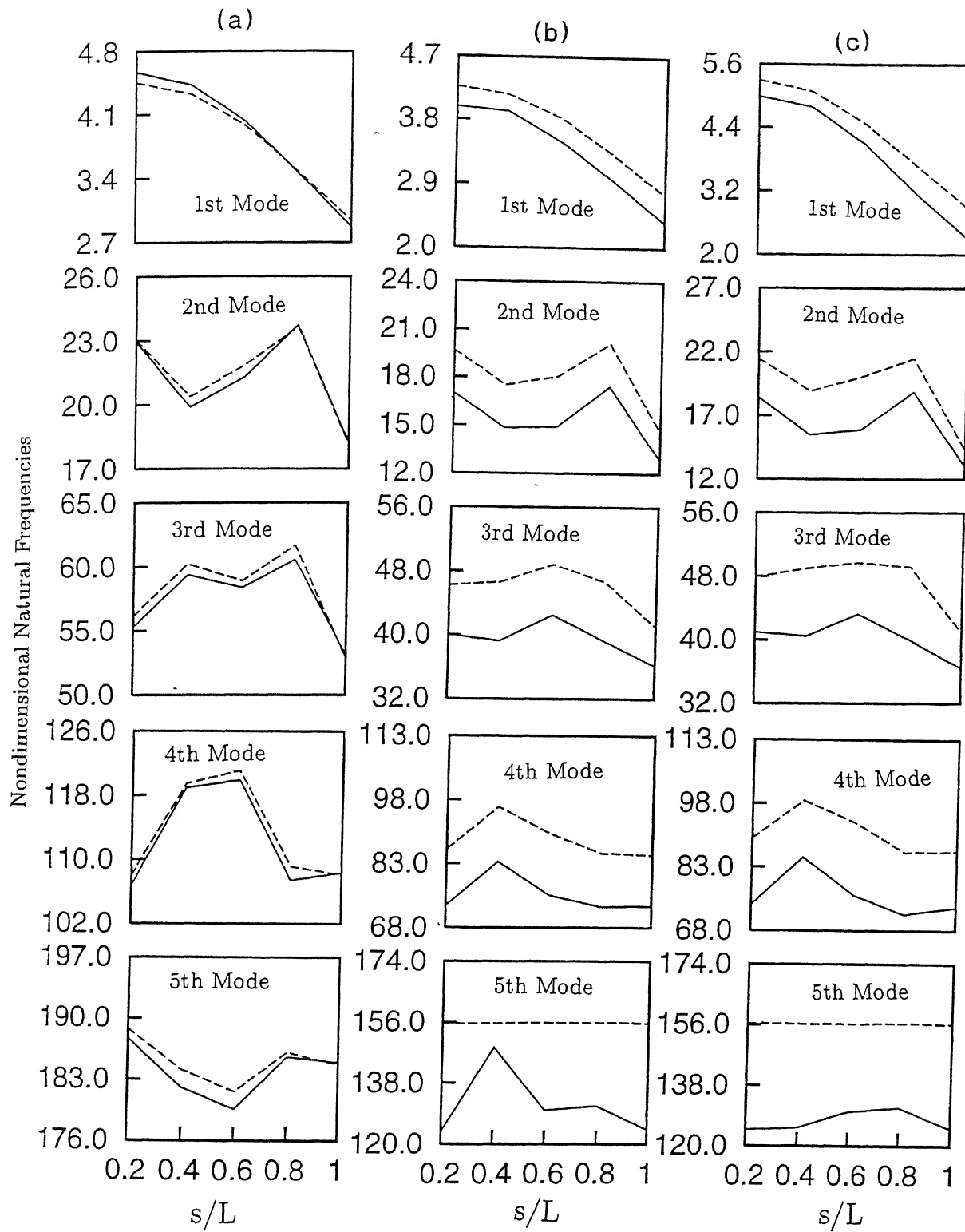


Fig.5.3. Effect of mass location on natural frequencies.
 (a) Width taper (b) height taper (c) width and height taper.
 Key same as Fig.5.2.

in the fifth mode, no significant change in frequency with the change in location of mass can be observed.

5.1.4. Natural Frequencies in Coupled Bending-Torsion Vibration

5.1.4.1 *Uniform Beam*

Results of a thin walled open section beam [69] and uniform section cantilever wing beam [70] have been selected for comparison purpose. Present theory has been used to obtain the results of uniform section beams as a special case of variable section beam for which the functions $f_1(s), \dots, f_5(s)$ in eq.(3.24) representing the variation of flexural stiffness, mass, torsional rigidity, mass polar moment of inertia and shear centre offset are taken unity.

Table 5.4 presents the natural frequency of coupled bending torsion vibration of thin walled open section beam with the following characteristics [69]

$L=5.0$ m, $m=2.45$ kg/m, $EI=5.8 \times 10^4$ N.m², $GJ=78.3$ N.m², $I_\alpha=0.02$ kg.m, $e=0.08$ m.

First five natural frequencies for clamped-free, clamped-clamped, pinned-pinned and free-free boundary conditions obtained by the present approach are compared with the results quoted in Ref.[69]. In the reference both approximate and exact results for the uniform beam are given. These results are only compared with the results obtained by present theory in Table 5.4.

Natural frequencies of a uniform cantilever wing is shown in Table 5.5 along with the results given in Ref.[70]. Wing characteristics are

$L=6.0$ m, $m=35.75$ kg/m, $EI=9.75 \times 10^6$ N.m², $GJ=9.88 \times 10^5$ N.m², $I_{\alpha}=8.65$ kg.m, $e=0.18$ m.

Table 5.4

*Natural Frequencies of Thin Walled Open Section Beams
in Coupled Bending-Torsion (Hz)*

End Cond.	Source of result	Mode Sequence Number				
		1	2	3	4	5
Cl-Fr	*	2.41	7.16	11.83	14.95	21.55
	Exact [69]	2.41	7.16	11.83	14.95	21.55
	Approx.[69]	2.40	7.13	11.78	14.85	21.27
Cl-Cl	*	6.06	12.31	18.45	24.81	31.07
	Exact [69]	6.07	12.32	18.45	24.81	31.07
	Approx.[69]	6.06	12.26	18.28	24.40	30.27
Pn-Pn	*	6.21	10.82	18.27	22.31	26.39
	Exact [69]	6.21	10.82	18.27	22.31	26.39
	Approx.[69]	6.20	10.77	18.09	22.07	26.12
Fr-Fr	*	11.13	12.89	18.84	24.29	30.99
	Exact [69]	11.12	12.89	18.84	24.29	30.99
	Approx.[69]	11.08	12.81	18.68	23.87	30.19

Table 5.5
Natural Frequencies of a Uniform Section Wing Beam
in Coupled Bending-Torsion (ω rad/s)

Source of result	Mode sequence Number				
	1	2	3	4	5
*	49.6	96.9	248.8	355.4	451.7
[70]	49.6	97.0	248.9	355.6	451.5

First five natural frequencies show excellent agreement with the published results.

5.1.4.2 Nonuniform beam

Actual wing of aircraft can be taken as an example of variable section bending-torsion coupled beam. Cross sectional properties of a wing of a small military aircraft have been measured at discrete span location [88]. Power series have been fitted in to the data to enable theoretical evaluation of natural frequencies using the proposed analytical approach. The following functions have been found to fit the actual data [Fig.5.4]

$$\begin{aligned}
 m(s) &= m(0) [1-0.39(s/L)] \\
 EI(s) &= EI(0) [1-1.11(s/L)+0.3(s/L)^2] \\
 GJ(s) &= GJ(0) [1-1.21(s/L)+0.33(s/L)^2] \\
 e(s) &= e(0) [1-.75(s/L)+0.27(s/L)^2] \\
 I_{\alpha}(s) &= I_{\alpha}(0) [1-0.87(s/L)]
 \end{aligned} \tag{5.4}$$

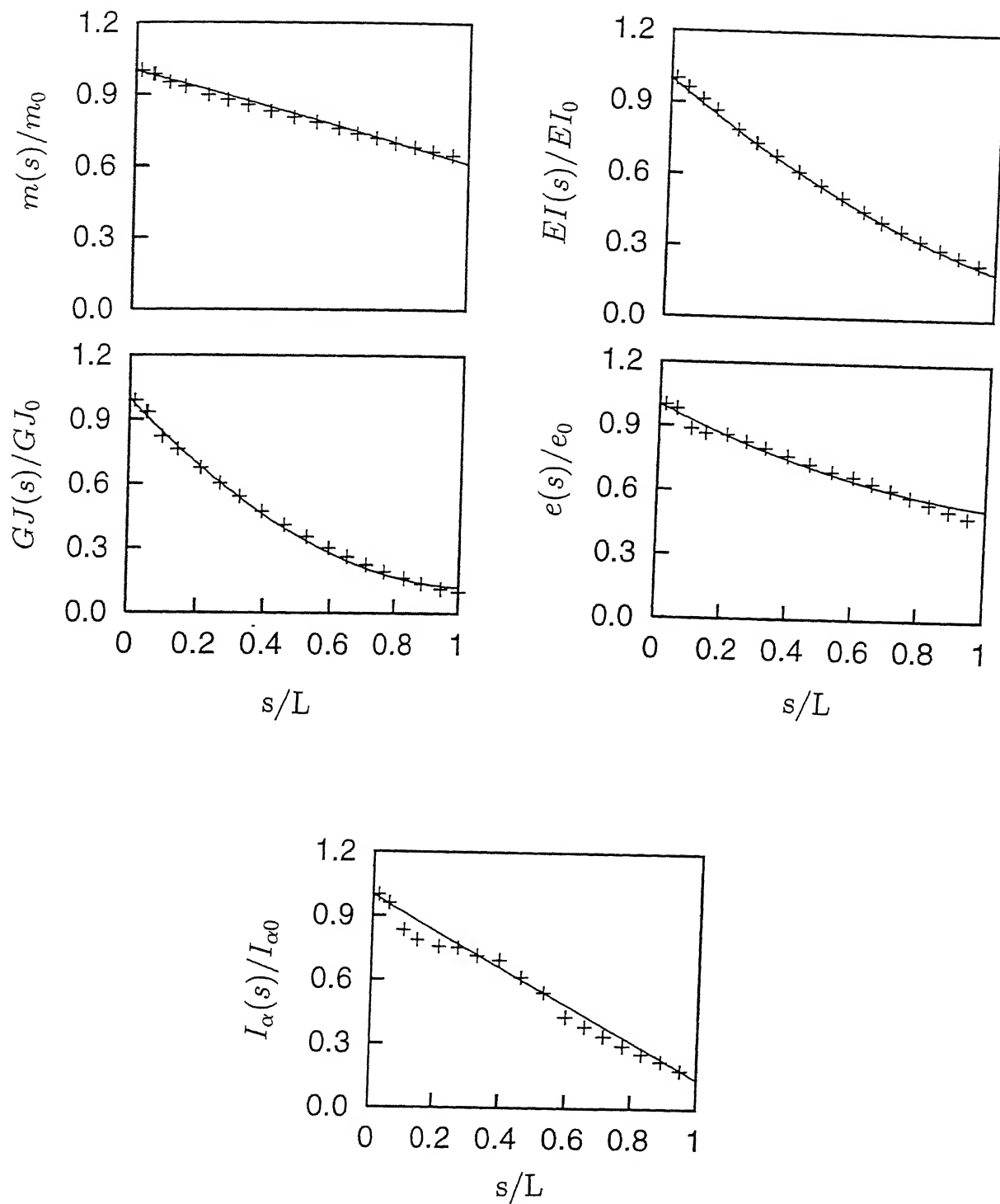


Fig.5.4. Polynomial fit of wing cross sectional properties.
 Key: Measured data [88] + + + + + , polynomial fit _____

where the nondimensional parameters at the root section are

$$m_0 e_0^2 / I_{\alpha 0} = 1.23 \text{ and } EI_0 / GJ_0 = 2.18$$

Table 5.6 gives the comparison between theoretical and experimental values. The closeness of the agreement indicates that the proposed approach may be employed for a general section for accurate evaluation of dynamic characteristics.

Table 5.6
*Comparison of theoretical and experimental values of
natural frequency (Hz)*

Mode No	Theory*	Experiment [88]
1	6.87	6.50
2	21.73	20.00
3	36.33	39.75
4	55.17	52.00
5	69.07	67.00

5.2 RESPONSE STATISTICS OF LINEAR VEHICLE MODEL

A passenger plane has been selected for the study. The following system data have been adopted to generate numerical results:

Aircraft:

Total mass (M_b): 1.469×10^5 Kg; Pitch Moment of inertia (I_s): 7.178×10^6 Kg m²; Roll moment of inertia: 6.325×10^5 Kg.m²; Fuselage length: 44.35 m; Main gear distance from aircraft c.g(l_1): 1.32 m; Nose gear distance from c.g (l_2): 16.68 m; Main

gear tread 6.3 m; Flexural rigidity of fuselage ($E_b I_b(0)$) 9.135×10^{10} N. m²; Torsional rigidity of fuselage at origin ($G_b J_b(0)$): 11.6×10^9 N.m²; Airframe viscous damping ($c_b(0)/m_b(0)$): 0.298 s^{-1} .

Landing Gears:

Nose gear mass (M_{u11}): 0.248×10^3 Kg; Main gears masses (M_{u22}, M_{u23}): 1.1105×10^3 Kg; Nose gear suspension spring constant (K_{s11}): 2.36×10^6 N/m; Two main gears spring constants (K_{s22}, K_{s23}): 14.5×10^6 N/m; Nose gear suspension damping (C_{s11}): 8.24×10^4 ; Main gears suspension dampings (C_{s22}, C_{s23}) 50.1×10^4 N.s/m; Nose and main wheel tyre stiffnesses ($K_{u11}, K_{u22}, K_{u23}$): 1.34×10^6 , 8.5×10^6 and 8.5×10^6 N/m; Nose and main wheels tyre damping ($C_{u11}, C_{u22}, C_{u23}$): 0.98×10^4 , 7.86×10^6 and 7.86×10^6 N.s/m

Wing:

Span (L_w): 20.0 m; Aspect ratio (A_T): 7.08; Mean chord ($c_h(0)$): 3.0 m; Flexural rigidity ($E_w I_w(0)$): 7.174×10^6 N.m²; Torsional rigidity ($G_w J_w(0)$): 4.662×10^6 N. m²; Mass moment of inertia about elastic axis ($I_{w\alpha}(0)$): $8.643 \text{ kg. m}^2/\text{m}$; Mass distribution at the root section ($m_w(0)$): 42.73 kg/m; Shear center offset ($e_w(0)$): 0.25 m; Linear damping ($c_w(0)/m_w(0)$): 0.16 s^{-1} ; Torsional damping ($\vartheta(0)/I_{w\alpha}(0)$): 0.008 s^{-1} ; Aerodynamic coefficients for lift and moment (C_L, C_{mac}): 0.8 and 0.1; Air density (ρ_a): 1.12 kg/m^3 .

Track and Pavement:

Runway length (L_p): 1400.0 m; Track mass (m_0): 3620 kg/m; Track flexural rigidity ($E_p I_p$): 1.38×10^7 N.m²; Foundation damping

$(c_f / m_0): 0.04 \text{ s}^{-1}$; Foundation spring constant $(k_f): 1.705 \times 10^8 \text{ N/m}^2$; Roughness constant $(A_r): 0.5025 \times 10^{-5}$; Correlation index $(k_r): 0.1012$; Track mean profile as in eq.(2.15) with $h_0 = h_2 = h_4 = \dots = 0$ and $h_1 = 0.001 + 2\pi A_0 / W_1$; $h_3 = -2\pi A_0 / (3! W_1^3)$; $h_5 = 2\pi A_0 / (5! W_1^5)$ etc. where $W_1 = 100\pi \text{ m}$ and $A_0 = 0.075 \text{ m}$ for nose wheel path, 0.04 m for left main wheel and 0.06 m for right main wheel path. This represents a combination of uniform slope and sinusoidal profiles followed by different wheels .

The response statistics of the aircraft model has been obtained for constant velocity, accelerating and decelerating runs during taxi, takeoff and landing on the runway. The response selected for the study are displacement, velocity and acceleration of the system generalised coordinates.

For the taxi run, three uniform aircraft velocities 40 Km/h , 60 Km/h and 80 Km/h have been considered. Response plots are shown for initial 20 seconds period of motion. In the takeoff run, responses are plotted for three forward acceleration of the aircraft - 1.6 m/s^2 , 1.8 m/s^2 and 2.0 m/s^2 . Time history plots are given from the start of forward motion till the aircraft reaches lift off velocity at 216 Km/h . In the landing run, time histories are shown from touch down instant to the stoppage of the forward motion of the aircraft. Responses are presented for sink velocities 0.6 , 0.9 and 1.2 m/s . The glide velocity and uniform slowing rate are assumed to be 215 Km/h and 1.5 m/s^2 .

The response in the three types of runs are being presented for the different models used in the study one by one.

5.2.1 Heave Model

5.2.1.1 *Taxi Run*

The aircraft is assumed to move forward at constant velocity in the taxi run. This corresponds to a situation of the vehicle moving at constant speed over a smooth surface and then suddenly encountering a rough terrain at $t = 0$, without any change in the forward velocity.

The mean displacement, velocity and acceleration of the generalised coordinates are presented in Fig.5.5. The mean displacements of the sprung and unsprung masses and the track modes in the later phase of taxi run follow the pattern of the mean track profile. The small initial transience gets damped out quickly. The magnitude of the mean displacements, during early phase of travel, do not show much variation with the vehicle velocity. However, with elapse of time, higher velocity seems to produce increased displacement. Due to presence of a rising gradient in the track mean used for the study, vehicle wheel experiences more height as it travels forward and more dynamic load is imposed on the pavement.

The mean velocities of the lumped masses and the track modes reveal stronger and more persistent transience. Except for the wing normal modes, which show very low values, the other steady state velocity responses have the same general pattern as the displacements with a difference in phase. The magnitude of the mean velocity is higher for higher vehicle forward velocity.

The mean acceleration of the lumped masses follow a pattern somewhat similar to their mean velocity, except for the difference

in phase. The magnitude of transient accelerations for all the response are higher in comparison to their steady state values. This may be due to the large force transmitted to the masses suddenly at transition from smooth to rough surface. The wing normal mode mean accelerations have been found to be sensitive to the vehicle forward velocity after elapse of some time. The mean acceleration of the track first three normal coordinates have initial transience on entry of vehicle over the track which is quickly damped out.

The displacement, velocity and acceleration mean responses of the wing first three normal coordinates have initial high transient values, diminishing to lower values at later stage of the taxi run. The higher vehicle velocity is found to produce larger amplitude for the wing response in its first three bending modes. The track input frequency seems to be dominant in the wing response in later stage.

The lumped mass mean response show that the track input frequency is dominant in the later stage of taxi run. The input frequency is also modified by the vehicle forward velocity as seen by the shift of peaks towards left with higher vehicle forward velocity. In all the modes, it is found that higher vehicle velocity is responsible for higher response. In most of the cases, the vehicle forward velocity is seen to modify the response frequency in the later part.

The response variances are presented in Fig.5.6. The displacement variances show that in early stage, the response is oscillatory with a high peak at the onset of vehicle motion. Subsequently the response subsides to reach a steady asymptotic

value. The steady state covariance magnitudes for displacements are higher for higher vehicle speeds. The track mode characteristics have low frequency variations in the steady state. The variances of the velocity response follow a trend similar to the displacements. The acceleration variances indicate dominant values at the initiation of motion. The steady state condition is reached within shorter time than that for displacement and velocity without any oscillations, showing progressively smaller peaks. The steady state values, however, are very low compared to the initial values.

Increase in the vehicle speed is seen to increase the magnitude of the response variances for all the coordinates. Comparison of response mean and variance in the first three flexible wing and track bending modes indicate that response magnitude decreases as the order of mode increases. This conforms to the usual assumption that the lower modes dominate the higher ones and inclusion of the first few lower modes in response computations is adequate.

5.2.1.2 *Takeoff Run*

During this run aircraft is assumed to start from rest, increasing its speed with uniform acceleration to lift off. The time history plots are from start of aircraft forward motion till it lifts off.

Fig.5.7 presents the mean response. Initial portion of the vehicle response show low magnitude transience. The accelerating vehicle takes some time to attain a certain level of velocity for the track input to become effective in setting up vibration in the

vehicle structure. Subsequently, mean response magnitude grows with increase in vehicle speed. Influence of the mean track profile is apparent in the vehicle mean response pattern - increasing level with sinusoidal variation. The constant frequency transient oscillation, as in taxi, is not observed in the takeoff run. Mean acceleration response of unsprung mass indicates a departure and has high frequency transience in the initial phase.

The mean displacement responses of the track beam for its first three normal coordinates show low initial response that grows as the vehicle accelerates to takeoff. The magnitude of the displacement is quite low compared to that in constant velocity run. This may be as the moving load is passing fast over the track beam, the track structure has little time to react to this load. The mean velocity has stronger initial transience and its magnitude is comparable to the response in the later phase of takeoff run. The mean acceleration of the first three normal coordinates of the track have high value prior to takeoff.

The response variances in takeoff run are presented in Fig.5.8. The variances for the vehicle response show very low values in the initial stage. As the vehicle accelerates from rest, its response variance show a steady increase till takeoff. The magnitude of the variances are seen to increase with the forward acceleration of the vehicle. The unsprung mass response variances are smaller compared to the sprung mass in displacement but larger in velocity and acceleration.

The variances of the first three track normal coordinates have an oscillatory pattern about an increasing mean level. There is a gradual increase in amplitude of oscillation till take off.

Higher vehicle accelerations induce increased response variances of track's first three normal coordinates. The oscillatory trend increases from displacement to velocity to acceleration response.

5.2.1.3 Landing Run

The response quantities studied during landing run are the same as in taxi and takeoff. The shock strut at the time of landing being under no load, is fully extended. This is utilised to obtain the initial displacements of the sprung and unsprung masses from their static values. The initial velocities for sprung and unsprung masses are the sink velocity of the aircraft. The initial conditions for the wing relative to the sprung mass and for the track are assumed to be zero. Response characteristics plots have been obtained from the instant of touch down till stoppage of the aircraft forward motion.

Fig.5.9 presents the mean displacement response of the vehicle-track system. The response pattern shows initial high value due to touch down impact, increasing with increase in sink velocity. After the initial impact energy is dissipated, the steady state response becomes dependent on the track roughness. The mean track input frequency is seen to play a dominant role in response during the later phase of landing run. As the vehicle loses its forward velocity, the effectiveness of input from the track decreases, reducing the system response. The magnitudes of response during impact phase are larger than that of the taxi and takeoff runs. The displacement and velocity means of the wing's first normal coordinates show the development of largest peak subsequent to impact. The velocity mean for the wing second normal coordinate indicates the presence of more than one frequency in

the oscillation during the impact phase.

Response variances are presented in Fig.5.10. Strong oscillatory patterns are present for all the displacements and for the vehicle velocity responses in the touch down phase which subsequently decrease gradually with the slowing of vehicle forward motion. The magnitude of the first peak seems to be higher with higher sink velocity. The wing third mode velocity variance rises to a peak after impact and then decreases with a slow rate showing little transience oscillations. The initial oscillations are absent for velocity variances of track modes also. These, however, indicate the presence of oscillation in the later phase of landing run. The initial impact oscillations are subdued in the acceleration variance showing only one or two peaks.

5.2.2 Heave Pitch Model with Rigid fuselage

For this model, response statistics are presented for ten coordinates -fuselage rigid body heave, pitch, nose and main gear heave degrees of freedom and first three generalised coordinates for the one wing and the track.

5.2.2.1 *Taxi Run*

The mean system response are presented in Fig.5.11. At transition from smooth to rough surface, the vehicle experiences a shock at $t=0$. This is indicated by strong initial mean for all the response coordinates considered. Influence of the mean track pattern is apparent in the vehicle lumped mass response. Increased forward velocity induces larger mean response magnitudes.

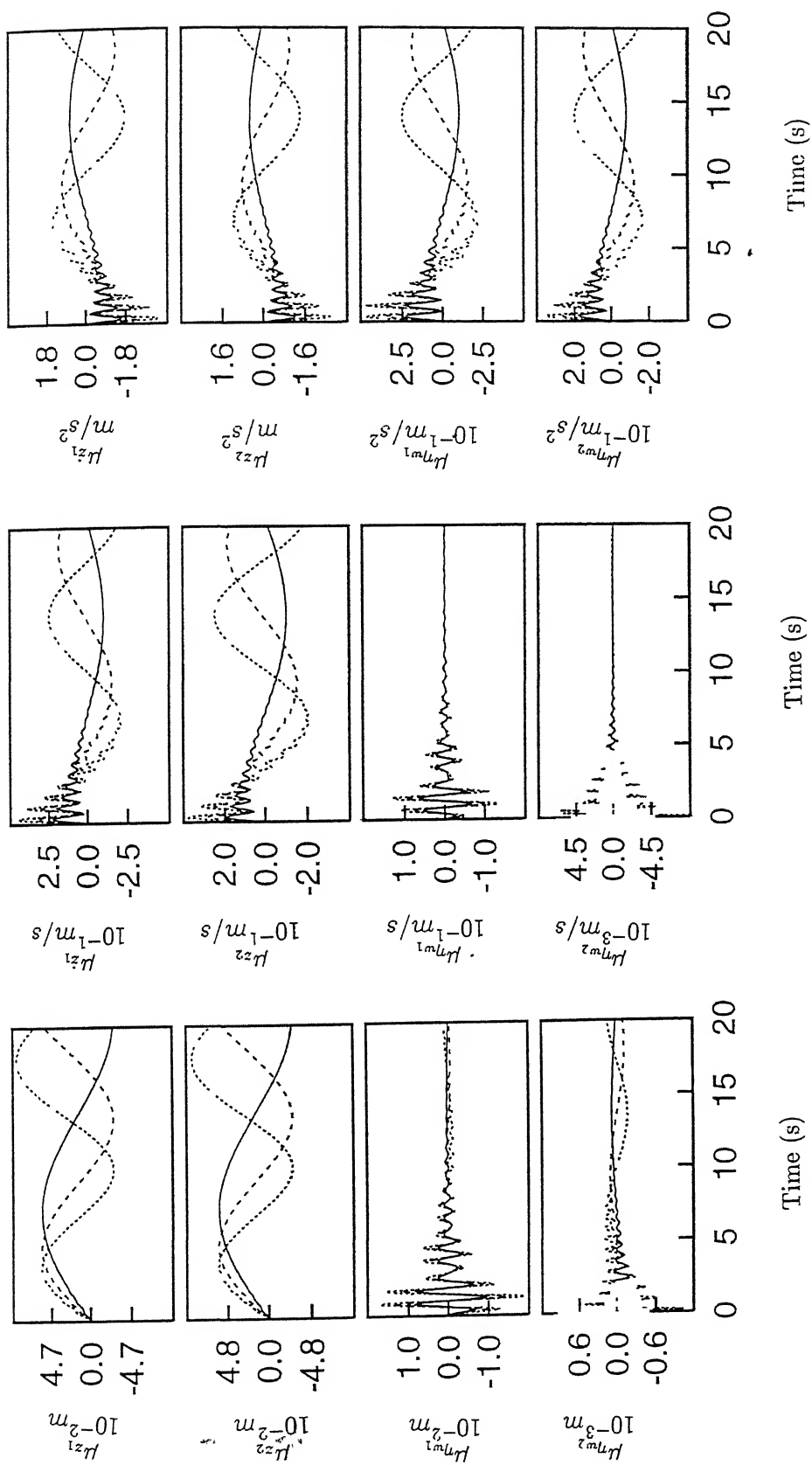


Fig.5.5. Heave Model- Mean response in taxi run.
 Key: Vehicle forward velocity, 40 Km/h ———, 60 Km/h - - - - -, 80 Km/h ,

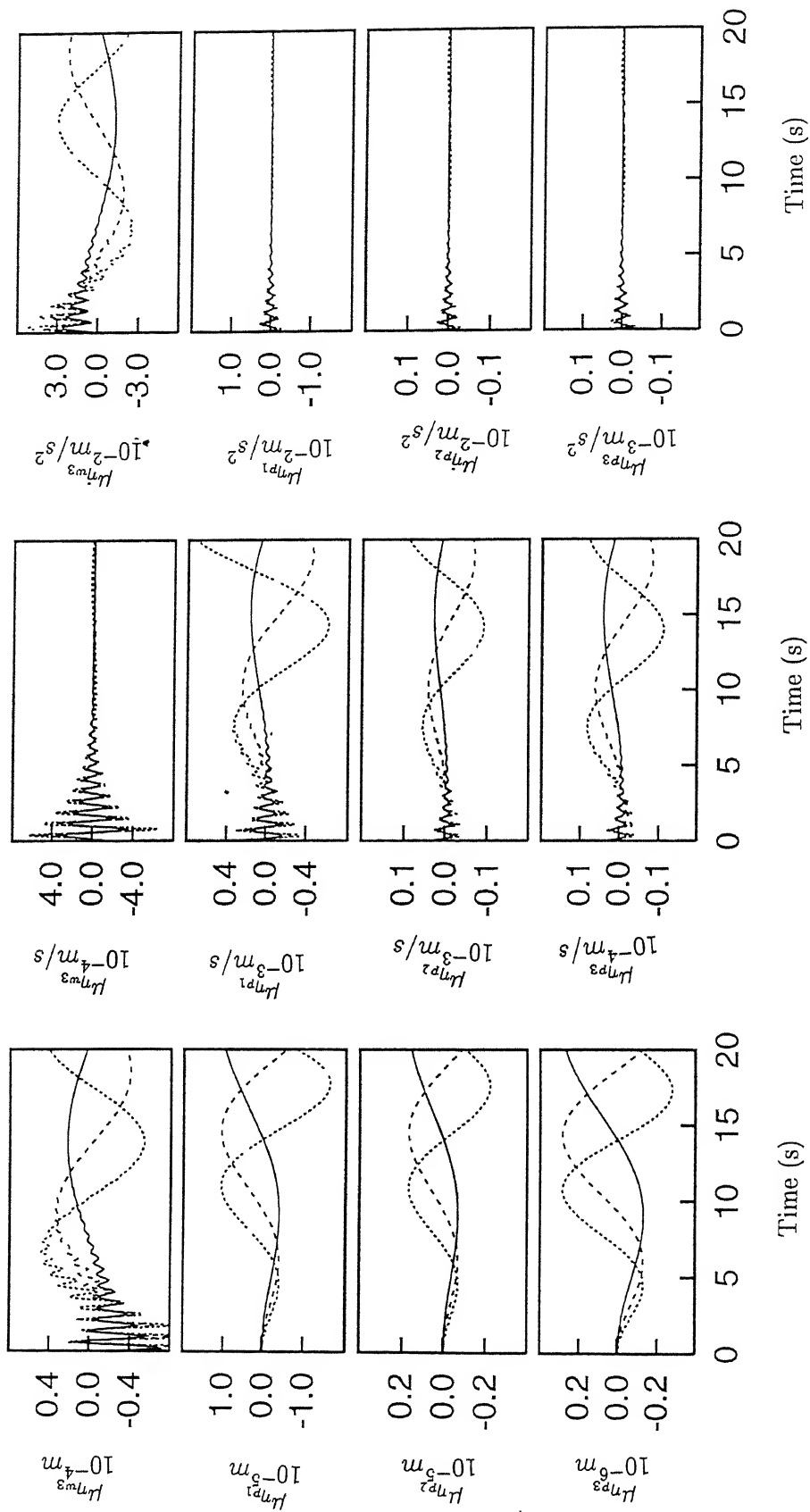


Fig.5.5(continued). Heave Model-Mean response in taxi run.
 Key: Vehicle forward velocity, 40 Km/h ———, 60 Km/h - - - - - ,
 80 Km/h ,

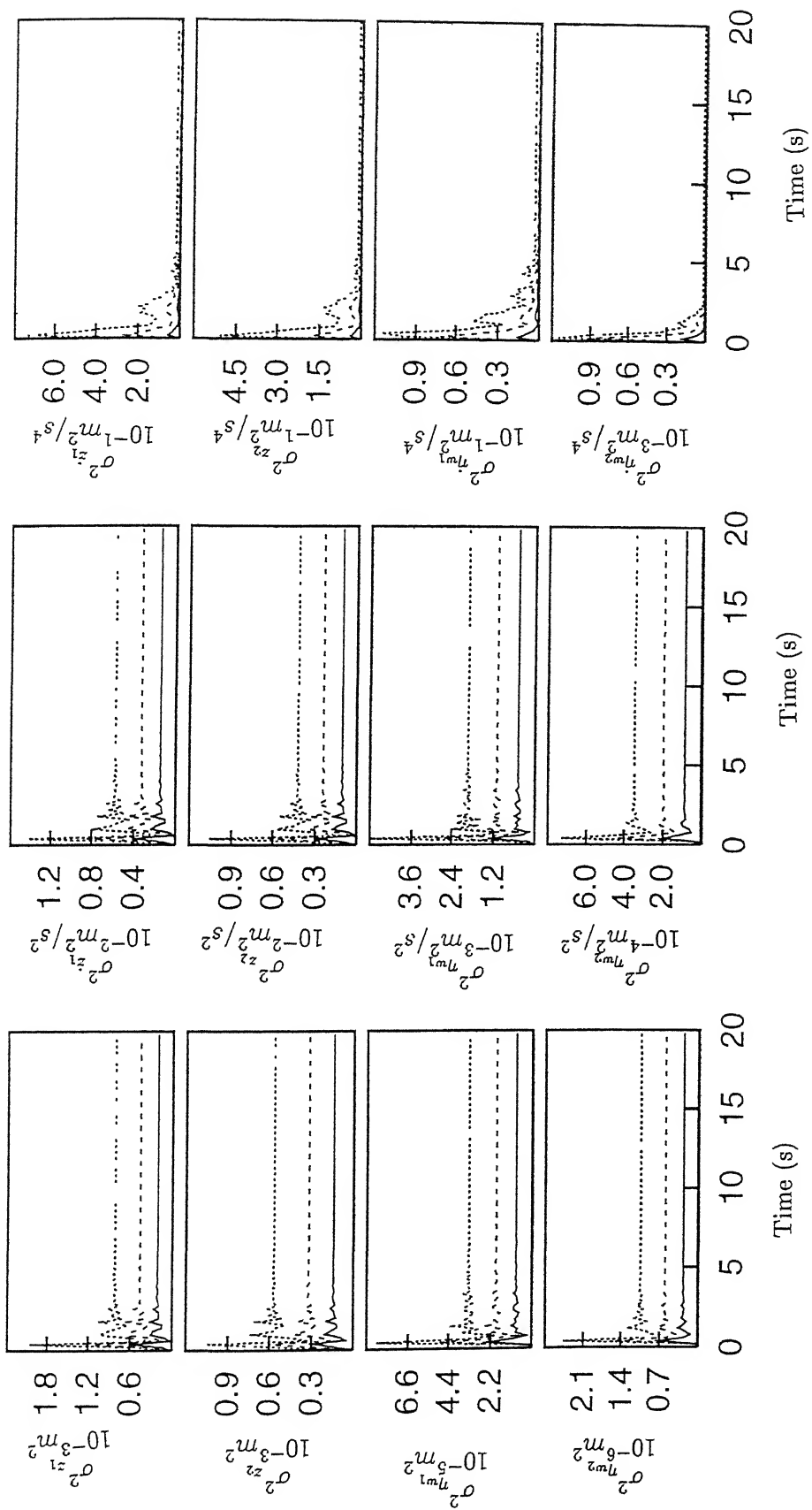


Fig.5.6. Heave Model-Response variance in taxi run.
Key same as Fig.5.5

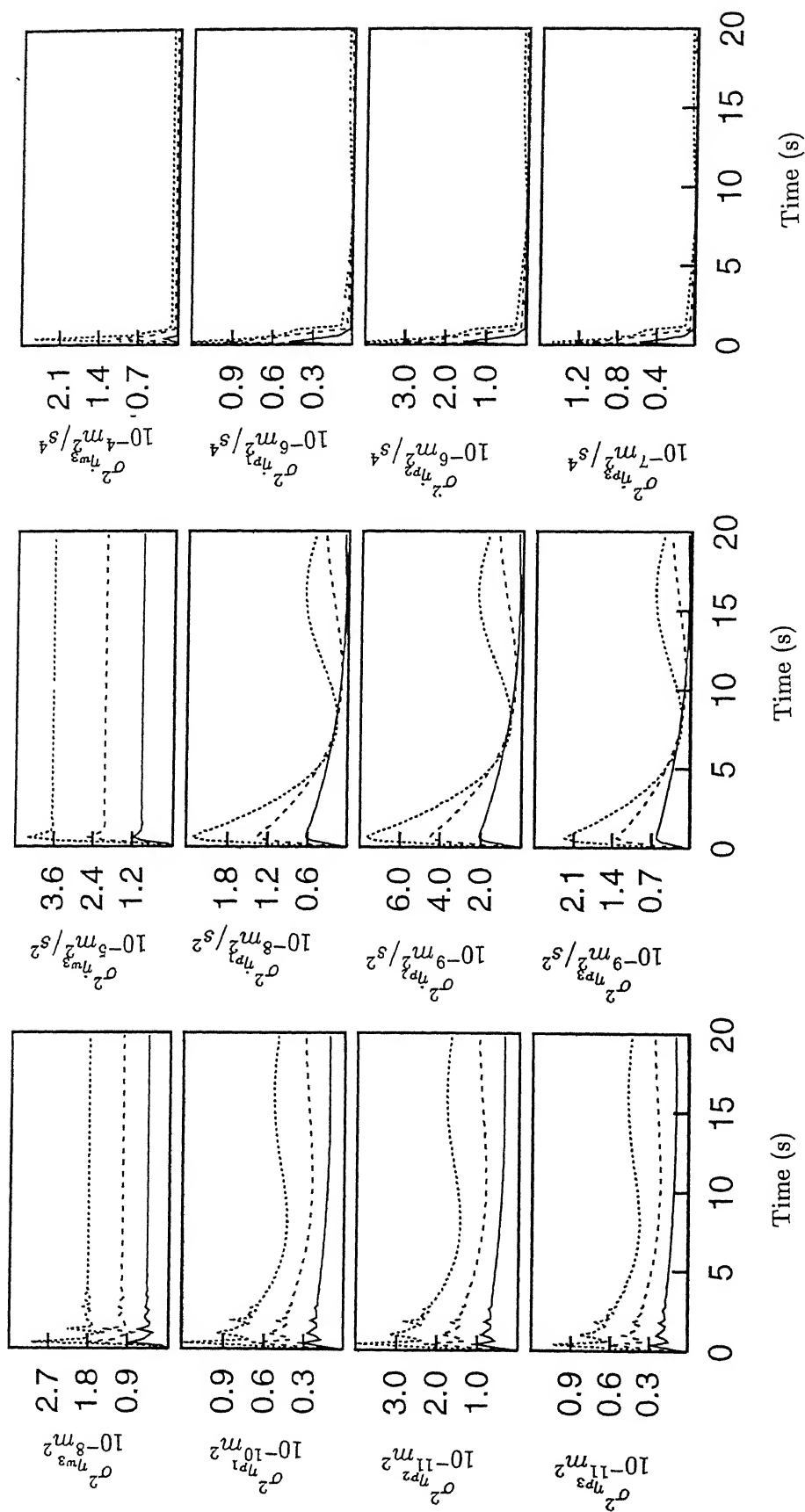


Fig.5.6(continued). Heave Model-Response variance in taxi run. Key same as Fig.5.5

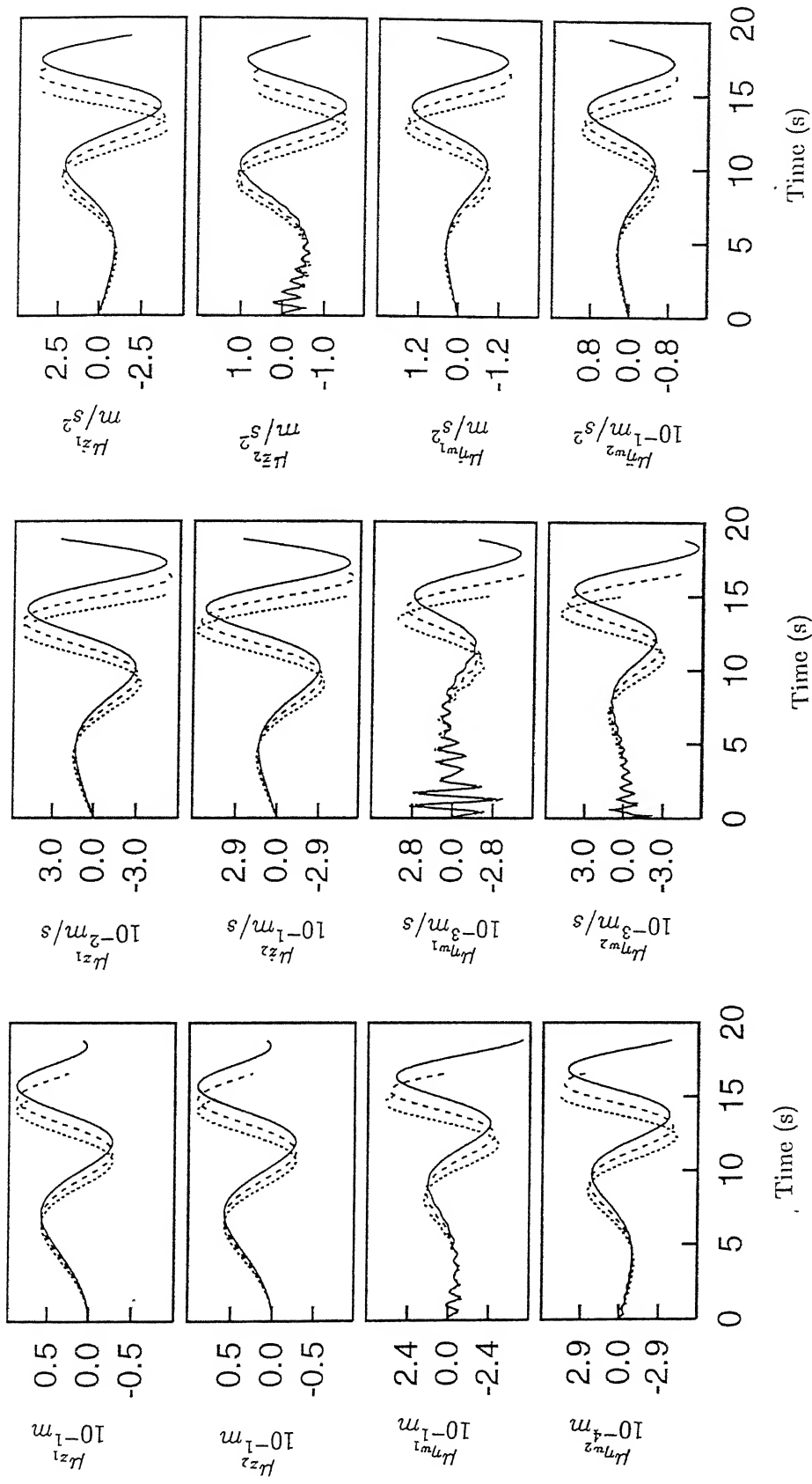


Fig.5.7. Heave Model -Mean response in takeoff run.
 Key: Vehicle forward acceleration, 1.6 m/s²,
 1.8 m/s², 2.0 m/s², 2.2 m/s²

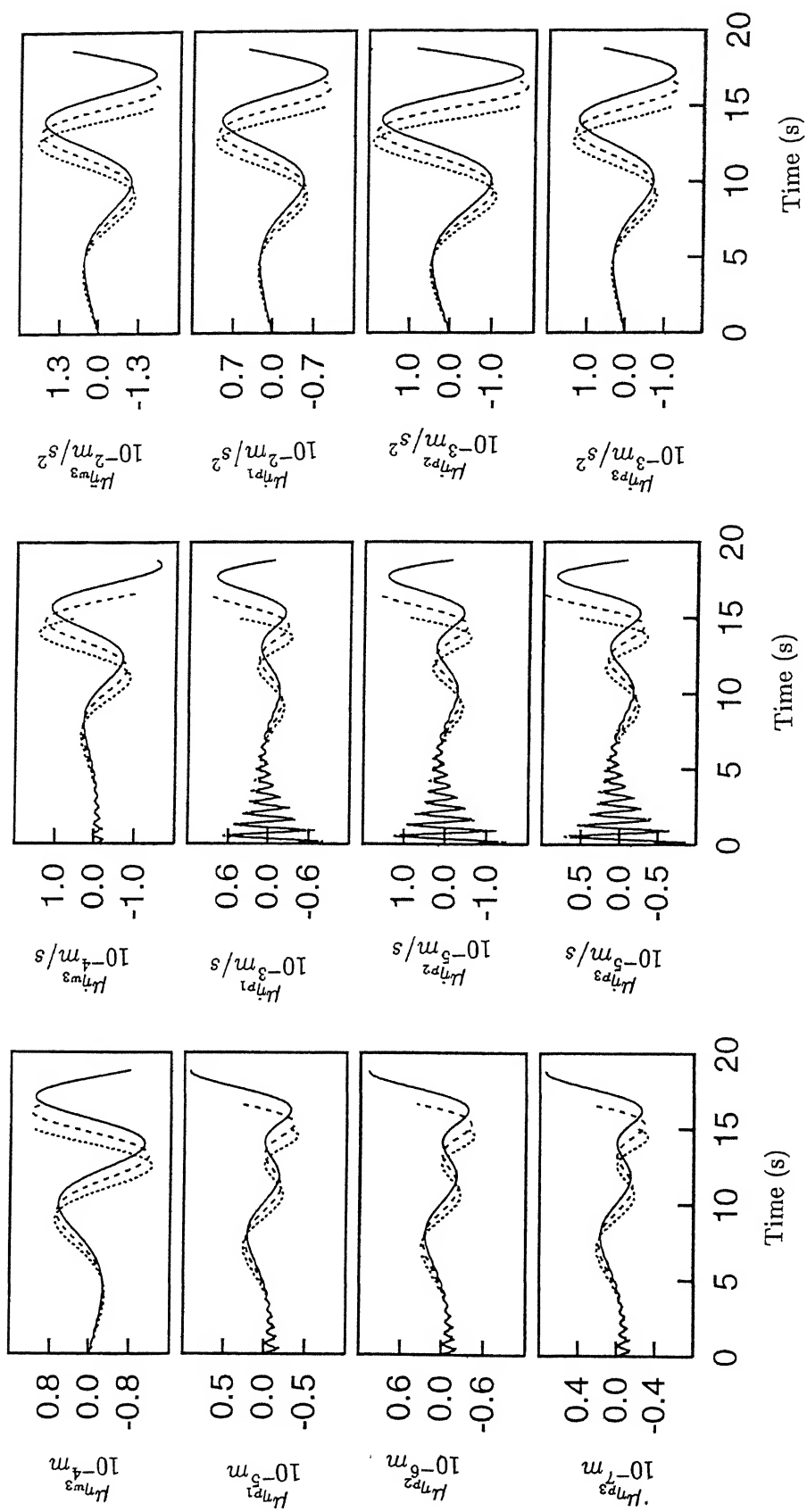


Fig.5.7(continued). Heave Model-Mean response in takeoff run
 Key: Vehicle forward acceleration, 1.6 m/s² —, 1.8 m/s² - - - - - , 2.0 m/s² ,

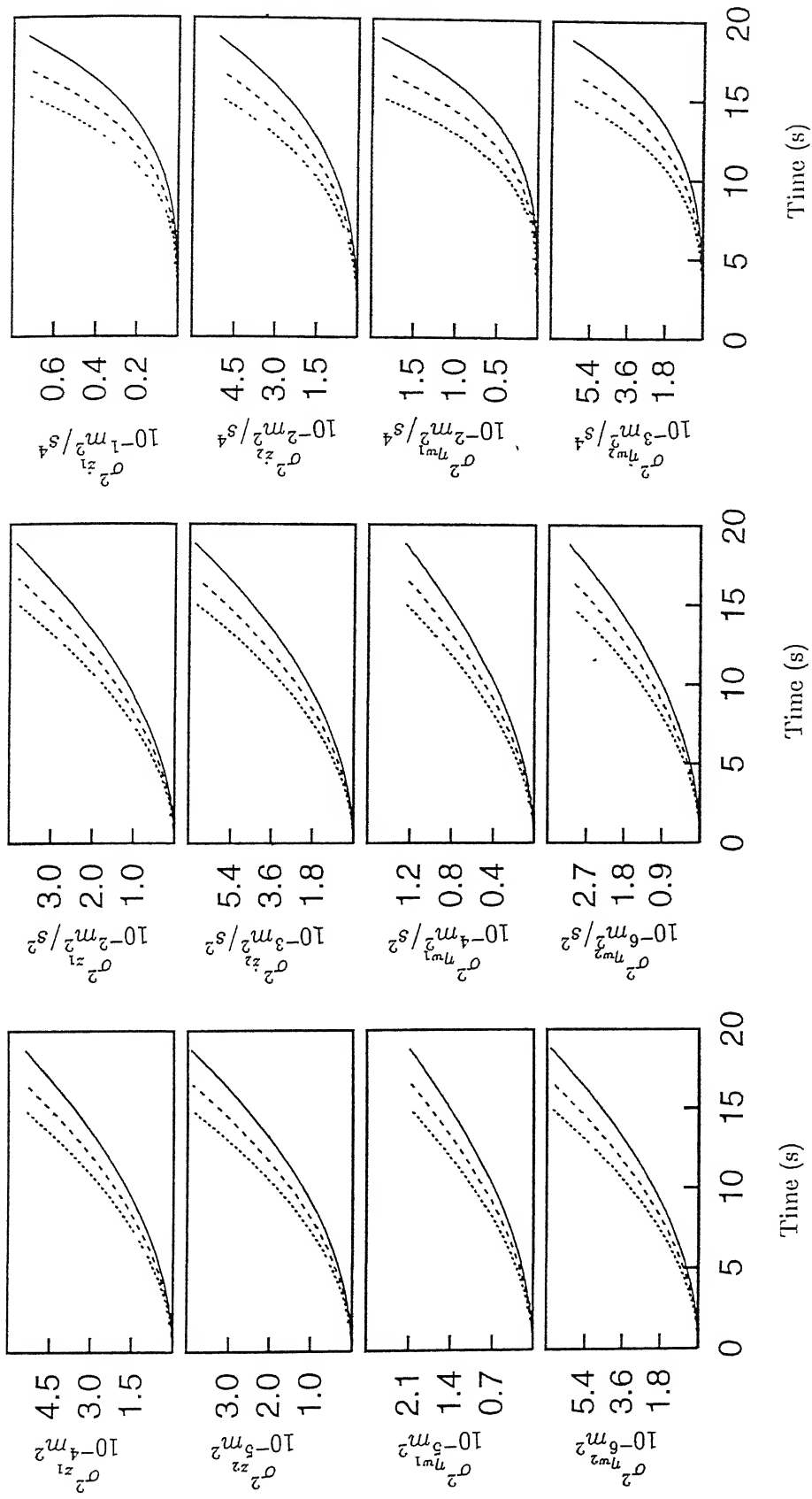


Fig.5.8. Heave Model-Response variance in takeoff run.
Key same as Fig.5.7.

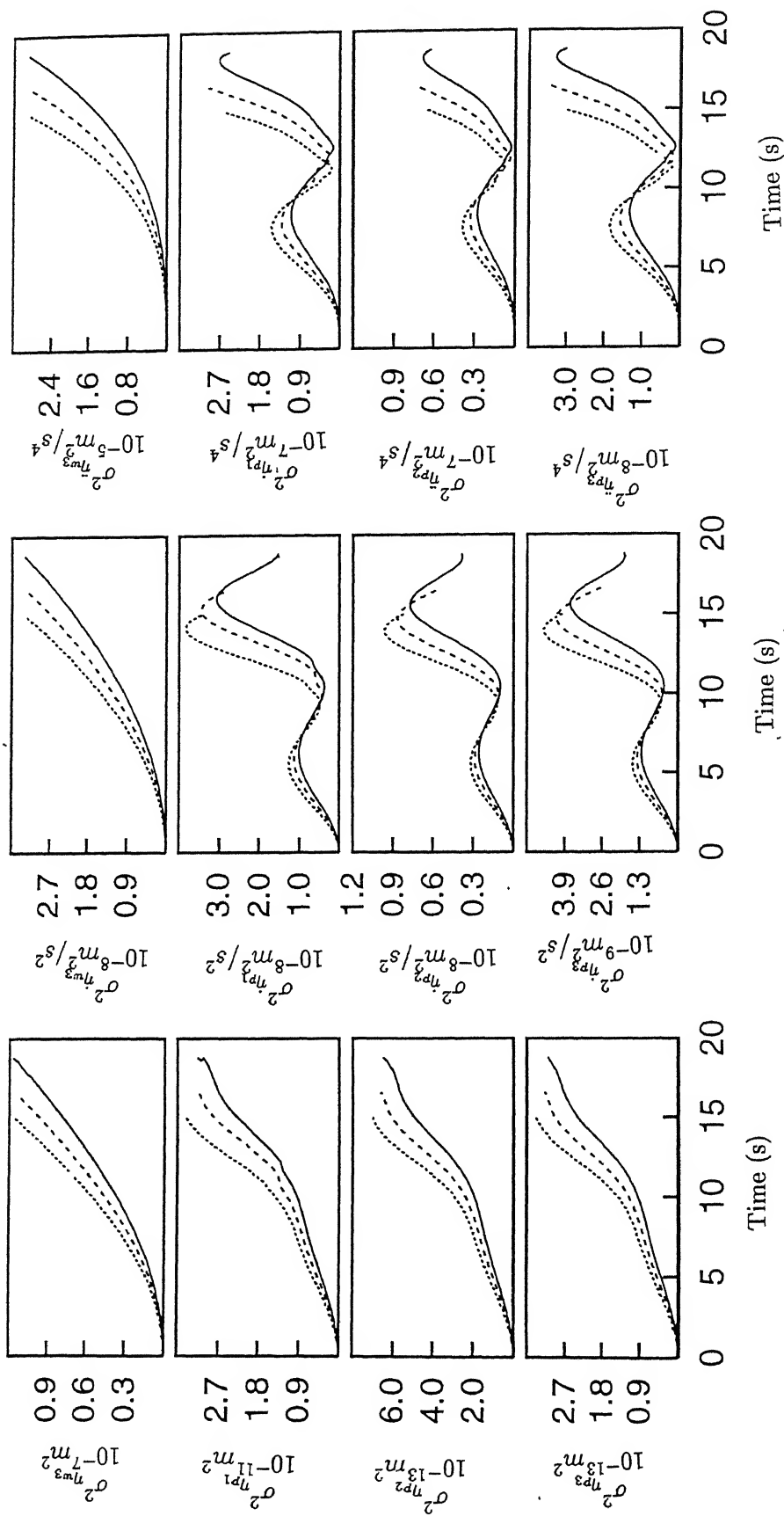


Fig.5.8(continued). Heave Model-Response variance in takeoff run. Key same as Fig.5.7

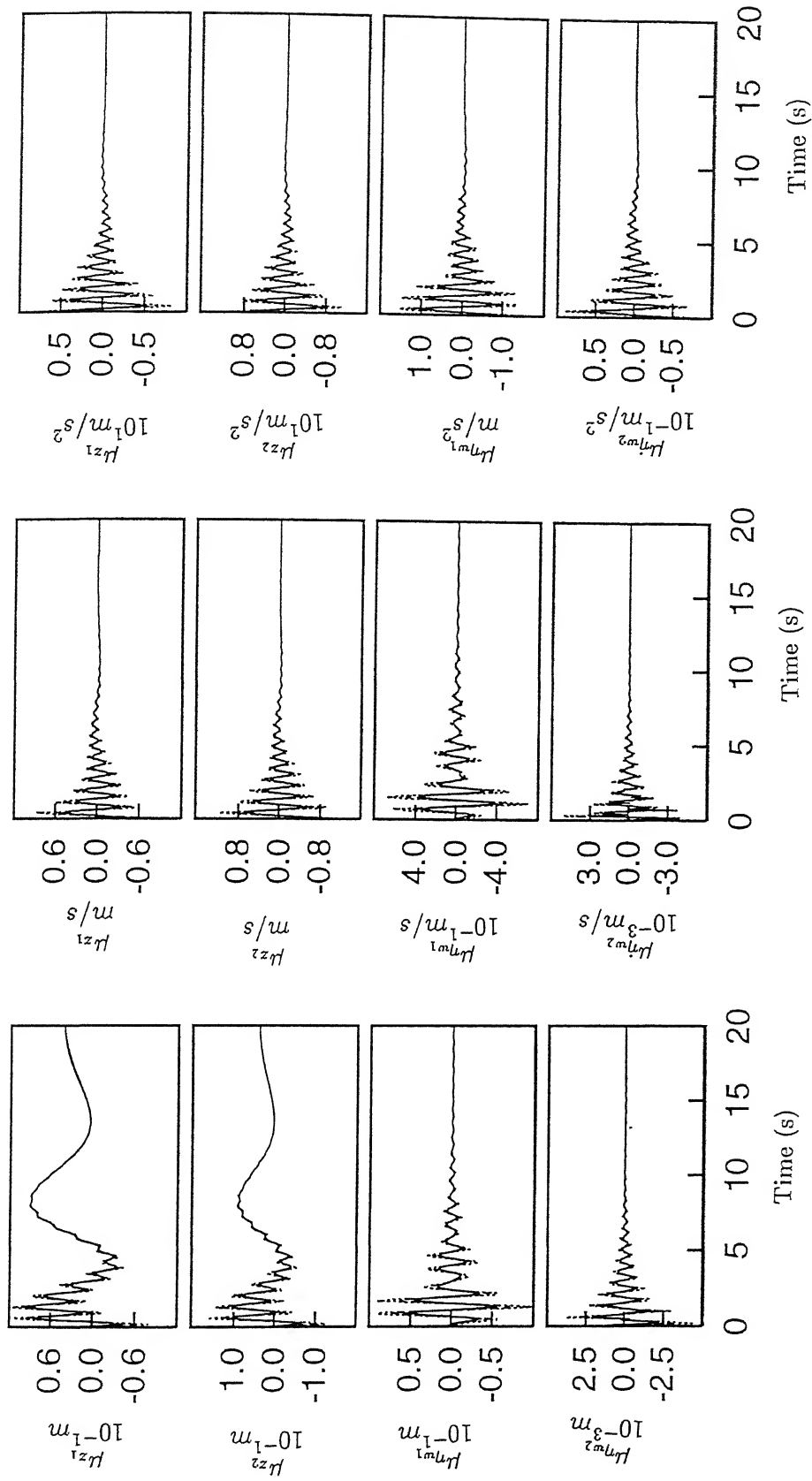


Fig.5.9. Heave Model-Mean response in landing run.
 Key: Aircraft sink velocity, 0.6 m/s ———, 0.9 m/s *-*-*-*-*
 1.2 m/s ~~~~~

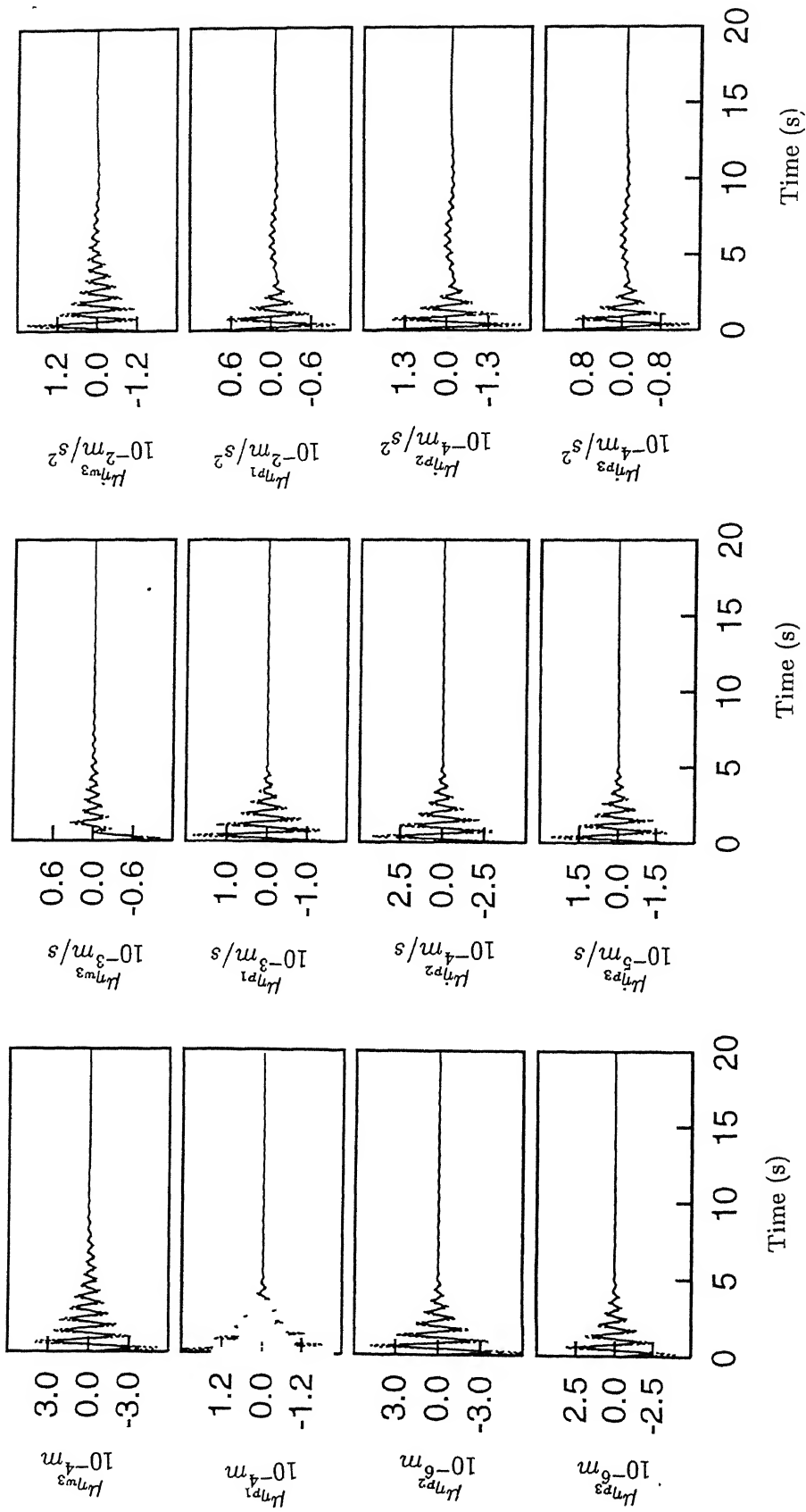


Fig.5.9(continued). Heave Model-Mean response in landing run
 Key: Aircraft sink velocity, 0.6 m/s ———, 0.9 m/s - - - - - , 1.2 m/s ,

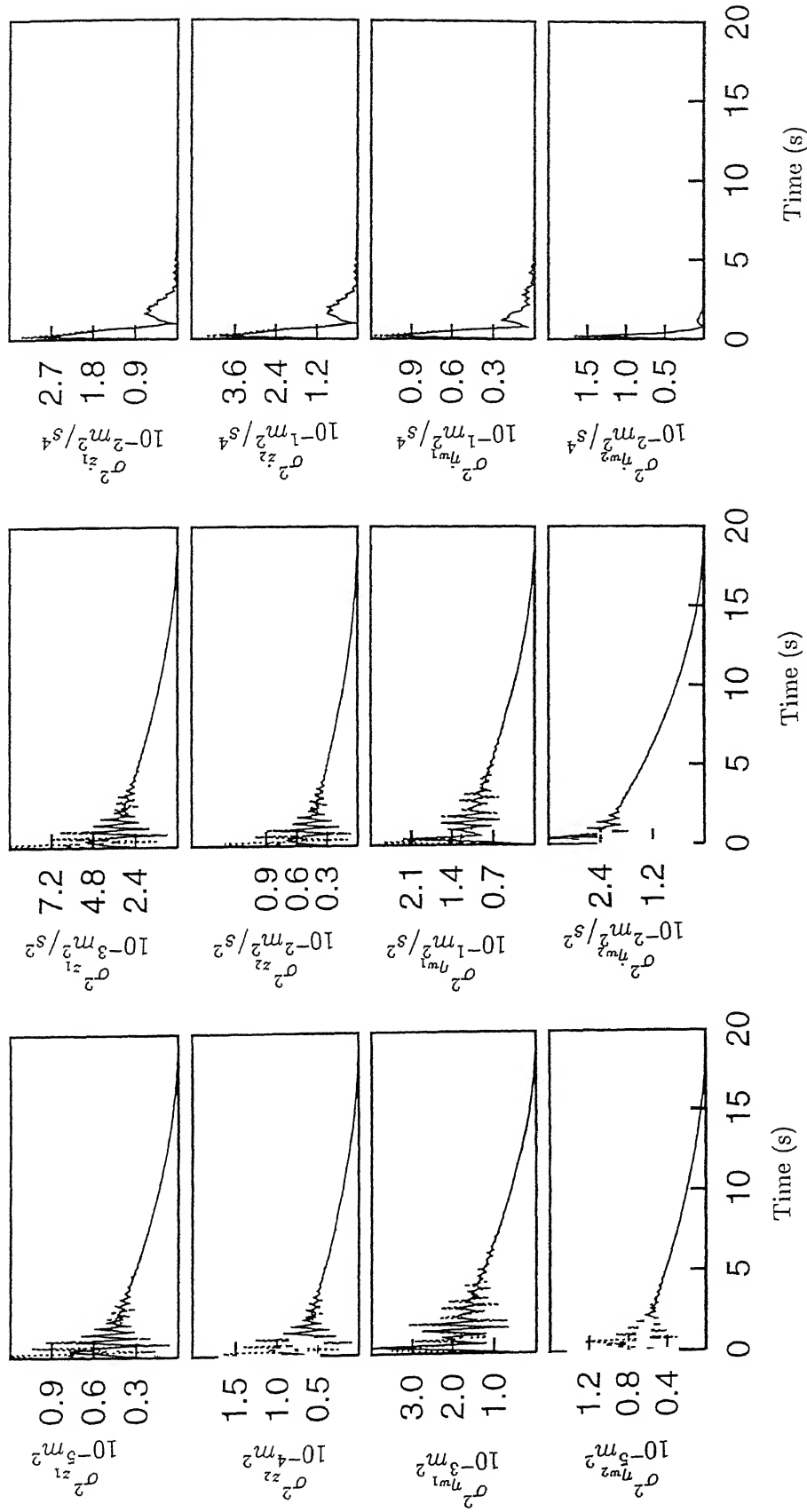


Fig.5.10. Heave Model-Response variance in landing run.
Key same as Fig.5.9.

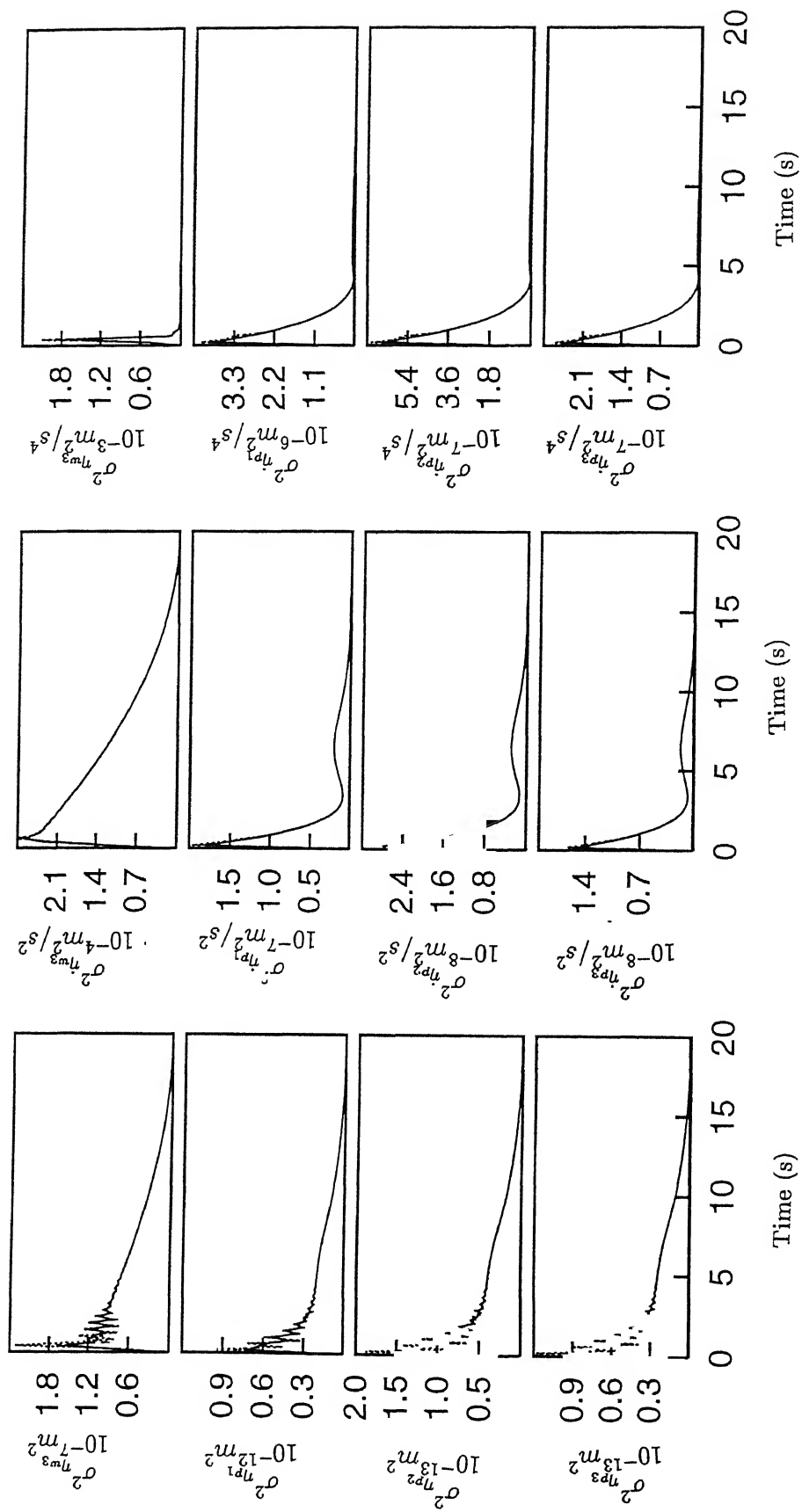


Fig.5.10(continued). Heave Model-Response variance in landing run. Key same as Fig.5.9

The input track frequency sensed by the vehicle is modified by its forward velocity and are higher for higher velocities. The mean response show low frequency components superimposed with higher frequency components. The lower frequency elements indicate sensitivity to the vehicle forward velocity. However, the higher frequency components undergo little modification with the forward velocity.

Mean responses of the wing normal coordinates show distinct single dominant frequency at transient stage which persist for a long duration. The response behaviour of track normal coordinates show low amplitude vibration at track input frequency which change with the change in the vehicle speed.

The response variances, presented in Fig.5.12, show large number of peaks, gradually decreasing with time. The distinctness of the pattern is reduced from displacement to velocity, to acceleration. Higher forward velocity induces stronger response. The higher frequency component does not show significant variation with change in forward velocity. The acceleration response attains steady state in a very short duration.

5.2.2.2 *Takeoff Run*

Fig.5.13 shows the mean response during takeoff. These have initial low values, subsequently rise with the increasing speed of the vehicle. Influence of mean track profile is apparent on the aircraft lumped masses showing low frequency components superimposed with small amplitude high frequency components. The low frequency component indicates sensitivity to the magnitude of the forward motion. The mean displacement and acceleration

decrease prior to takeoff. The aircraft pitch rotations are found to be oscillatory in pattern. The track normal coordinates also have oscillatory pattern that gradually increase in magnitude with passage of time. The longest takeoff time induces highest track mean response.

Fig.5.14 represents the response variances during takeoff. As the vehicle starts from rest, increasing its speed gradually, it takes some time for the track input to become effective. When the effective speed level is attained, variances are found to increase with the increase in speed showing an oscillatory pattern over an increasing mean value. The high frequency components reduce with the time derivative of the response for the continuous member, being lower in velocity and acceleration.

5.2.2.3 *Landing Run*

Mean responses are presented in Fig.5.15. The effect of impact at touch down, which increases with increase in the sink velocity, is revealed in the mean response. With the progress of landing run, initial energy gets dissipated and response shows dependence only on the track roughness inputs. Pitching motion of the sprung mass is found less dependent on the sink velocity. The nose gear mean displacement and velocity show much slower dissipation of impact energy. Main gear response magnitudes are less compared to the nose gear mean characteristics. Track normal coordinate displacement means are found to be more sensitive to the change of sink velocity compared to the velocity and acceleration response. The track acceleration shows a high value at touch down impact which steeply falls with time to a very low value.

Response variances during landing run are presented in Fig.5.16. The variance pattern is oscillatory in general. The effect of touch down impact is also seen here with initial high peak response which subsequently decreases with reduction in the vehicle speed. The magnitude of the peak is higher for higher sink velocity. Effect of sink velocities is seen to be present in the wing higher normal modes. Track normal coordinate displacement variances show pronounced fluctuations compared to velocity and acceleration variance. Displacement variance magnitude has greater dependence on the sink velocity.

The wing has coupled bending - torsion behaviour and a space distribution of the bending - torsion displacement ratios in the first three modes are shown in Fig.5.17. The figure reveals strong coupling between the two motions in the second and third modes compared to the first one. The first mode response is mainly dominated by the bending deformation towards the tip for the system parameters selected in the study.

5.2.3 Heave-Pitch Model with Fuselage flexible in Bending

For this model, first five flexural modes of the fuselage are considered out of which first two represent rigid body heave and pitch degrees of freedom. The other three represent elastic bending modes. Besides these, two lumped masses heave degrees of freedom, wing and track first three generalised coordinates are considered as in the previous rigid model. The response characteristics of the thirteen generalised coordinates are presented for the taxi, takeoff and landing run. Results have been presented for one wing only.

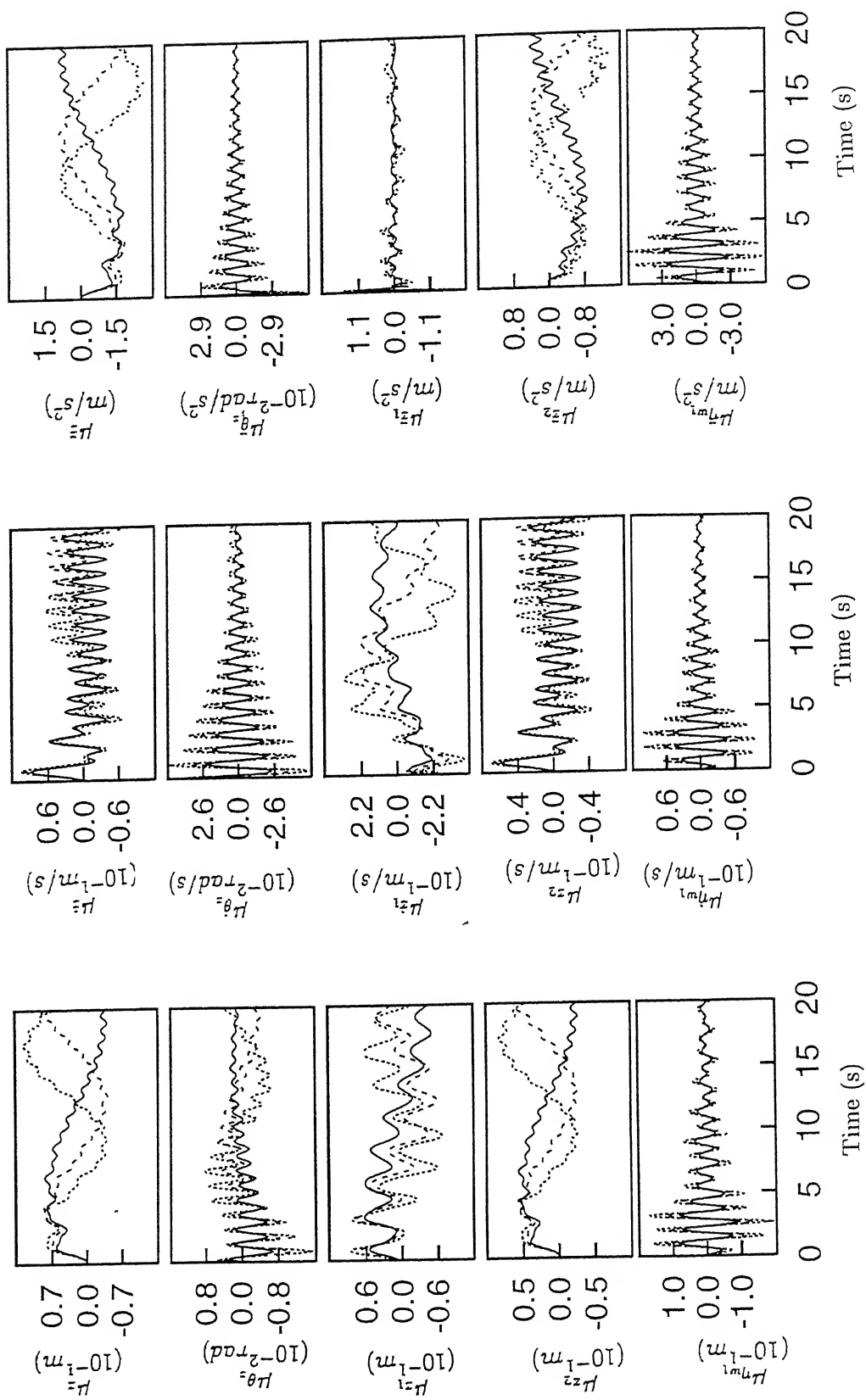


Fig.5.11. Heave-Pitch Model (Rigid fuselage)-Mean response in taxi run. Key same as Fig.5.5

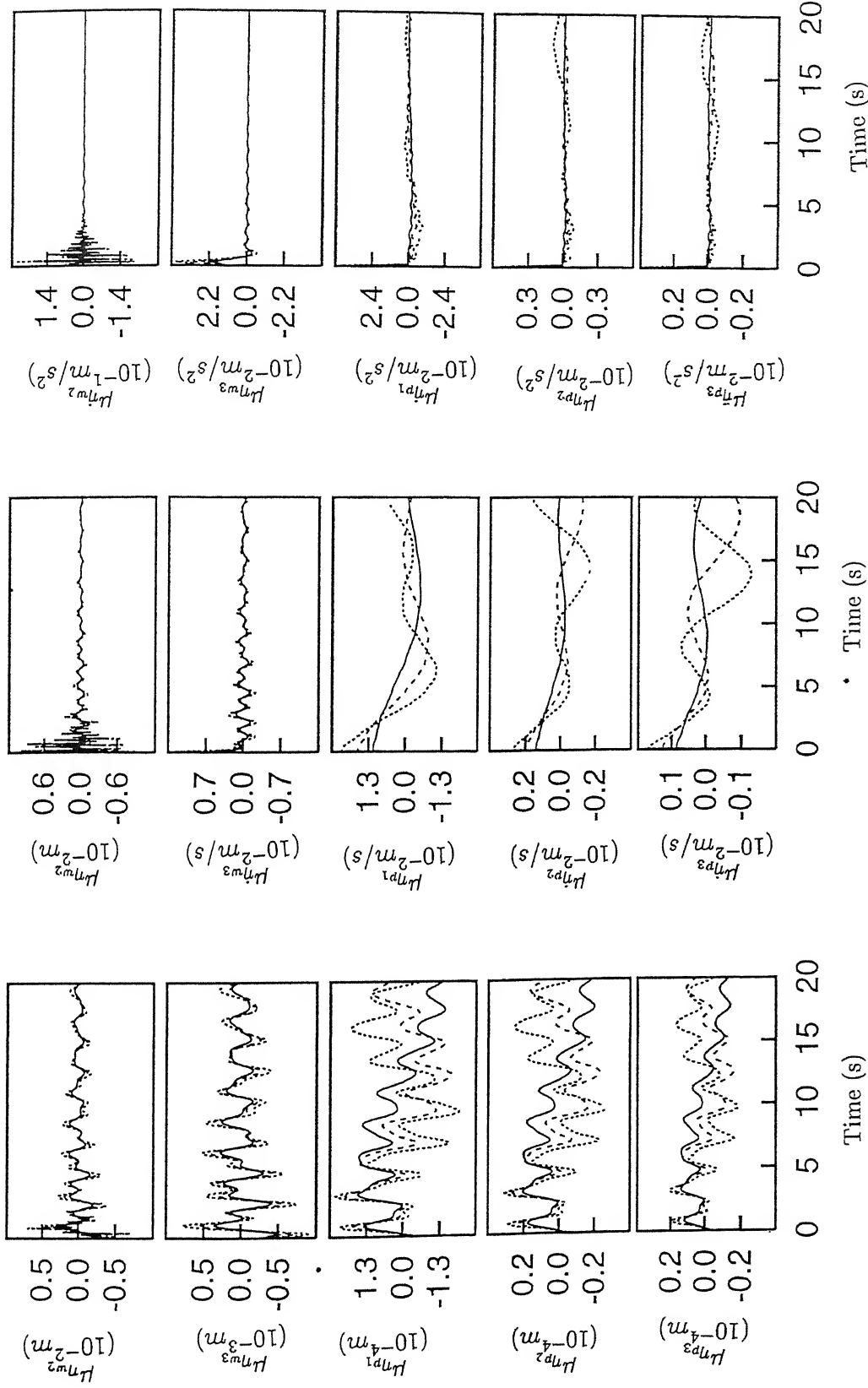


Fig.5.11(continued). Heave-Pitch Model (Rigid fuselage)-Mean response in taxi run. Key same as Fig.5.5

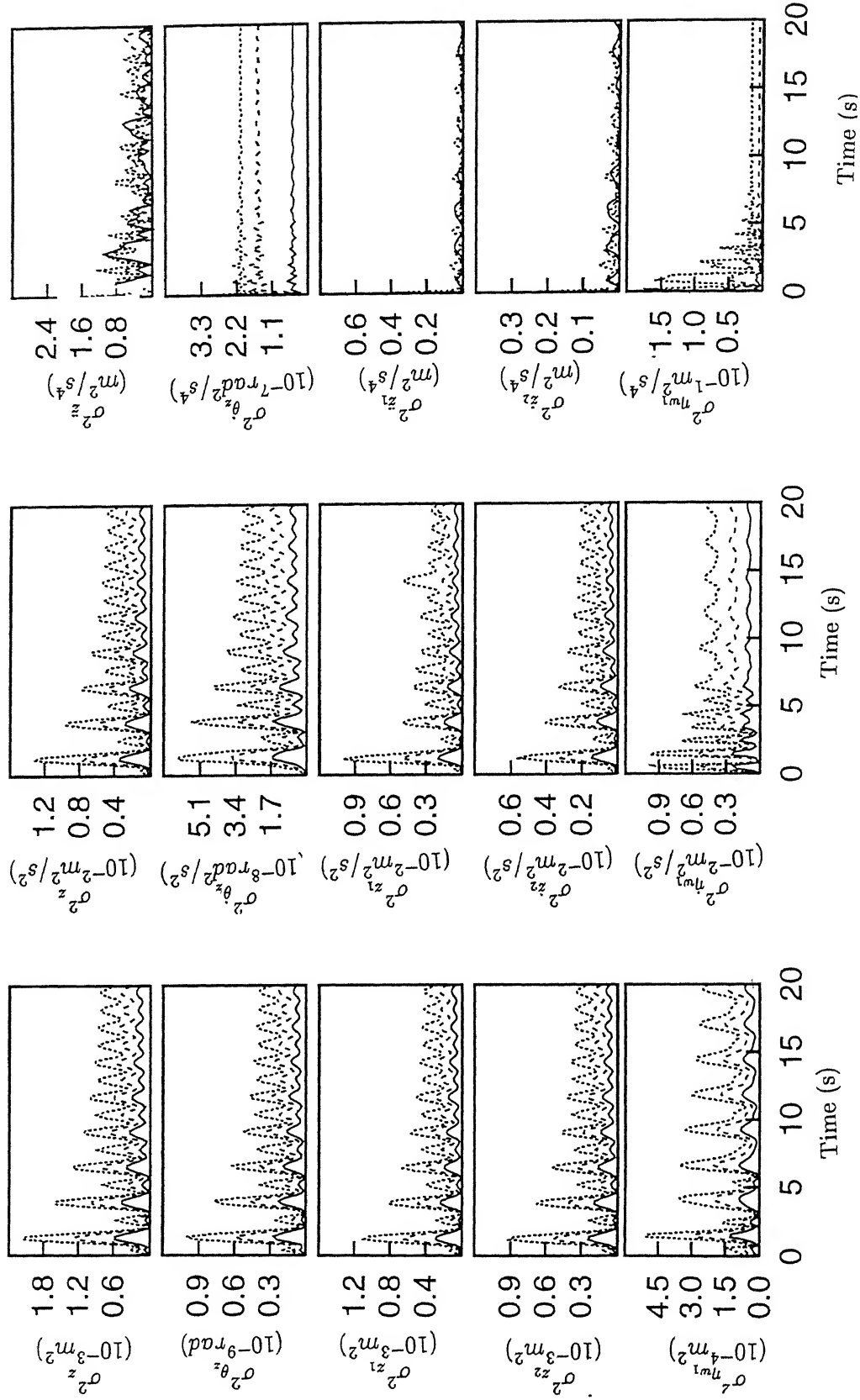


Fig.5.12. Heave-Pitch Model (Rigid fuselage)- Response variance in taxi run. Key same as Fig.5.5

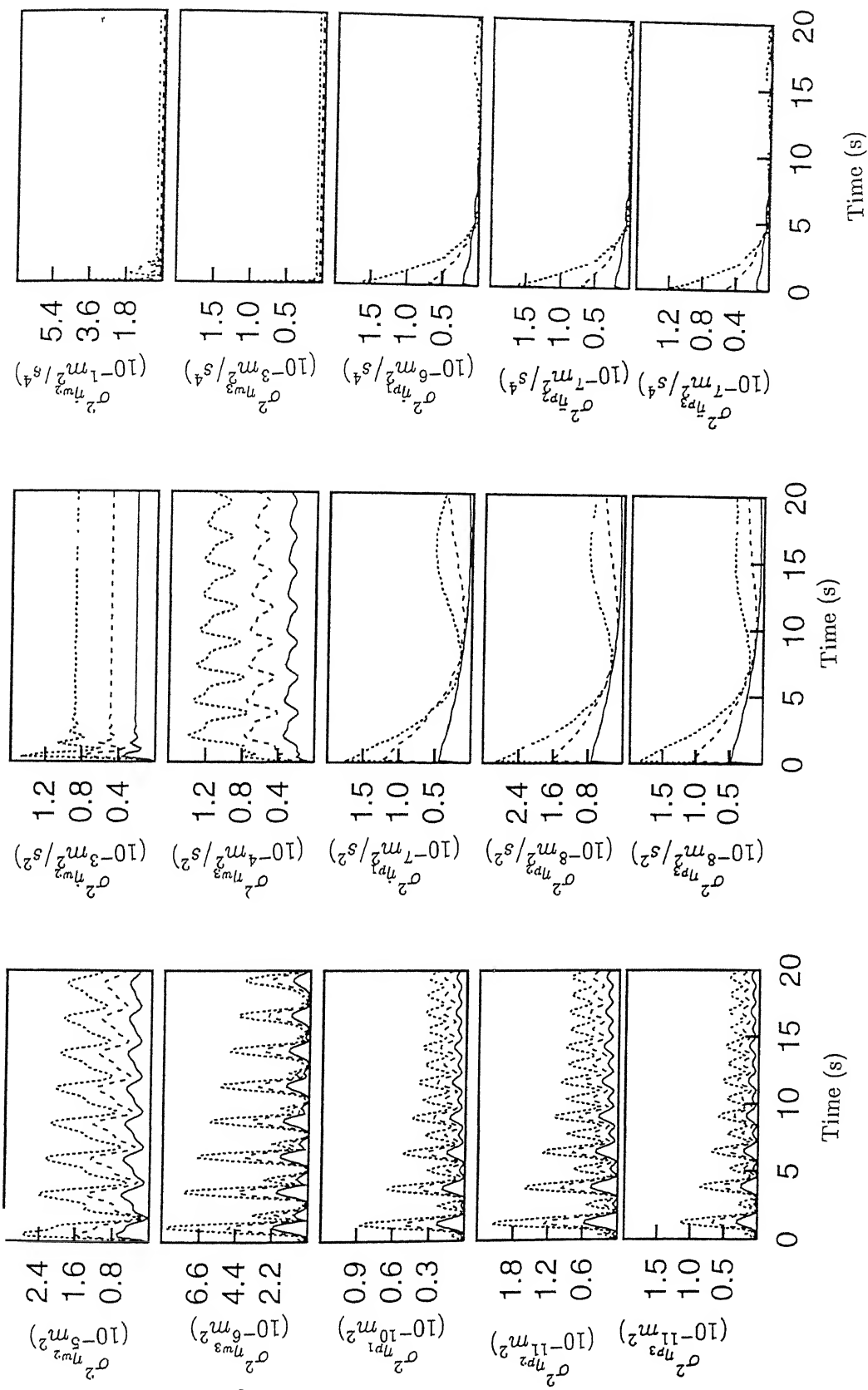


Fig.5.12(continued). Heave-Pitch Model (Rigid fuselage)-
Response variance in taxi run. Key same as Fig.5.5

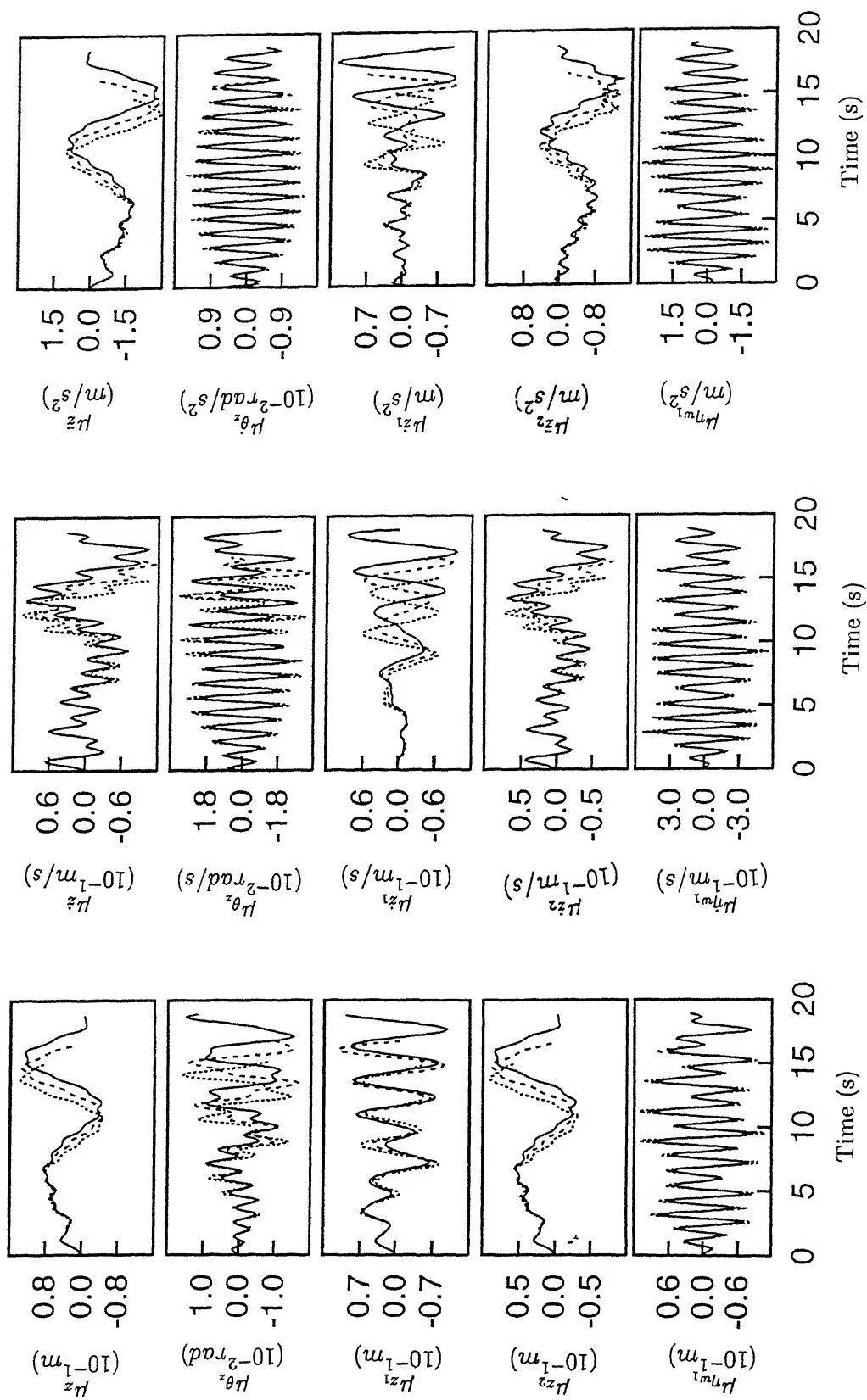


Fig.5.13. Heave-Pitch Model (Rigid fuselage)-Mean response in takeoff run. Key same as Fig.5.7

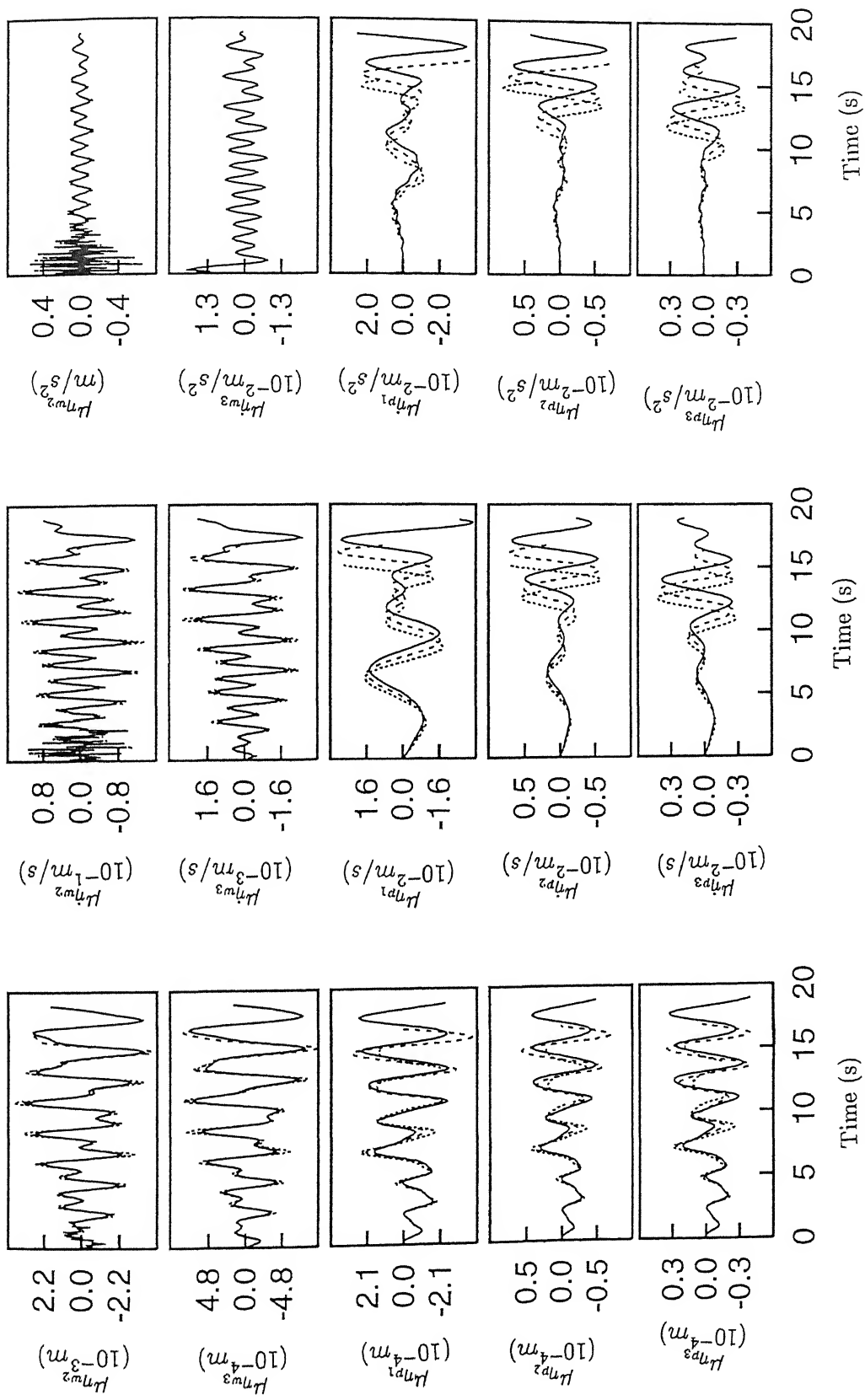


Fig.5.13(continued). Heave-Pitch Model (Rigid fuselage)-Mean response in takeoff run. Key same as Fig.5.7

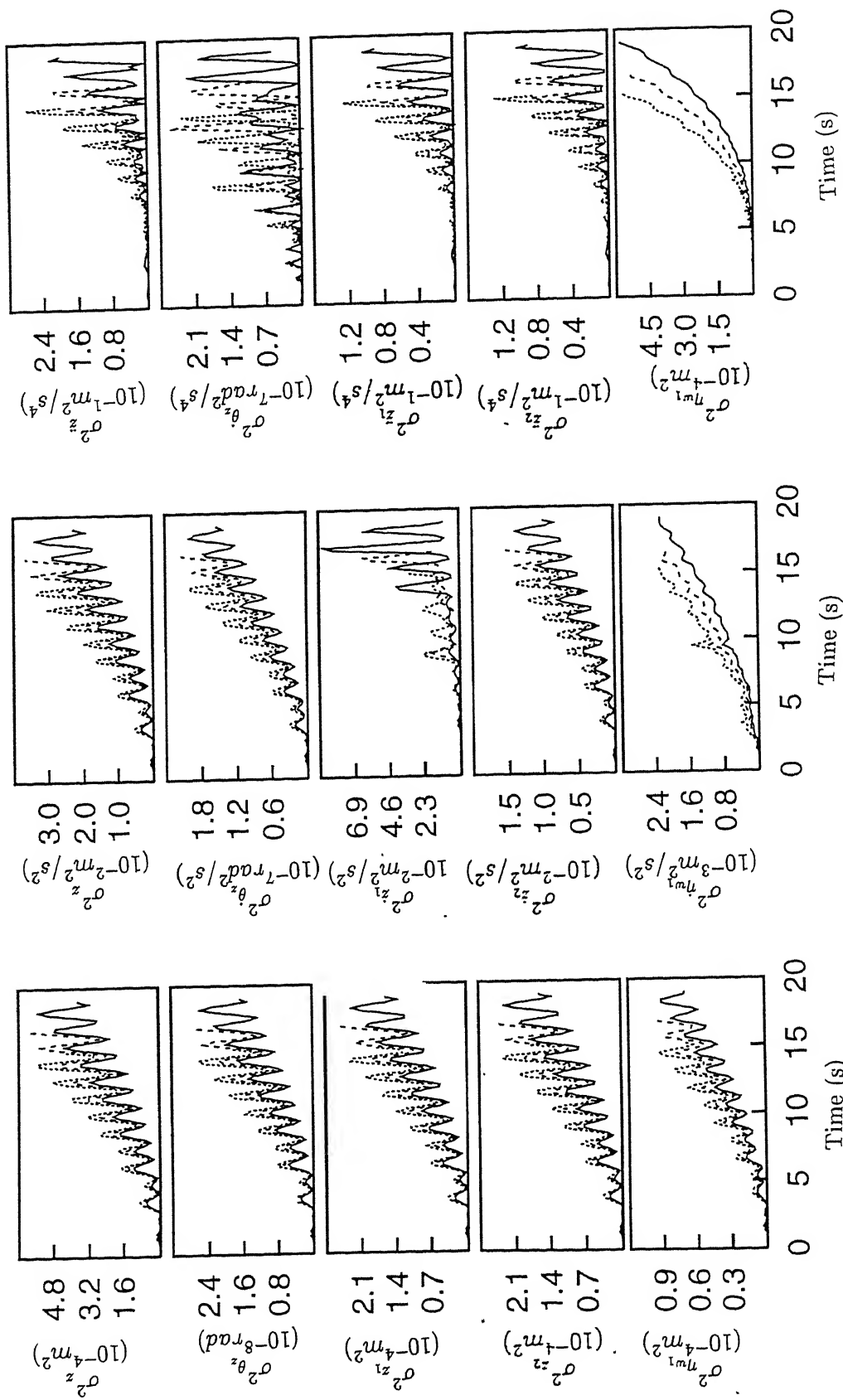


Fig.5.14. Heave-Pitch Model (Rigid fuselage)-Response variance in takeoff run. Key same as Fig.5.7

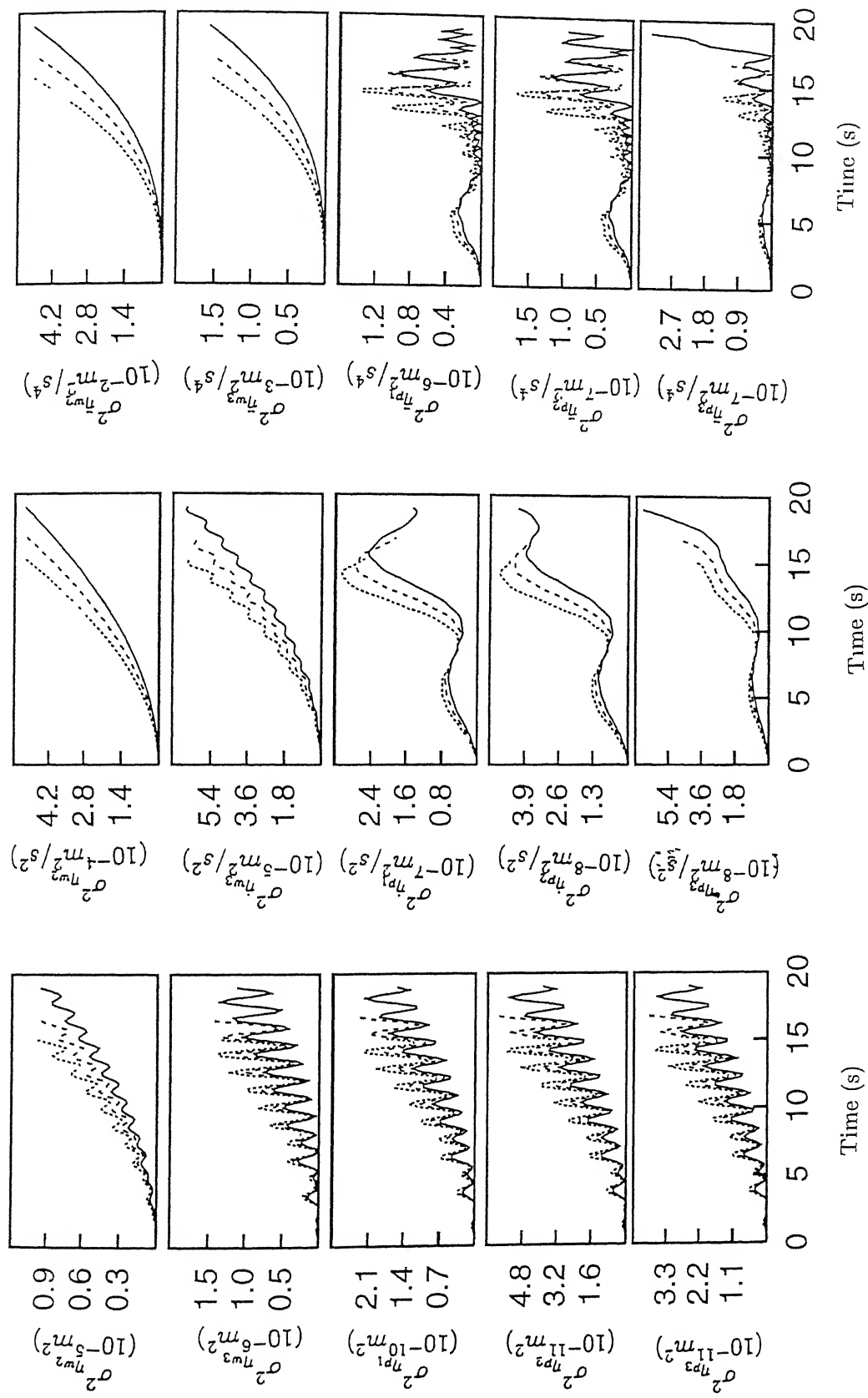


Fig.5.14.(continued). Heave-Pitch Model (Rigid fuselage)-
Response variance in takeoff run. Key same as Fig.5.7

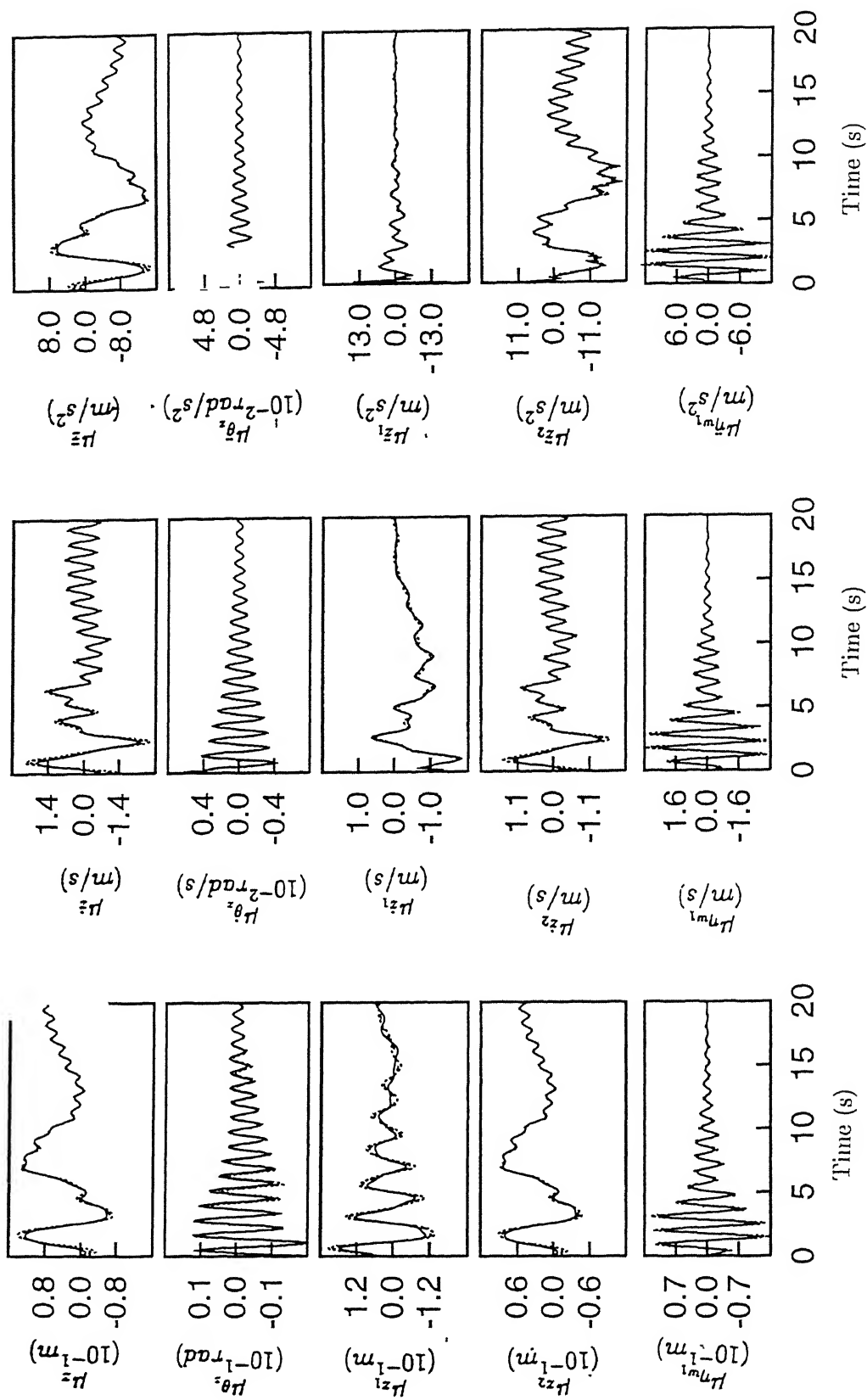


Fig.5.15. Heave-Pitch Model (Rigid fuselage)-Mean response in landing run. Key same as Fig.5.9

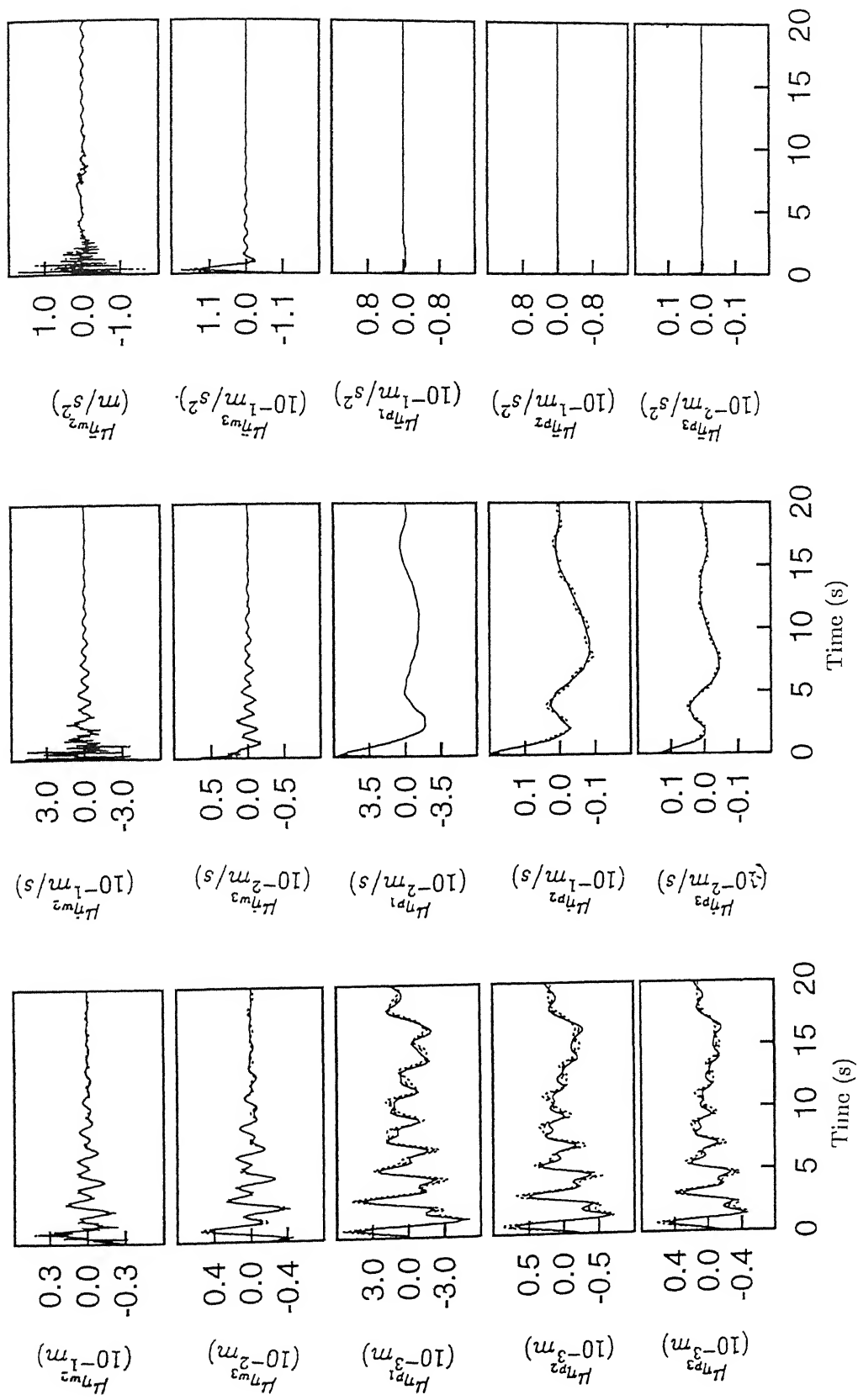


Fig.5.15(continued). Heave-Pitch Model (Rigid fuselage)-Mean response in landing run. Key same as Fig.5.9

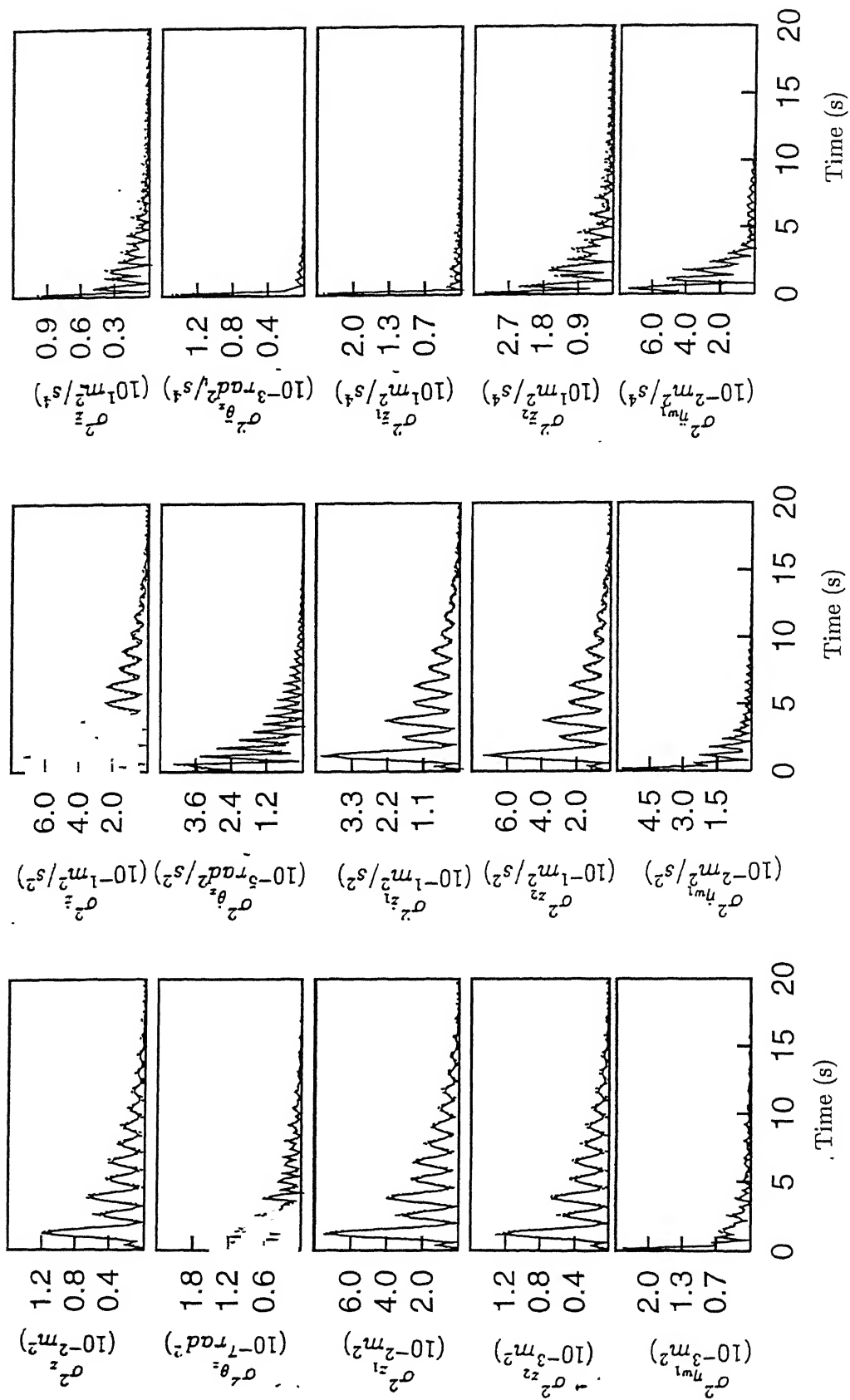


Fig.5.16. Heave-Pitch Model (Rigid fuselage)-Response variance in landing run. Key same as Fig.5.9

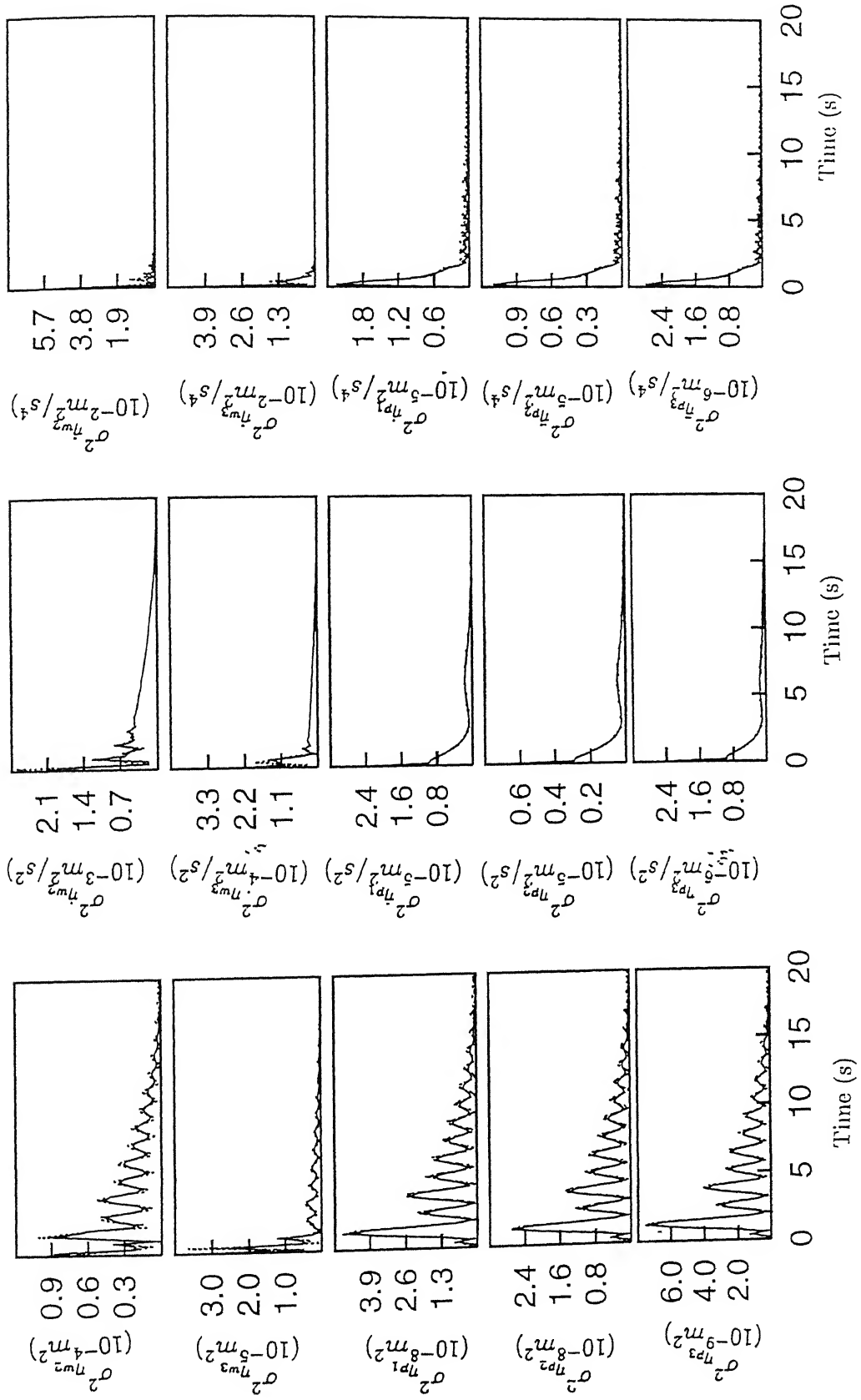


Fig.5.16(continued). Heave-Pitch Model (Rigid fuselage)-
Response variance in landing run. Key same as Fig.5.9

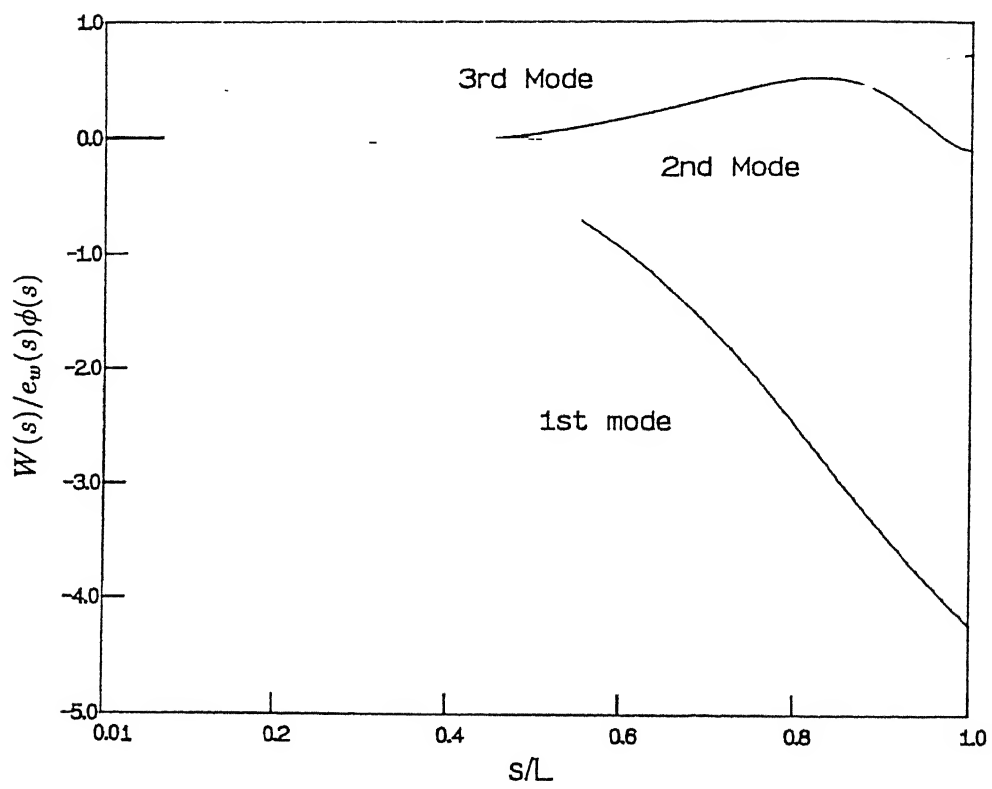


Fig.5.17. Bending-torsion displacement ratio of wing.

5.2.3.1 Taxi Run

The mean system response are presented in Fig.5.18. Rigid body vertical motion and bending deformations of the fuselage show the influence of mean track profile. Track input frequency is modified by the vehicle forward velocity. Flexural response have low values at the end of taxi run compared to rigid body vertical heave motion. Pitch motion exhibits high frequency components initially, which diminished with passage of time. Wheel response also have more or less a similar pattern. Acceleration of the nose gear shows high initial value which gradually decreases to reach a low steady state value. Initial oscillations do not show much variations with the change in vehicle velocity. This points to their association with structural modes rather than the external excitation.

Mean response of wing's normal coordinates shows less sensitivity to track influence in the lower modes. Higher mode response, however, indicates a increase in frequency with increase in the vehicle speed. Track normal coordinate displacement and velocity means show an increase in magnitude with increasing level of track mean height experienced by the wheels. Track accelerations have higher values at the onset of motion. This may be due to the shock on entry of the vehicle over the track.

Response variance during taxi run are presented in Fig.5.19. Variances are oscillatory in the initial stage with a high peak at the initiation of motion. These subside to reach steady asymptotic levels with passage of time. The acceleration variances achieve steady value within a shorter time compared to displacement and velocity. Track mode characteristics show low

frequency variation in the steady state part. Higher vehicle velocity is found to increase the response magnitudes. The response of the elastic members indicate substantial contributions from the lower modes also.

5.2.3.2 Takeoff Run

Fig.5.20 presents mean response during takeoff. Fuselage generalised coordinates have dominant low frequency components with small amplitude high frequency components superimposed over it. The response amplitudes show an initial low value which gradually builds up with increase in speed and track mean level. Higher forward acceleration generates higher response. Differences are observed at take off instant depending on its location in the low frequency cycle. Influence of mean track profile is apparent in the air frame as well as main wheel response. Nose wheel response during takeoff is found to be smaller compared to the main wheel. The airframe and wing lower modes show marginal reduction in amplitude with progress in time. Track normal coordinates mean response also show a dominant low frequency component with gradually increasing amplitude. The velocity response have superimposed high frequency small amplitude components while the acceleration response have some low frequency components also.

Fig.5.21 represents the response variances during takeoff. When the effective speed level for the aircraft is achieved, variances are found to increase steadily with the increase in vehicle speed. Oscillatory pattern over an increasing mean value is noticeable in most of the cases. A gradual increase in response

variance is also observed in the track normal coordinates. The oscillatory pattern over increasing mean level and amplitude is more pronounced for the track modes.

5.2.3.3. *Landing Run*

Mean responses are presented in Fig.5.22. The effect of impact at touchdown, which increases with increase in sink velocity, is revealed in the mean response. As in the previous model, with the progress of the landing run, impact energy gets dissipated and response shows dependence only on the track roughness input. Higher bending modes of the fuselage show increasing mean of the response pattern with progress of the landing run. Main wheel displacement response has faster dissipation of the impact energy compared to the nose wheel.

Wing generalised coordinate mean responses have much higher peaks at impact phase compared to the response amplitudes in the later part of the landing run. Response in the wing's higher modes are found to damp out much faster than the lower modes for velocity and acceleration. Mean responses of the track generalised coordinate also reveal the effect of landing impact. The magnitude of the track response at touchdown instant is higher than the constant velocity and accelerated runs.

Response variances for the landing run of the aircraft are presented in Fig.5.23. Oscillatory patterns are present for all the displacements and velocity response in the touchdown phase. Magnitudes of the first peaks seem to be higher with higher sink velocity. Response variances of the wing's second and third normal coordinates show single dominant peak at touch down phase which

steeply falls to lower values during the landing run. Track normal coordinates displacement variance show oscillations with higher frequency variation while velocity and acceleration responses have dominant low frequency components.

5.2.4 Heave-Pitch-Roll Model (Flexible fuselage in bending with rigid roll)

In this model, response of five generalised coordinates of fuselage flexure , rigid body roll of fuselage, three unsprung masses vertical bounce motion, first three normal coordinates of left and right wing coupled bending-torsion modes and first three flexural modes of the track have been considered. The first two fuselage generalised coordinates give the rigid body heave and pitch motion. Plots have been presented for eighteen generalised system modes in taxi, takeoff and landing runs of the aircraft.

5.2.4.1 *Taxi Run*

Mean system response are presented in Fig.5.24. Fuselage rigid body bounce motion shows increase in displacement with increasing height of the track mean profile in presence of rising gradient selected for this study. Mean velocity and acceleration response show high transience set up at the onset of vehicle forward motion which tends to diminish with passage of time. The response magnitude is higher at the transient stage compared to value at the later stage. Pitch response reveals the presence of high frequency components which persists in transient and the steady state part. Change of vehicle forward velocity shows minor effect in case of pitch velocity and acceleration.

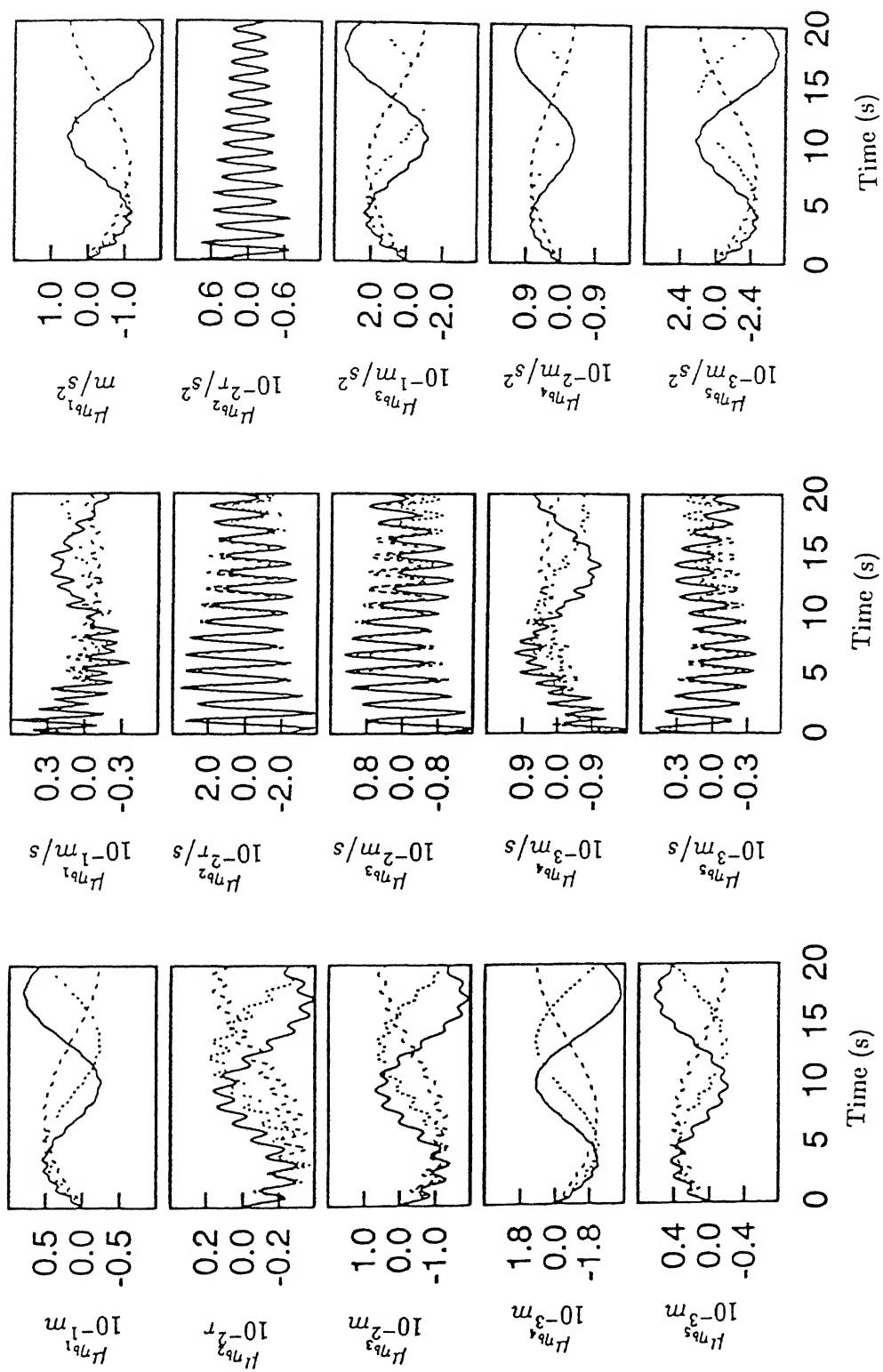


Fig.5.18. Heave-Pitch Model (Flexible fuselage in bending) - Mean response in taxi run.
Key: Vehicle forward velocity, 40 Km/h - - - - - , 60 Km/h....., 80 Km/h _____

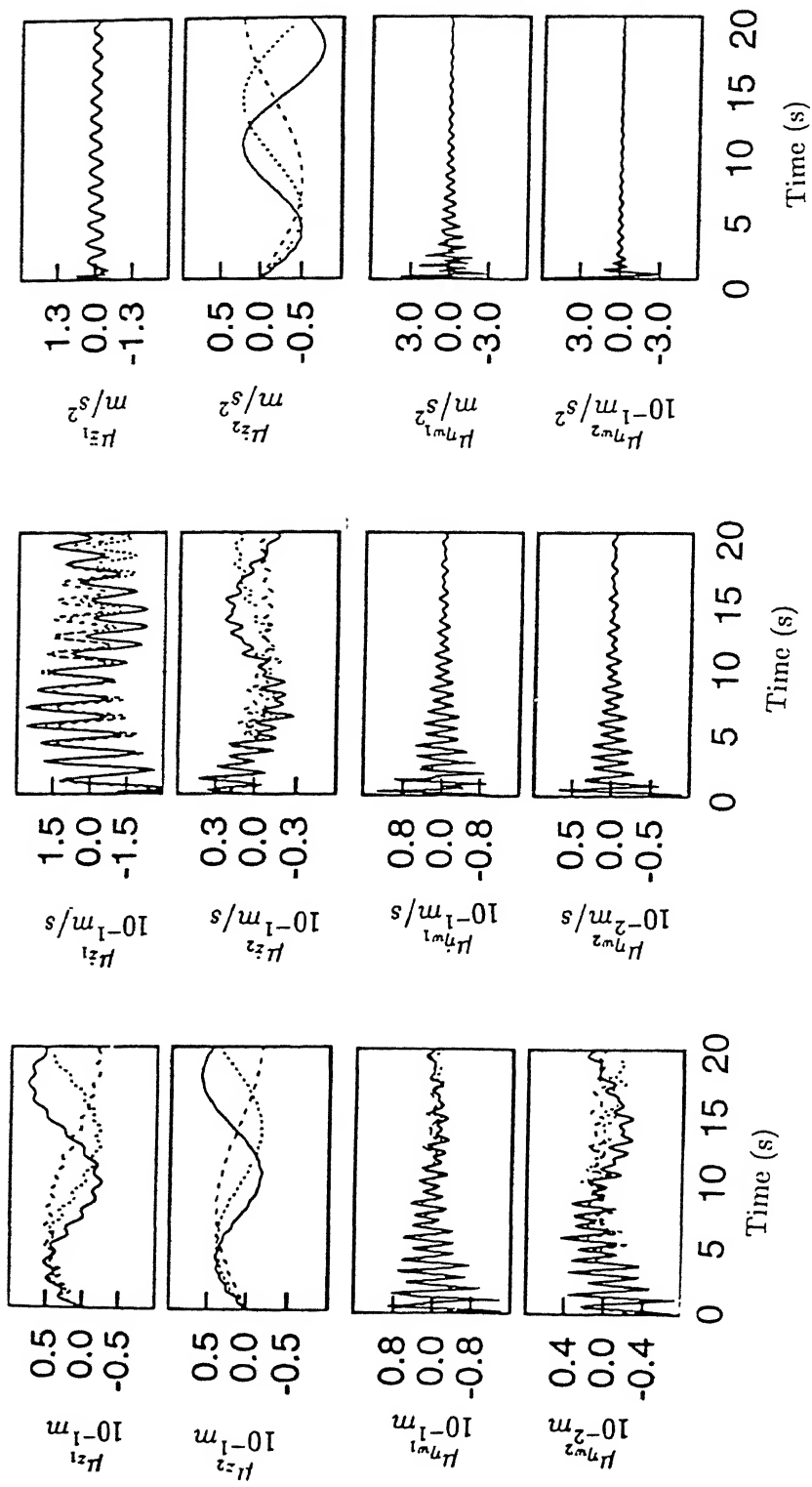


Fig.5.18(continued). Heave-Pitch Model (Flexible fuselage in bending)-Mean response in taxi run.
Key: Vehicle forward velocity, 40 Km/h ———, 60 Km/h....., 80 Km/h_____

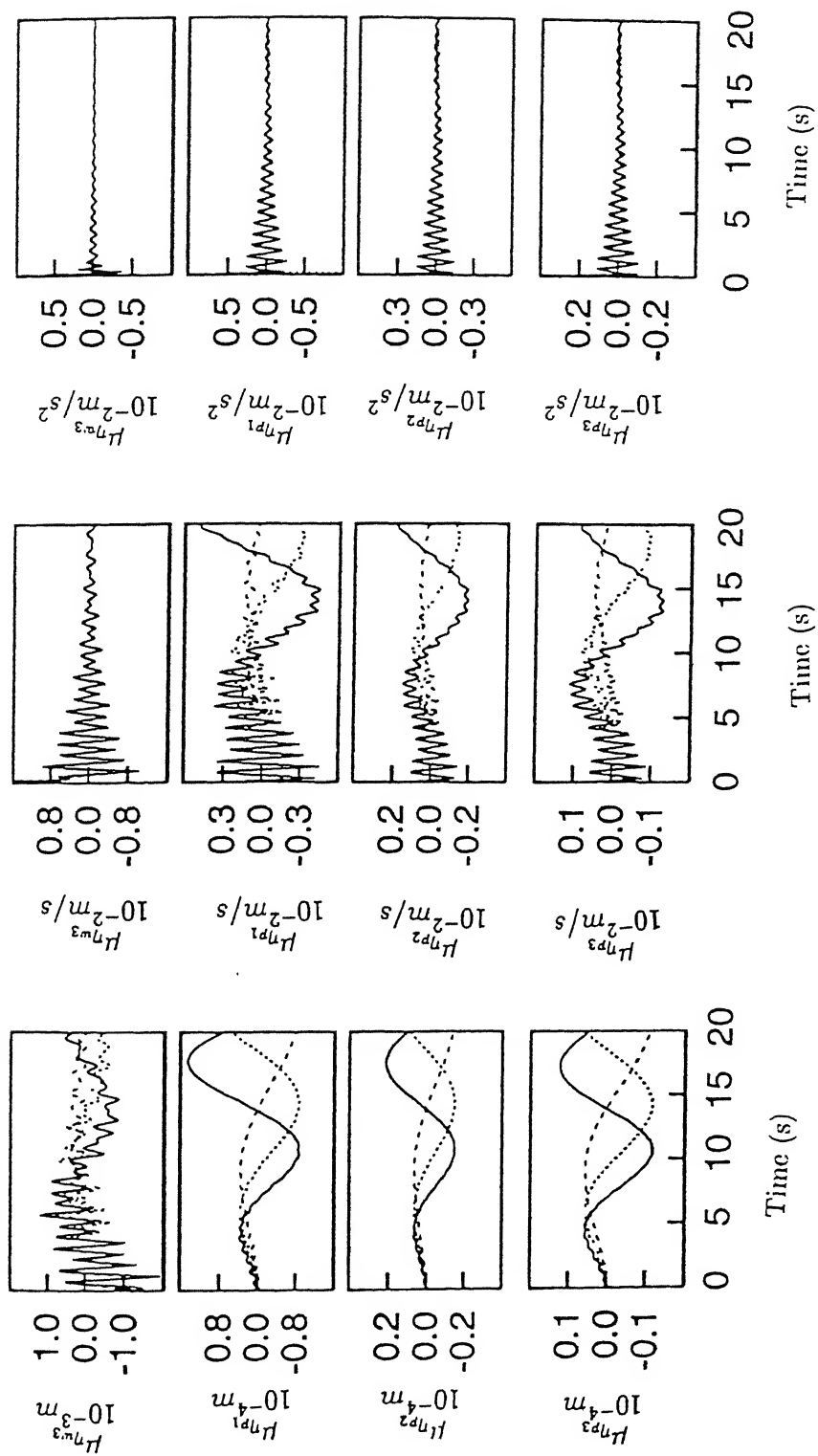


Fig.5.18(continued). Heave-Pitch Model (Flexible fuselage in bending)-Mean response in taxi run.
Key: Vehicle forward velocity, 40 Km/h —, 60 Km/h ---, 80 Km/h

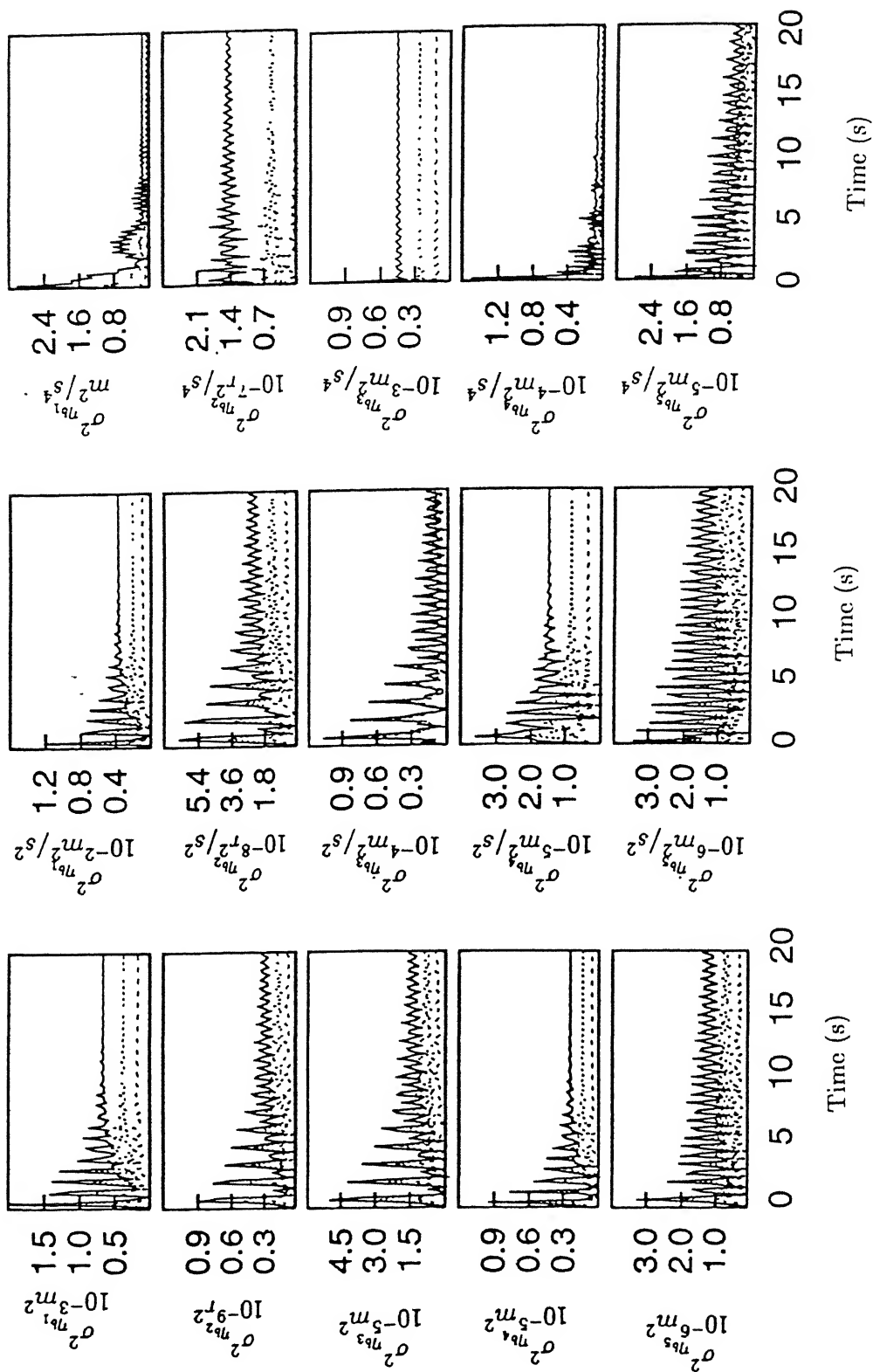


Fig.5.19. Heave-Pitch Model (Flexible fuselage in bending) - Resonse variance in taxi run. Key same as Fig.5.18

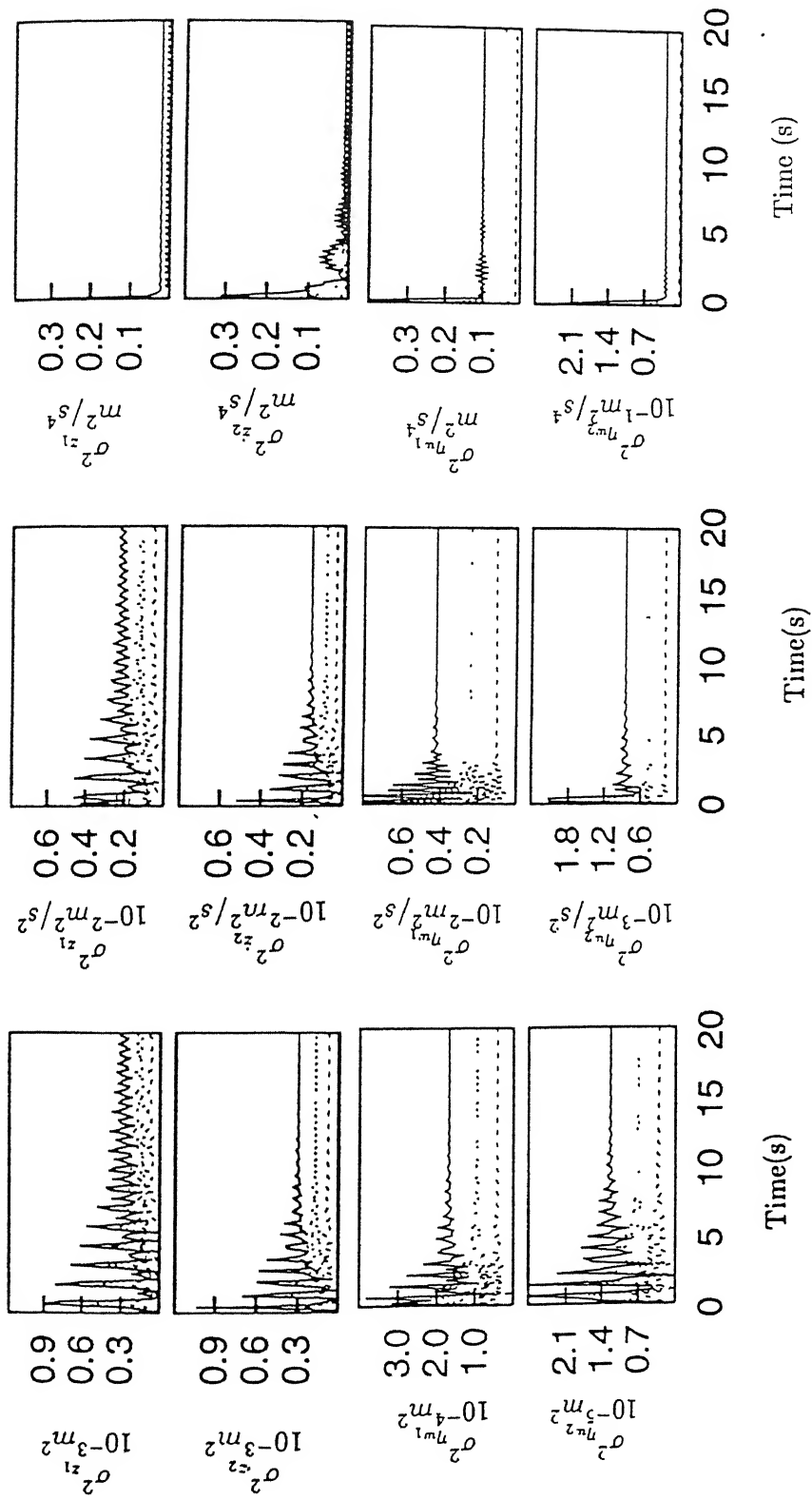


Fig.5.19(continued). Heave-Pitch Model (Flexible fuselage in bending)-Response variance in taxi run. Key same as Fig.5.18

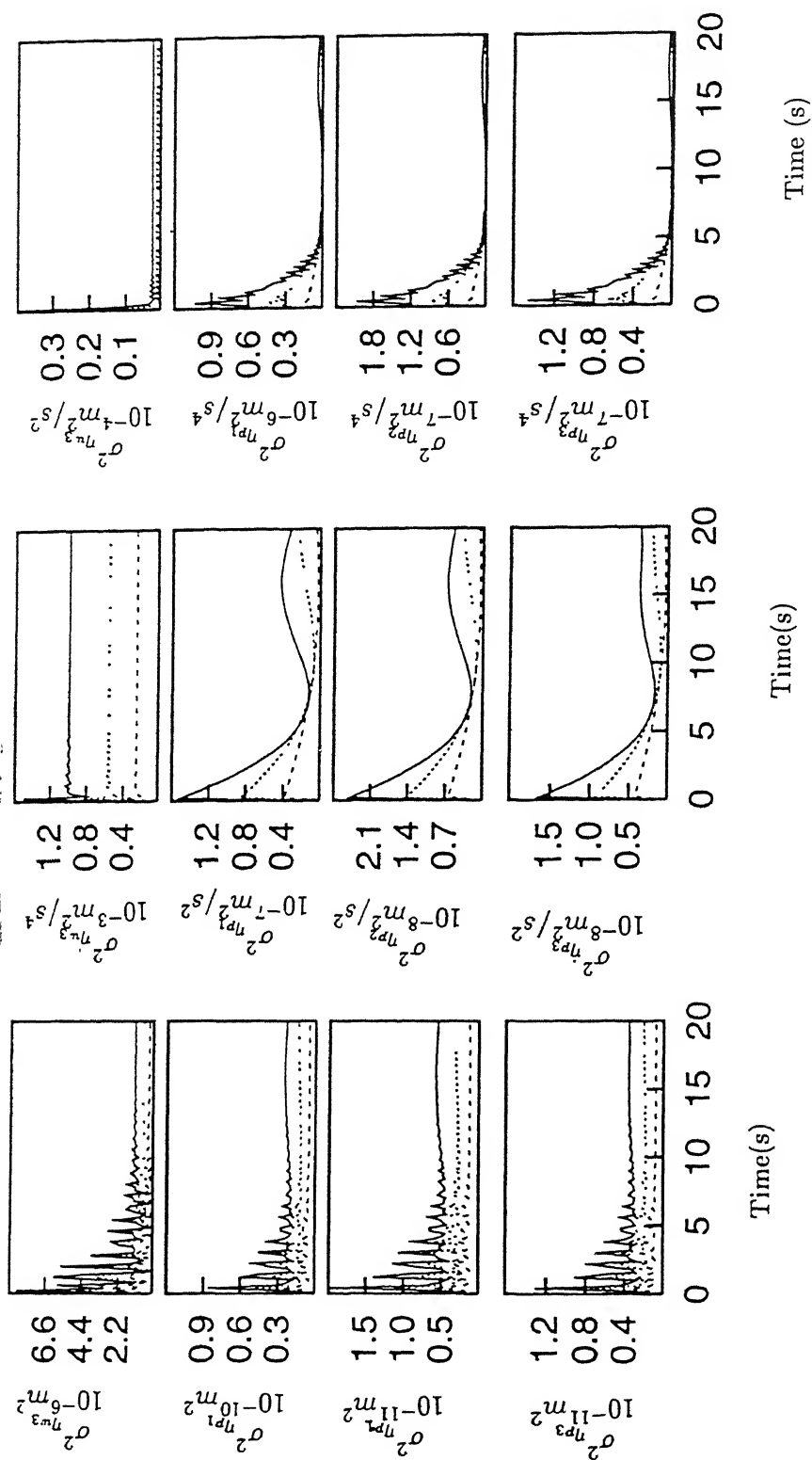


Fig.5.19(continued). Heave-Pitch Model (Flexible fuselage in bending)-Response variance in taxi run. Key same as Fig.5.18

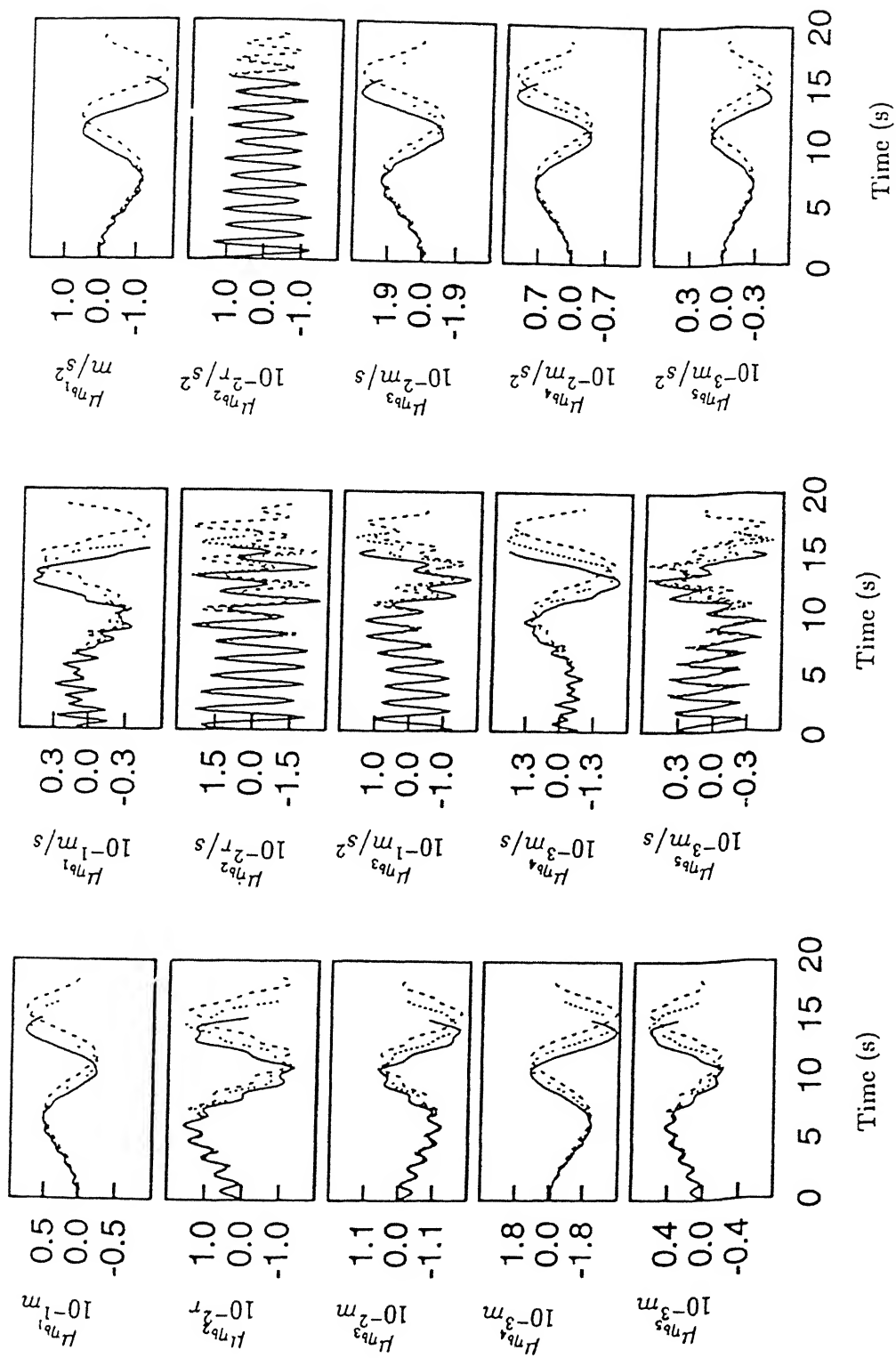


Fig.5.20. Heave-Pitch Model (Flexible fuselage in bending)-
Mean response in takeoff run.

Key: Vehicle forward acceleration, 1.6 m/s² ---, 1.8 m/s²,
2.0 m/s² _____

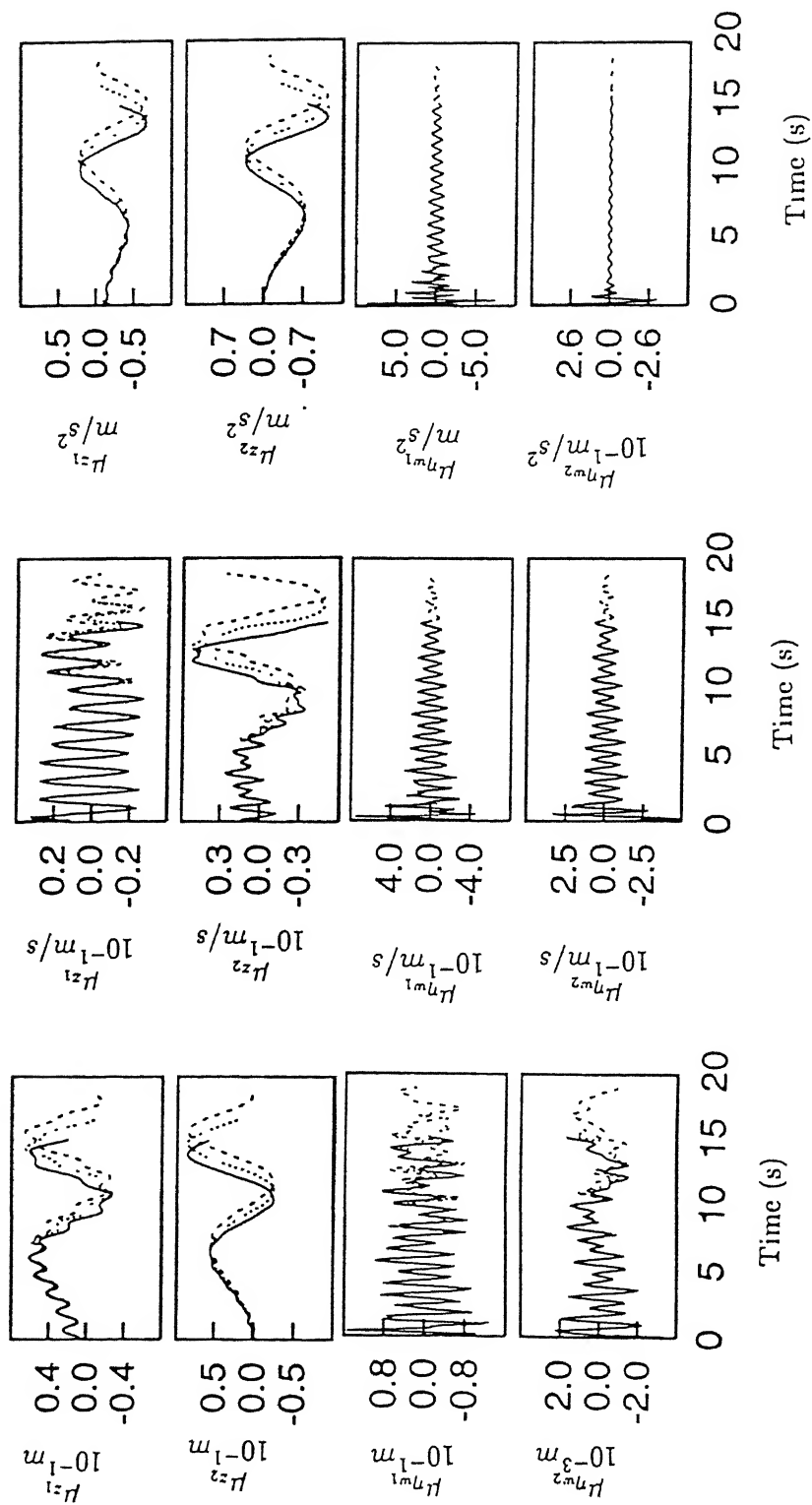


Fig.5.20(continued). Heave-Pitch Model (Flexible fuselage in bending)-Mean response in takeoff run.
Key: Vehicle forward acceleration, 1.6 m/s² — — — — —, 1.8 m/s²....., 2.0 m/s²_____

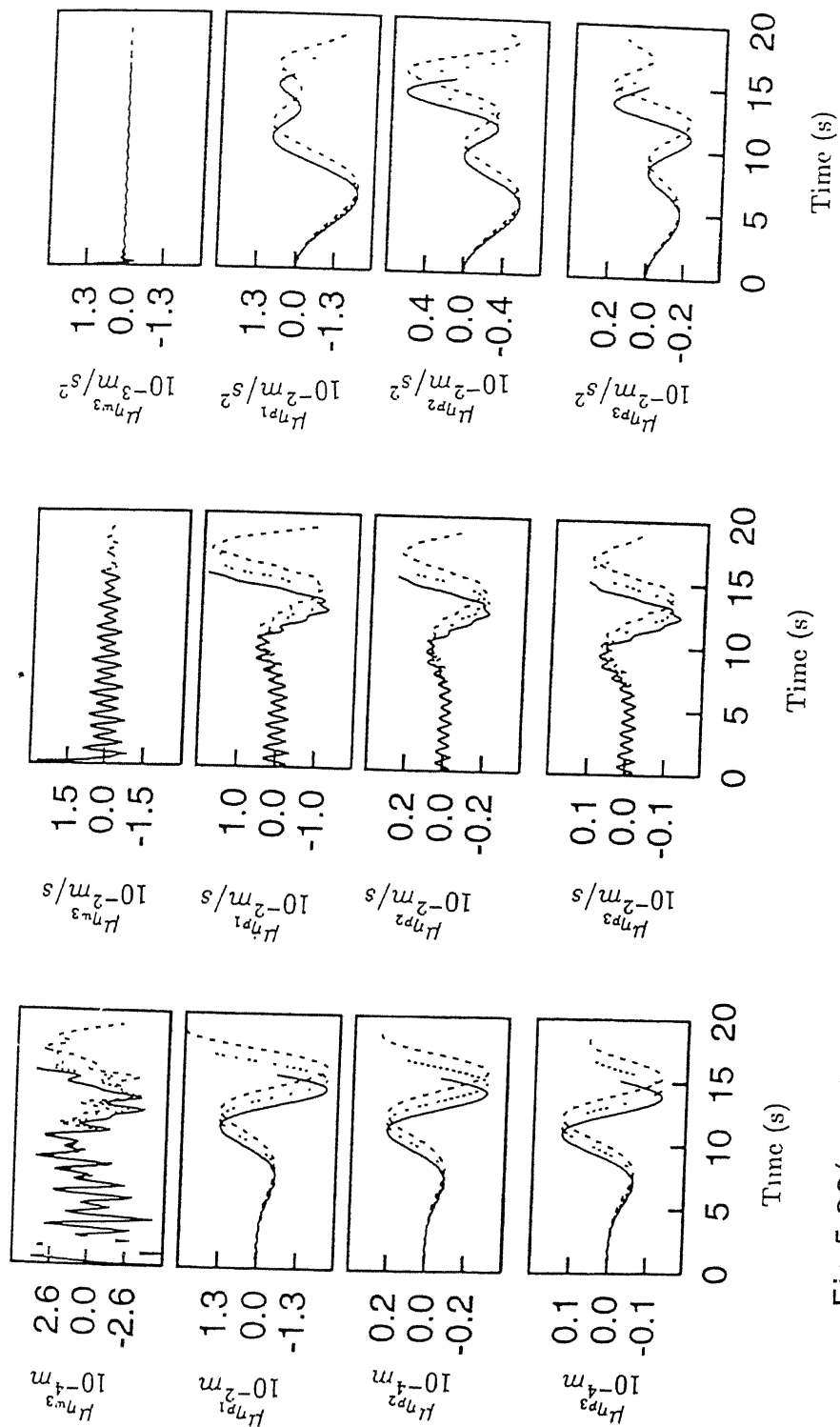


Fig.5.20(continued). Heave-Pitch Model (Flexible fuselage in bending)-Mean response in takeoff run.
Key: Vehicle forward acceleration, 1.6 m/s^2 —, 1.8 m/s^2 — — —, 2.0 m/s^2 — — — — —.

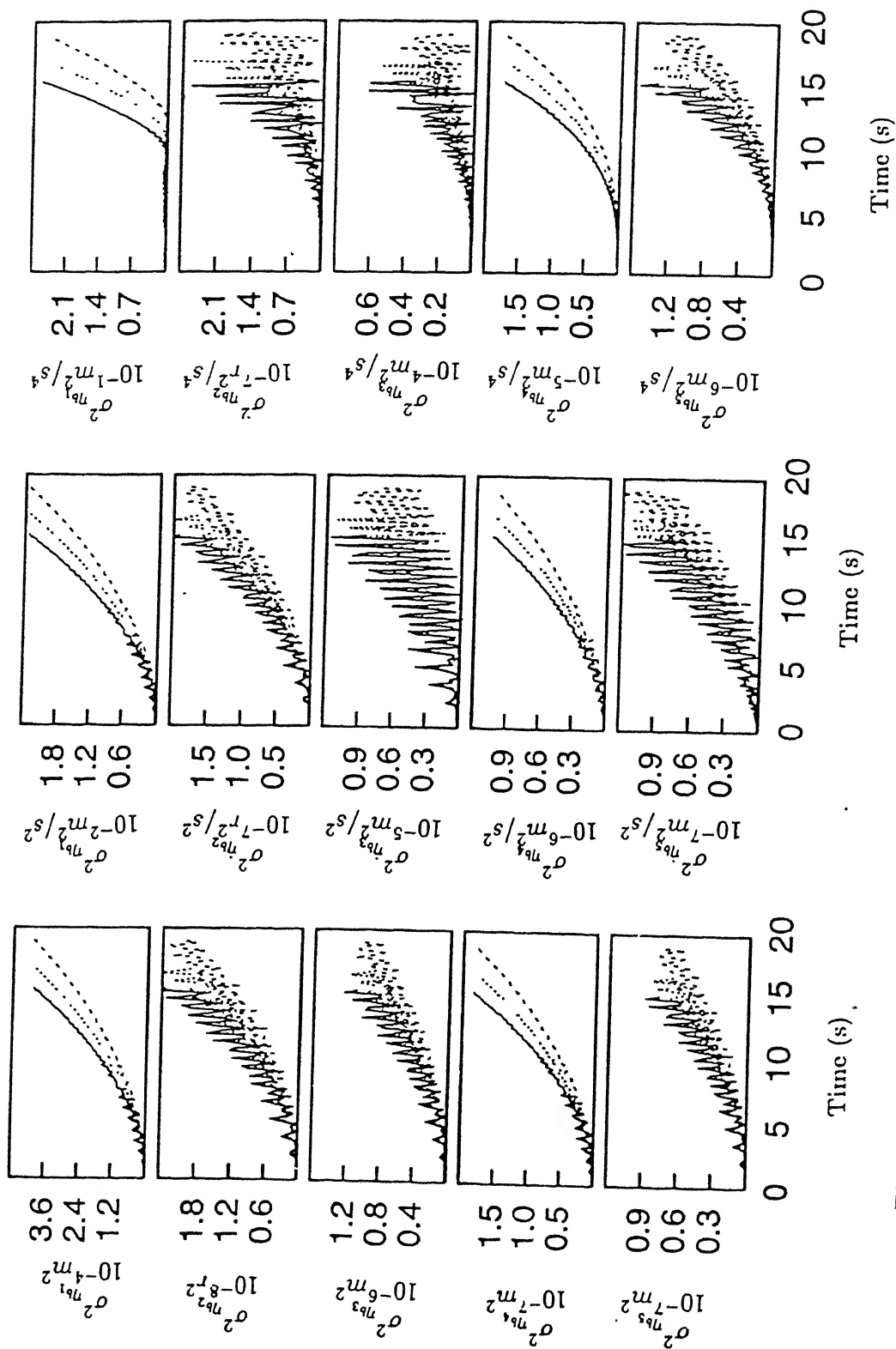


Fig.5.21. Heave-Pitch Model (Flexible fuselage in bending)-
Response variance in takeoff run.
Key same as Fig.5.20

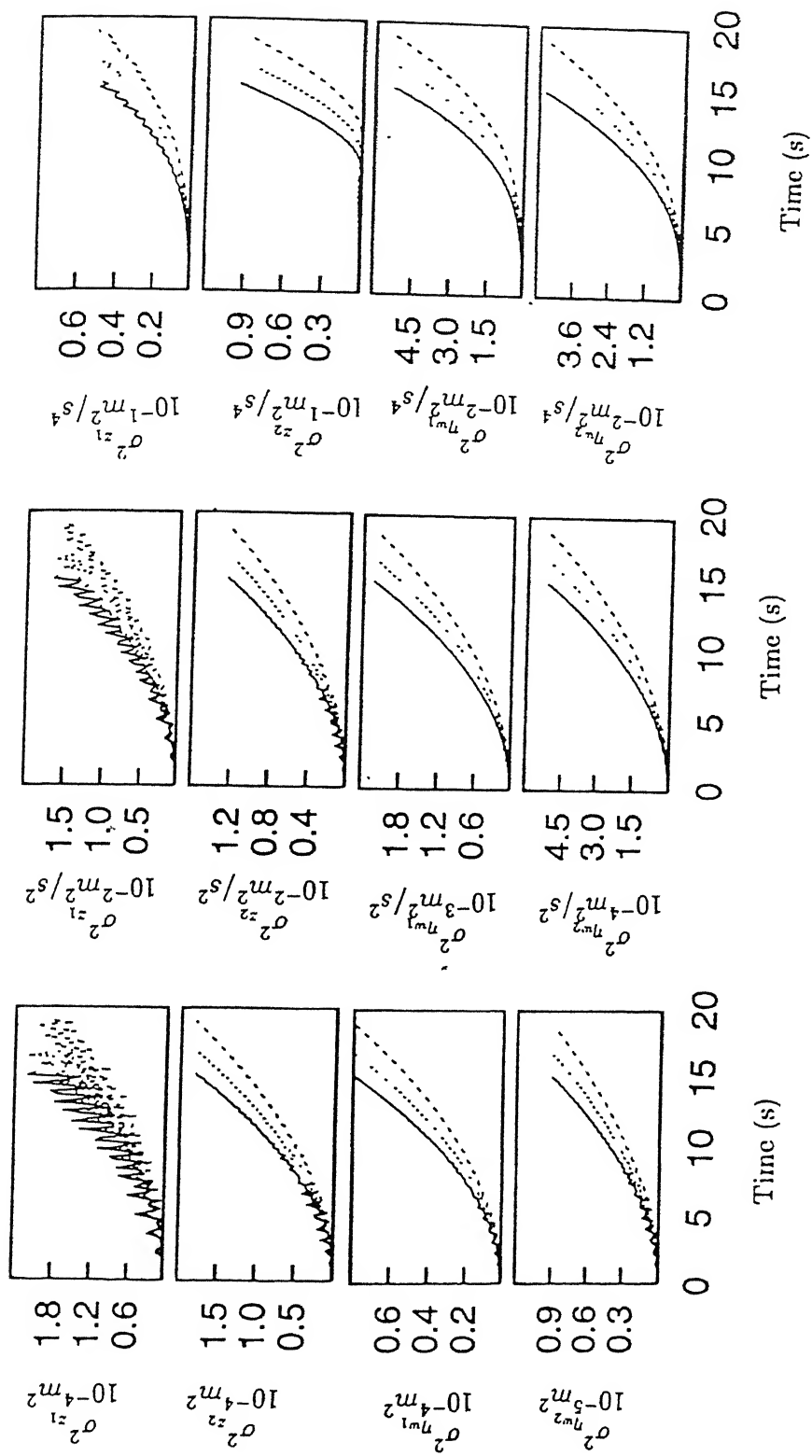


Fig.5.21(continued). Heave-Pitch Model (Flexible fuselage in bending)-Response variance in takeoff run. Key same as Fig.5.20

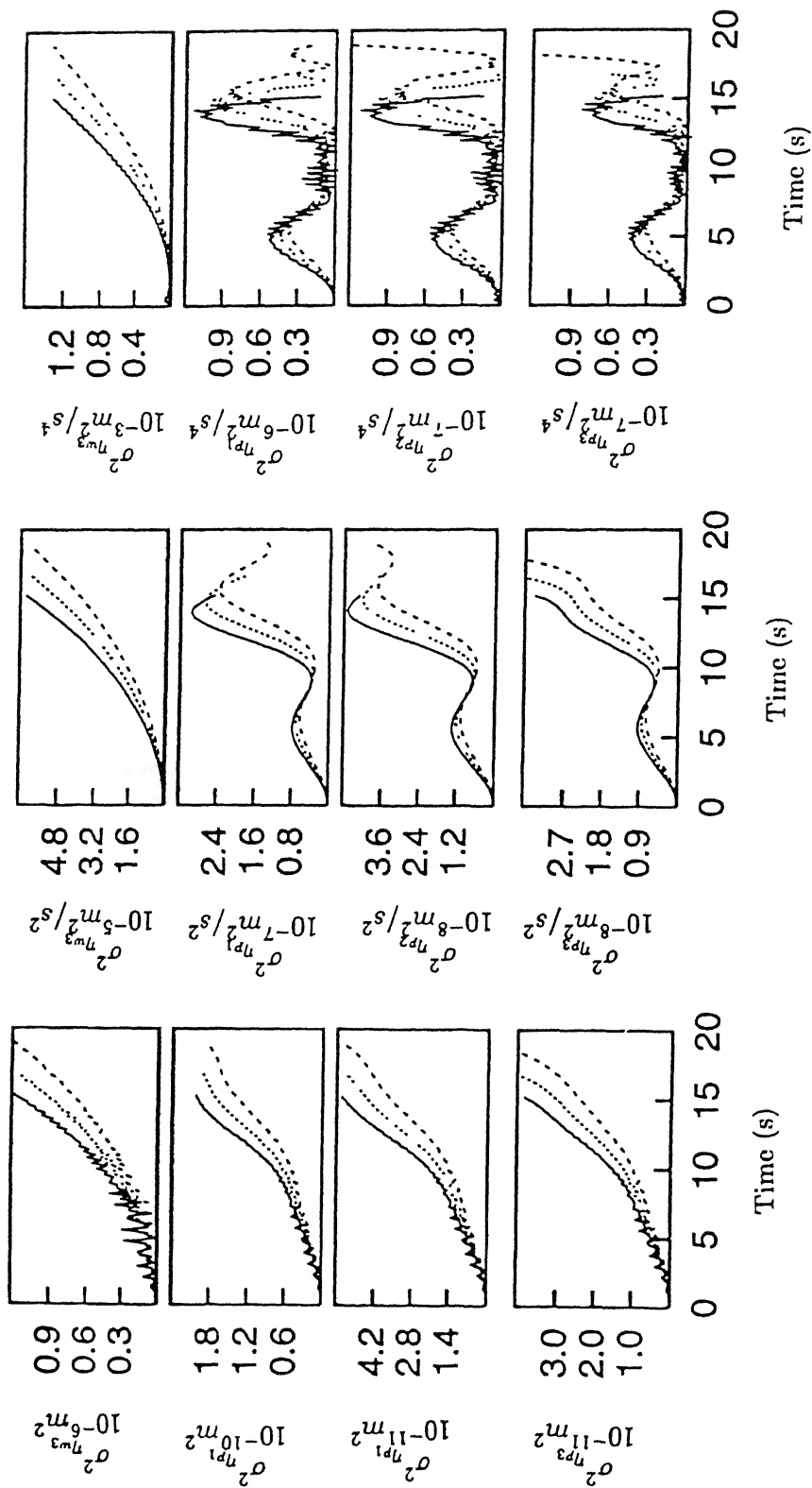


Fig.5.21(continued). Heave-Pitch Model (Flexible fuselage in bending)-Response variance in takeoff run. Key same as Fig.5.20

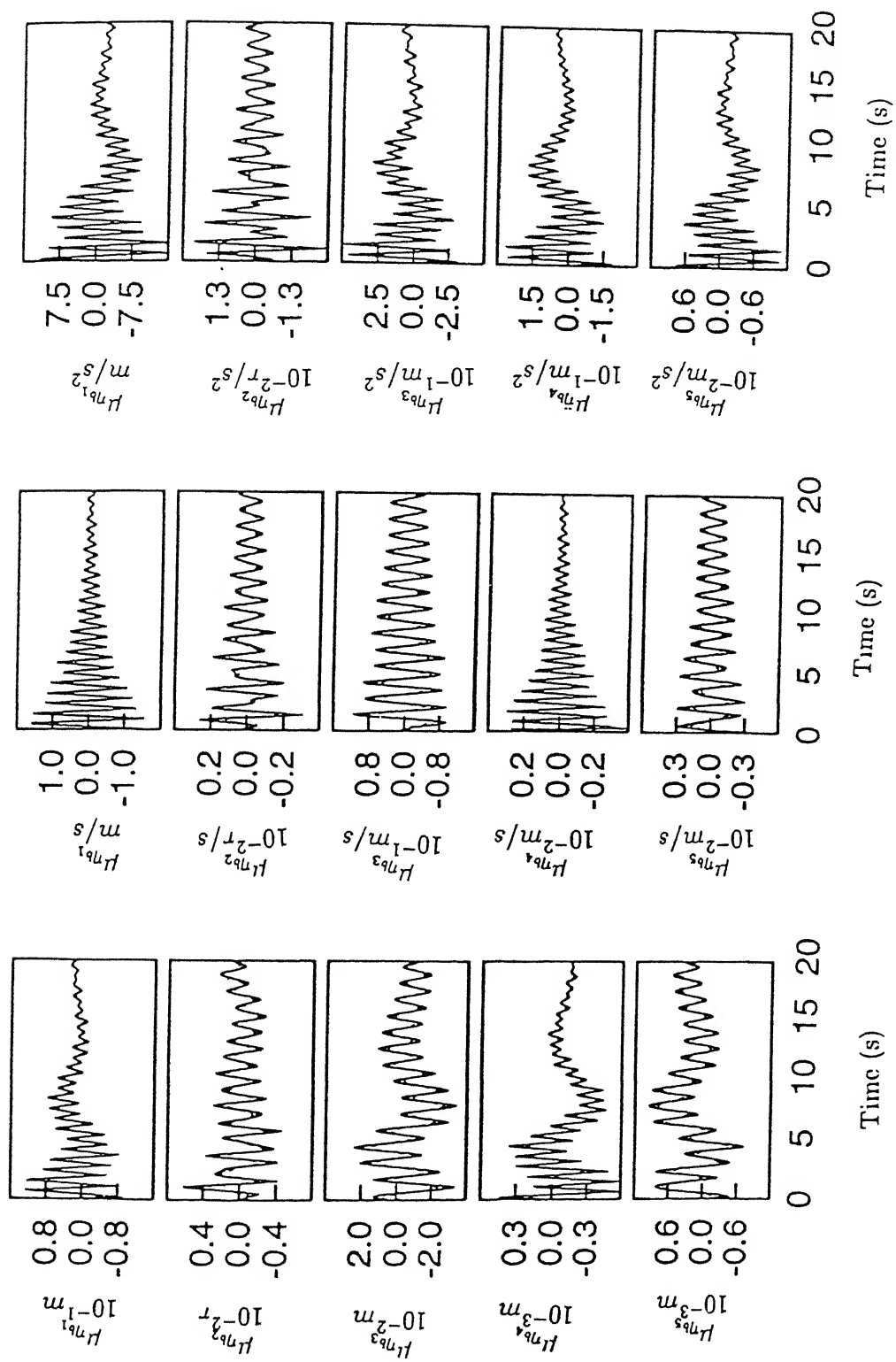


Fig.5.22. Heave-Pitch Model (Flexible fuselage in bending)-
Mean response in landing run.

Key: Aircraft sink velocity, 0.6 m/s —, 0.9 m/s ----, 1.2 m/s .

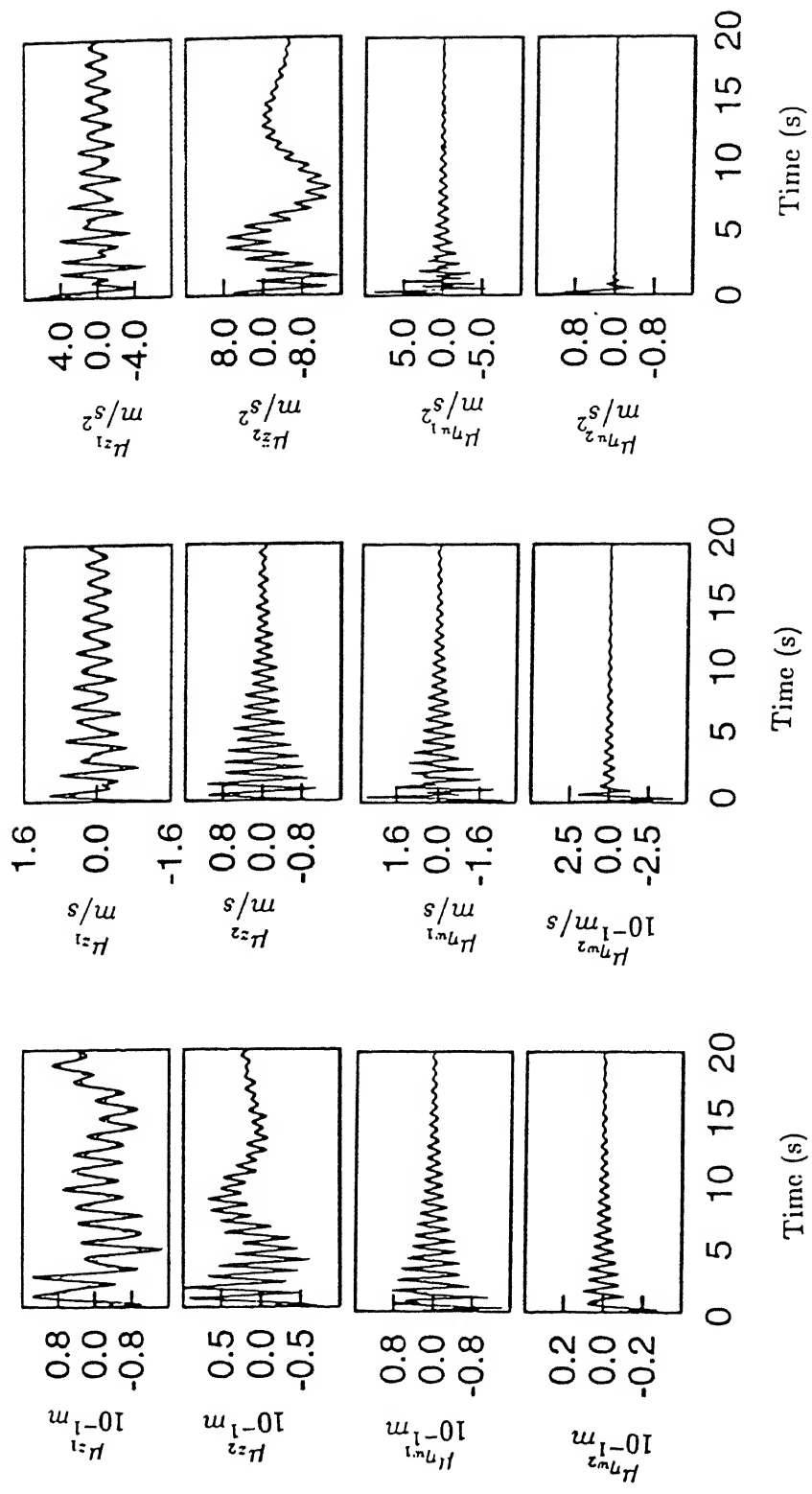


Fig.5.22(continued). Heave-Pitch Model (Flexible fuselage in bending)-Mean response in landing run.
 Key: Aircraft sink velocity, 0.6 m/s ---, 0.9 m/s....., 1.2 m/s —

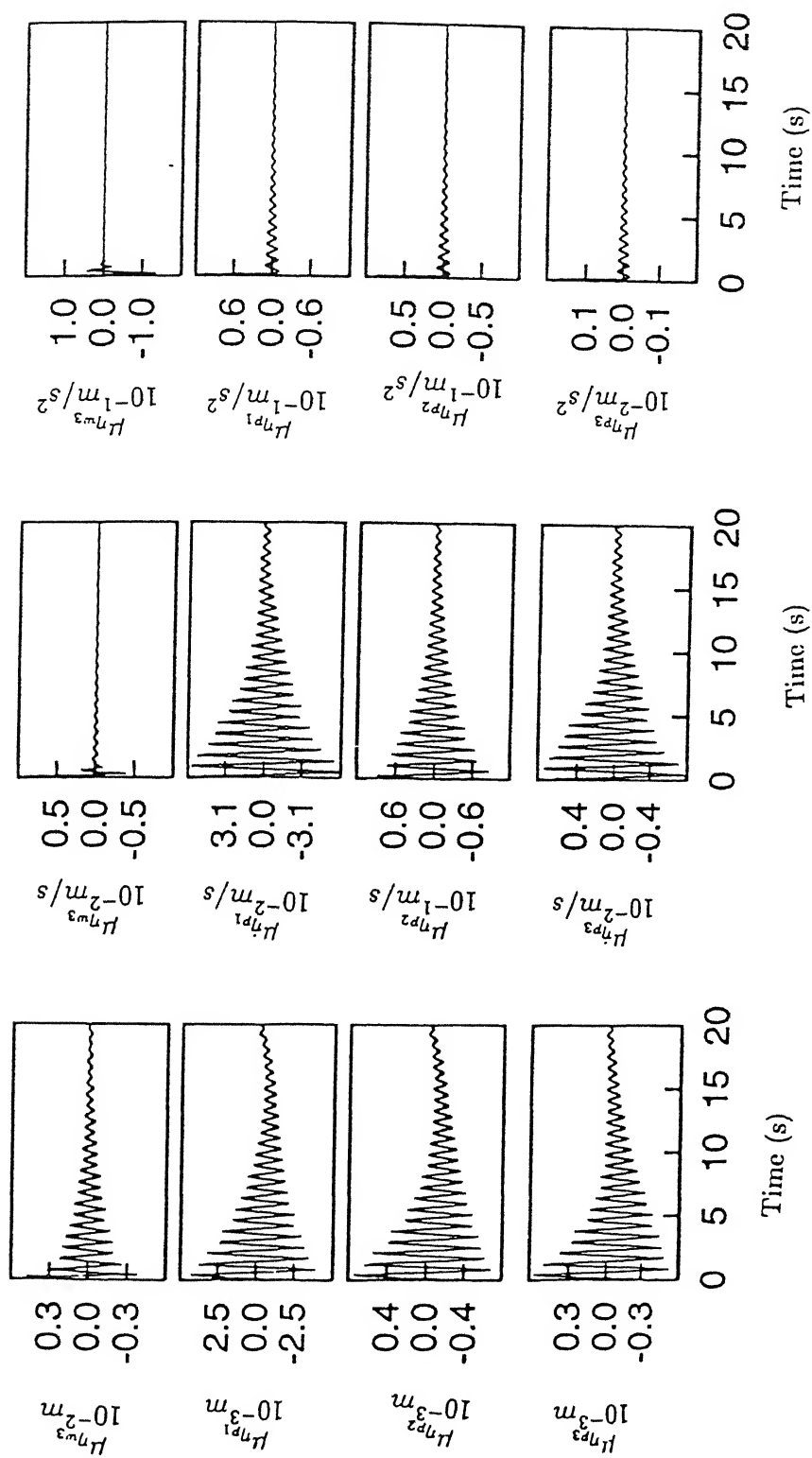


Fig.5.22(continued). Heave-Pitch Model (Flexible fuselage in bending)-Mean response in landing run.

Key: Aircraft sink velocity, 0.6 m/s --- , 0.9 m/s --- , 1.2 m/s ---

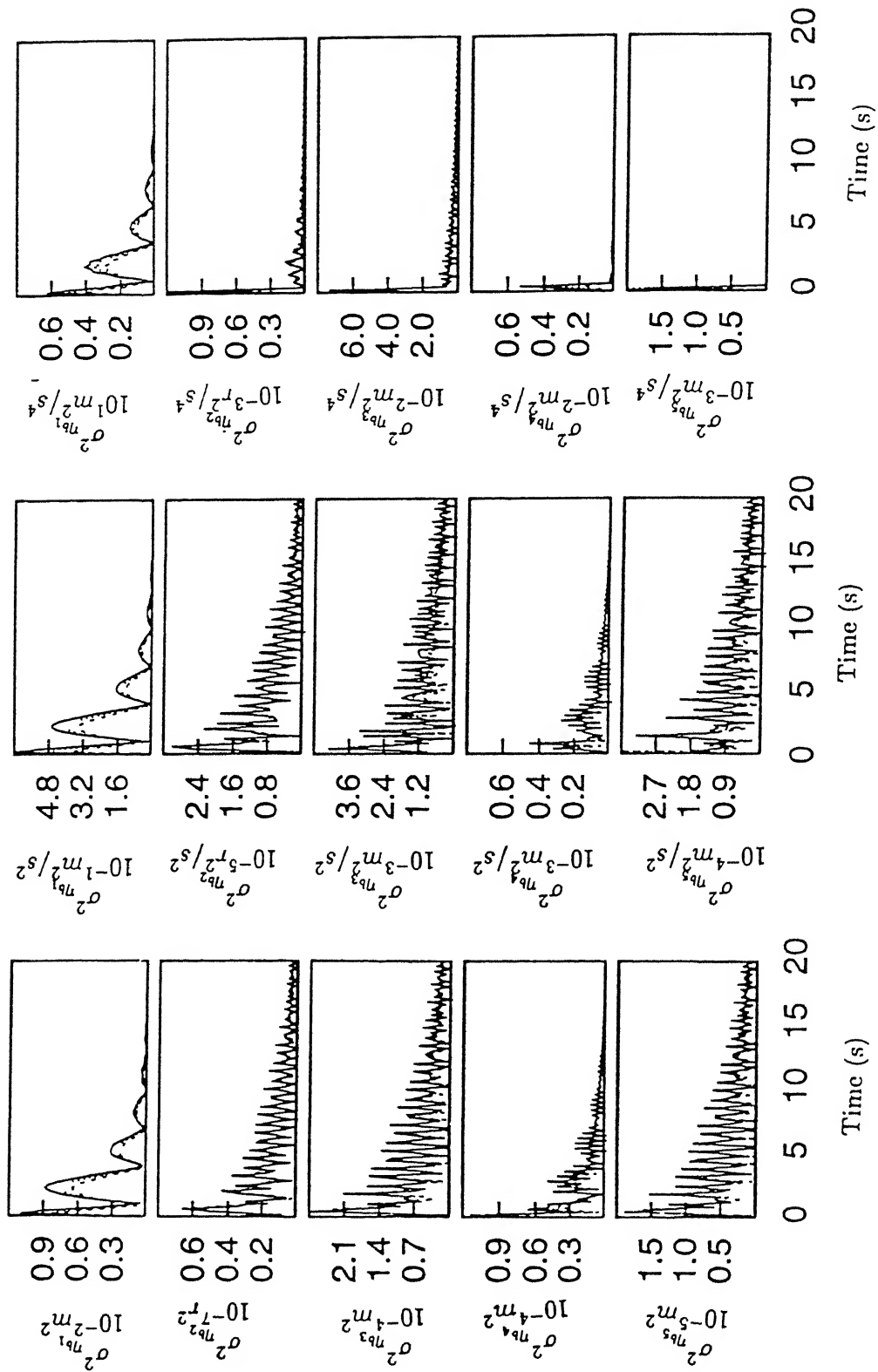


Fig.5.23. Heave-Pitch Model (Flexible fuselage in bending)-
Response variance in landing run.
Key same as Fig.5.22

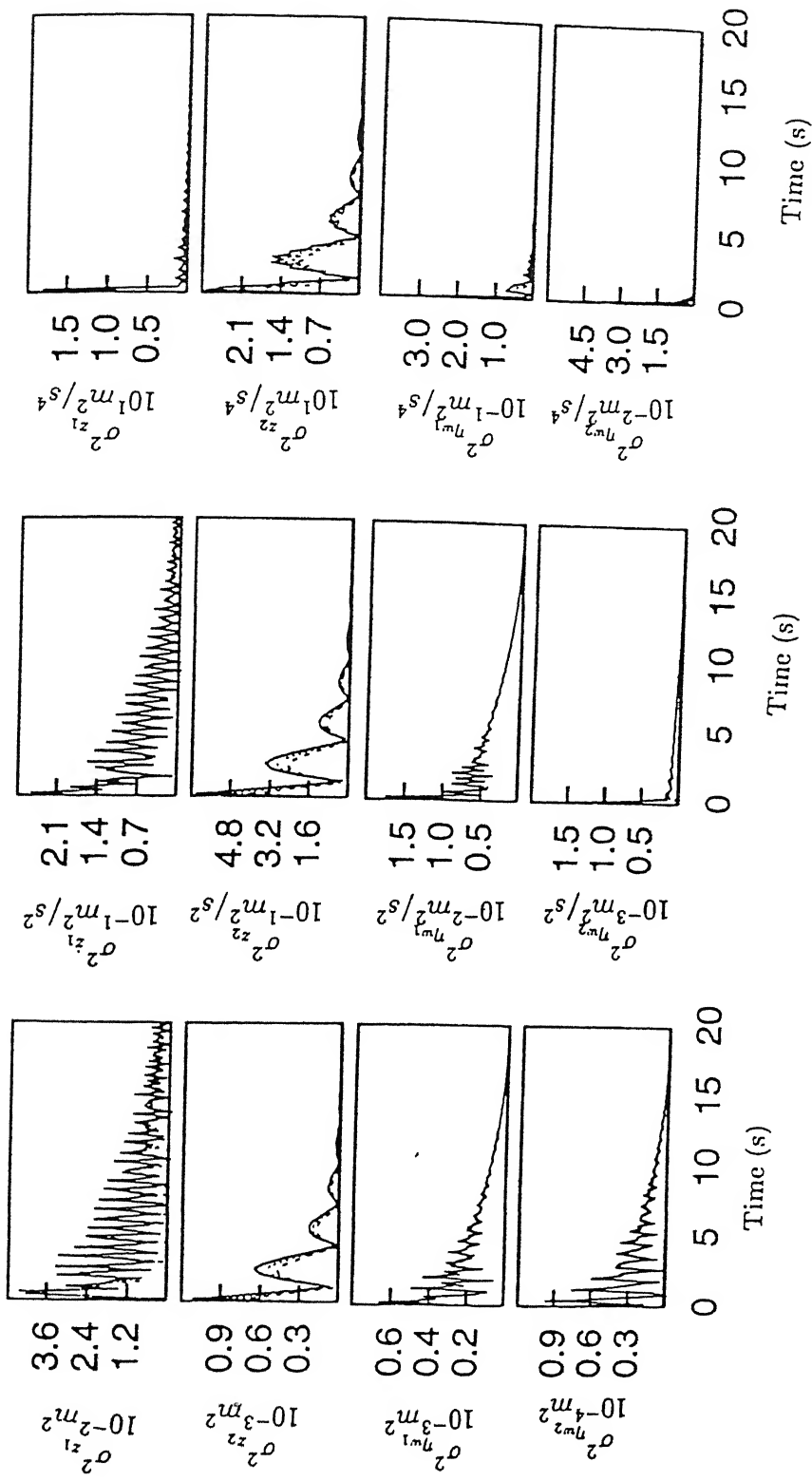


Fig.5.23(continued). Heave-Pitch Model (Flexible fuselage in bending)-Response variance in landing run. Key same as Fig.5.22

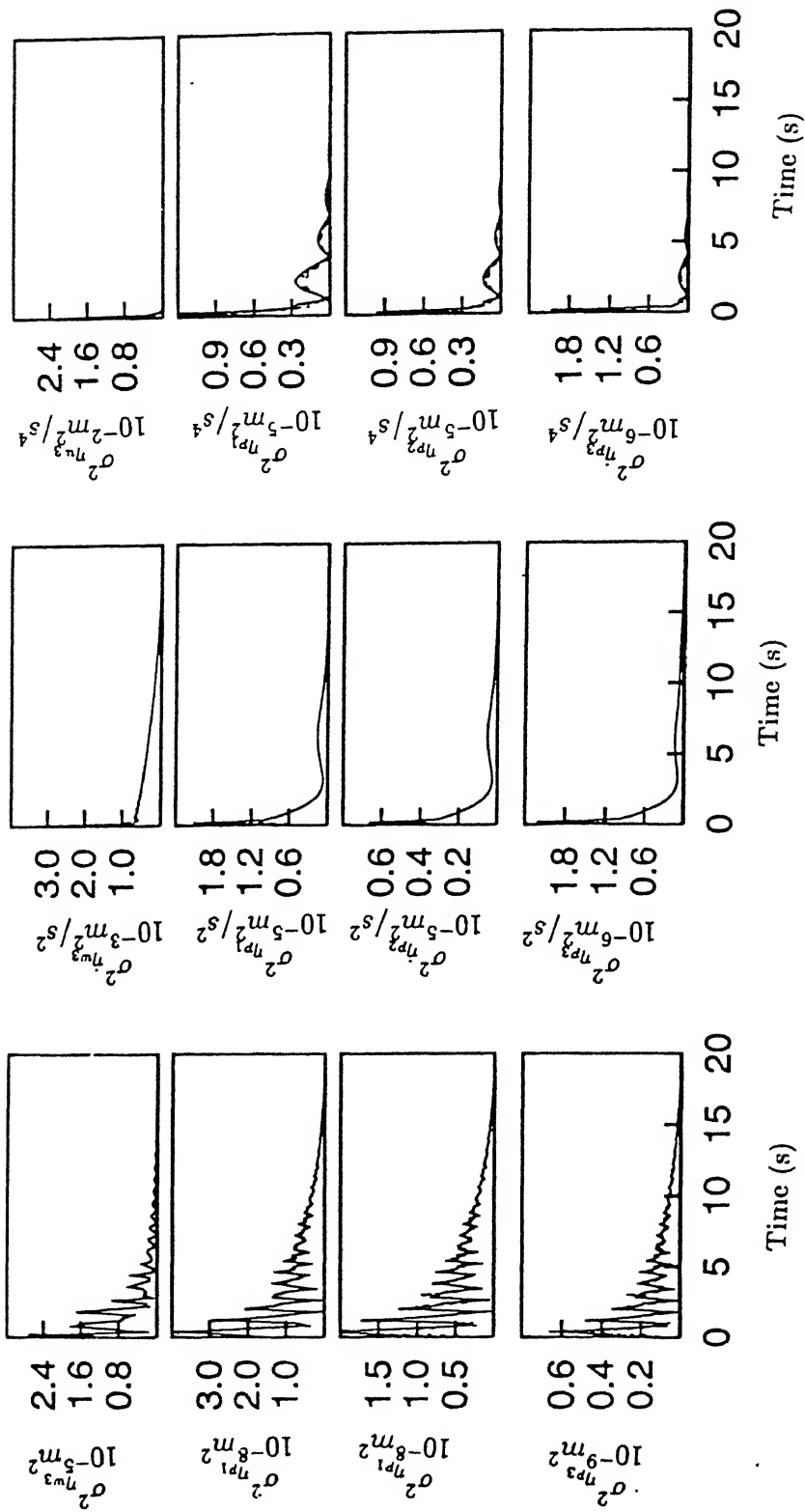


Fig.5.23(continued). Heave-Pitch Model (Flexible fuselage in bending)-Response variance in landing run. Key same as Fig.5.22

Mean response of third, fourth and fifth normal coordinates of fuselage elastic modes show the influence of mean track profile as in the case of rigid body heave motion. However, response magnitudes are smaller compared to the rigid body heave motion. Fuselage rigid body rolling pattern shows steady state condition at constant velocity run. Effect of change of vehicle forward velocity has more pronounced effect in the roll compared to pitch response. Wheel mean displacements are seen to be influenced by track mean variation and vehicle forward speed. Nose wheel velocity and acceleration mean has low steady state response. The two main wheel response characteristics show a difference, indicating the effect of fuselage rolling. Similar is the case for the left and right wing's generalised coordinate's mean response which differ in magnitude as well as phase.

Track normal coordinates mean response grow in magnitude with increasing track mean level and vehicle speed. Higher vehicle forward velocity is seen to induce higher response in the track. Acceleration mean of the track show large value on entry of vehicle over the track.

Variance of displacement, velocity and acceleration of the system generalised coordinates are presented in Fig.5.25. Variance of displacement and velocity of the fuselage rigid body heave and pitch motion has oscillatory pattern in the early stages which tend to an asymptotic value with time. Pitch acceleration variance has initial high value which decreases to a low asymptotic value with low amplitude fluctuation. Variance of fuselage third, fourth and fifth normal coordinates, rigid body rolling and wheel heave

degrees of freedom reveal similar characteristics. Response variance of left and right wing normal coordinates show fluctuation in early stage which subside to reach asymptotic values. Steady value is reached much faster in case of velocity and acceleration response.

Track normal coordinates response variance indicate low frequency variation in later part of taxi runs which become more pronounced in velocity response at higher forward velocity.

5.2.4.2 *Takeoff Run*

Fig.5.26 presents mean response during takeoff of the aircraft. Rigid body heave motion show gradual building up of the response with increase in vehicle forward speed. Longer takeoff run is seen to induce higher displacement magnitude for the heave motion. Pitch acceleration during takeoff is seen to decrease after initial transience as aircraft proceeds to takeoff. Pitch acceleration is found to have less dependence on the change of vehicle forward acceleration. Mean response of fuselage elastic bending reveals high frequency components in the initial stage of motion. High frequency oscillation show low sensitivity to vehicle forward acceleration. Rigid body roll of the airplane indicates low value at the initiation of motion. Higher vehicle forward acceleration induce higher roll acceleration in the airplane. Nose wheel displacement and velocity response show high frequency components which tends to diminish as the takeoff run progresses. Response of two main wheels are found different. At takeoff instant mean displacement of right wheel is seen to have larger

magnitude compared to that of left wheel. Mean response of left and right wing's first and second normal coordinate show more persistent transience compared to that in the third normal coordinate.

Track normal coordinate mean response show growing up of amplitude with increasing speed. High frequency components present in the response indicates less sensitivity to vehicle forward acceleration.

Response variances are presented in Fig.5.27. Variance of fuselage rigid body heave motion shows gradual building up of the amplitude with increase in vehicle speed. Acceleration variance show very low value which steeply increases during takeoff time. Pitch displacement and velocity have a fluctuating pattern which is not present in acceleration response. Fuselage normal coordinates response variance in elastic bending modes follow a pattern similar to the rigid body heave mode. Roll variance also indicates a rising tendency with the increase in vehicle forward velocity. Oscillations are more pronounced at higher vehicle forward acceleration. Nose and main wheel response variance follow a pattern similar to the fuselage response. High frequency components are more prominent in wheels acceleration response variance.

Left and right wing response variance magnitudes increase with vehicle forward speed. Acceleration variance of right wing's second normal coordinate, however, indicate the presence of asymptotic level at takeoff instant. Track normal coordinate response variance reveal low frequency oscillation which is more

apparent in velocity and acceleration. Acceleration response of third normal coordinate is found to have a steep rise at takeoff instant.

5.2.4.3 Landing Run

Mean system response in landing run have been presented in Fig.5.28. Fuselage rigid body modes have high frequency oscillation during the impact phase. Response is gradually damped out with the slowing of vehicle forward motion. Higher sink velocity induces higher heave response. Pitch response also show the effect of landing impact. Fuselage third and fifth coordinate's mean displacements reveal low frequency oscillation in the later stage of landing run. Mean displacement and velocity of rigid body rolling has second peak higher than the first one after touch down whereas the peaks progressively reduce in the acceleration response. Wheels response also reveal the effect of impact at landing touch down which gradually decays and the response become dependent on track mean input.

Wing mean response show dominant values at impact phase with a cluster of closely spaced peaks. Effect of landing impact dies out soon showing very low response in the later phase of the landing run. Mean response of the track generalized coordinates capture the high frequency oscillation after the vehicle causes impact on the track. Response magnitude decreases with the slowing of the vehicle forward motion.

Response variance during landing run are presented in Fig.5.29. Out of the fuselage first five normal coordinates, rigid

body heave motion show less number of peaks compared to other normal coordinate response variance. Acceleration variances of second, third, fourth and fifth generalised coordinates are found to decay faster compared to displacement and velocity. Displacement and velocity variance of rigid body rolling has first peak of much higher magnitude compared to subsequent peaks. Two main wheels response variances follow the pattern similar to the heave response variance. Nose gear displacement and velocity show slower dissipation of impact energy compared to the two main wheels. Nose gear acceleration variance at touch down instant has higher value compared to main wheels. Wing's response are oscillatory in the early stage. The oscillatory nature reduces from displacement to velocity to acceleration. Wing acceleration variance in the first mode indicate two peaks, first peak being much higher compared to second one whereas acceleration variance in second and third mode indicates single dominant peak.

Track normal coordinates displacement variance show oscillatory pattern with high frequency components in the impact phase. Velocity and acceleration show low frequency variation in the later stage of the landing run.

5.2.5 Heave-Pitch-Roll Model (Flexible fuselage in bending and torsion)

First five flexural modes and first four torsional modes of the airframe have been considered in this three point input model out of which first two in flexure represent rigid body heave and pitch while first one in torsion is for the rigid rolling of the

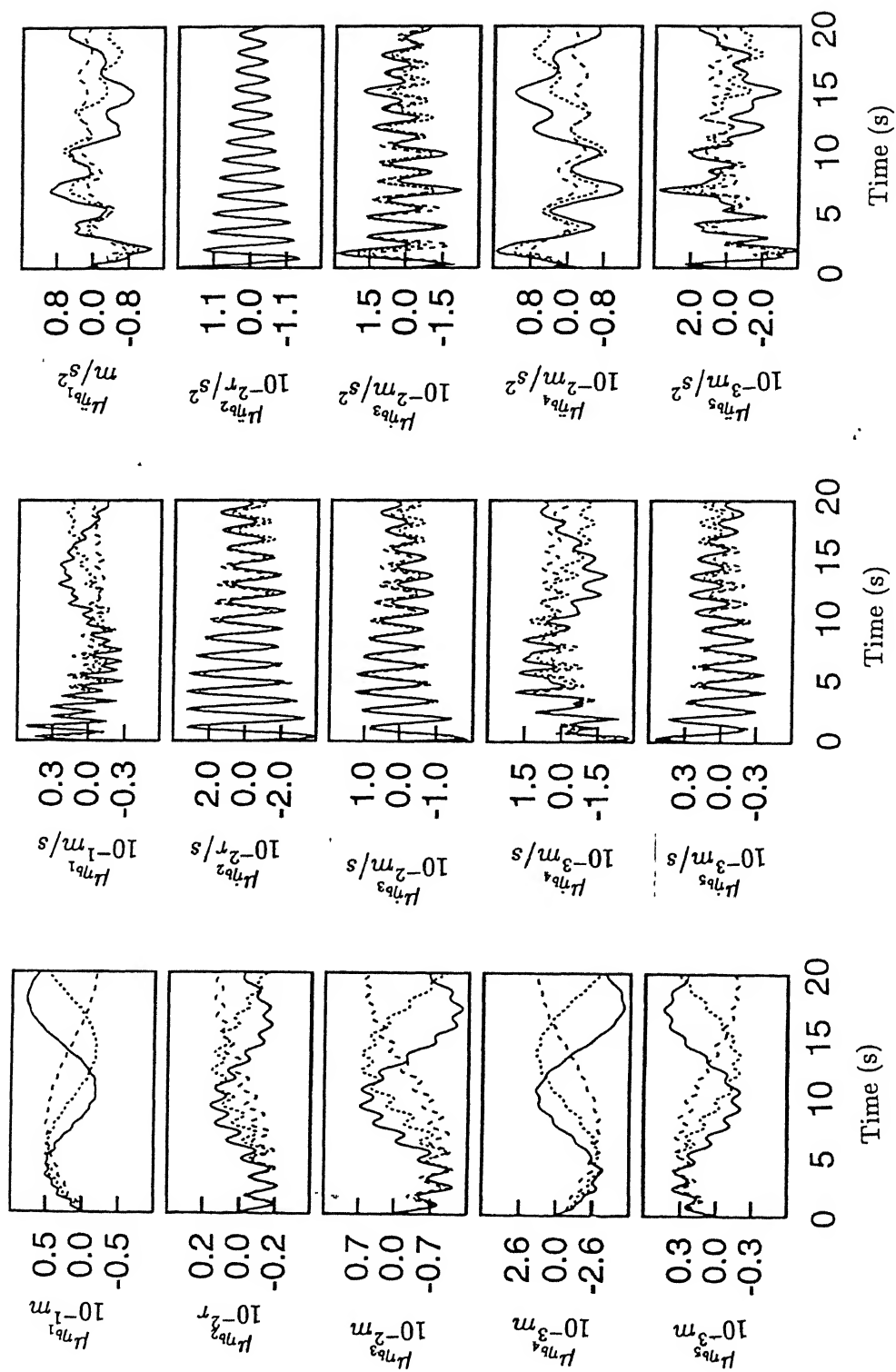


Fig.5.24. Heave-Pitch-Roll Model (Flexible fuselage in bending with rigid roll)-Mean response in taxi run. Key same as Fig.5.18

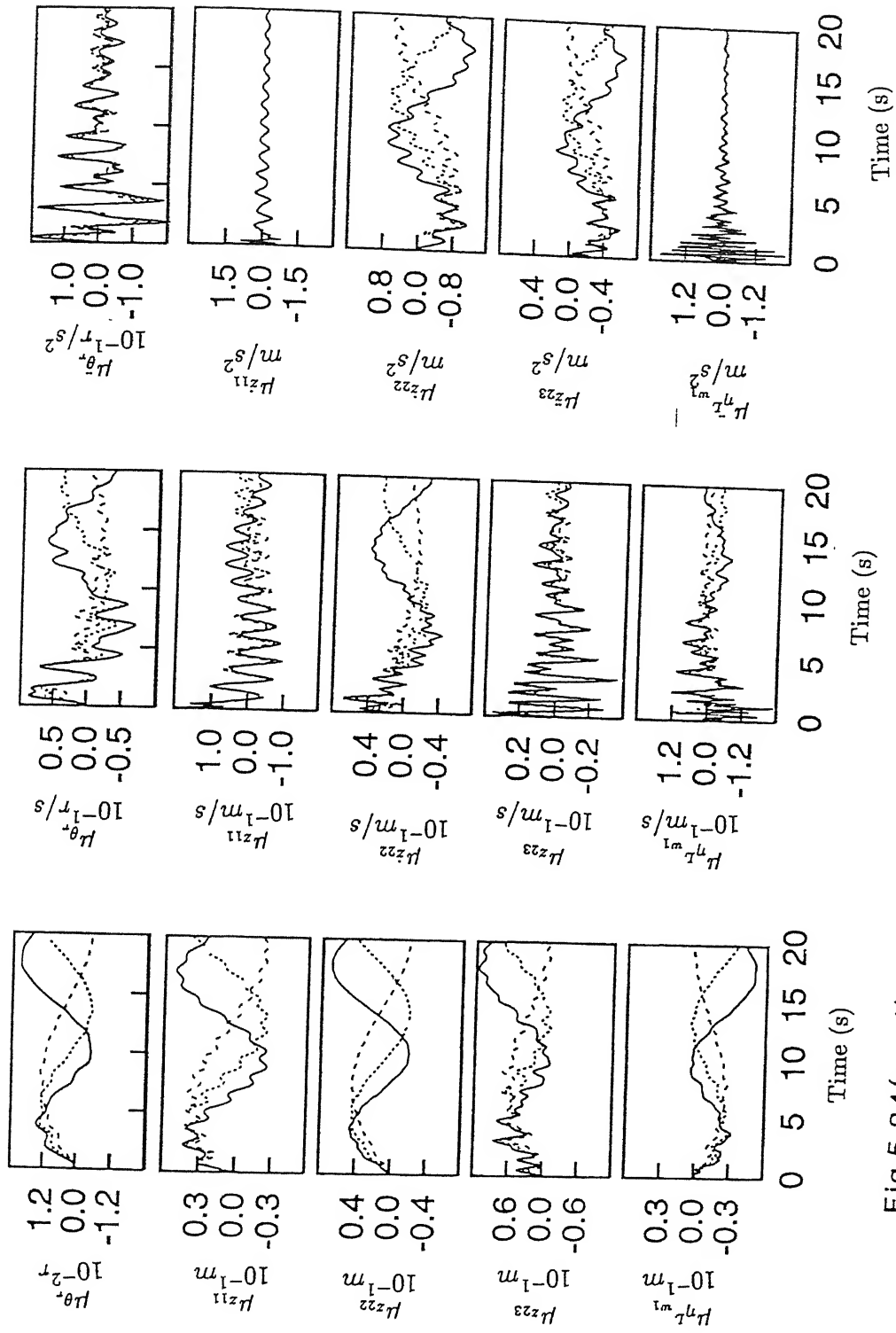


Fig.5.24(continued). Heave-Pitch-Roll Model (Flexible) fuselage in bending with rigid roll)-Mean response in taxi run. Key same as Fig.5.18

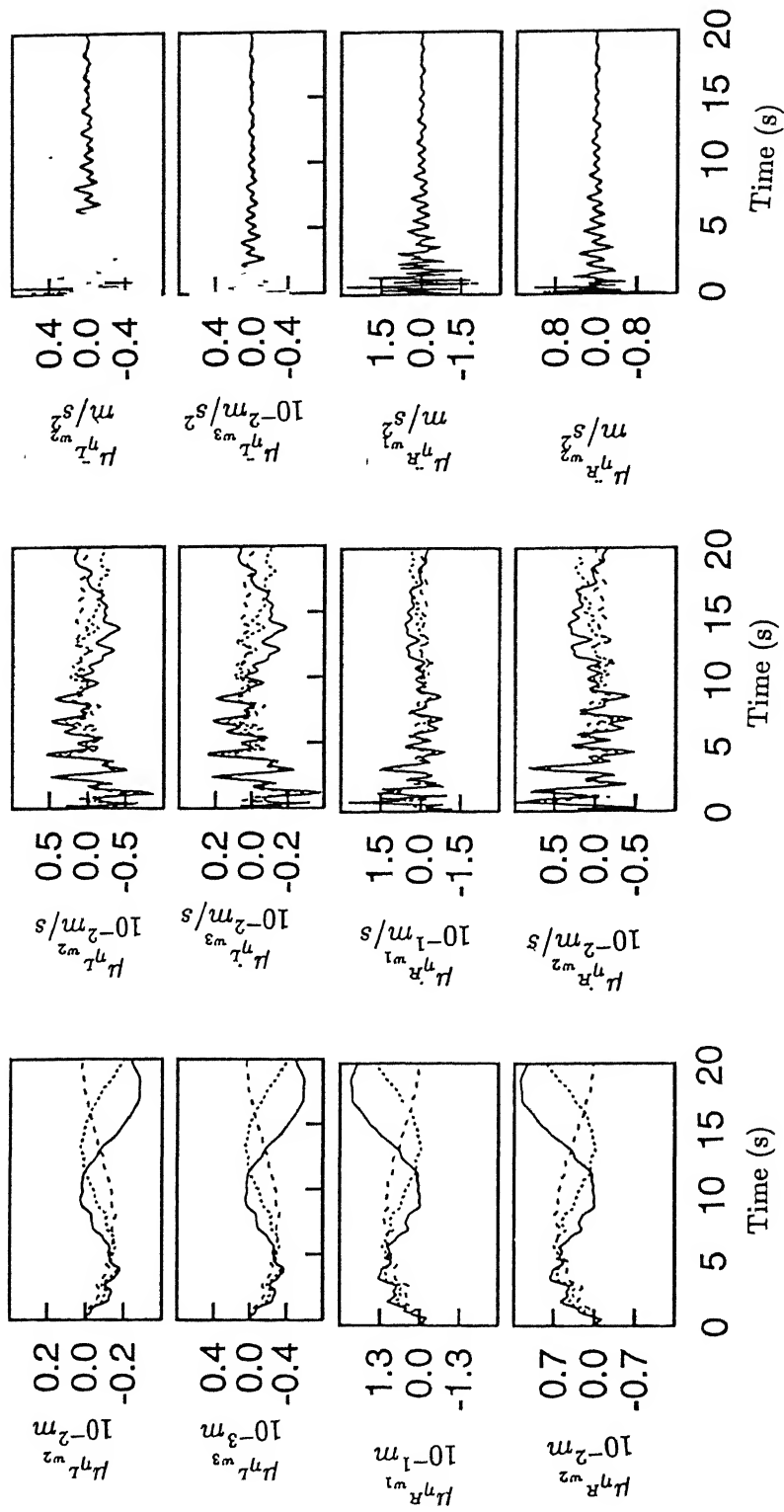


Fig.5.24(continued). Heave-Pitch-Roll Model (Flexible fuselage in bending with rigid roll)-Mean response in taxi run. Key same as Fig.5.18

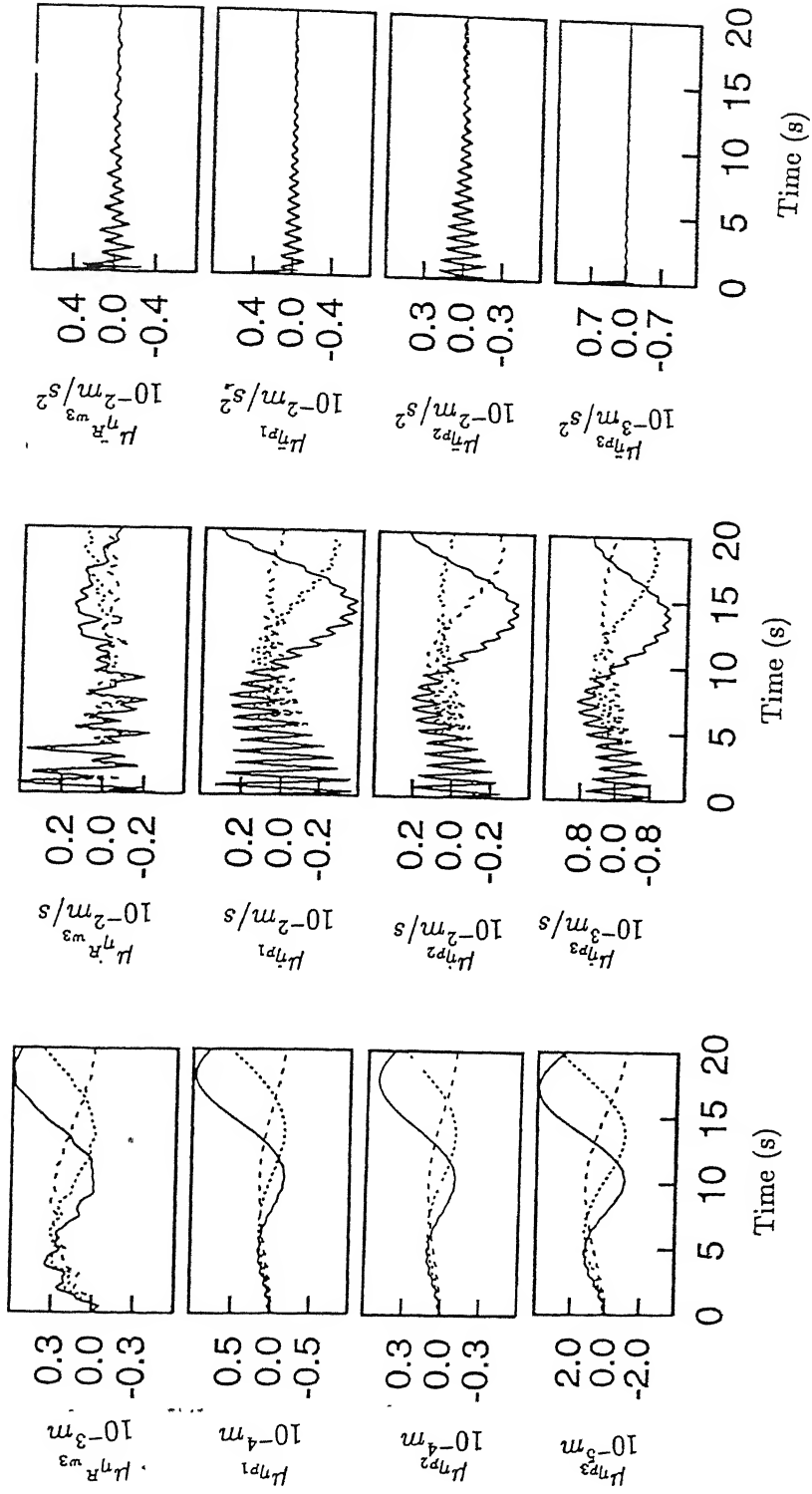


Fig.5.24(continued). Heave-Pitch-Roll Model (Flexible fuselage in bending with rigid roll)-Mean response in taxi run. Key same as Fig.5.18

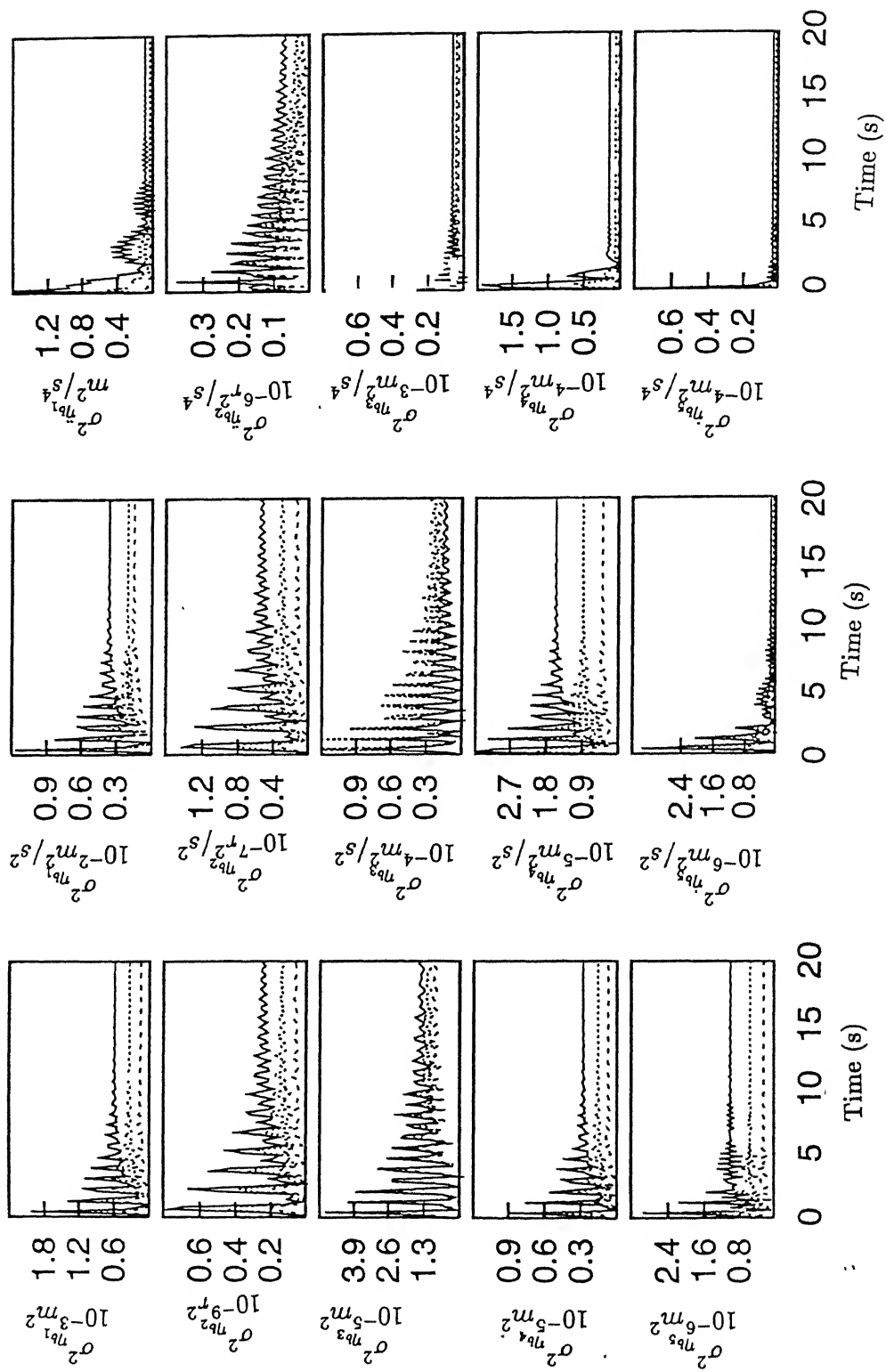


Fig.5.25. Heave-Pitch-Roll Model (Flexible fuselage in bending with rigid roll)-Response variance in taxi run. Key same as Fig.5.18

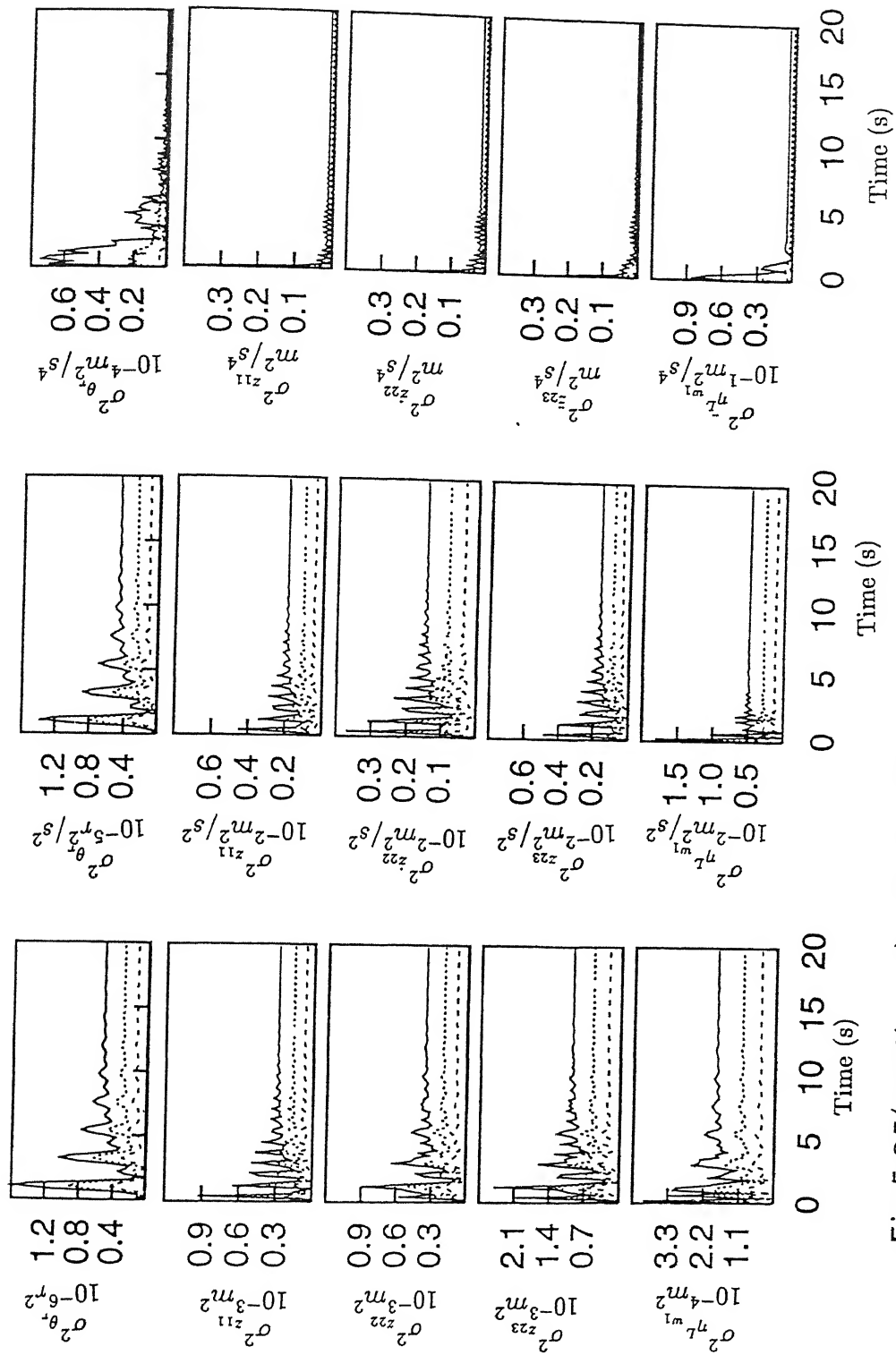


Fig.5.25(continued). Heave-Pitch-Roll Model (Flexible) fuselage in bending with rigid roll)-Response variance in taxi run. Key same as Fig.5.18

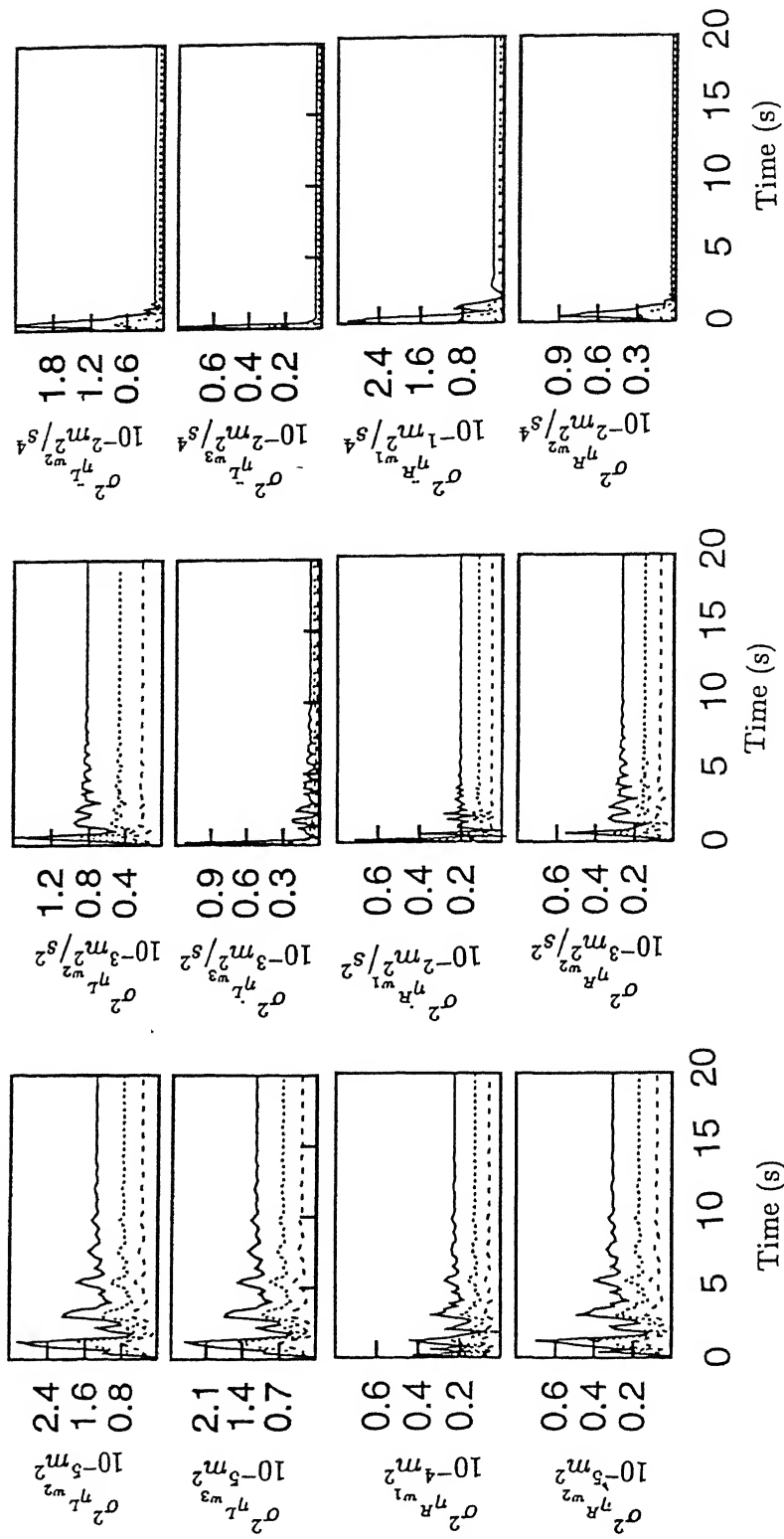


Fig.5.25(continued). Heave-Pitch-Roll Model (Flexible fuselage in bending with rigid roll)-Response variance in taxi run. Key same as Fig.5.18

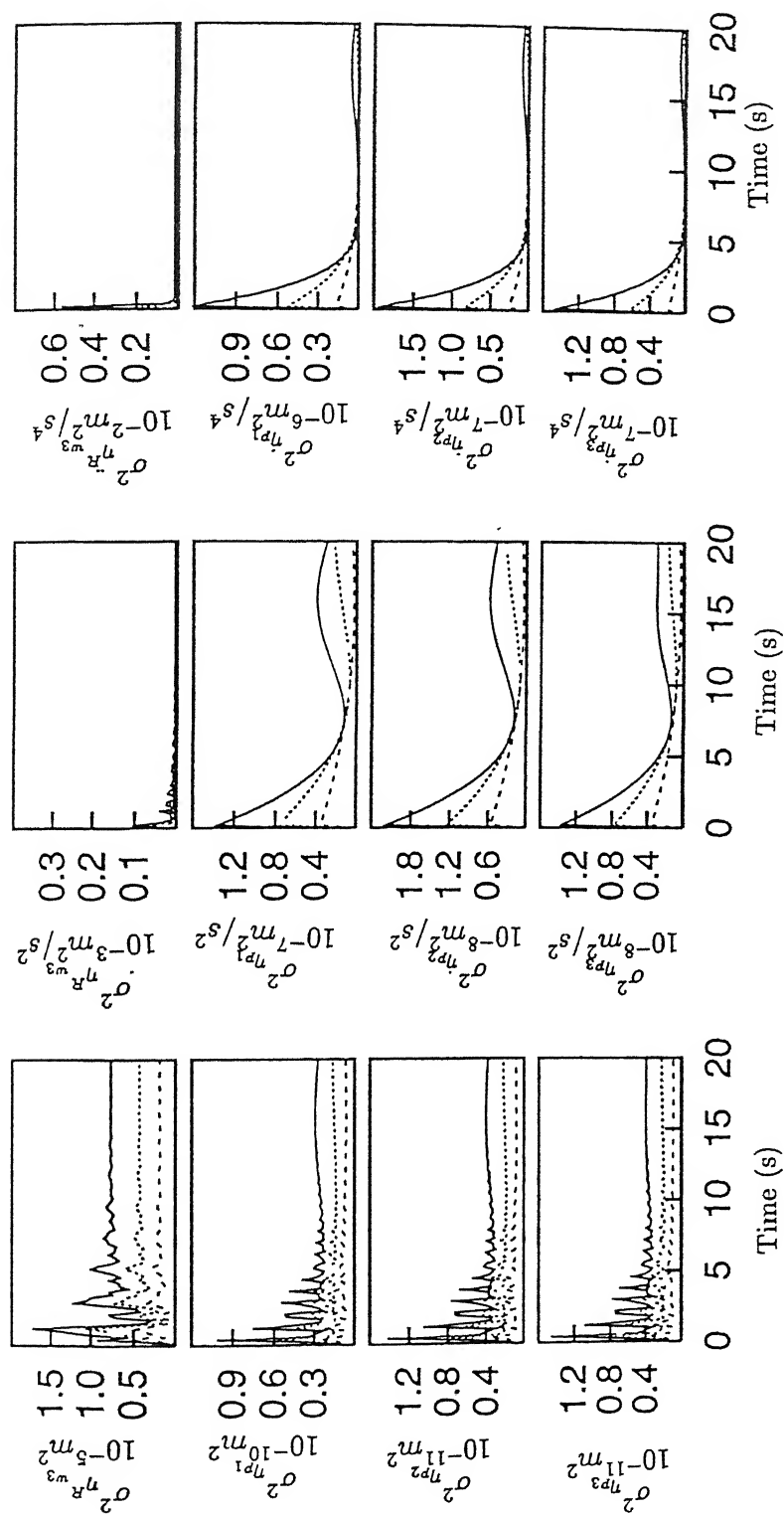


Fig.5.25(continued). Heave-Pitch-Roll Model (Flexible fuselage in bending with rigid roll)-Response variance in taxi run. Key same as Fig.5.18

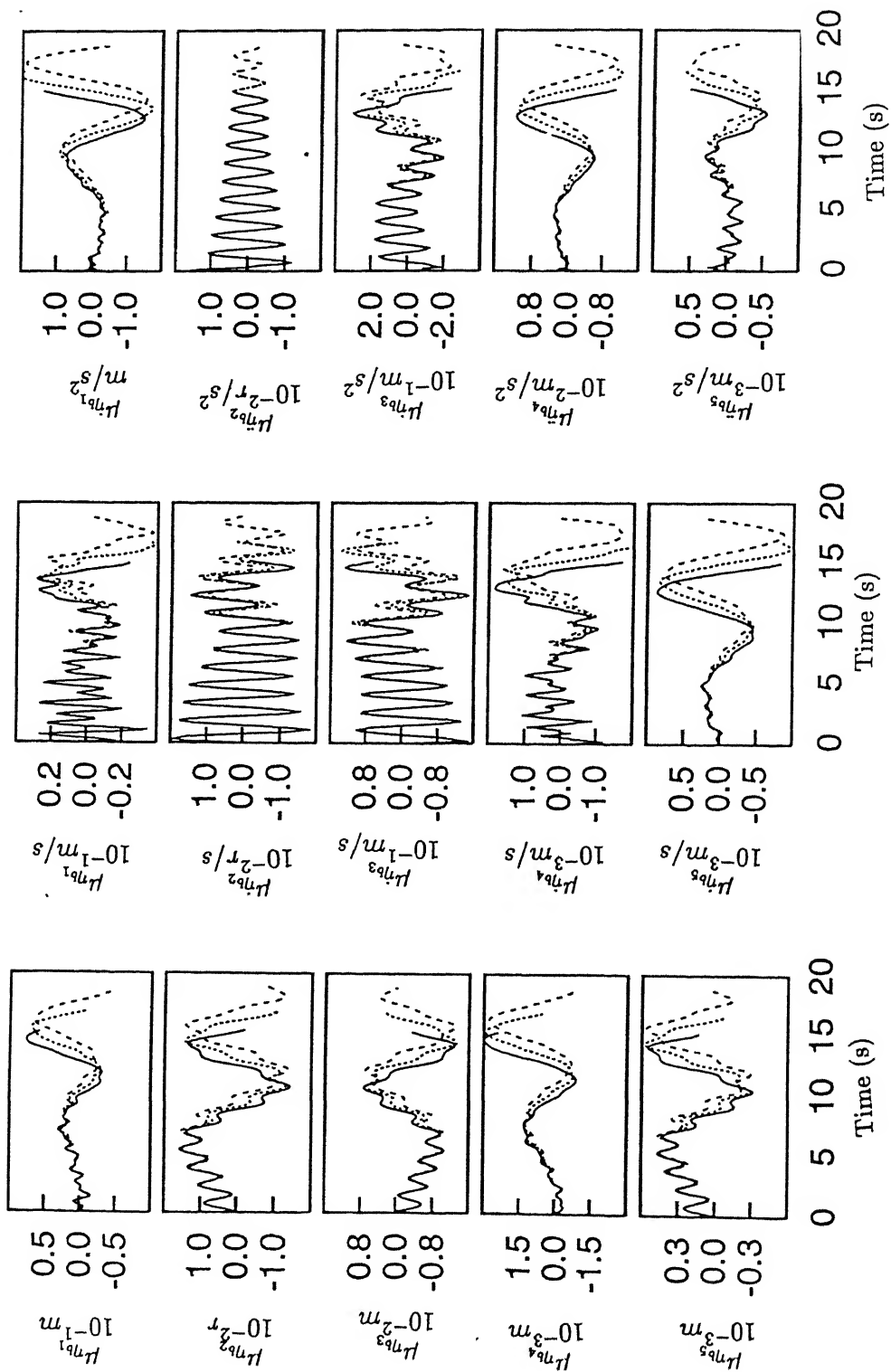


Fig.5.26. Heave-Pitch-Roll Model (Flexible fuselage in bending with rigid roll)-Mean response in takeoff run. Key same as Fig.5.20

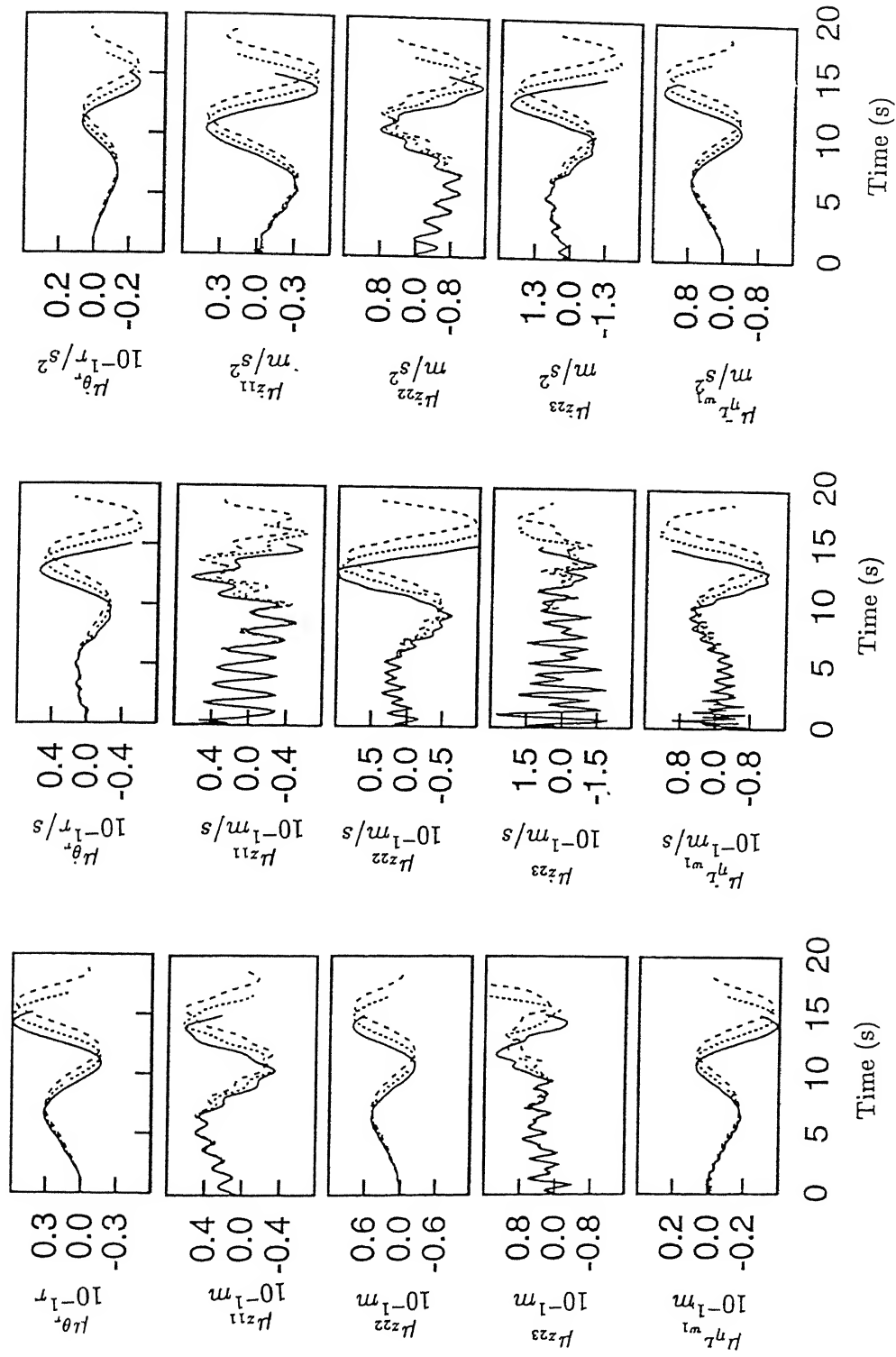


Fig.5.26(continued). Heave-Pitch-Roll Model (Flexible fuselage in bending with rigid roll)-Mean response in takeoff run. Key same as Fig.5.20

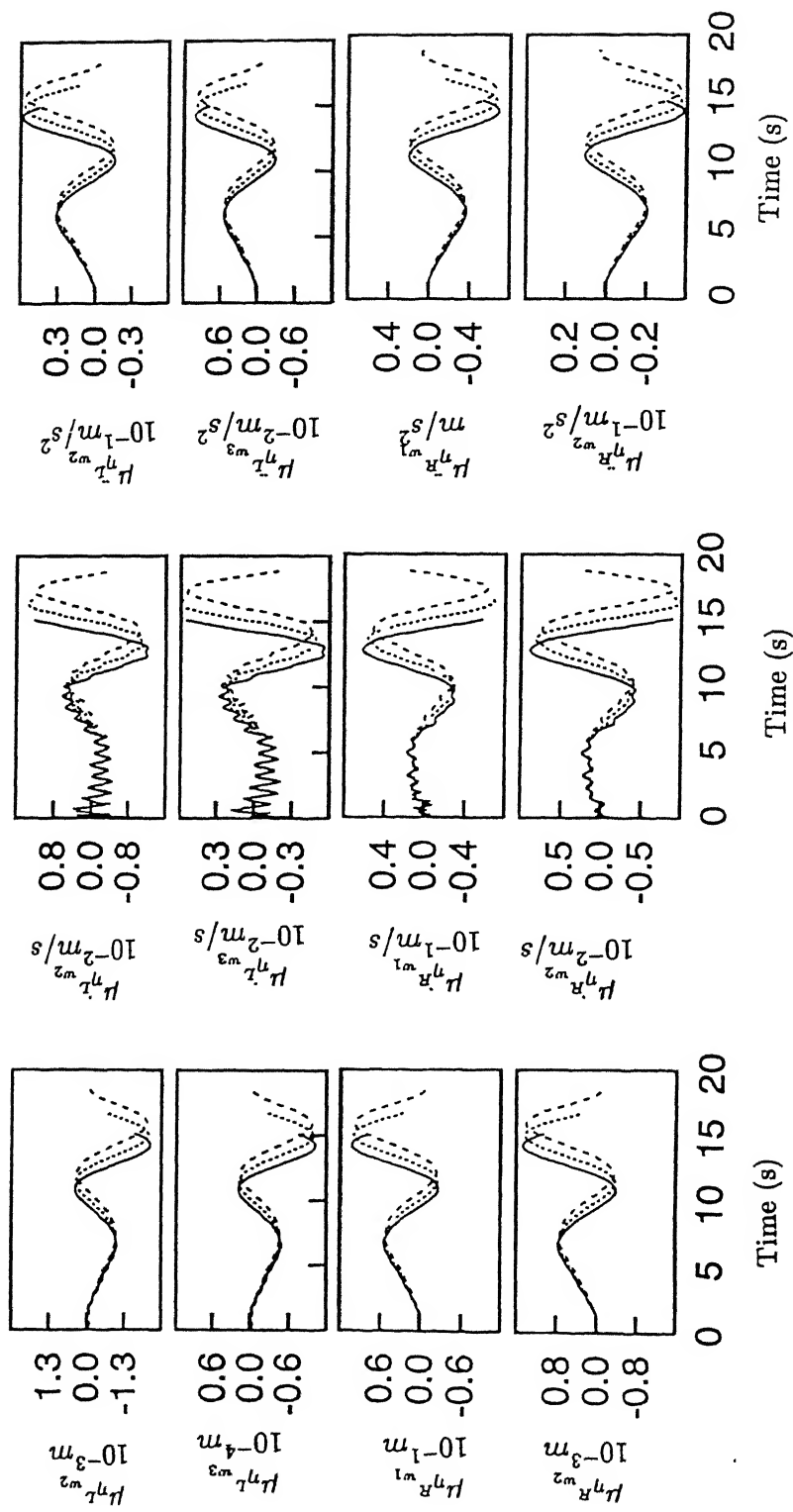


Fig.5.26(continued). Heave-Pitch-Roll Model (Flexible fuselage in bending with rigid roll)-Mean response in takeoff run. Key same as Fig.5.20

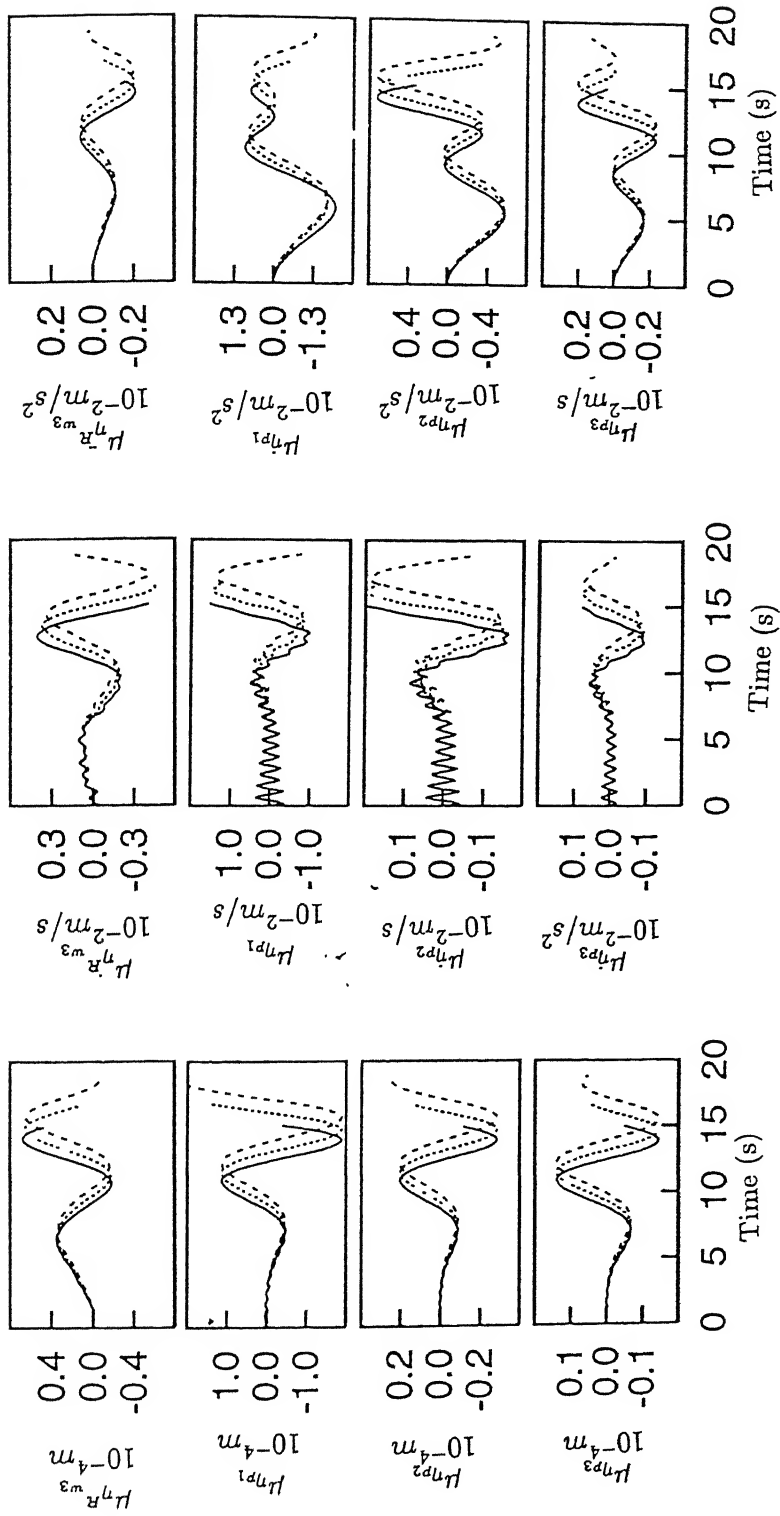


Fig.5.26(continued). Heave-Pitch-Roll Model (Flexible fuselage in bending with rigid roll)-Mean response in takeoff run. Key same as Fig.5.20

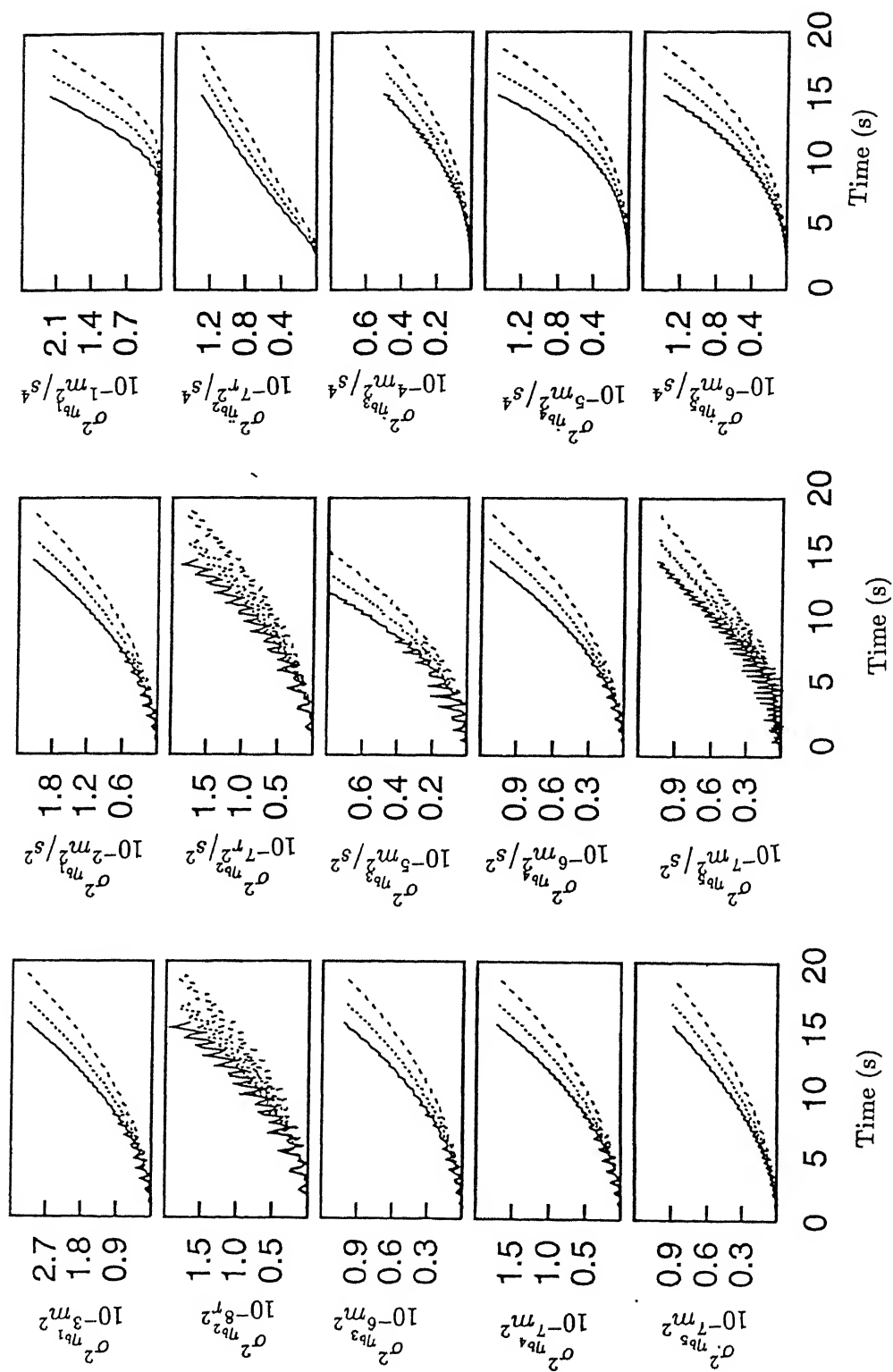


Fig.5.27. Heave-Pitch-Roll Model (Flexible fuselage in bending with rigid roll)-Response variance in takeoff run. Key same as Fig.5.20

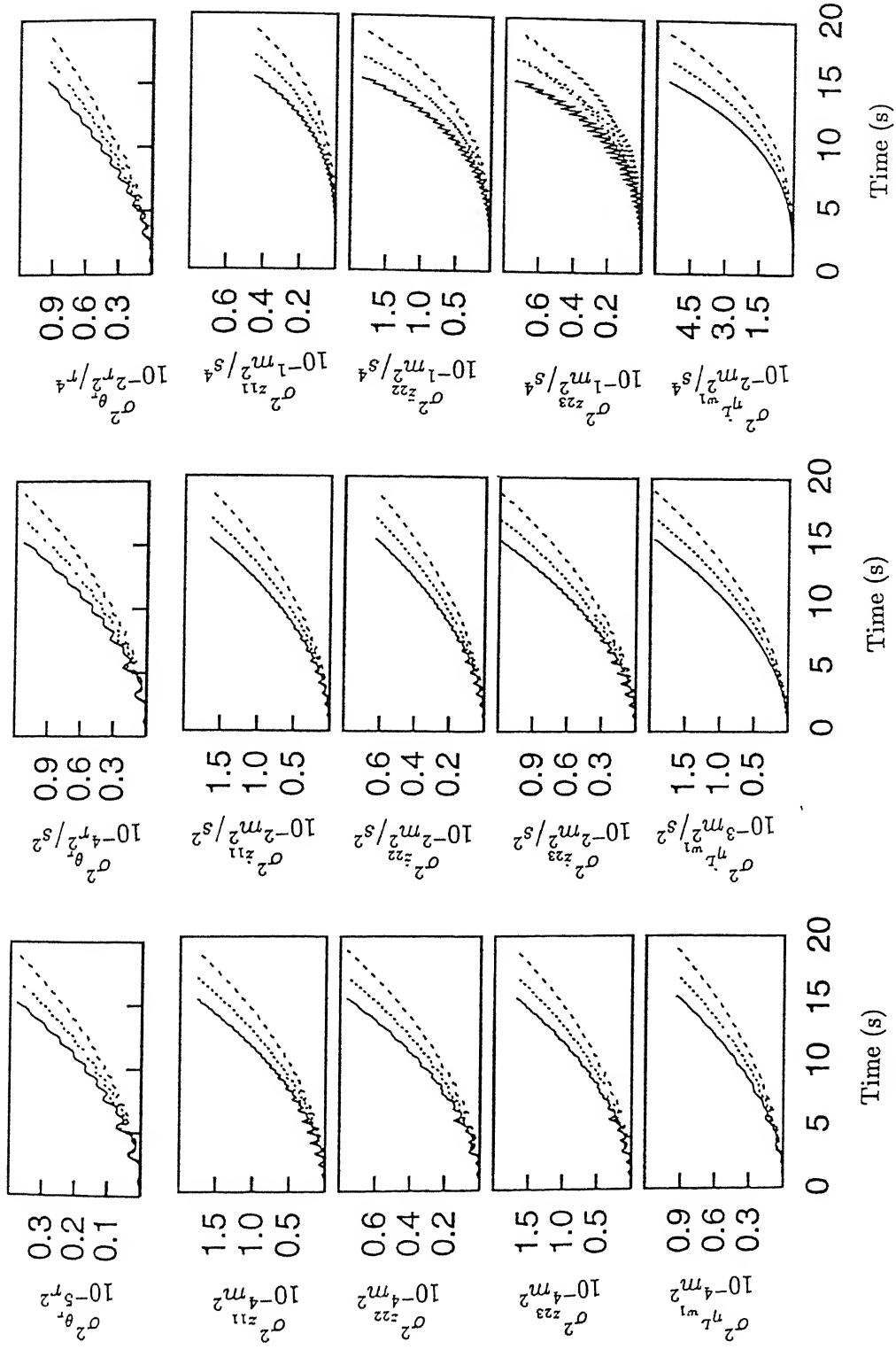


Fig.5.27(continued). Heave-Pitch-Roll Model (Flexible fuselage in bending with rigid roll)-Response variance in takeoff run. Key same as Fig.5.20

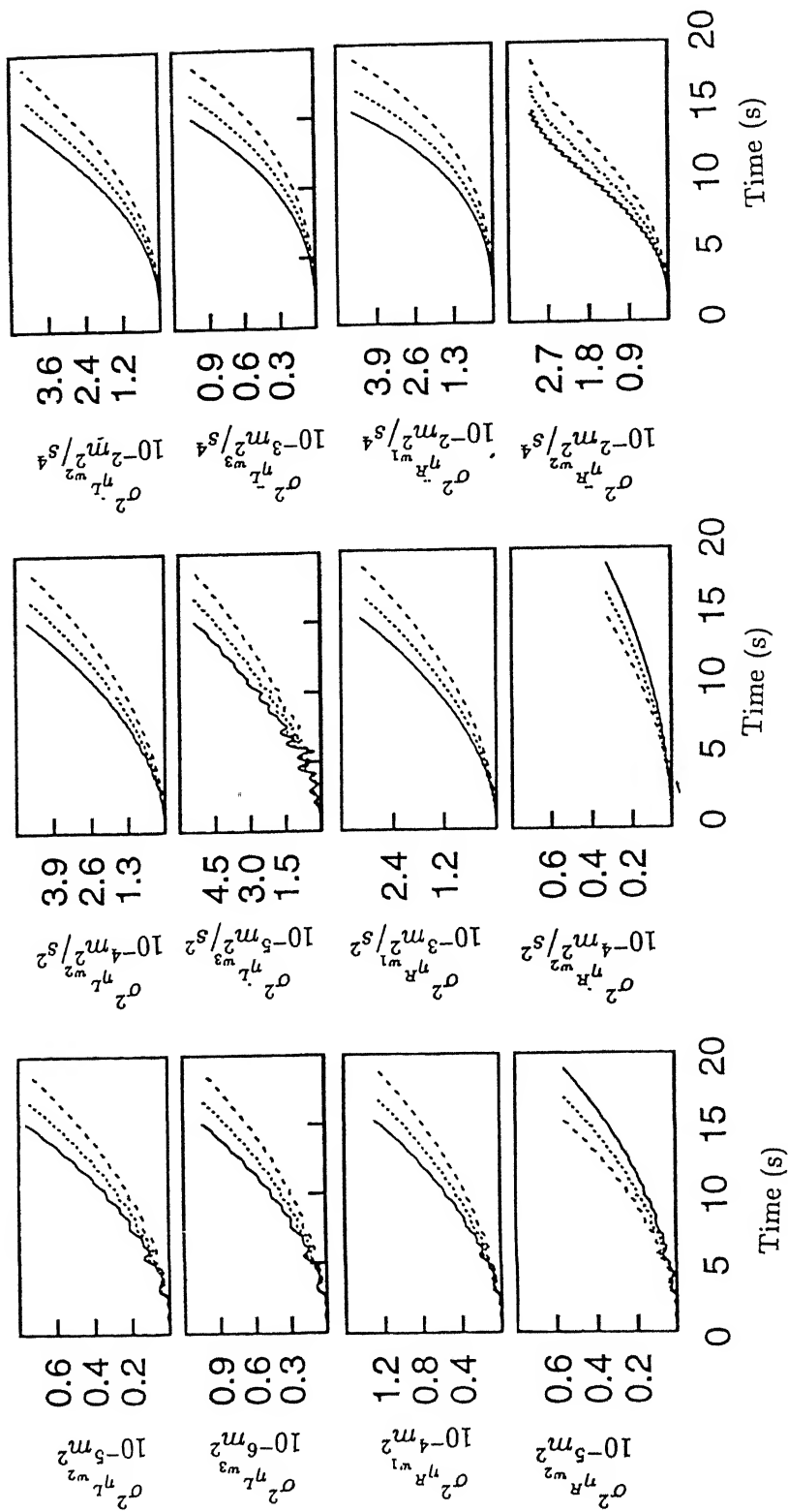


Fig.5.27(continued). Heave-Pitch-Roll Model (Flexible fuselage in bending with rigid roll)-Response variance in takeoff run. Key same as Fig.5.20

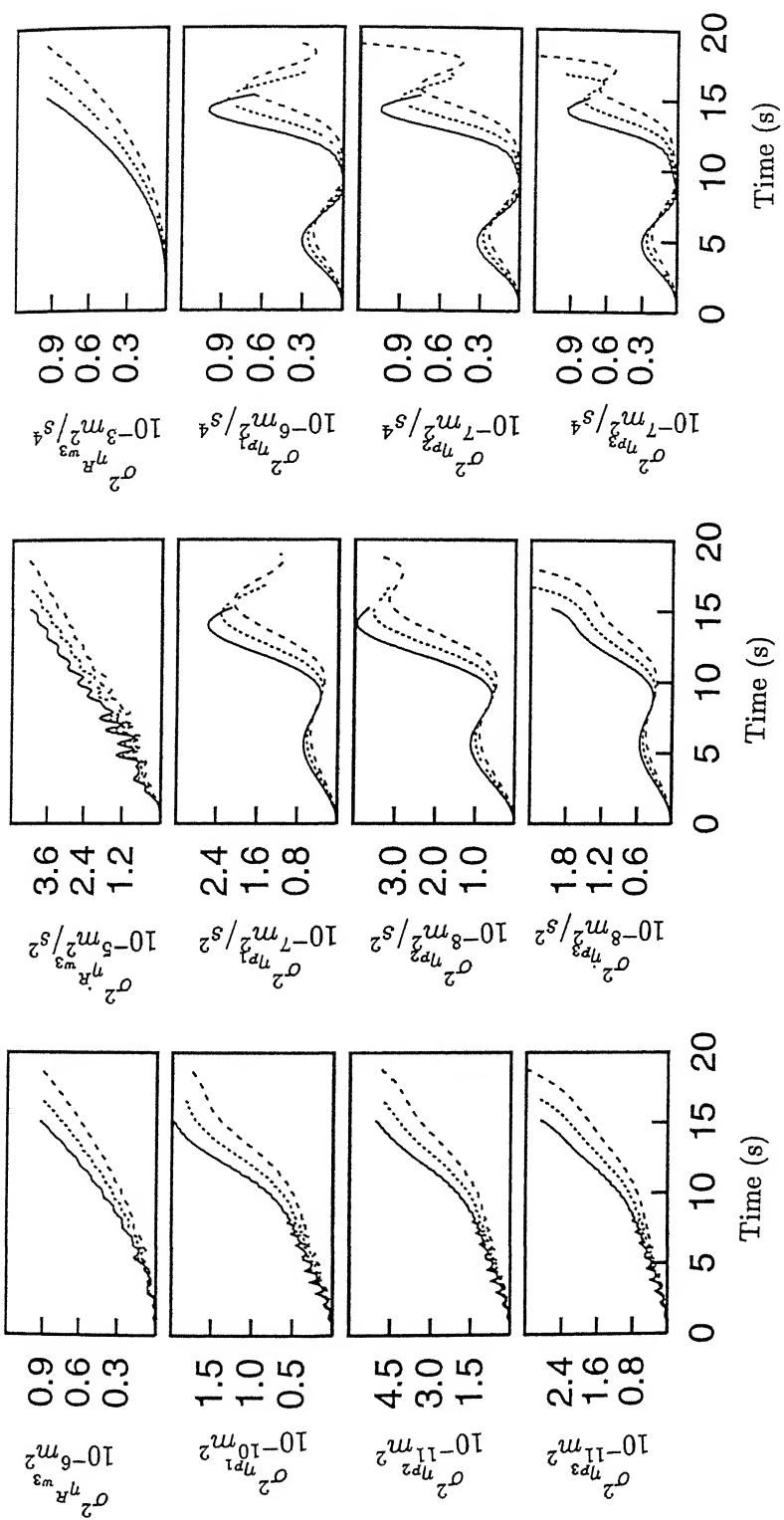


Fig.5.27(continued). Heave-Pitch-Roll Model (Flexible fuselage in bending with rigid roll)-Response variance in takeoff run. Key same as Fig.5.20 .

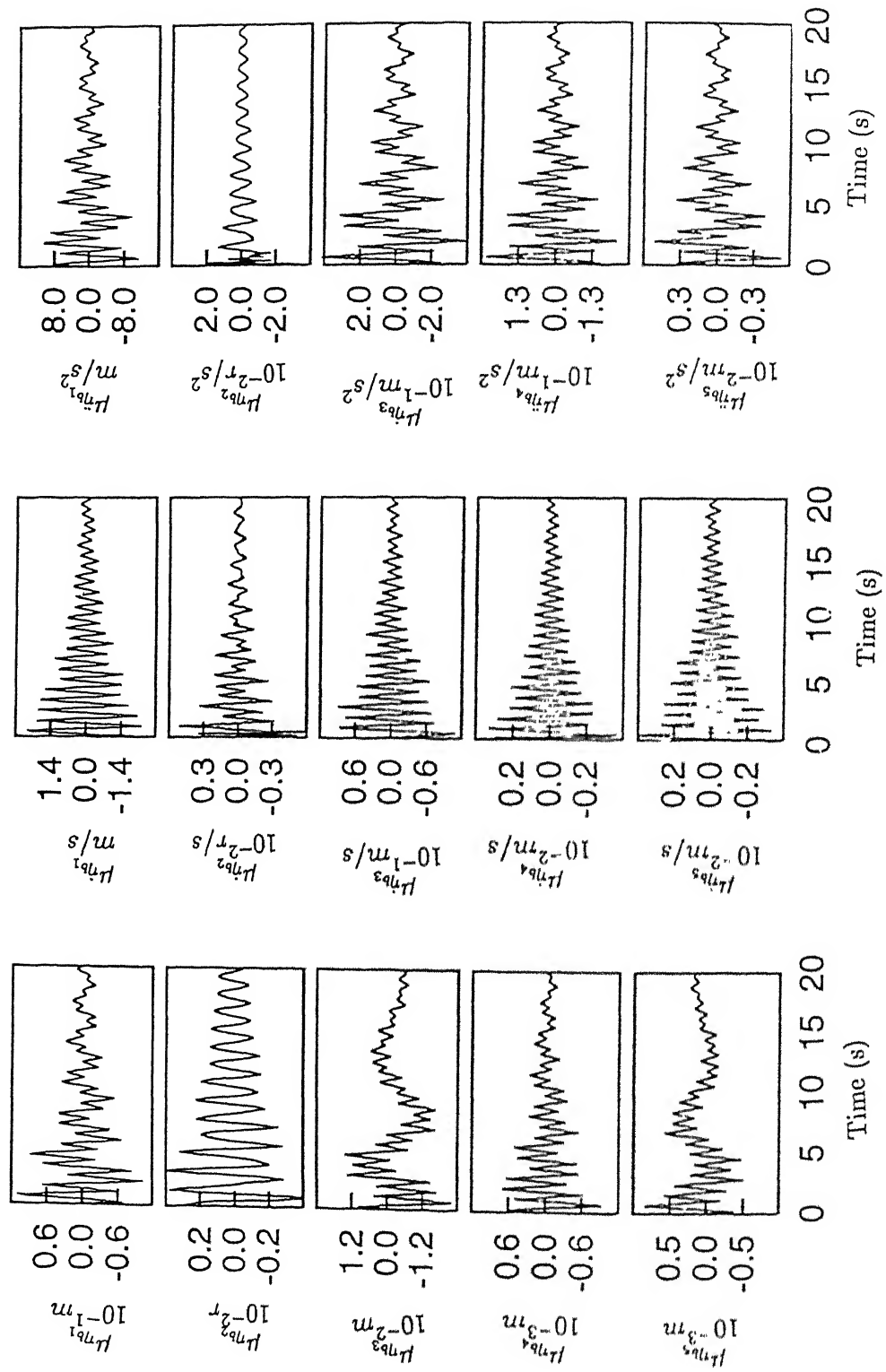


Fig.5.28. Heave-Pitch-Roll Model (Flexible fuselage in bending with rigid roll)-Mean response in landing run. Key same as 5.22

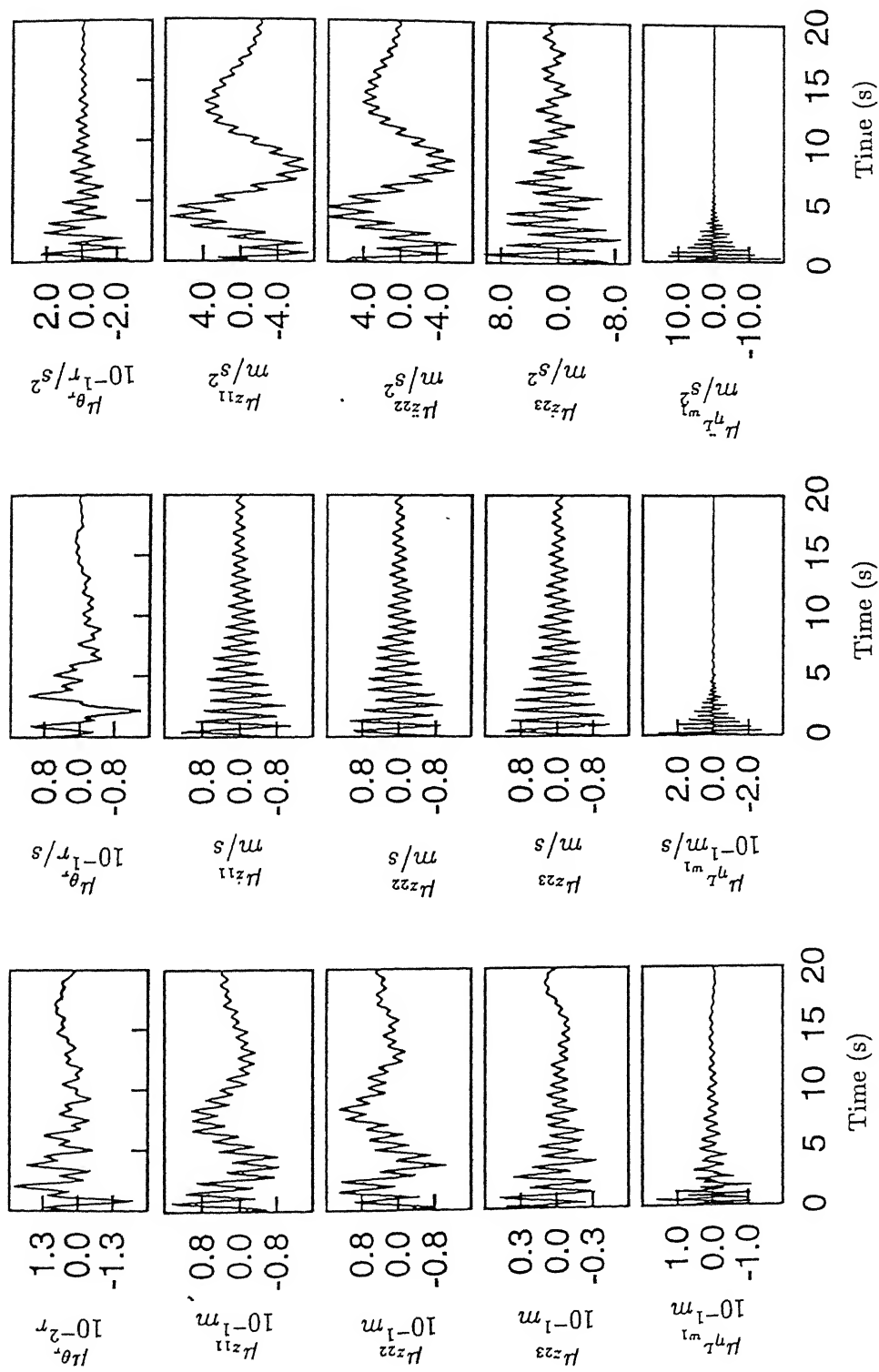


Fig.5.28(continued). Heave-Pitch-Roll Model (Flexible fuselage in bending with rigid roll)-Mean response in landing run. Key same as Fig.5.22

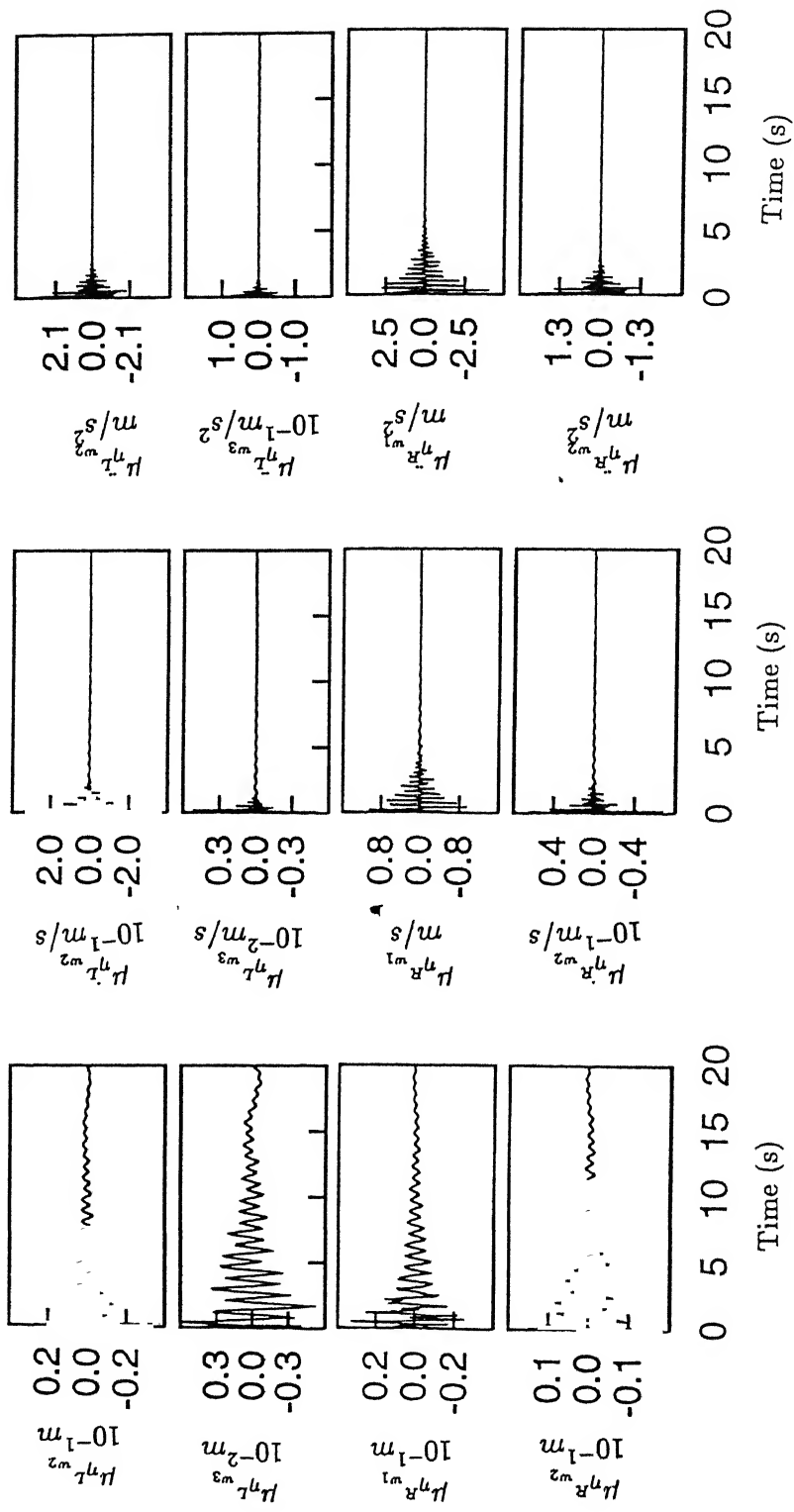


Fig.5.28(continued). Heave-Pitch-Roll Model (Flexible fuselage in bending with rigid roll)-Mean response in landing run. Key same as Fig.5.22

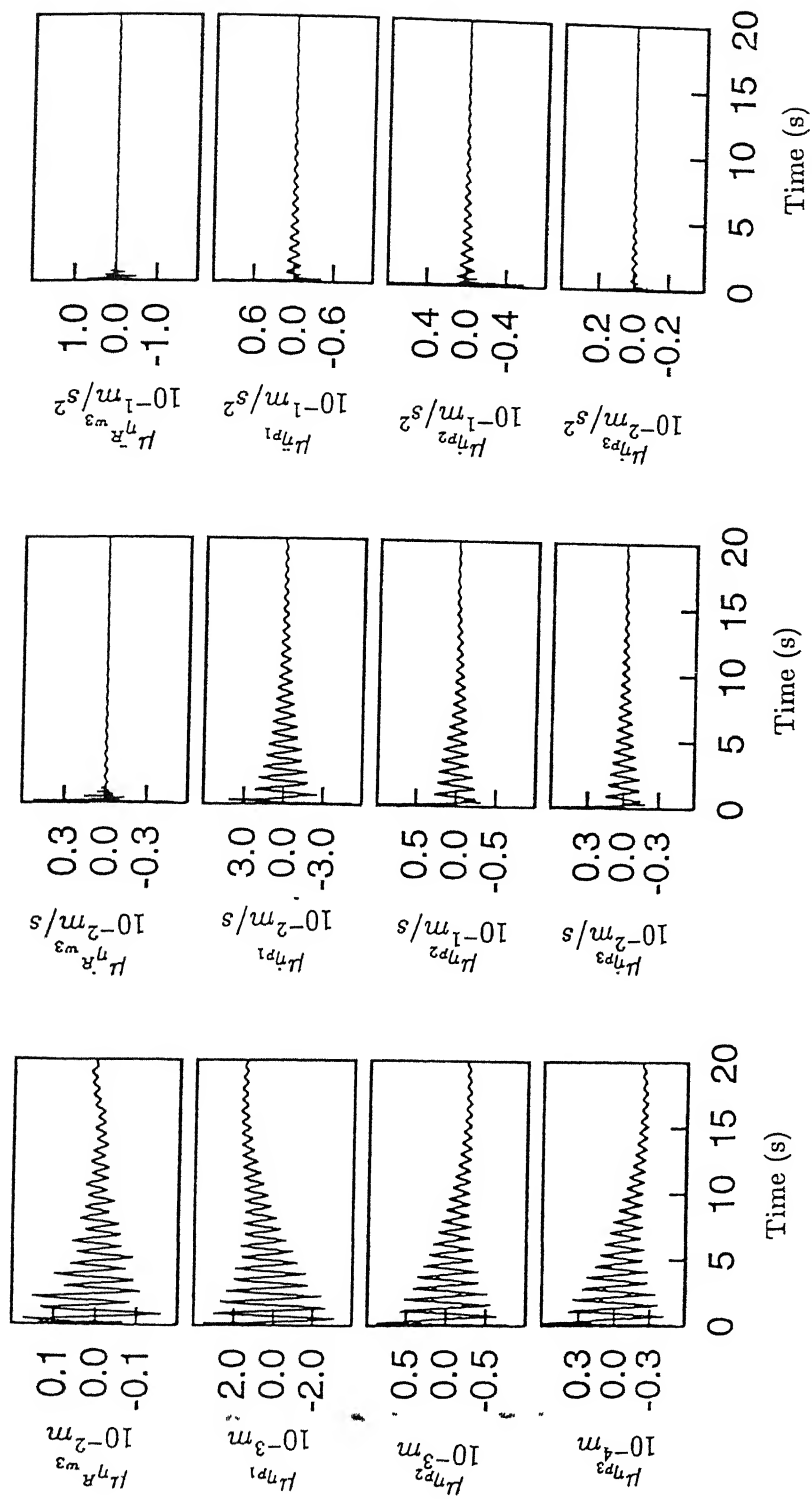


Fig.5.28(continued). Heave-Pitch-Roll Model (Flexible fuselage in bending with rigid roll)-Mean response in landing run. Key same as Fig.5.22

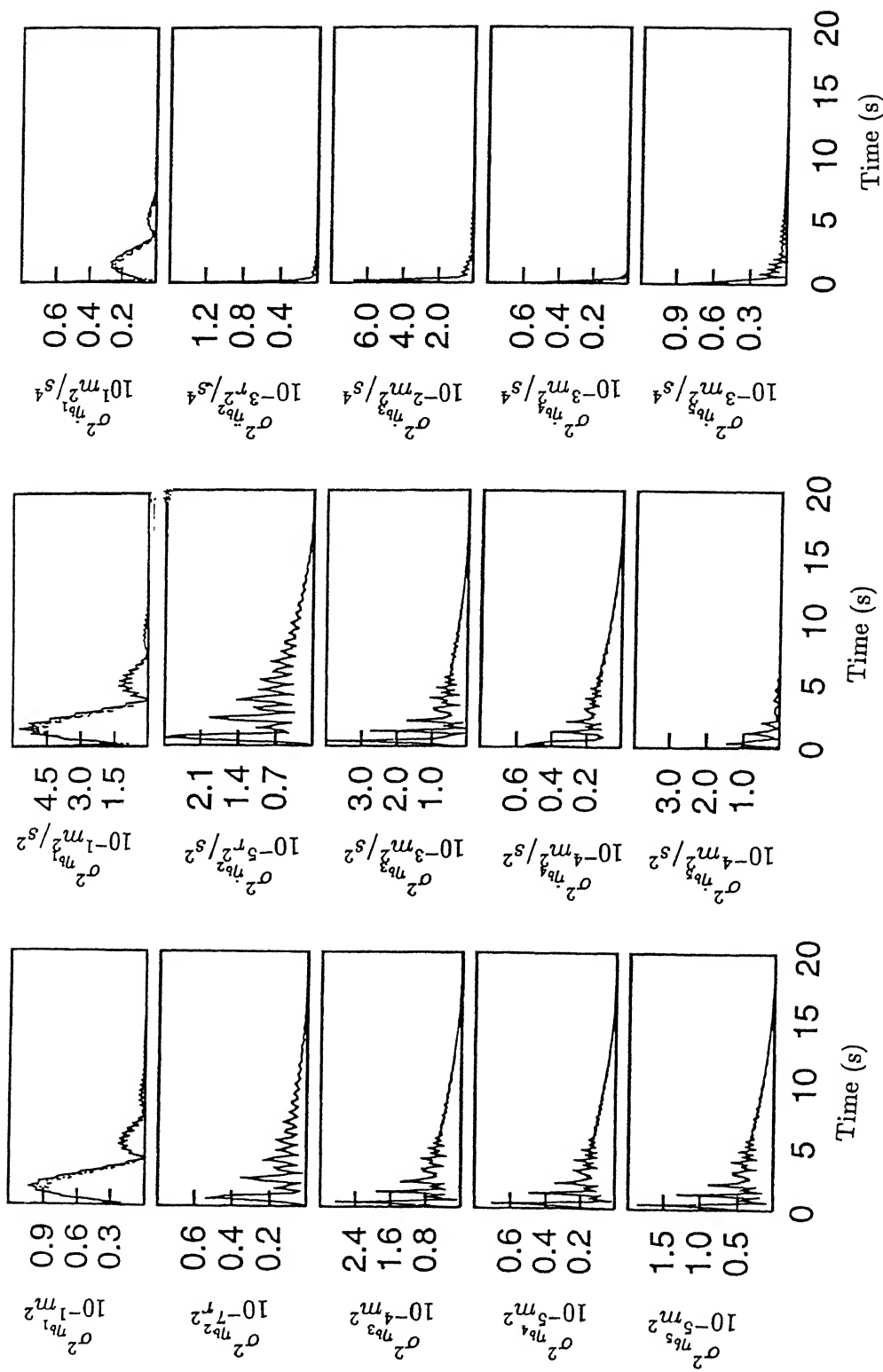


Fig.5.29. Heave-Pitch-Roll Model (Flexible fuselage in bending with rigid roll)-Response variance in landing run. Key same as Fig.5.22

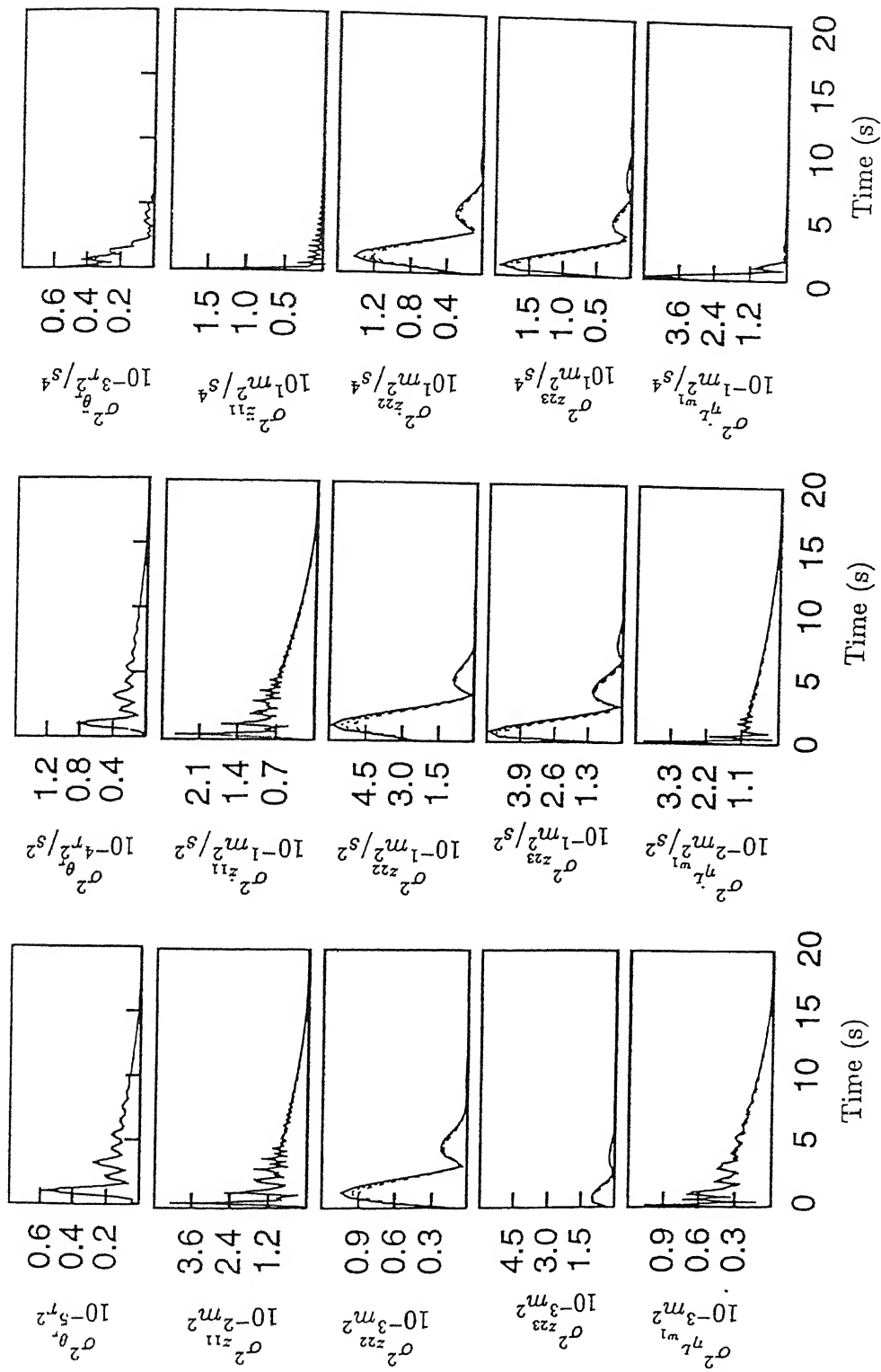


Fig.5.29(continued). Heave-Pitch-Roll Model (Flexible fuselage in bending with rigid roll)-Response variance in landing run. Key same as Fig.5.22

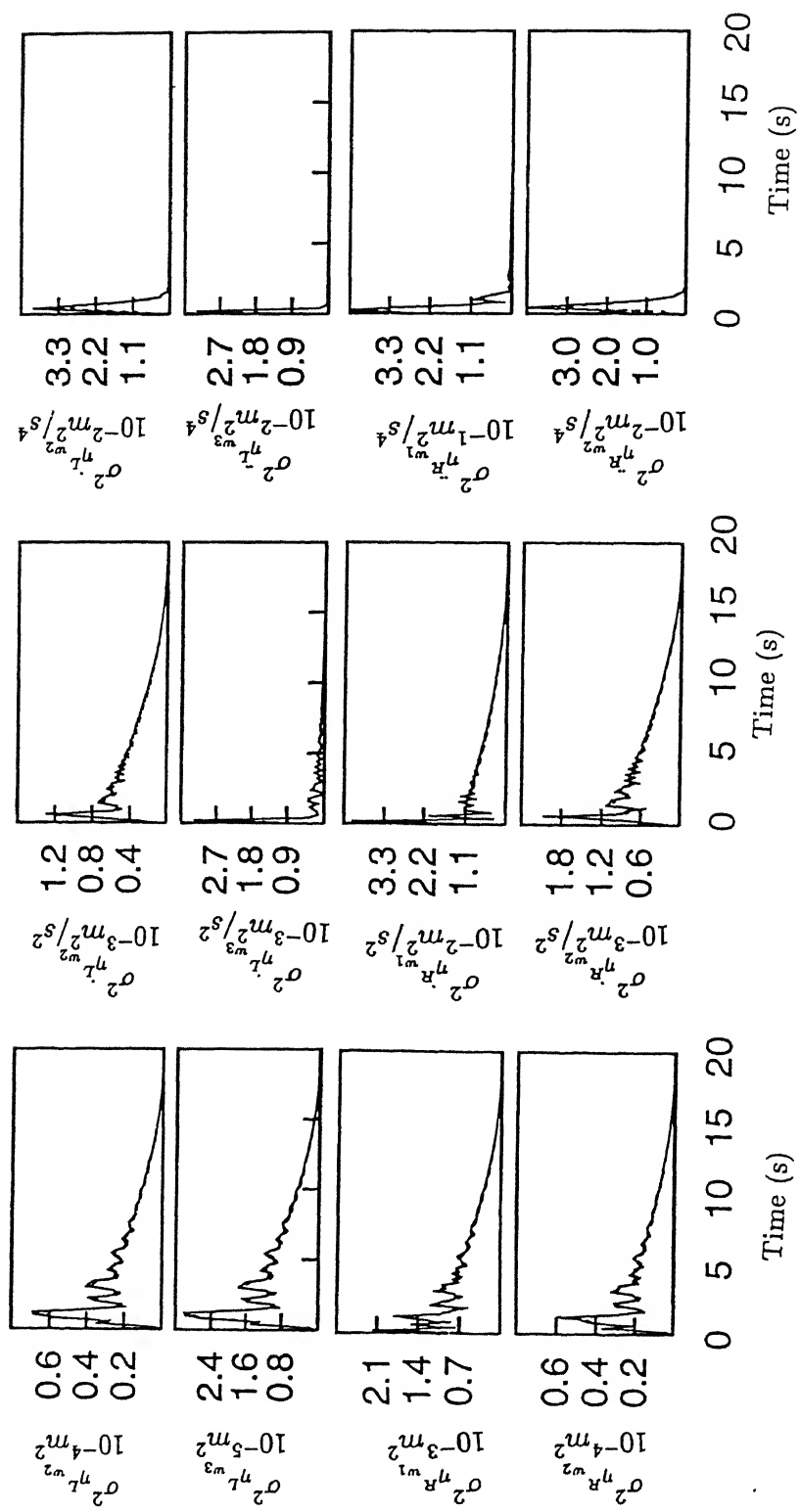


Fig.5.29(continued). Heave-Pitch-Roll Model (Flexible fuselage in bending with rigid roll)-Response variance in landing run. Key same as Fig.5.22

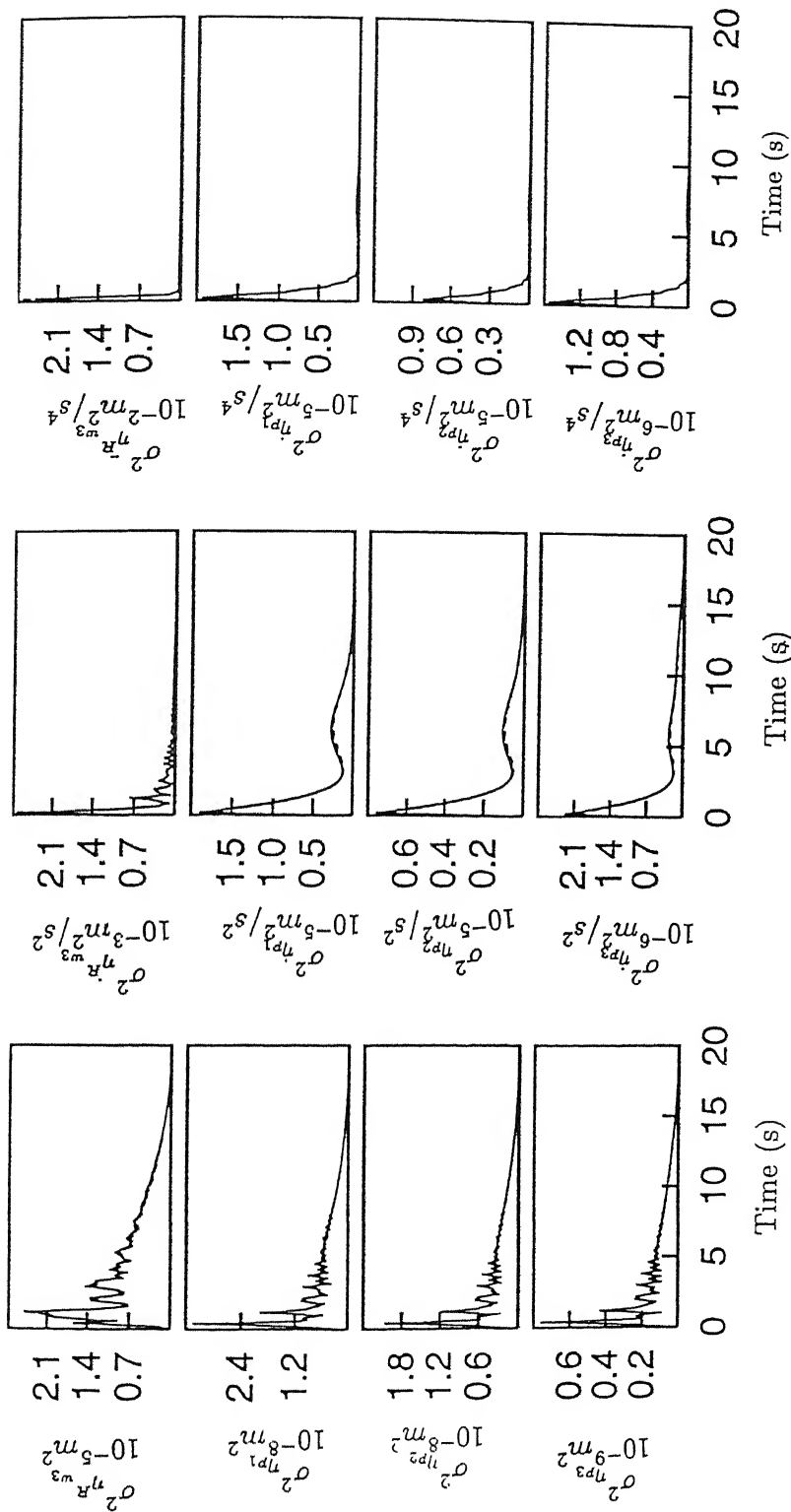


Fig.5.29(continued). Heave-Pitch-Roll Model (Flexible fuselage in bending with rigid roll)-Response variance in landing run. Key same as Fig.5.22

airframe. First three coupled bending - torsional modes of both the wings and first three flexural modes of the track have been taken into account. Along with the heave response of the three unsprung masses, results have been obtained for twentyone generalised coordinates for this model.

5.2.5.1 *Taxi Run*

Mean response are presented in Fig.5.30. Rigid body heave, pitch and roll displacement of the airframe show influence of input process mean shape. Initial transience are more prominent in velocity and acceleration mean. Out of the two angular rigid body modes, rolling motion is more affected by the change in vehicle forward velocity. Fuselage first three elastic modes in bending and torsion reveal the presence of high frequency components in mean response for the initial phase which gradually diminish to reach steady state patterns. Single dominant frequency in the steady state part which gets modified by the change in vehicle forward velocity can be observed. High frequency oscillations in the transient stage, however, are less sensitive to the change in vehicle velocity.

Unsprung masses response exhibit the similarity in pattern with the rigid body heave motion. Nose wheel acceleration mean shows high transience initially and takes considerable time to reach steady state. Two main wheels mean response characteristic are not found exactly identical. This signifies the effect of rolling of the vehicle on account of transverse variation of the track level.

Left wing mean displacements exhibit clear steady state pattern in constant velocity run which is subdued in mean velocity and acceleration. The velocity and acceleration mean are highly effected by the transience set up at the onset of motion. Right wing mean response behaviour is found to follow the trend of the left wing response except that the difference in phase in later phase of taxi run.

Track normal coordinates displacement and velocity mean show an increase in magnitude with increasing level of track mean height experienced by the wheels. Track acceleration mean has strong transience at the onset of motion and low steady state value. This may be due to shock on entry of the vehicle over the track.

Response variances of the system generalised coordinates in taxi run are presented in Fig.5.31. The displacement variances have an oscillatory pattern with high peak at the onset of the vehicle motion. Subsequently the response subsides to reach a steady asymptotic value. The variances of the velocity response follow a trend similar to the displacements. The acceleration variances indicate dominant values at the initiation of motion. The asymptotic value is reached within shorter time than that for displacement and velocity, showing progressively smaller peaks. The asymptotic values, however, are very low compared to the initial value.

5.2.5.2 Take off Run

Fig.5.32 presents the mean system response during takeoff. The vehicle is assumed to start from rest, runs with gradually increasing velocity till liftoff. Initial portion of the mean response shows low transience. Mean response magnitudes are seen to build up gradually with the increase in vehicle forward speed and track mean level which has a rising gradient. However, as the aircraft proceeds to takeoff, mean response shows decrease in amplitude. Rigid body motion in roll seems to be more pronounced with increasing velocity. Response behaviour of the right main wheel is different from the left main wheel showing strong interaction of rolling in the accelerating runs.

Mean response of the generalised coordinates of the left wing are found to be different from the right wing. Less transience is observed in the right wing mean response. However, phase difference is noticed between the response of the two wings. The track normal coordinate mean response shows initial low values which subsequently increase as the vehicle vibration picks up with increase in speed imposing more dynamic loads.

Response variances of the system generalised coordinates are presented in Fig.5.33. The variances for the vehicle response show very low values in the initial stage. Variances are seen to increase with forward acceleration of the vehicle, but at takeoff instances, differences in magnitudes are not appreciable.

Variances of the first three track normal coordinates have low frequency components in their response characteristics, which are more prominent in velocity and acceleration. For the slower.

takeoff acceleration, the track mode response variance seems to have higher magnitudes.

5.2.5.3 *Landing Run*

Fig.5.34 presents the mean system response during landing run. The effect of impact at touchdown, which increase with the increase in sink velocity, is revealed in the mean response of all the degrees of freedom considered in the model. With the progress of landing run, impact energy gets dissipated and response shows dependence only on the track roughness input. The effect of the mean input excitation is seen in fuselage elastic bending modes in displacement. However, in the airframe elastic torsional mode mean response the effect of input mean excitation is subdued. Torsional modes of the fuselage have faster dissipation of energy compared to rigid body mode in rolling.

Nose and main wheel response mean are found to have similar pattern. However, impact energy dampens quickly in case of right gear mean response. Response mean of wings generalised coordinates have very closely spaced peaks caused by the landing impact. These dampen out as the vehicle runs at decreasing speed. Wing's higher mode response mean shows slight dependence on the track roughness in the latter phase of landing run. Mean response of the track generalised coordinates also reveal the effect of landing impact. The magnitude of the track response at touch down instant is higher than for constant velocity and takeoff run.

Response variances for the landing run of the aircraft are presented in Fig. 5.35. Oscillatory patterns are observed for all

the rigid body and flexible modes of the airplane during touchdown impact. Rigid body pitch and roll response variances are quite similar in pattern. Number of peaks in roll response variance are smaller compared to pitch variance. The effect of impact persists for slightly longer duration for the roll acceleration variance. Nose wheel response variance shows slower dissipation of impact energy than the main wheels response.

Wing response variance pattern resemble the vehicle response variance. Two peaks are seen in acceleration variance of both left and right wing's first normal coordinates. Amplitude of the first peak is much higher than the second peak. Track normal coordinate's displacement variance show oscillations with high frequency components while velocity and acceleration response have dominant low frequency components.

5.2.6 Comparison of Some Linear Models Behaviour

In response analysis, selection of model is very important. The purpose of the present section is to present a comparative study of response behaviour of different vehicle models so that a approximate guidelines for the selection of model can be framed. Four different vehicle models have been considered. These are (1) Model 1- Heave -Pitch rigid aircraft model (2) Model 2 - Heave - Pitch flexible aircraft model with bending flexibility of the fuselage. (3) Model 3 - Heave - Pitch - Roll model with fuselage bending and rigid roll. (4) Model 4 - Heave - Pitch - Roll model including fuselage bending and torsional flexibility.

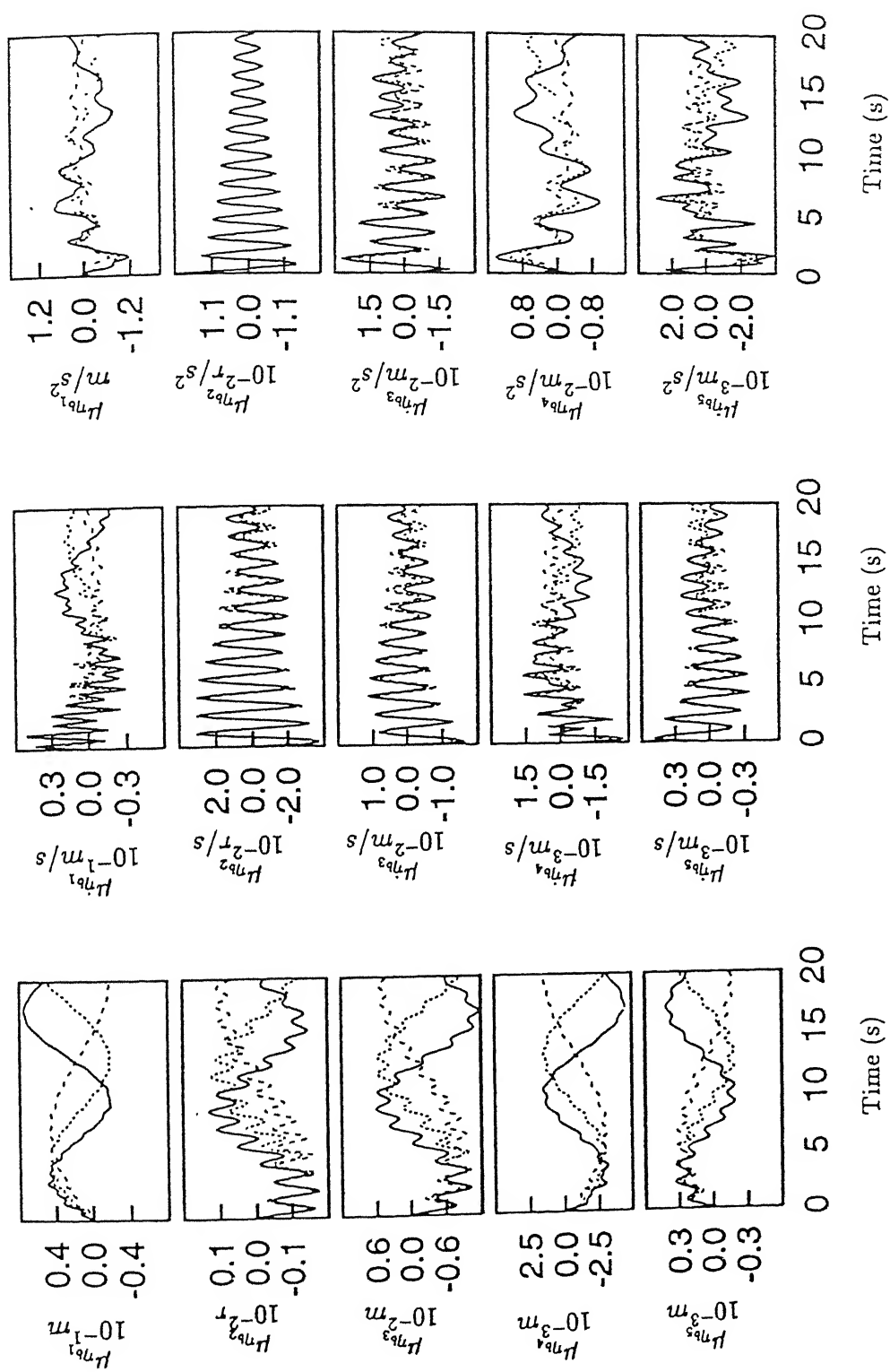


Fig.5.30. Heave-Pitch-Roll Model (Flexible fuselage in bending and torsion)-Mean response in taxi run. Key same same as Fig.5.18

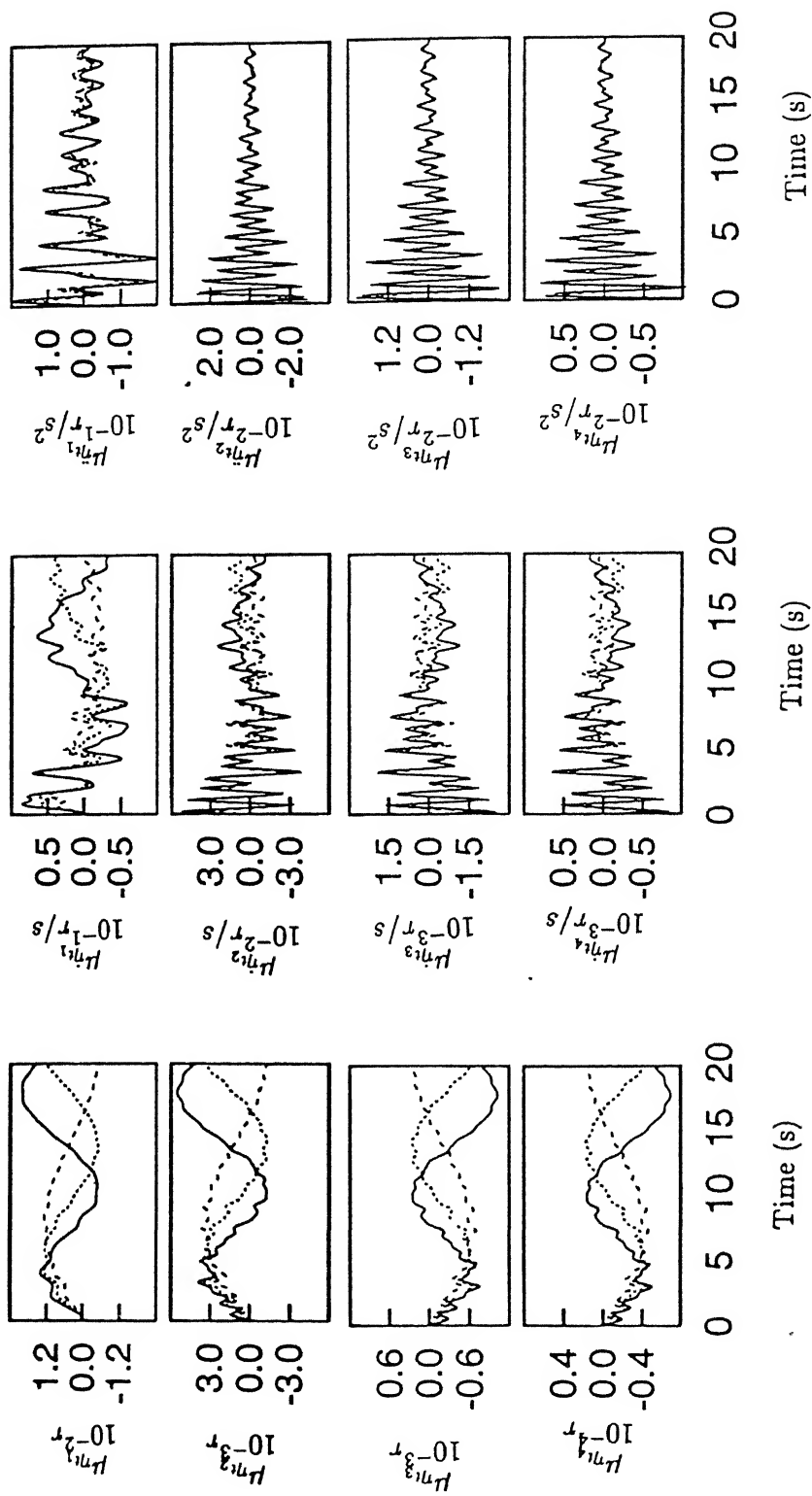


Fig.5.30(continued). Heave-Pitch-Roll Model (Flexible fuselage in bending and torsion)-Mean response in taxi run. Key same as Fig.5.18

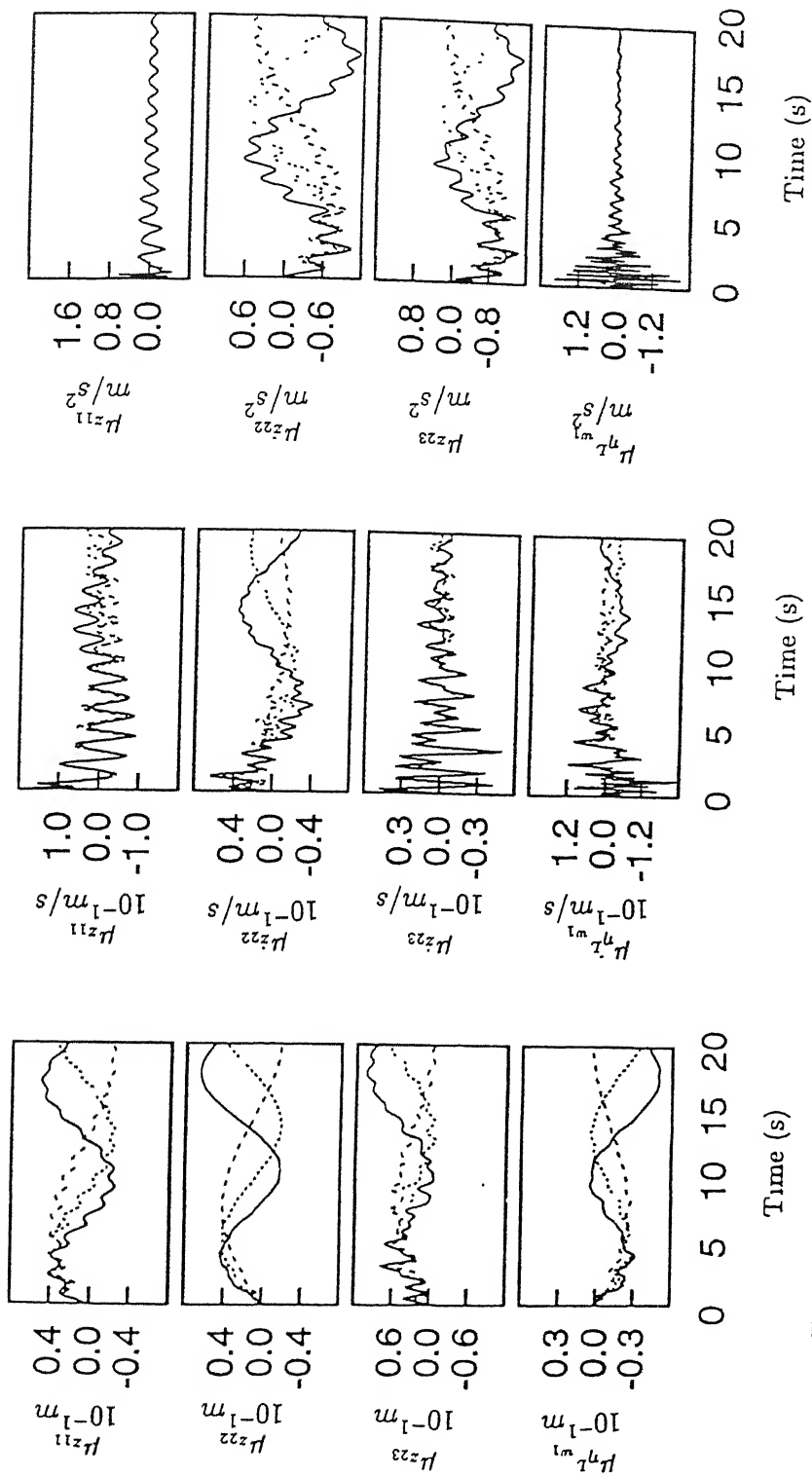


Fig.5.30(continued). Heave-Pitch-Roll Model (Flexible fuselage in bending and torsion)-Mean response in taxi run. Key same as Fig.5.18

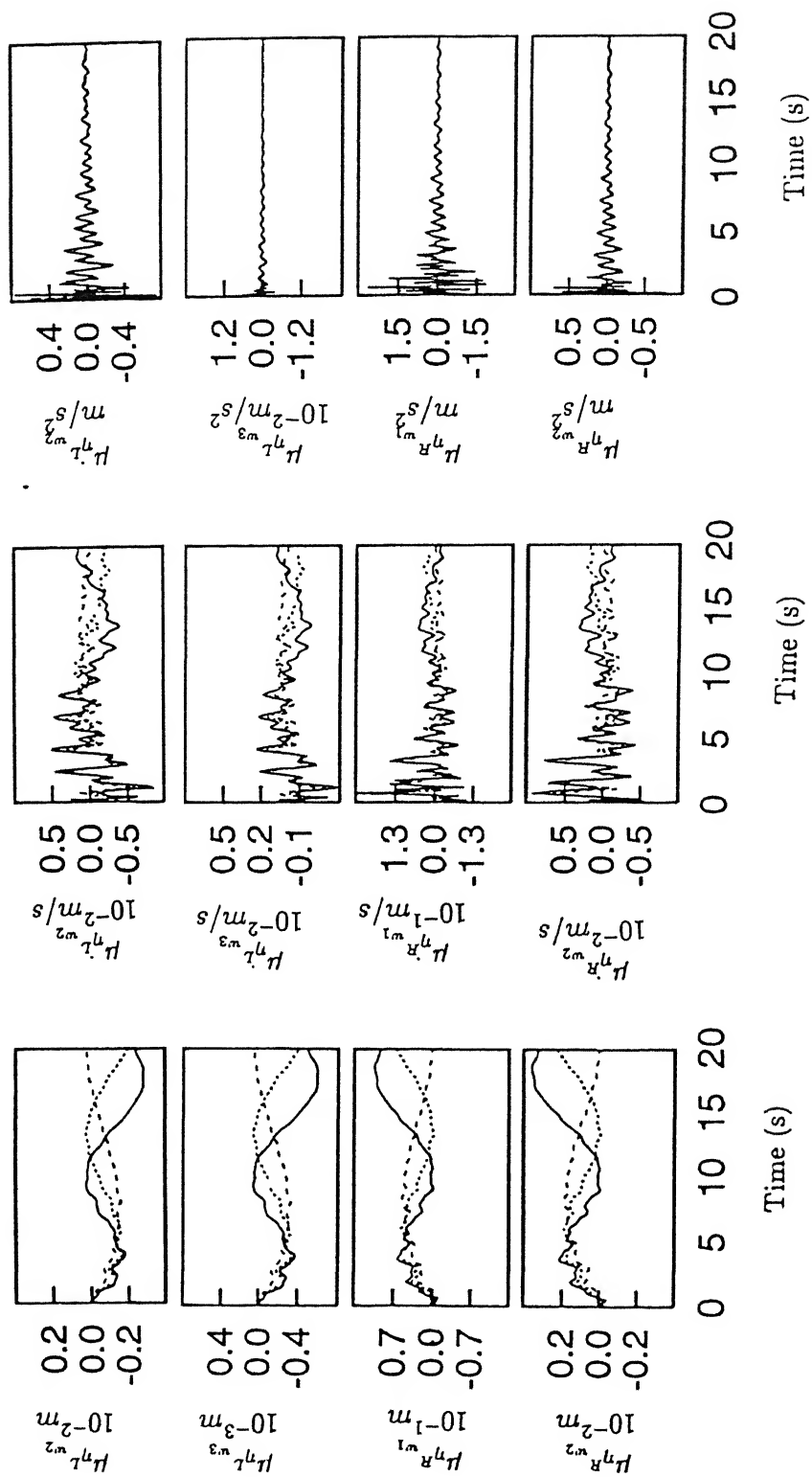


Fig.5.30(continued). Heave-Pitch-Roll Model (Flexible fuselage in bending and torsion)-Mean response in taxi run. Key same as Fig.5.18

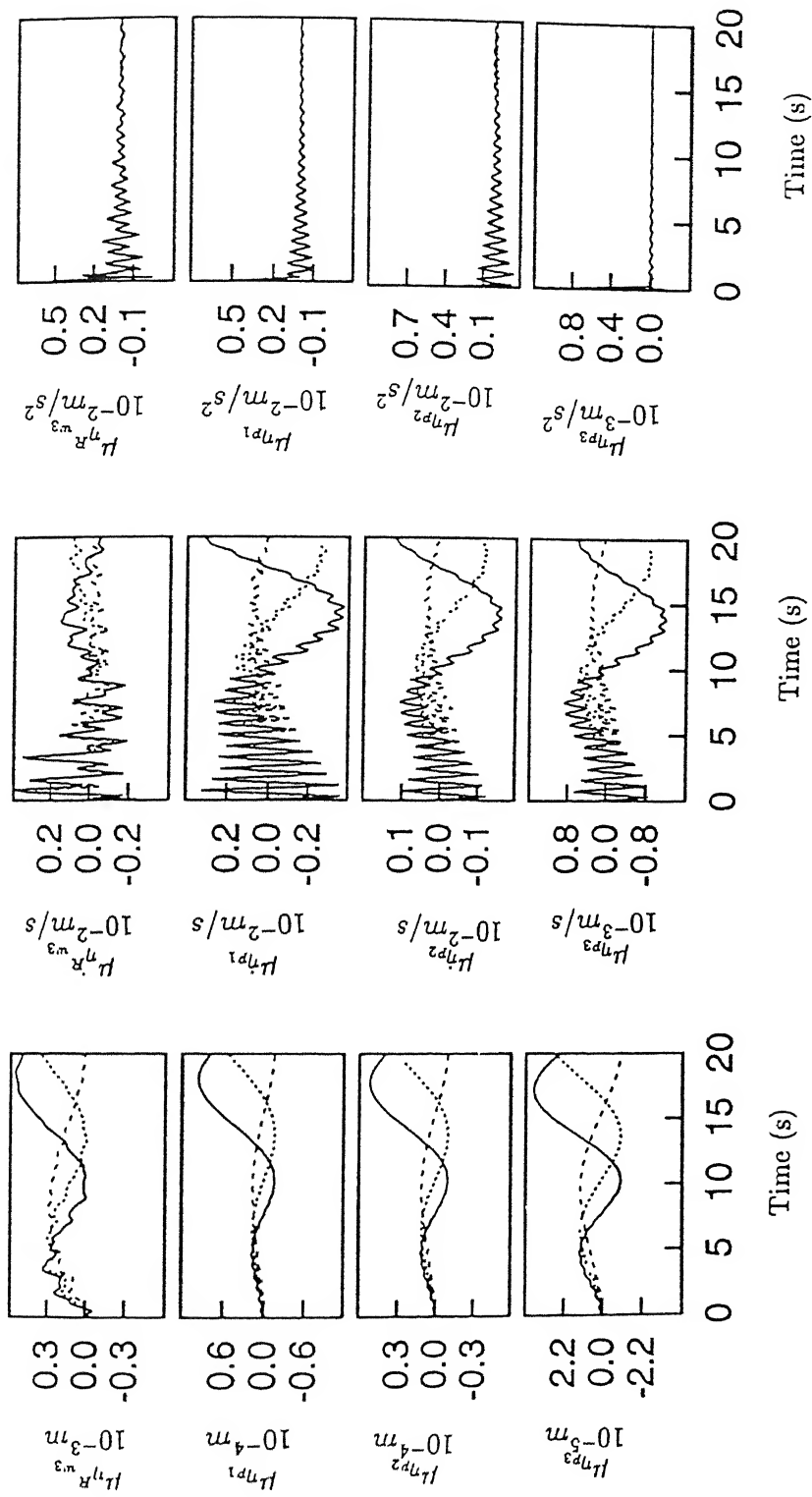


Fig.5.30(continued). Heave-Pitch-Roll Model (Flexible fuselage in bending and torsion)-Mean response in taxi run. Key same as Fig.5.18

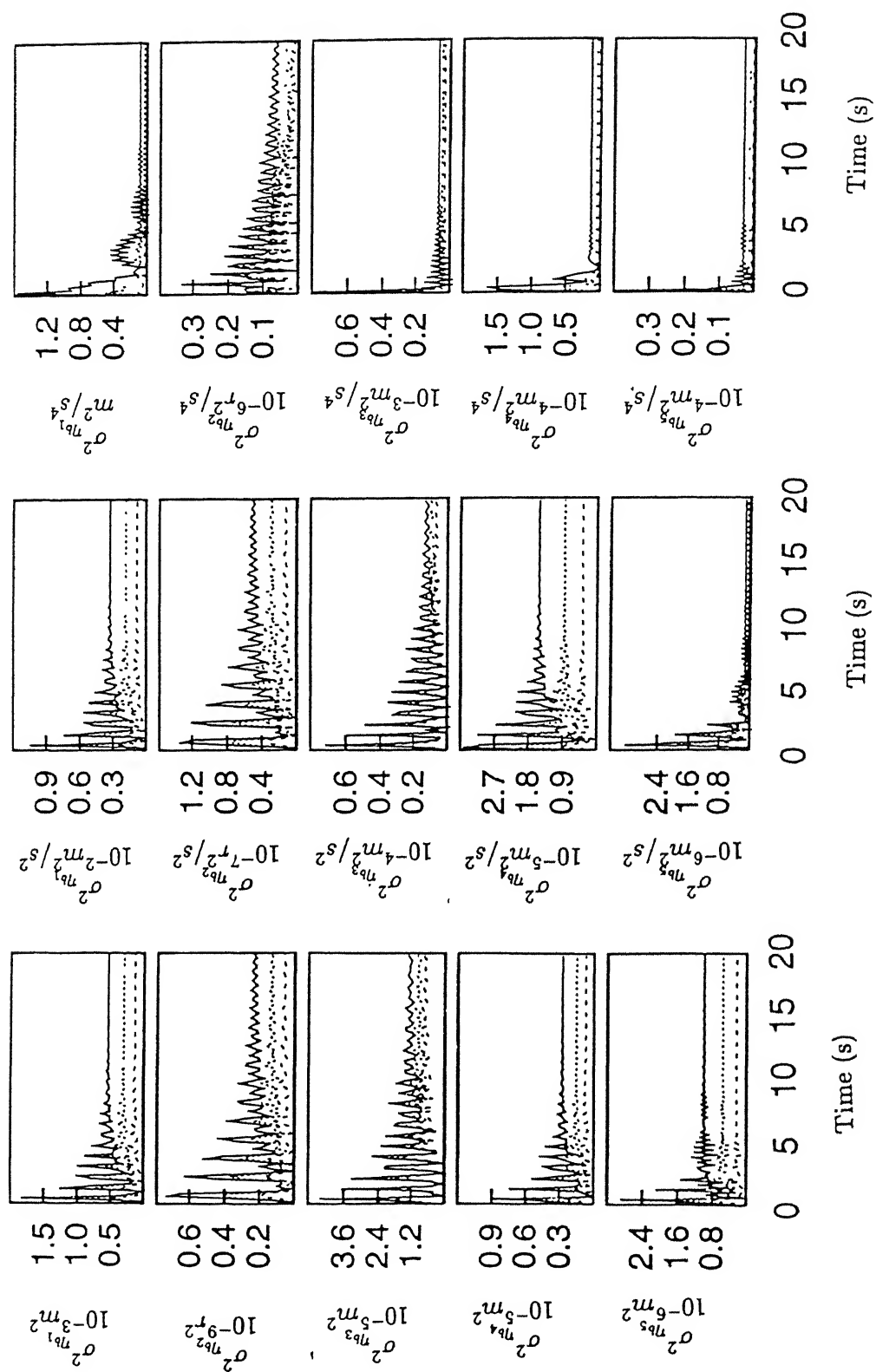


Fig.5.31. Heave-Pitch-Roll Model (Flexible fuselage in bending and torsion)-Response variance in taxi run. Key same as Fig.5.18

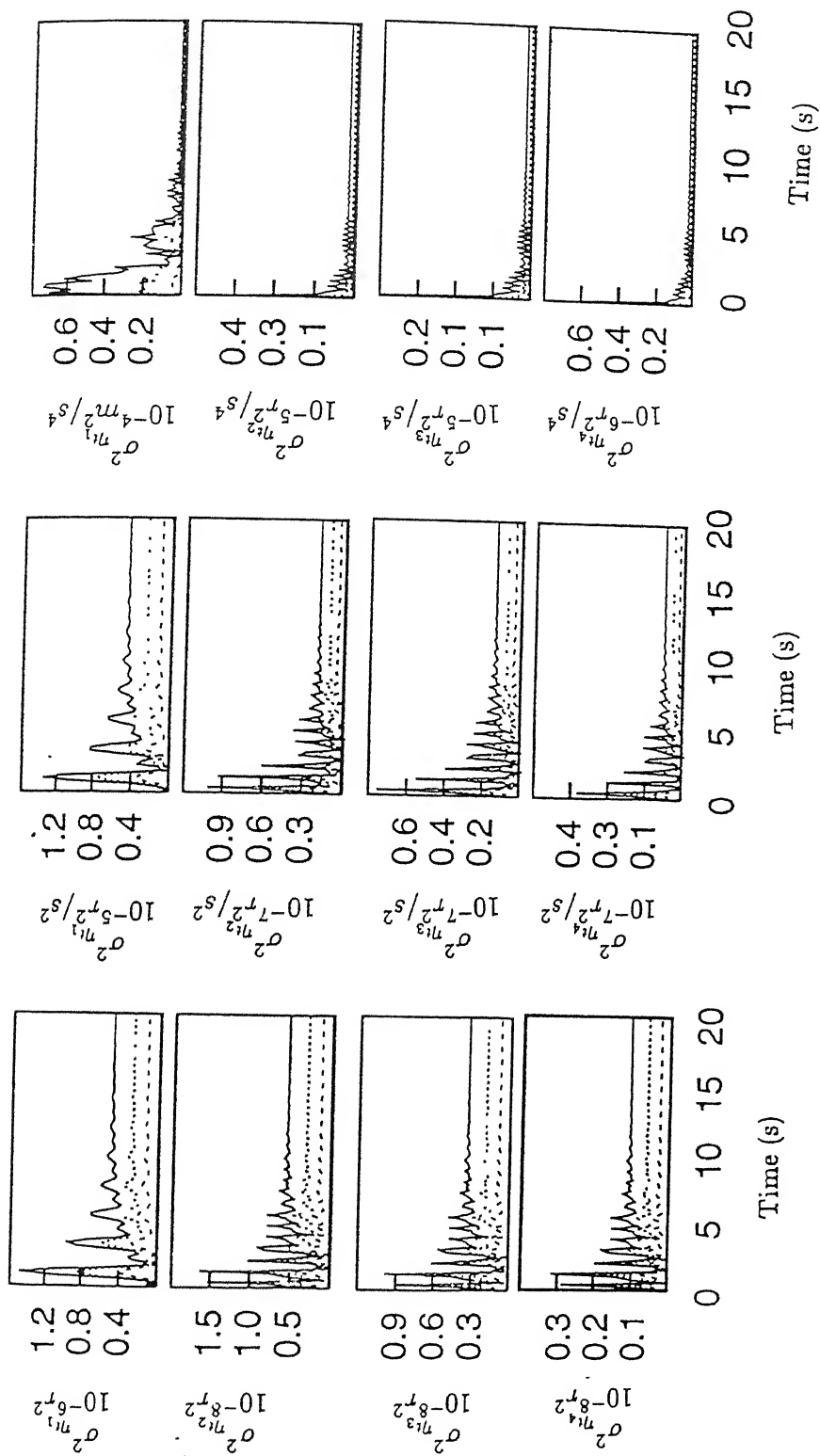


Fig.5.31(continued). Heave-Pitch-Roll Model (Flexible fuselage in bending and torsion)-Response variance in taxi run. Key same as Fig.5.18

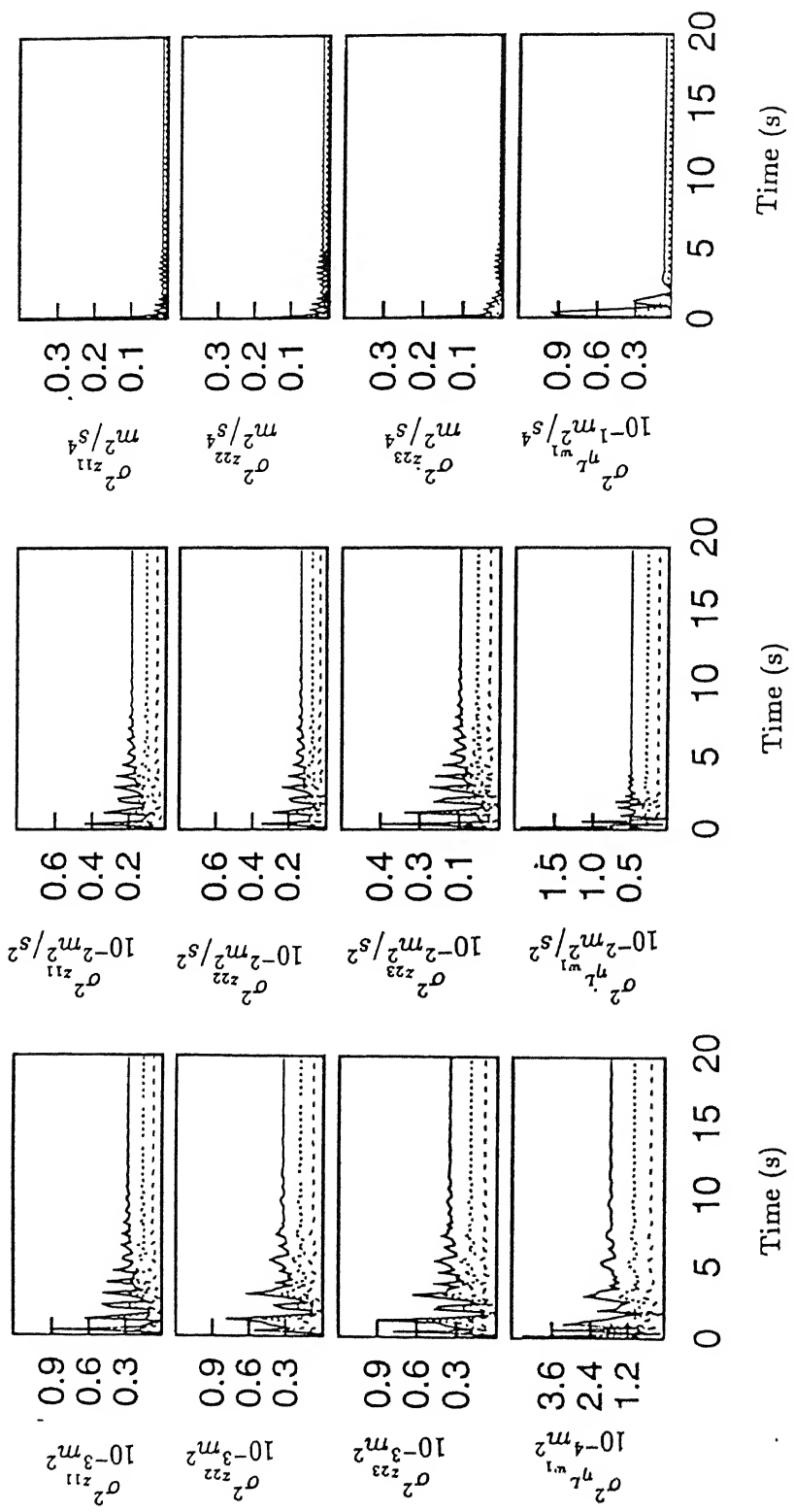


Fig.5.31(continued). Heave-Pitch-Roll Model (Flexible fuselage in bending and torsion)-Response variance in taxi run. Key same as Fig.5.18

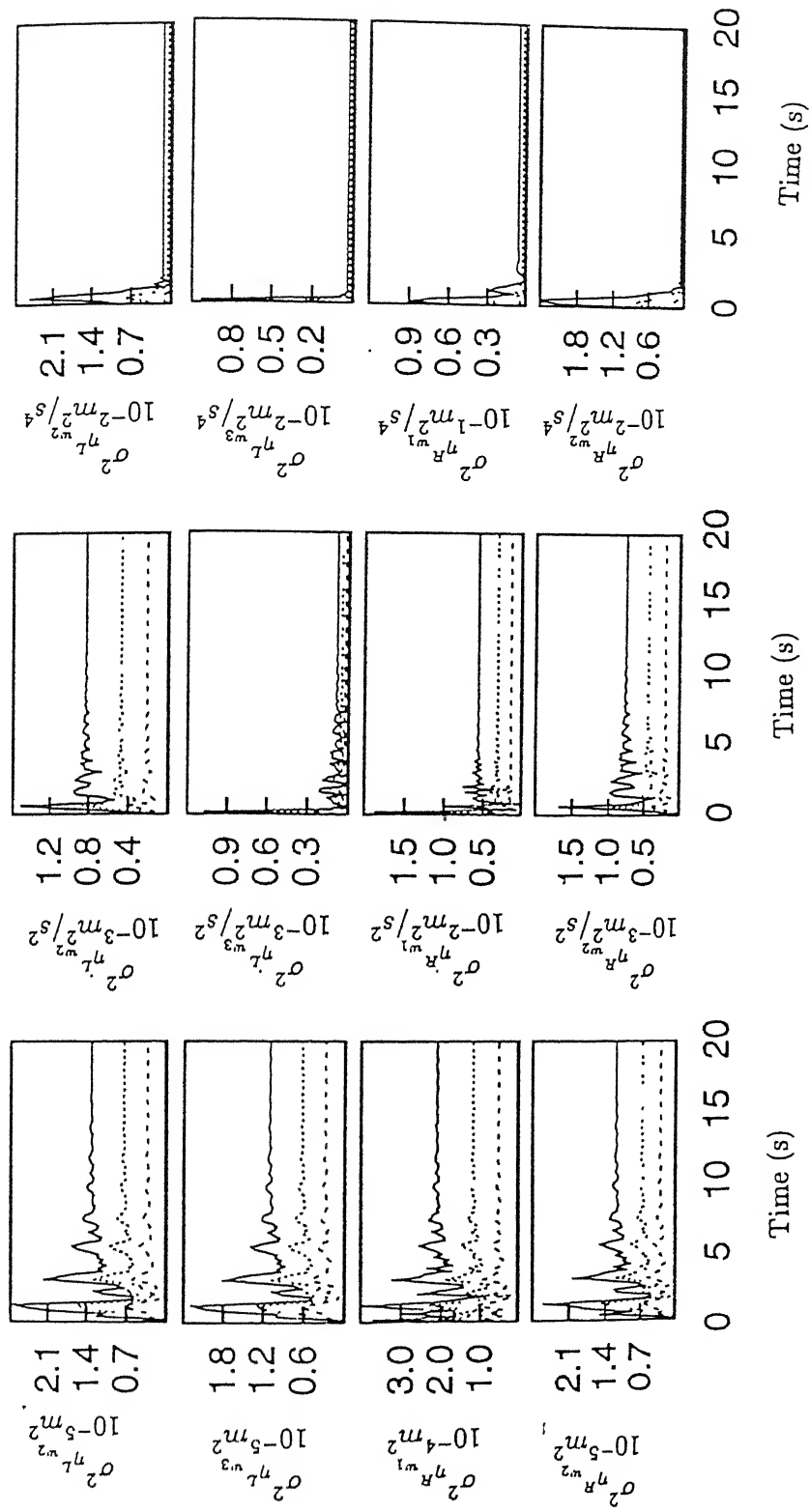


Fig.5.31(continued). Heave-Pitch-Roll Model (Flexible fuselage in bending and torsion)-Response variance in taxi run. Key same as Fig.5.18

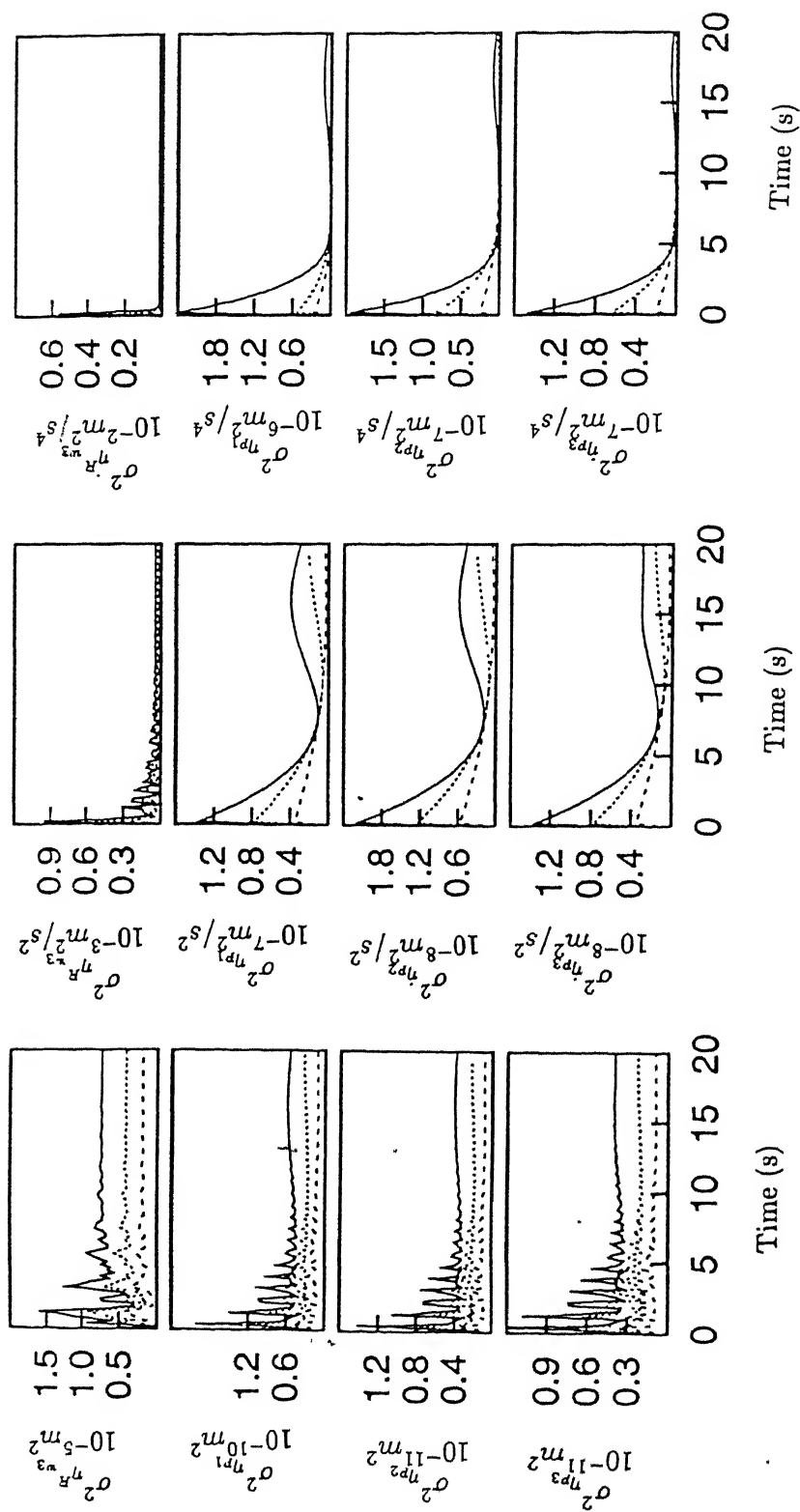


Fig.5.31(continued). Heave-Pitch-Roll Model (Flexible fuselage in bending and torsion)-Response variance in taxi run. Key same as Fig.5.18

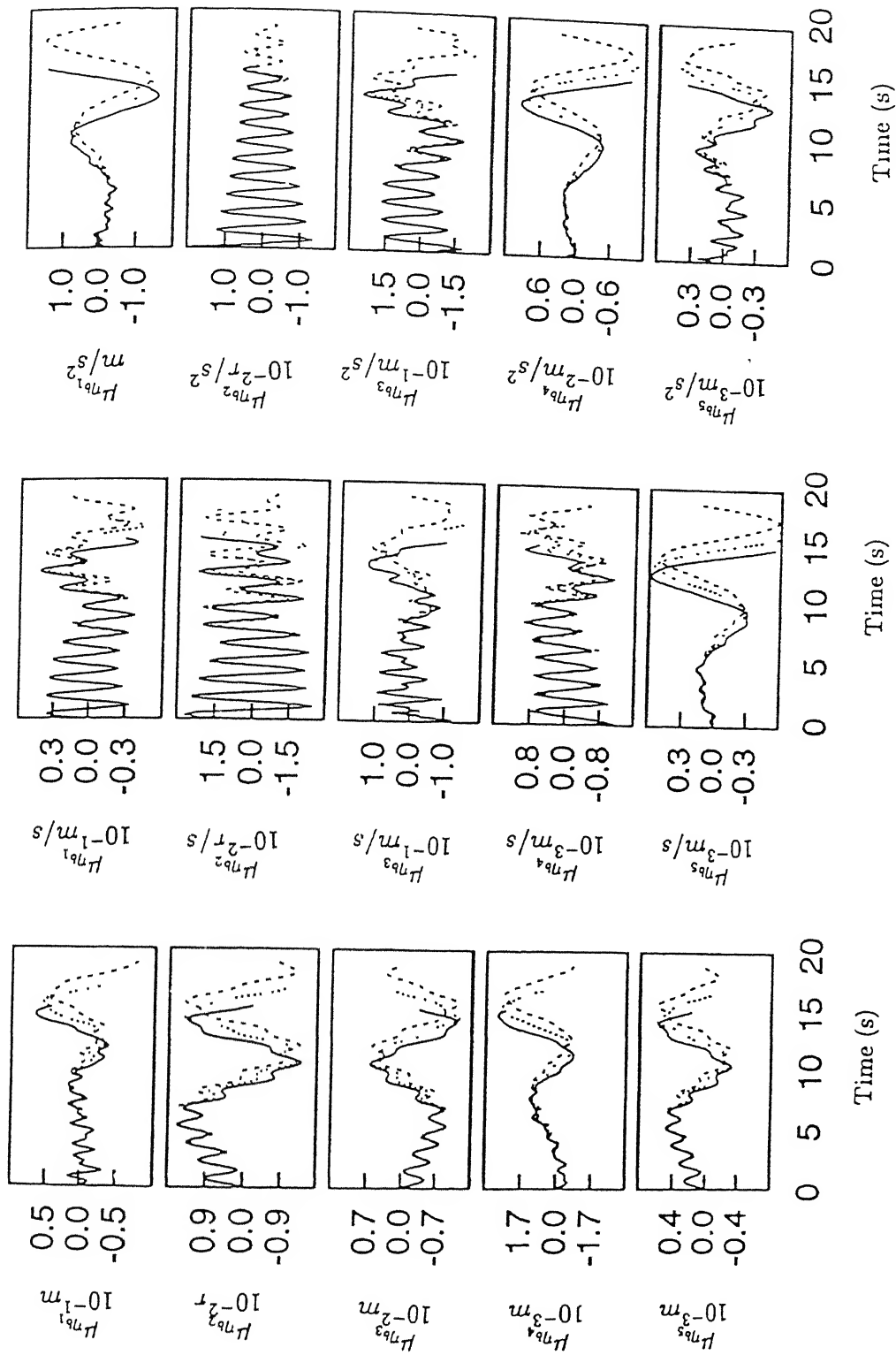


Fig.5.32. Heave-Pitch-Roll Model (Flexible fuselage in bending and torsion)-Mean response in takeoff run. Key same as Fig.5.20

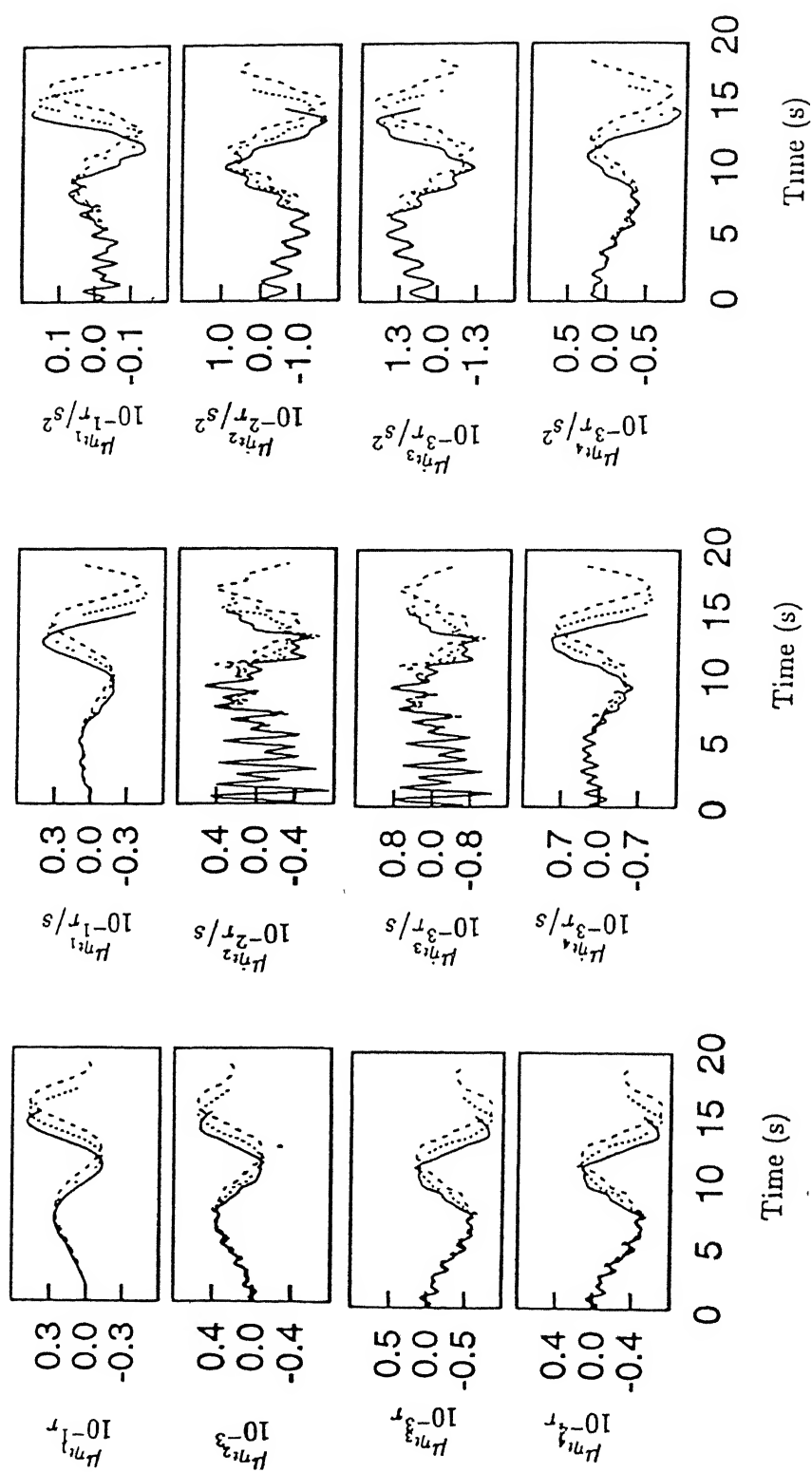


Fig.5.32(continued). Heave-Pitch-Roll Model (Flexible fuselage in bending and torsion)-Mean response in takeoff run. Key same as Fig.5.20

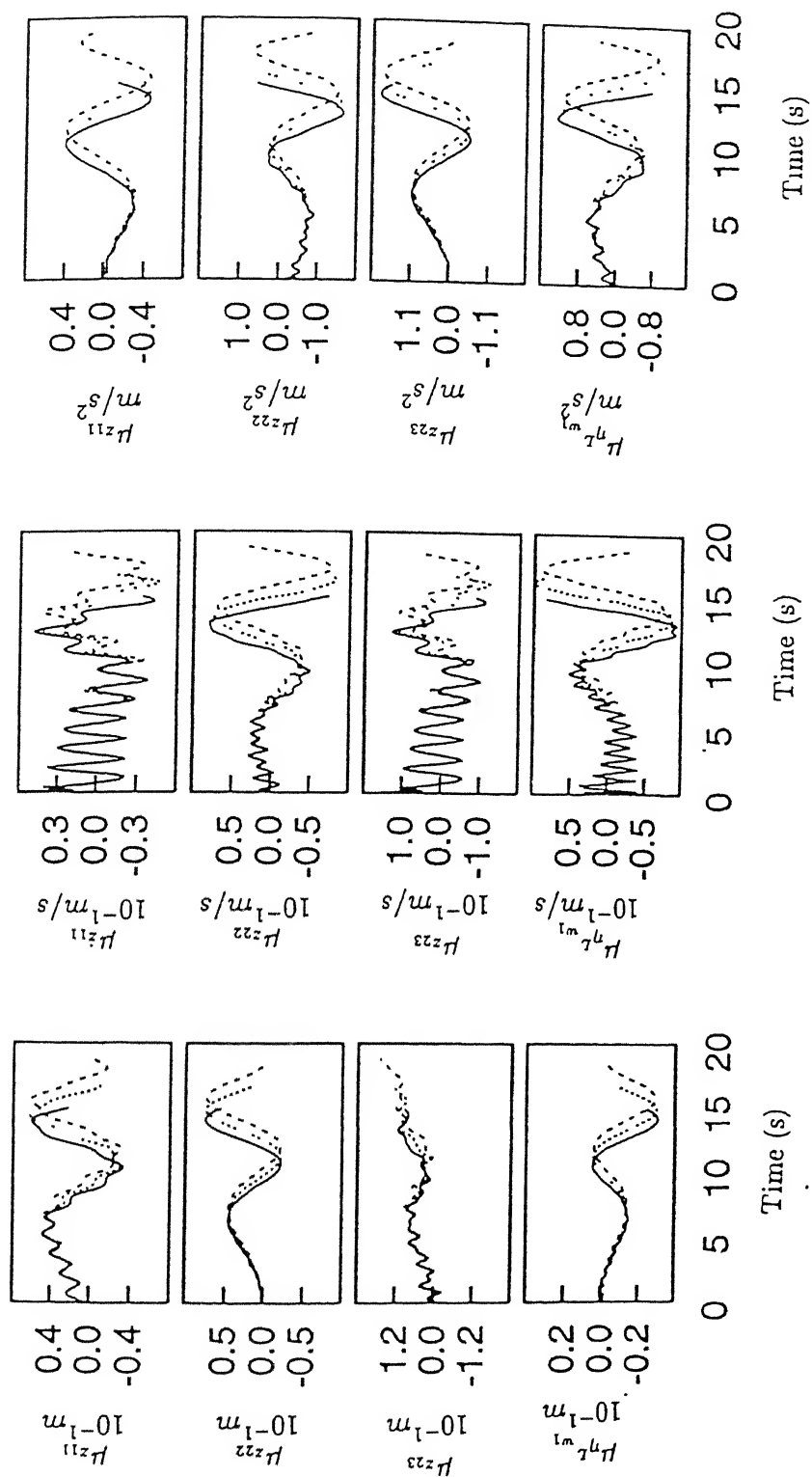


Fig.5.32(continued). Heave-Pitch-Roll Model (Flexible fuselage in bending and torsion)-Mean response in takeoff run. Key same as Fig.5.20

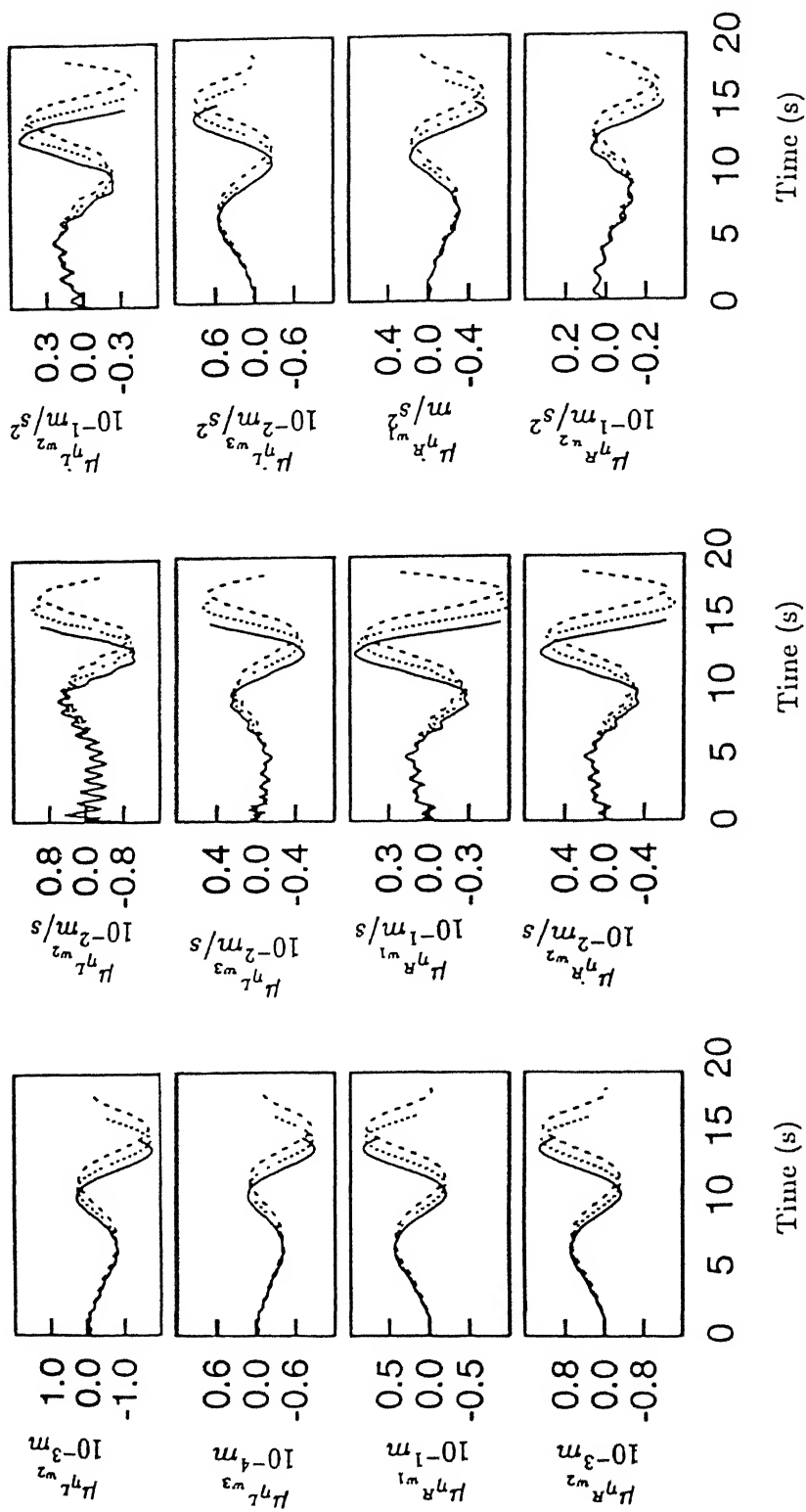


Fig.5.32(continued). Heave-Pitch-Roll Model (Flexible fuselage in bending and torsion)-Mean response in takeoff run. Key same as Fig.5.20

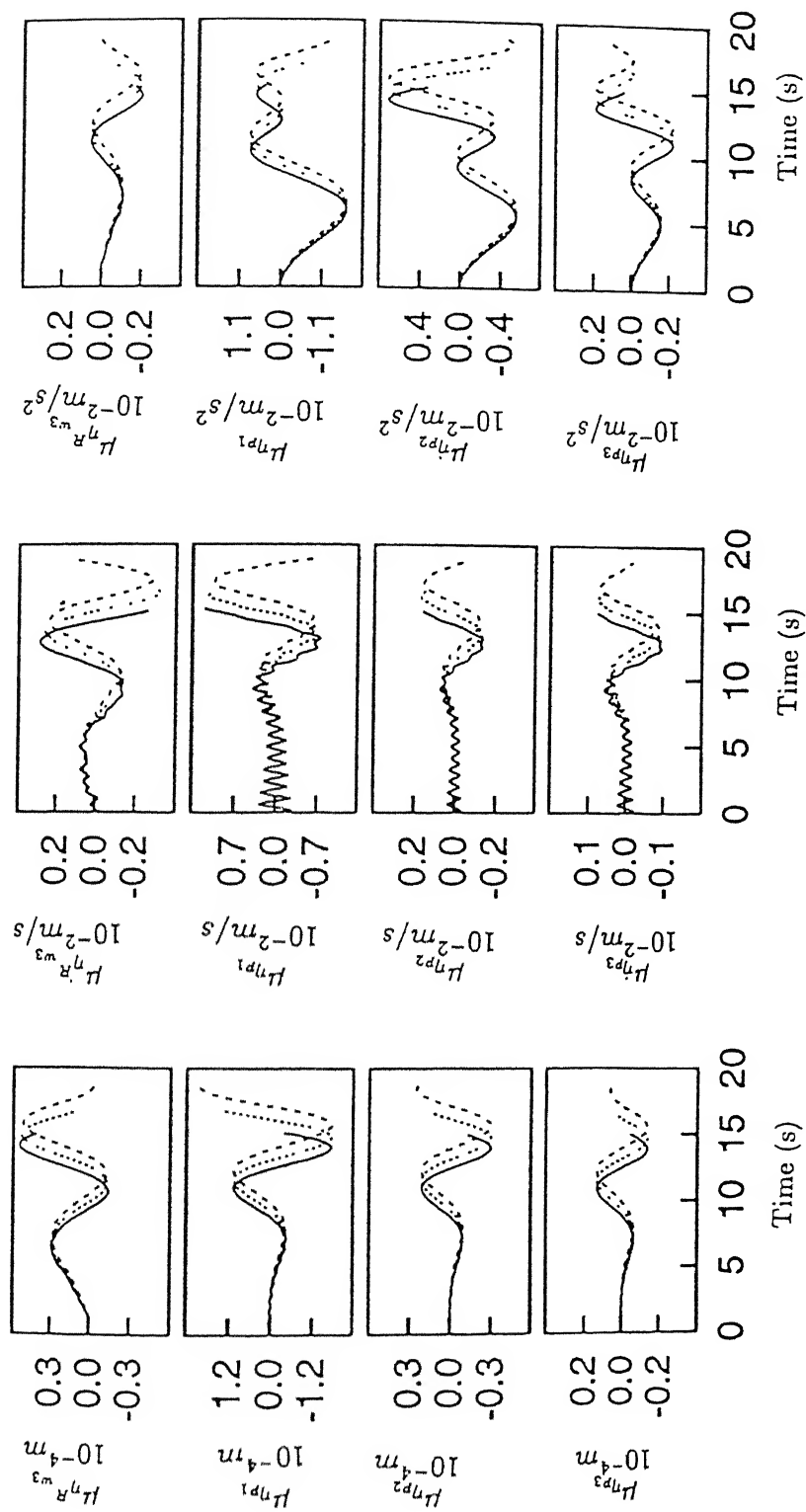


Fig.5.32(continued). Heave-Pitch-Roll Model (Flexible fuselage in bending and torsion)-Mean response in takeoff run. Key same as Fig.5.20

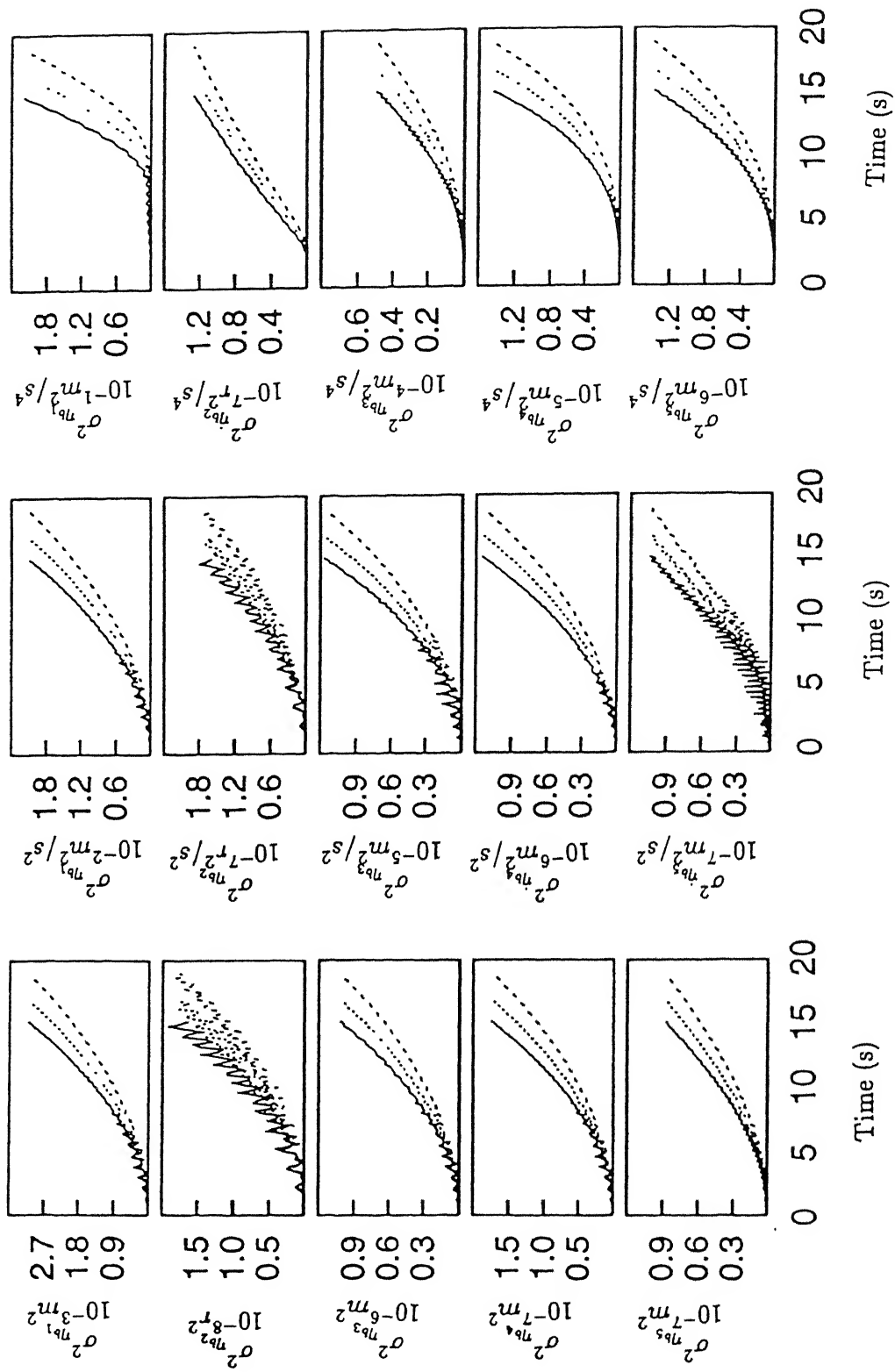


Fig.5.33. Heave-Pitch-Roll Model (Flexible fuselage in bending and torsion)-Response variance in takeoff run. Key same as Fig.5.20

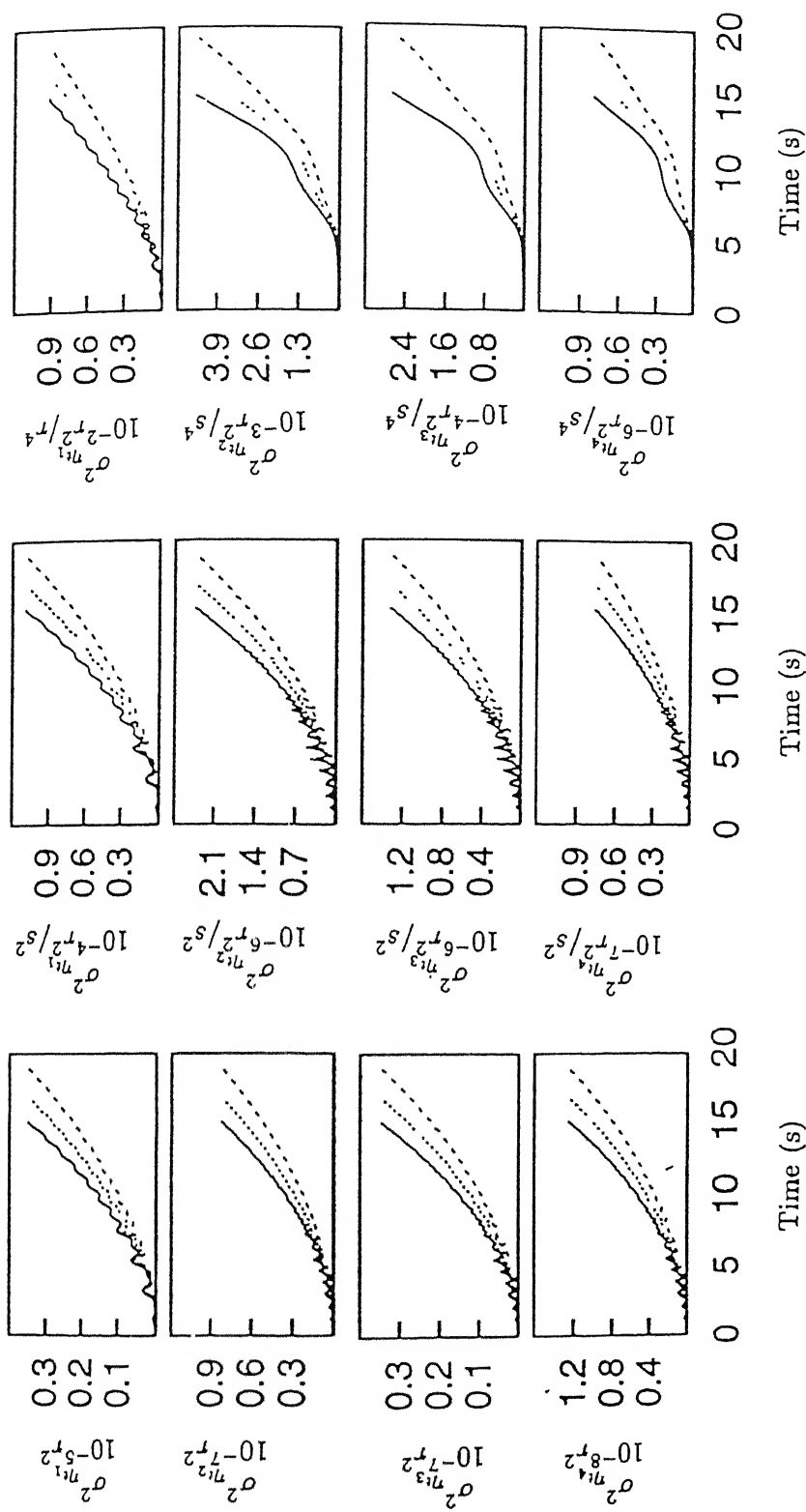


Fig.5.33(continued). Heave-Pitch-Roll Model (Flexible fuselage in bending and torsion)-Response variance in takeoff run. Key same as Fig.5.20

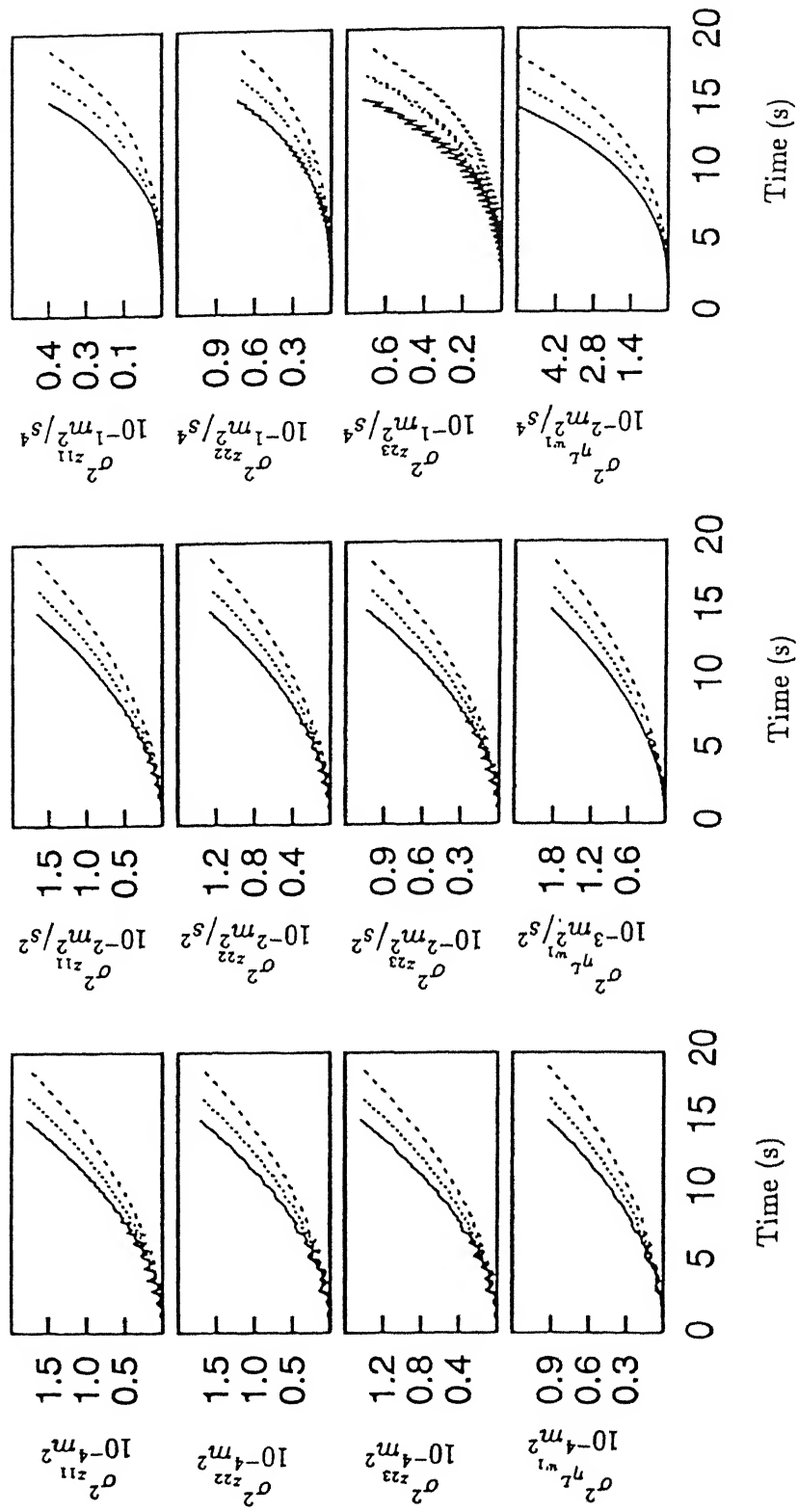


Fig.5.33(continued). Heave-Pitch-Roll Model (Flexible fuselage in bending and torsion)-Response variance in takeoff run. Key same as Fig.5.20

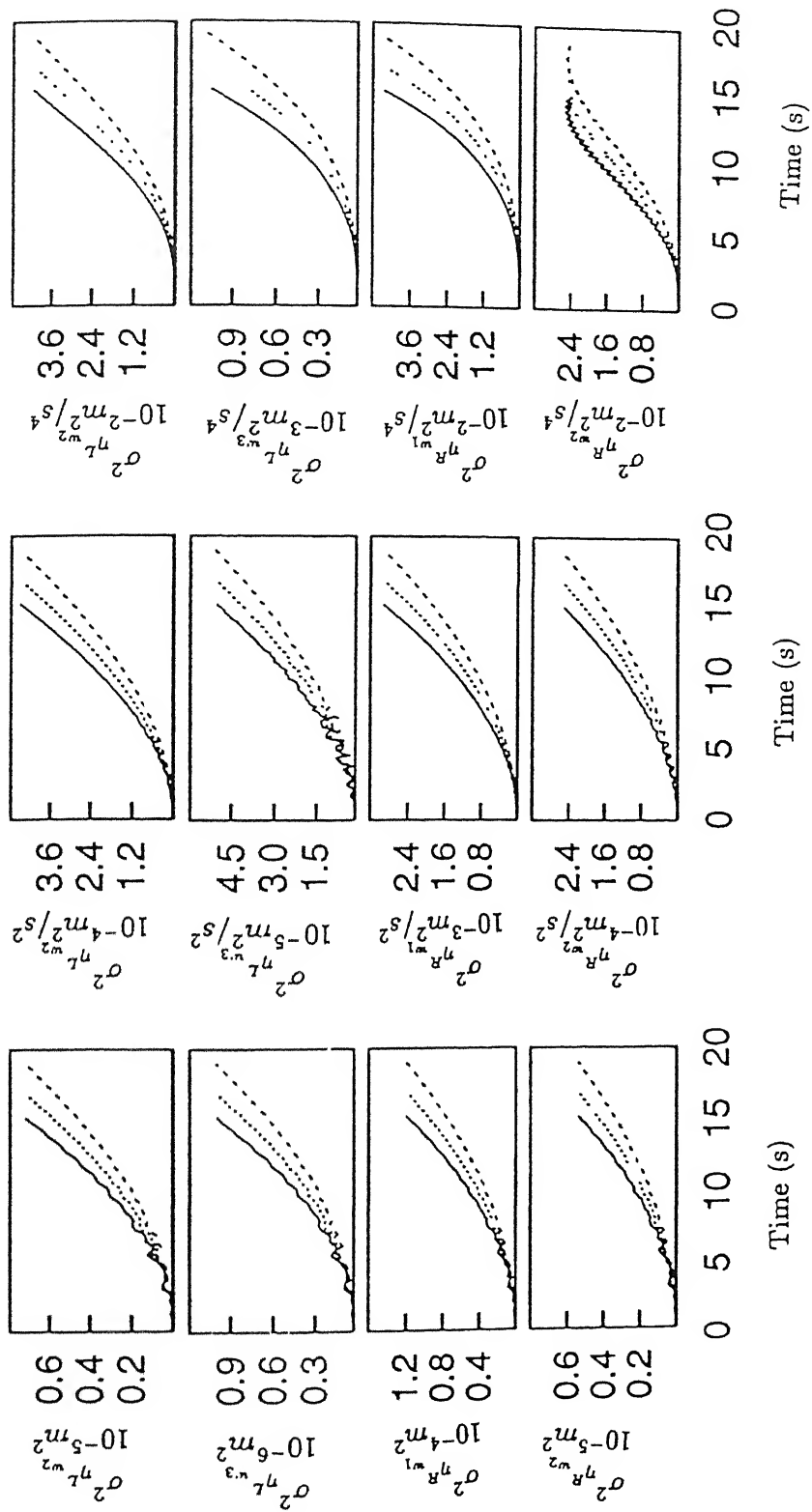


Fig.5.33(continued). Heave-Pitch-Roll Model (Flexible fuselage in bending and torsion)-Response variance in takeoff run. Key same as Fig.5.20

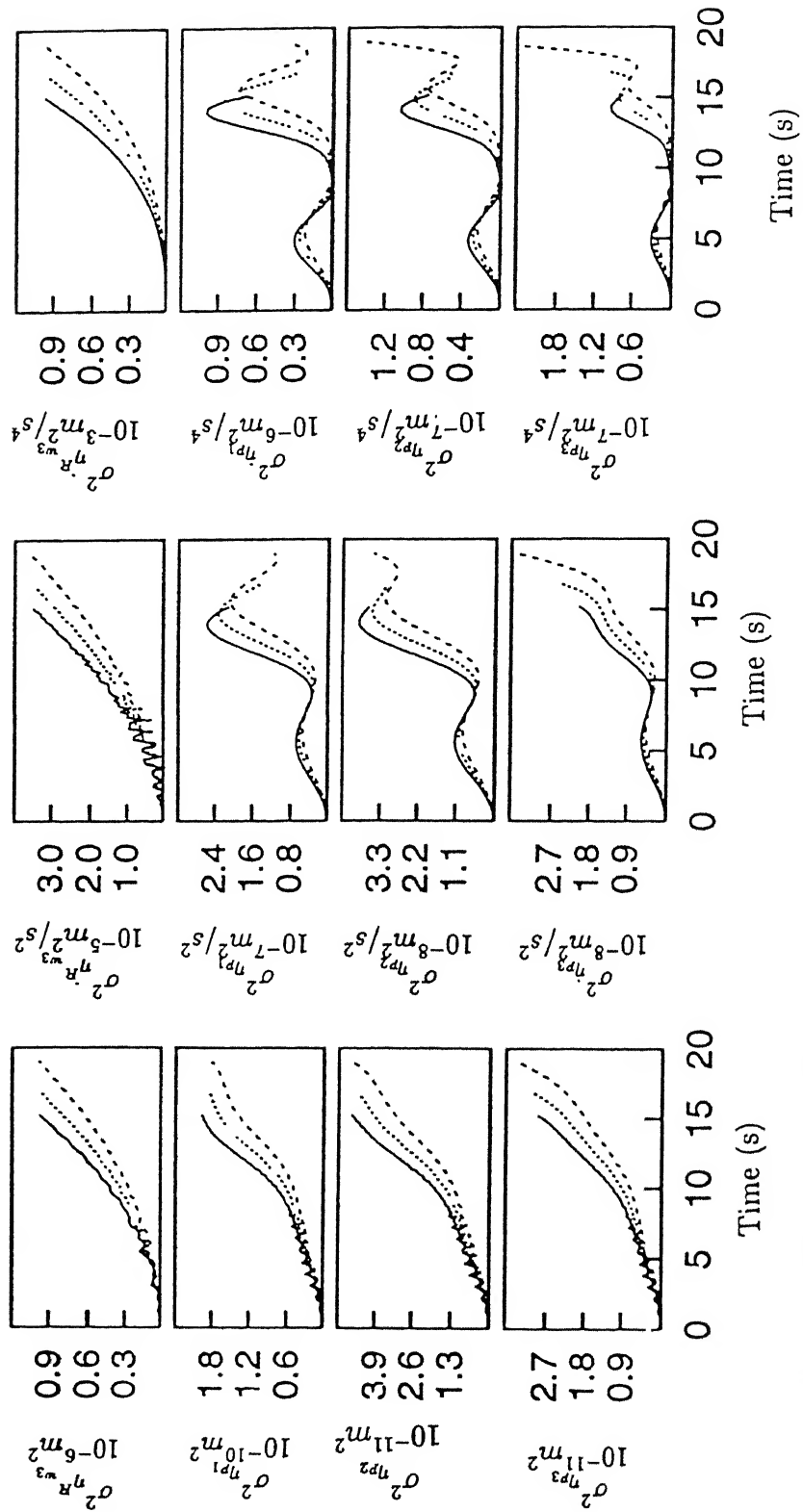


Fig.5.33(continued). Heave-Pitch-Roll Model (Flexible fuselage in bending and torsion)-Response variance in takeoff run. Key same as Fig.5.20

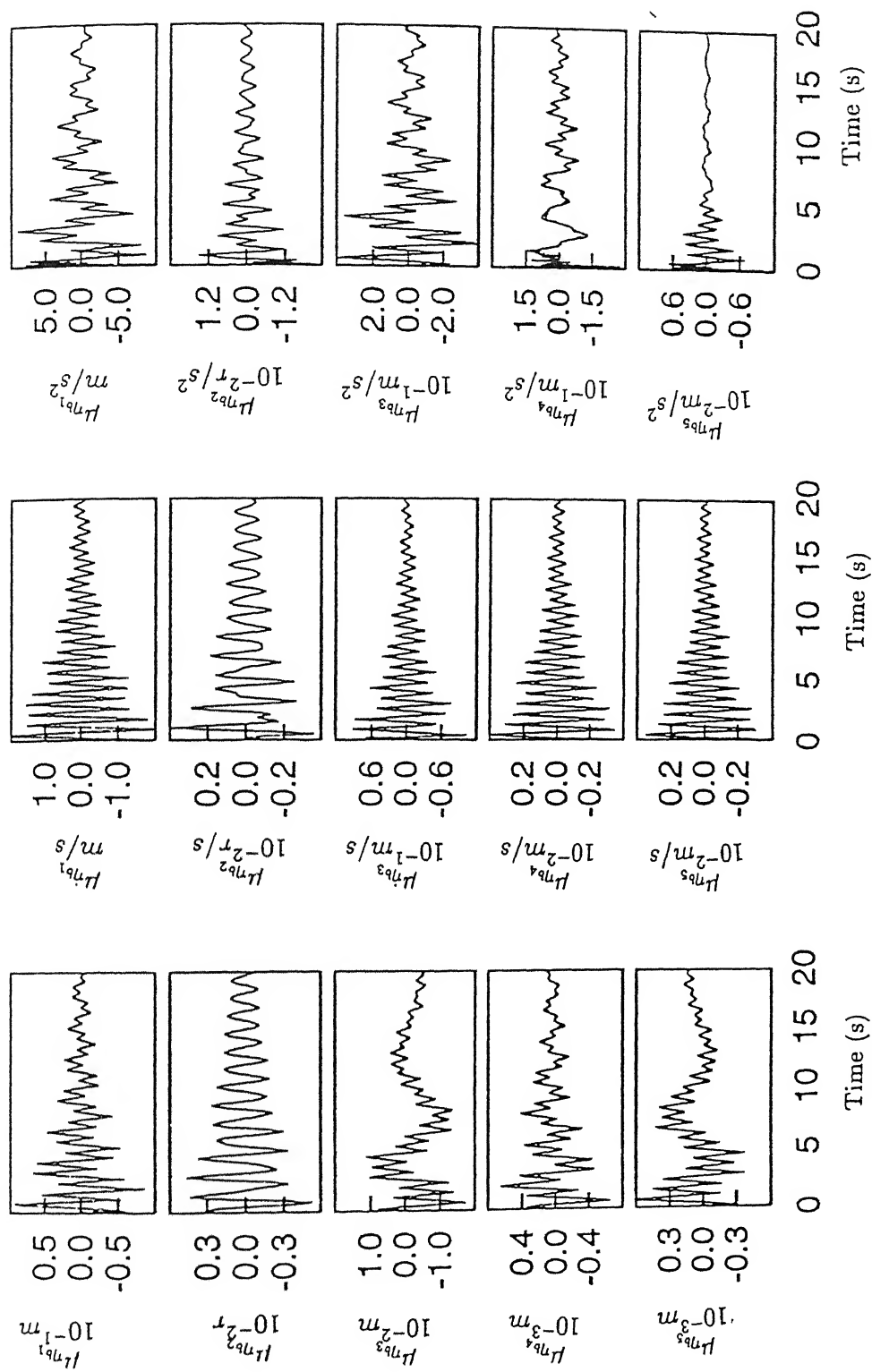


Fig.5.34. Heave-Pitch-Roll Model (Flexible fuselage in bending and torsion)-Mean response in landing run. Key same as Fig.5.22

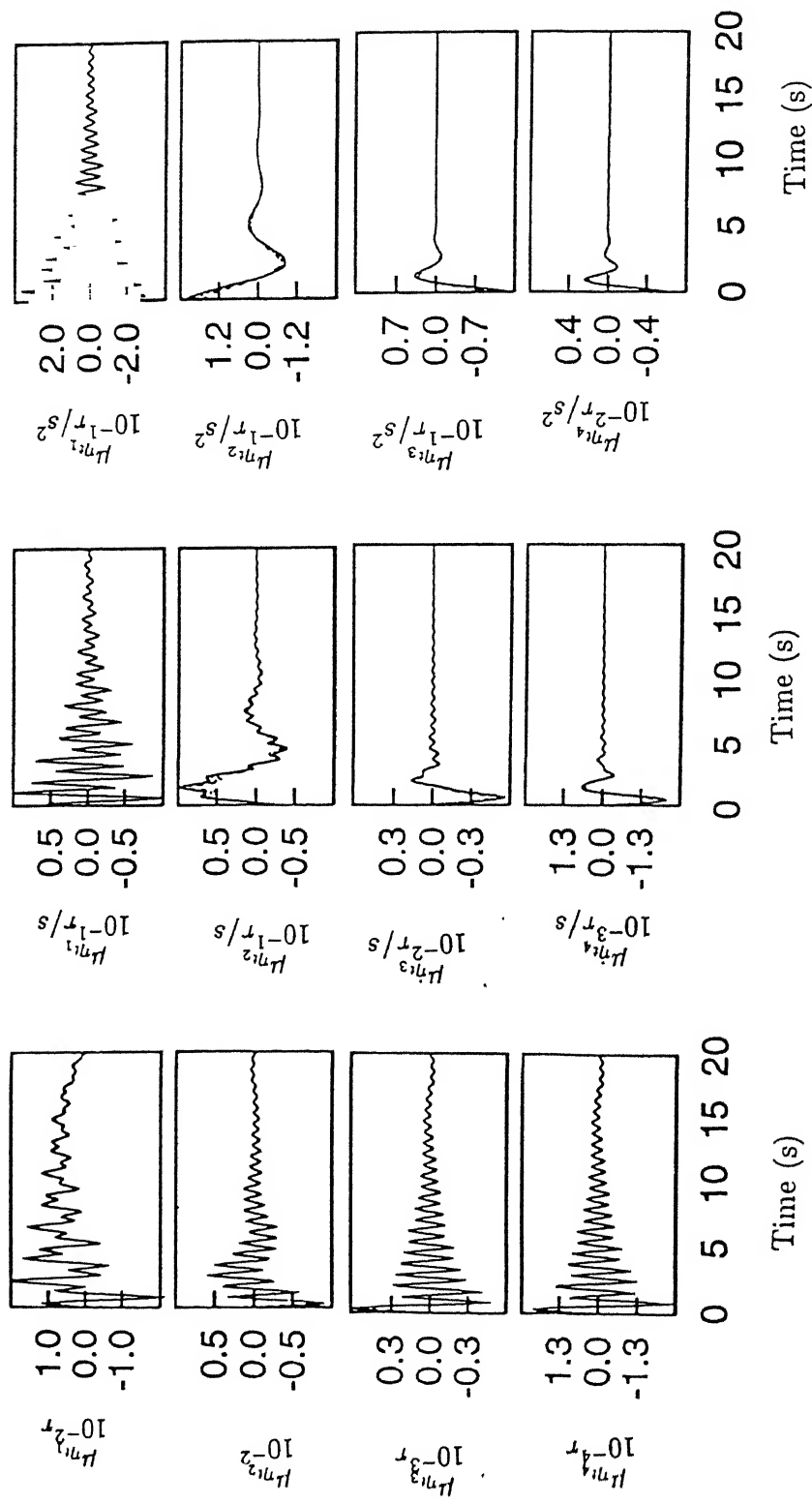


Fig.5.34(continued). Heave-Pitch-Roll Model (Flexible fuselage in bending and torsion)-Mean response in landing run. Key same as Fig.5.22

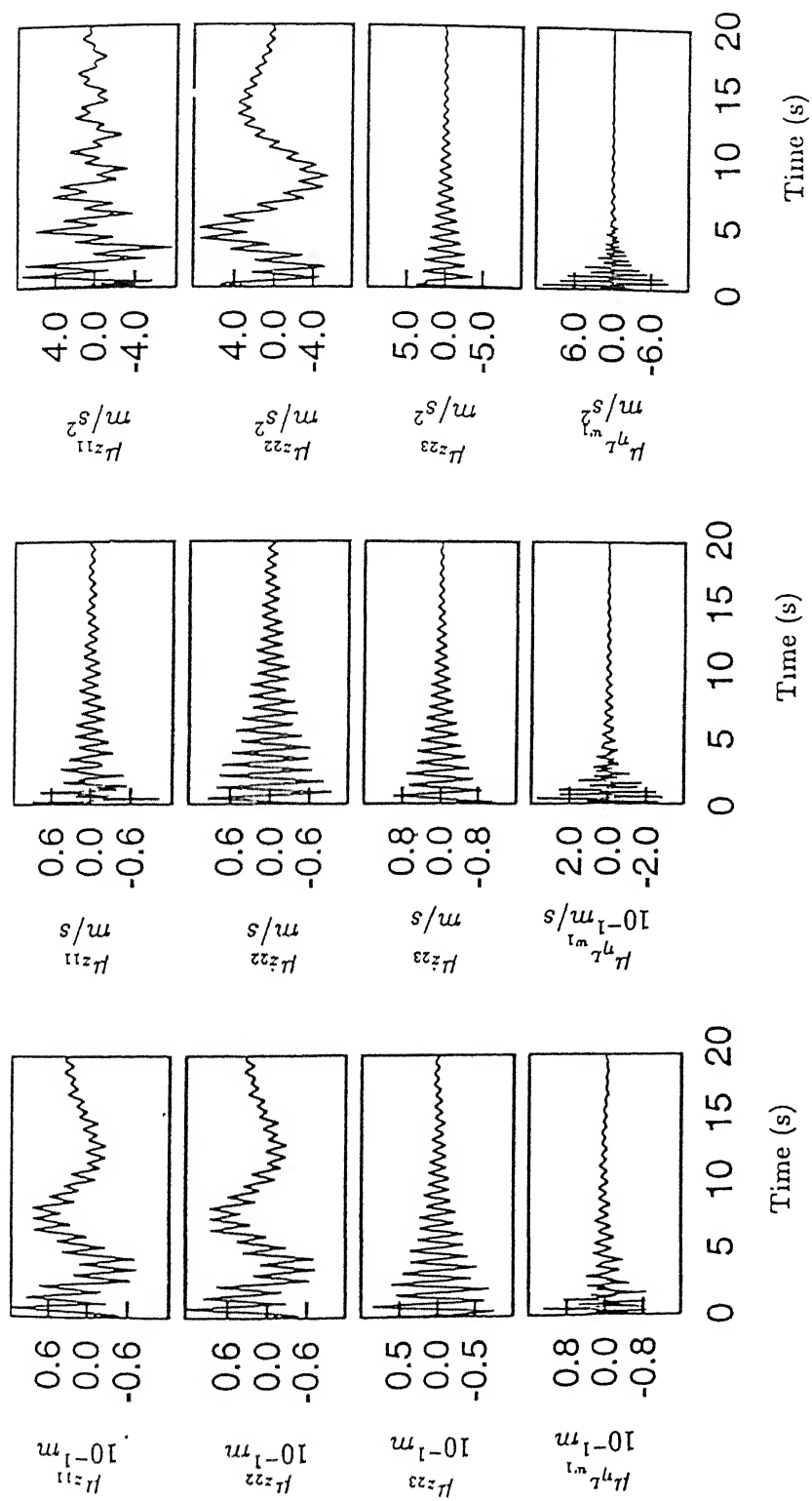


Fig.5.34(continued). Heave-Pitch-Roll Model (Flexible fuselage in bending and torsion)-Mean response in landing run. Key same as Fig.5.22

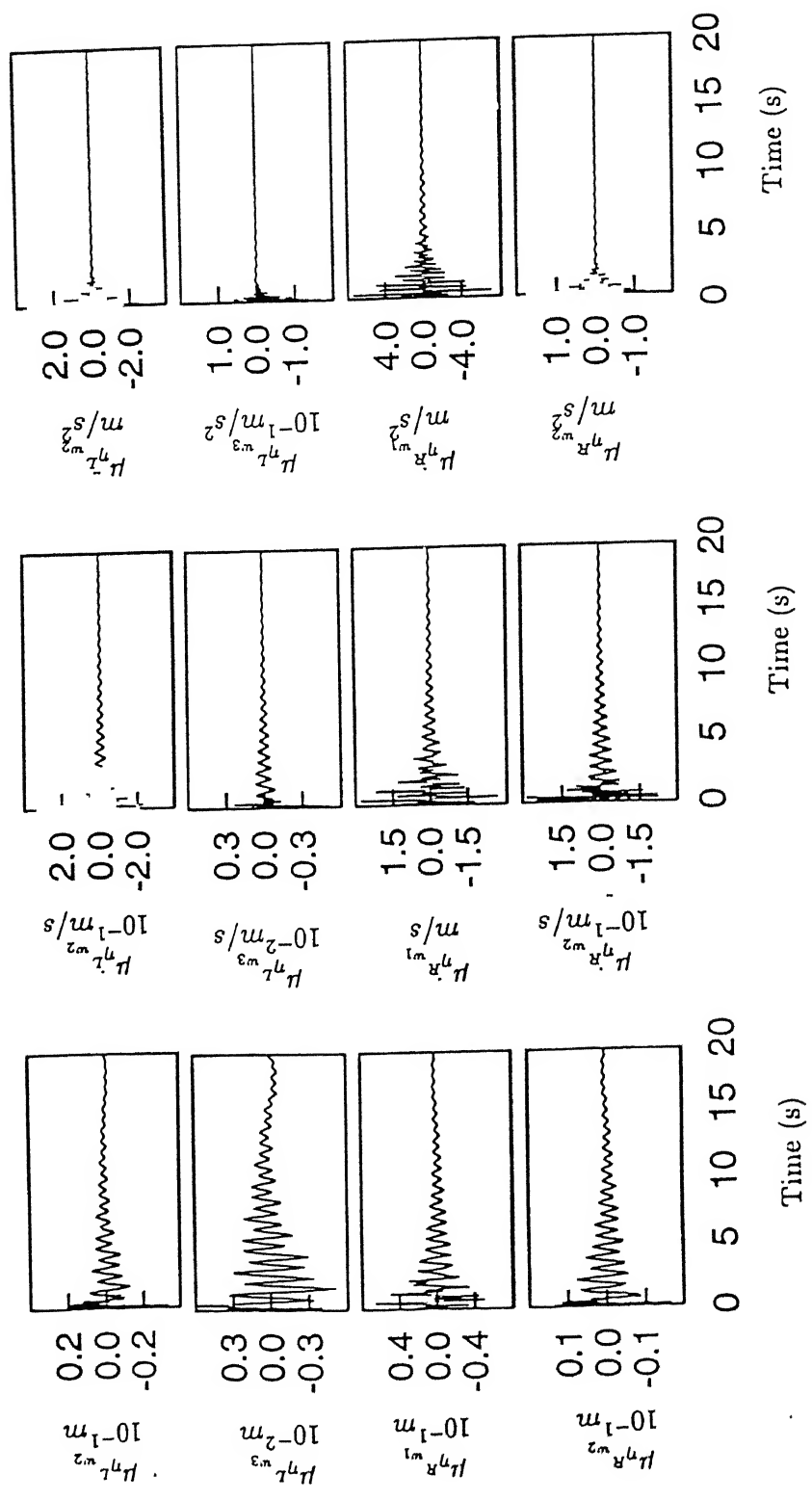


Fig.5.34(continued). Heave-Pitch-Roll Model (Flexible fuselage in bending and torsion)-Mean response in landing run. Key same as Fig.5.22

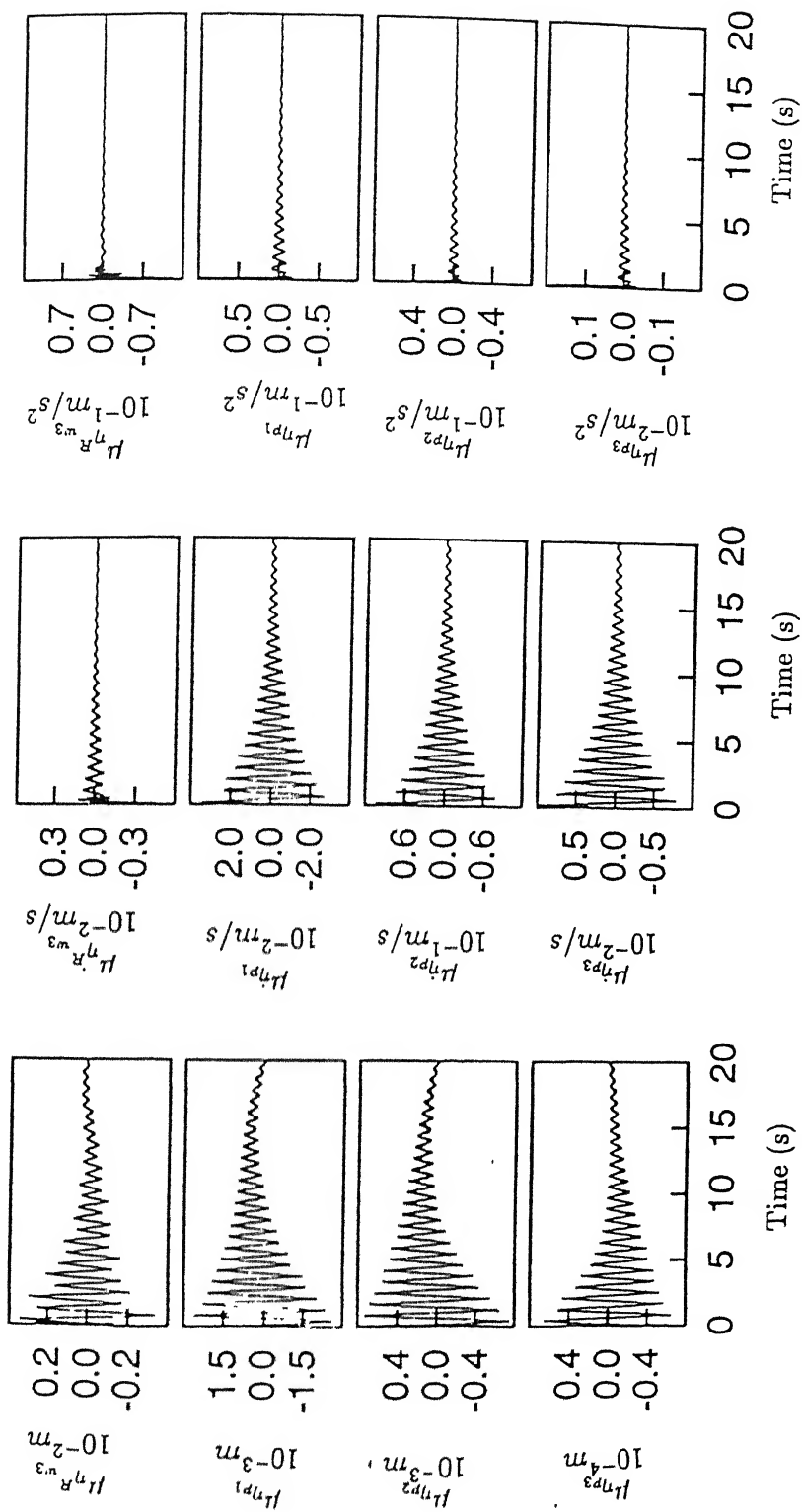


Fig.5.34(continued). Heave-Pitch-Roll Model (Flexible fuselage in bending and torsion)-Mean response in landing run. Key same as Fig.5.22

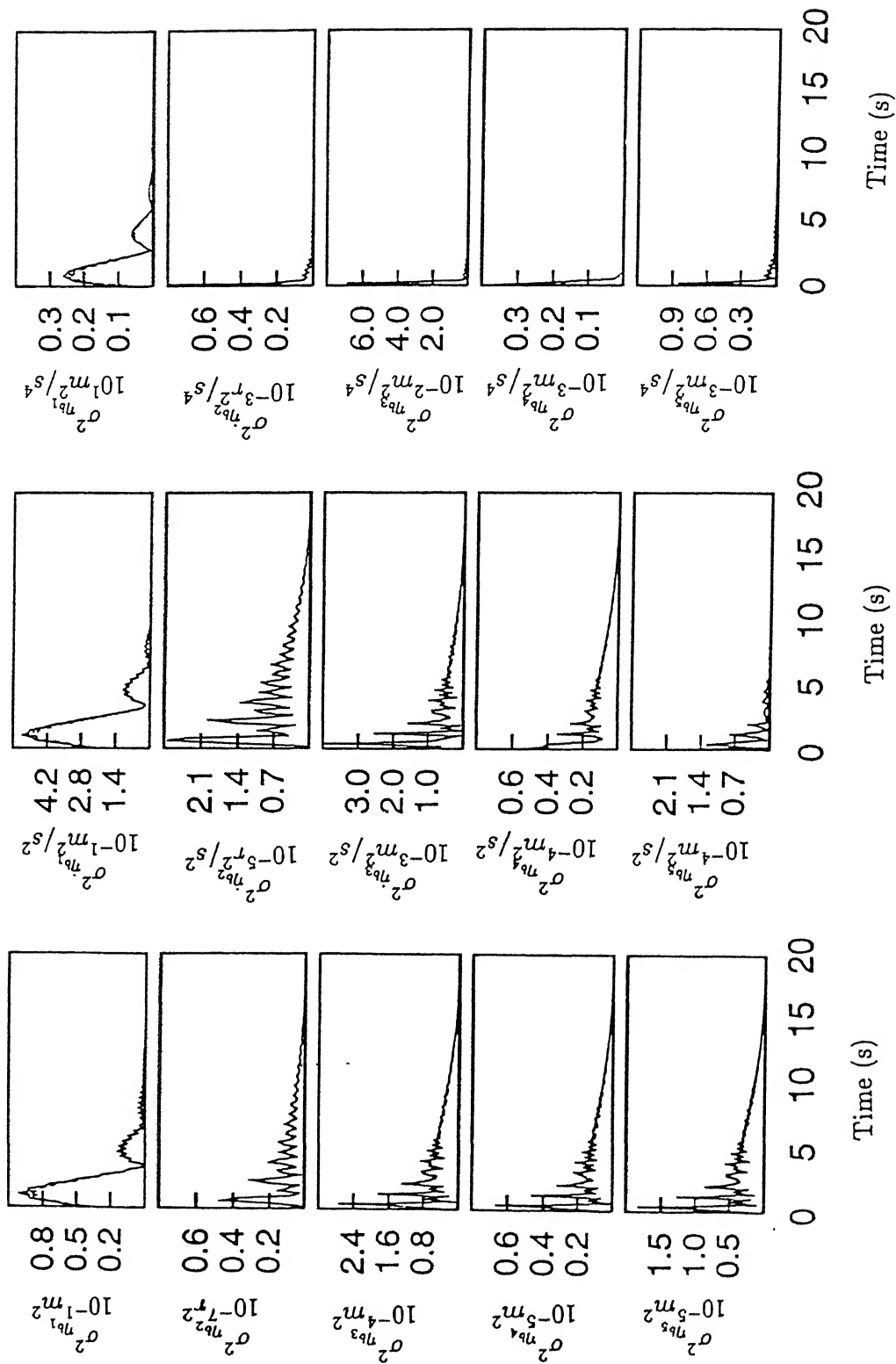


Fig.5.35. Heave-Pitch-Roll Model (Flexible fuselage in bending and torsion)-Response variance in landing run. Key same as Fig.5.22

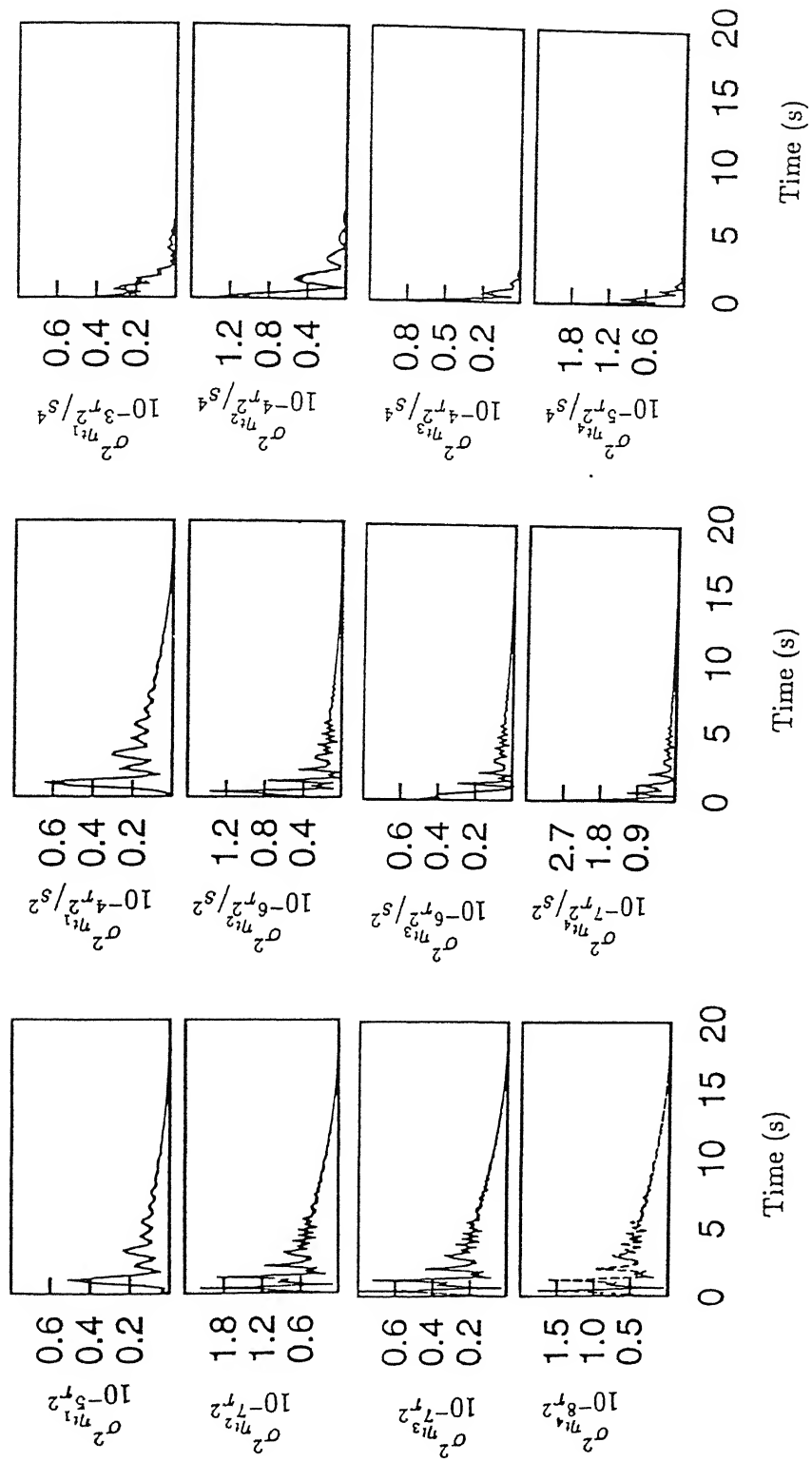


Fig.5.35(continued) Heave-Pitch-Roll Model (Flexible fuselage in bending and torsion)-Response variance in landing run. Key same as Fig.5.22

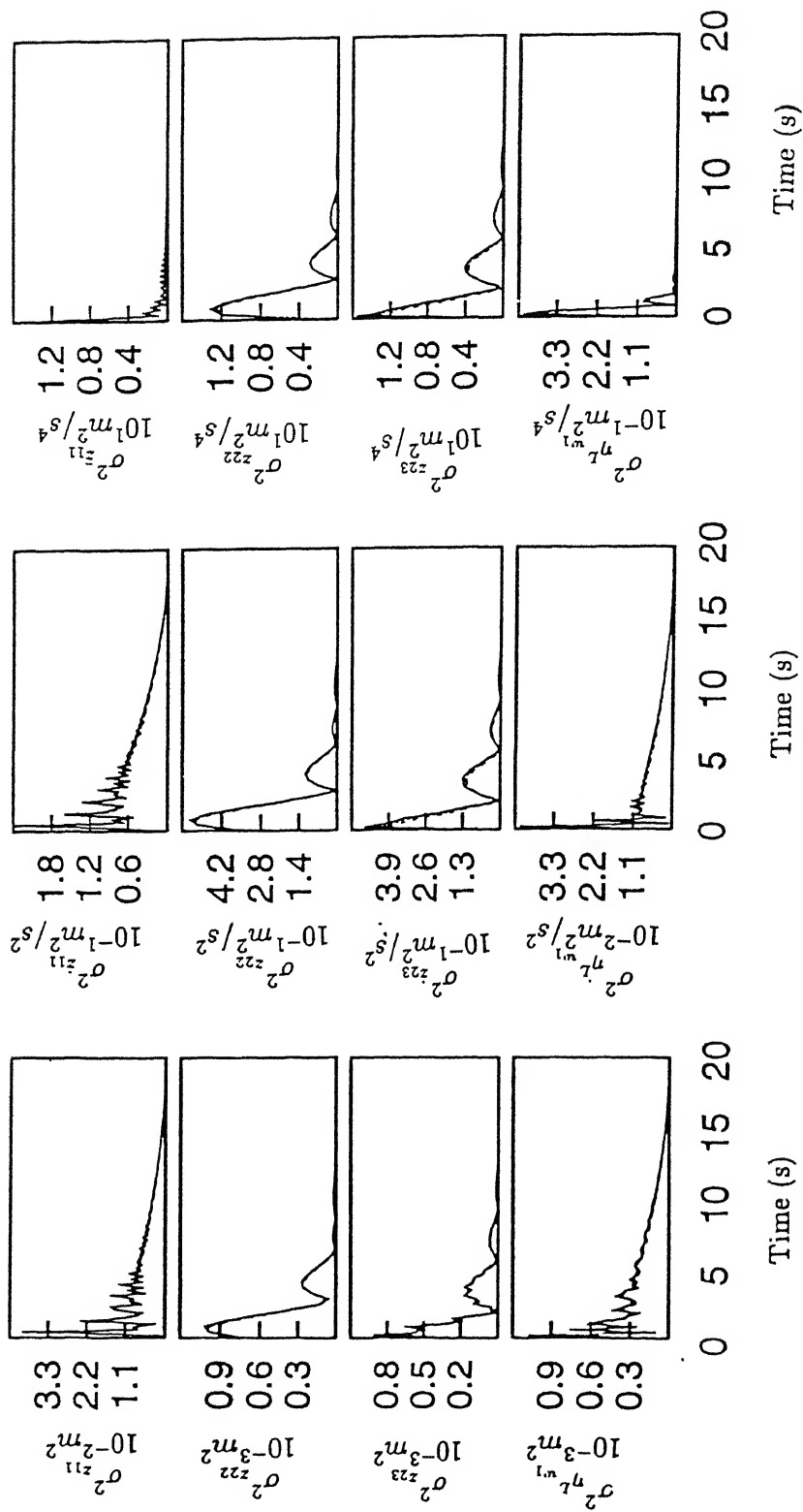


Fig.5.35(continued) Heave-Pitch-Roll Model (Flexible fuselage in bending and torsion)-Response variance in landing run. Key same as Fig.5.22

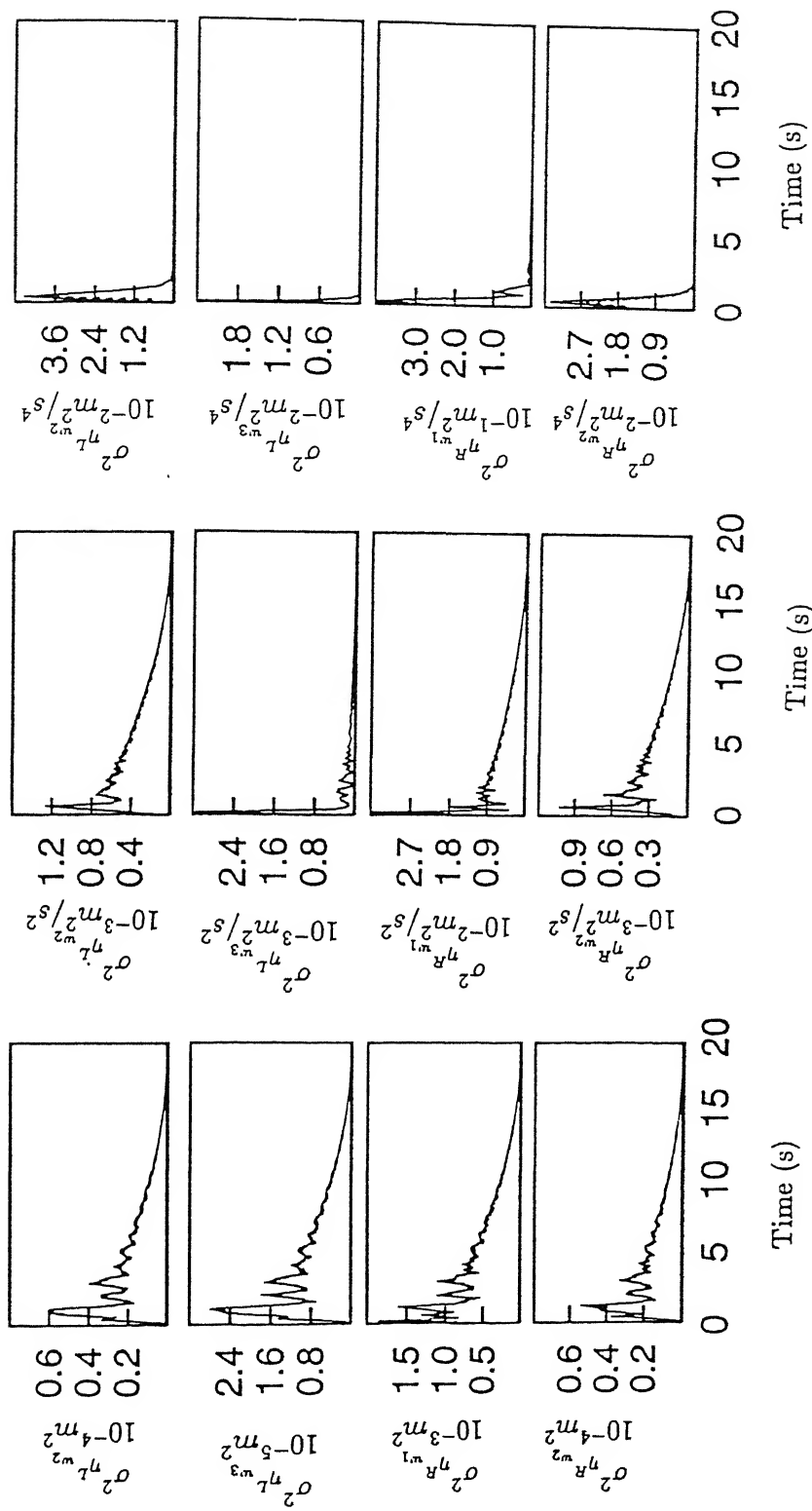


Fig.5.35(continued) Heave-Pitch-Roll Model (Flexible fuselage in bending and torsion)-Response variance in landing run. Key same as Fig.5.22

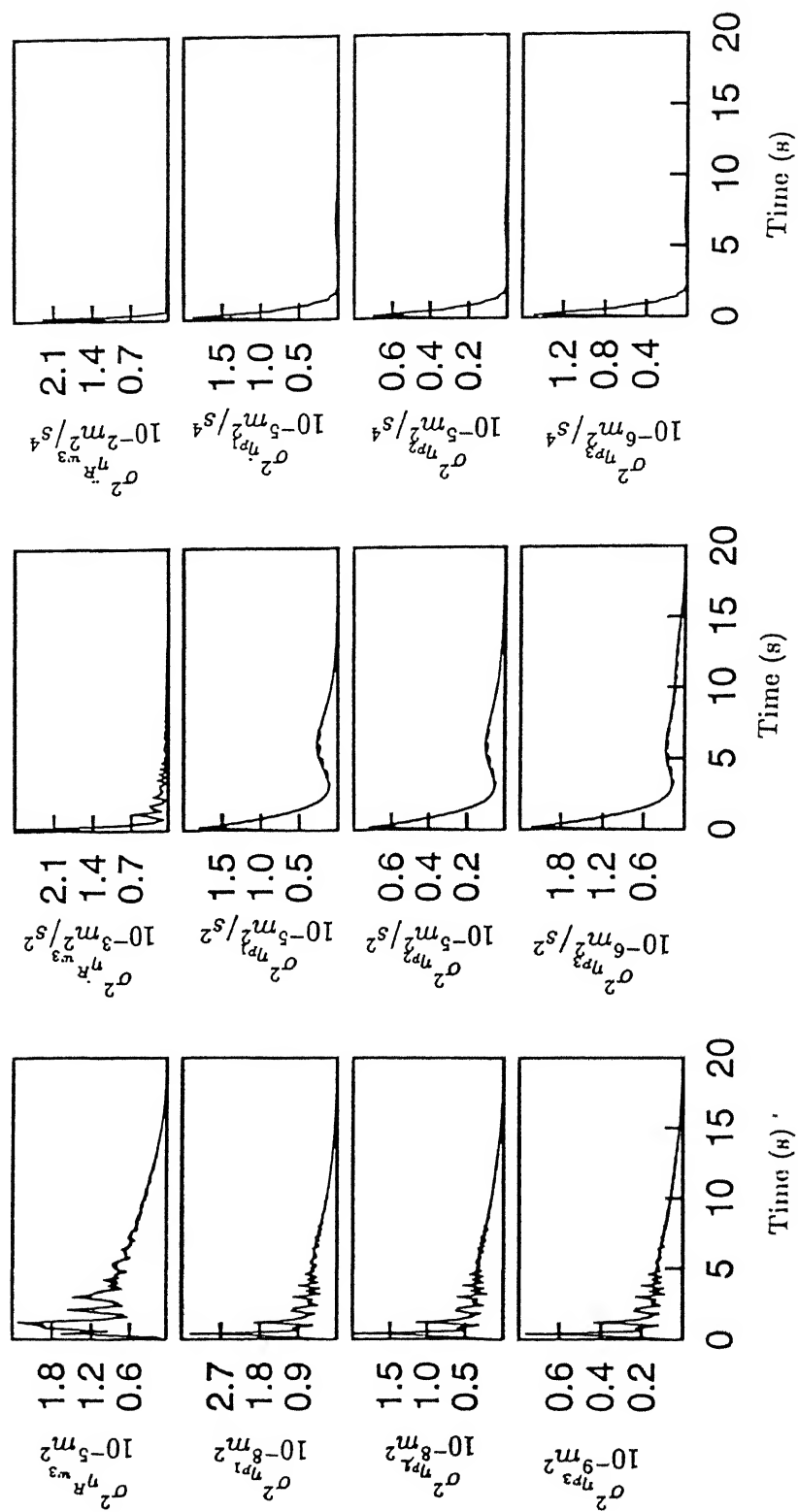


Fig.5.35(continued) Heave-Pitch-Roll Model (Flexible fuselage in bending and torsion)-Response variance in landing run. Key same as Fig.5.22

Displacement means and variances of rigid body heave, pitch, roll with first two elastic bending modes of the fuselage, nose and one main wheel response, first two coupled bending - torsion modes of one wing and track first normal coordinate have been presented for comparison. Taxi, takeoff and landing run have been studied with vehicle speed 80 Km/h in taxi, forward acceleration 2.0 m/s^2 in takeoff and sink velocity 1.2 m/s in landing runs.

Fig.5.36 presents the displacement means and variances in constant velocity runs. Response mean of the rigid body modes of the vehicle shows steady state oscillation representing track mean profile for all the models considered. Rigid vehicle model (Model 1) predicts higher response mean and variances for the heave and pitch degree of freedom. In flexible structures, a part of the dynamic energy is being utilised to cause elastic deformation. As the vehicle body becomes more flexible, displacements in rigid body modes are further reduced. Roll response mean and variance of the Model 4 shows slightly lower value compared to that of Model 3 which is assumed torsionally rigid. High frequency oscillation in the nose gear response is more prominent in Model 1 with higher amplitudes than other models considered. In case of main wheel response, slightly higher value is obtained in three point input models (Model 3 and 4). Fuselage elastic bending modes response mean and variance has less value in Model 4. Wing mean and variance in two point input models (Model 1 and 2) show predominant high frequency oscillation which are found to be less in three point input models (Model 3 and 4). Influence of mean track profile is more apparent in the higher mode mean response of

wing in Model 1 and 2. Track first normal coordinate's mean displacement reveals high value of the transient response for Model 1. In Model 3 and 4, the effect of roll motion is seen to reduce the response mean and variance of track deflections.

Fig.5.37 presents the comparison of response mean and variance in takeoff run. Rigid model shows high value of response mean and variance for the heave and pitch degree of freedom. Variances are found oscillatory in the rigid model. Torsional flexibility is found more effective to reduce the response magnitude in case of rigid body roll motions induced in three point input model (Model 4) during takeoff run. Nose gear responses have more high frequency components in Model 1 compared to other models. Main wheel response for all the models do not reveal much difference in various models except the variance is found to fluctuate about an increasing mean in Model 1. Fuselage elastic bending response in flexible three point input models (Model 3 and 4) retains similar characteristics. Flexible wing's first and second normal coordinate mean response in Model 3 and 4 show appreciable deviation from that of Model 1 and 2. Track response builds up gradually with increase in speed in flexible models (Model 2, 3 and 4)

Mean displacement and variances in landing run of the aircraft are compared in Fig.5.38. Heave and pitch motion of the aircraft has slightly higher peaks in the impact phase for Model 1 and 2. Mean and variance of the rigid body rolling of the vehicle in Model 3 and 4 have similar behaviour at touchdown impact with little difference in the amplitude. In case of fuselage second

elastic bending mode mean displacement, peak developed at touch down instant has higher magnitude in Model 3 and 4. However, variance shows peaks of low magnitude and faster dissipation of impact energy compared to two point input models (Model 1 and 2). Flexible wing's normal coordinate mean and response variance in rigid model show much significant effect of the landing impact. In the latter phase of landing run, response behaviour in all the models are quite similar. Track behaviour are similar in all the models with higher peaks developed due to impact of rigid vehicle on the track. However, some departure in response behaviour is noticed during the progress of landing run.

Comparative study shows that, in general, rigid vehicle response magnitudes are higher than the flexible models although evolution of mean and variances with time predicts similar nature. Inclusion of elastic torsional mode of the vehicle shows minor influence on the response behaviour as compared to elastic bending mode.

5.3 NONLINEAR MODEL RESPONSE STATISTICS

Results of the heave model of aircraft with tapered flexible wing are obtained with the system parameters mentioned earlier. Shock absorber characteristics of the nonlinear suspension are assumed as

Initial air pressure (P_{a0}): 3.6×10^6 N/m², pneumatic area and volume (A_{a0} , V_{a0}): 0.65×10^{-2} m² and 0.2518×10^{-2} m³, hydraulic and orifice area (A_h , A_n): 80.5×10^{-4} m², 3.044×10^{-4} m², coefficient of orifice discharge: 0.6, fluid

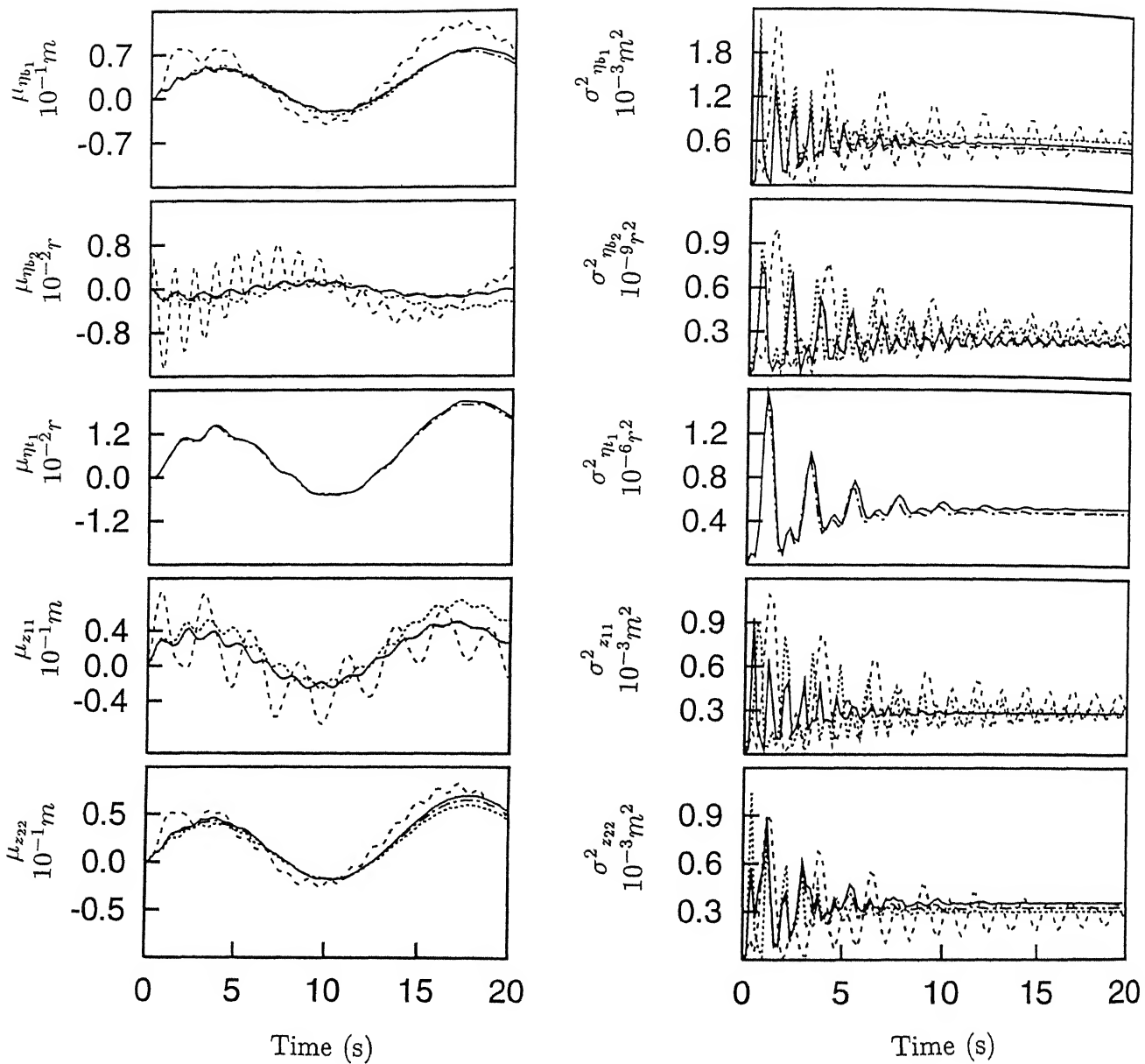


Fig.5.36. Comparison of mean and variance of displacement in taxi run.
 Key: Model 1 _ _ _ _ _ , model 2 , model 3 ———— ,
 model 4 — · — · — · .

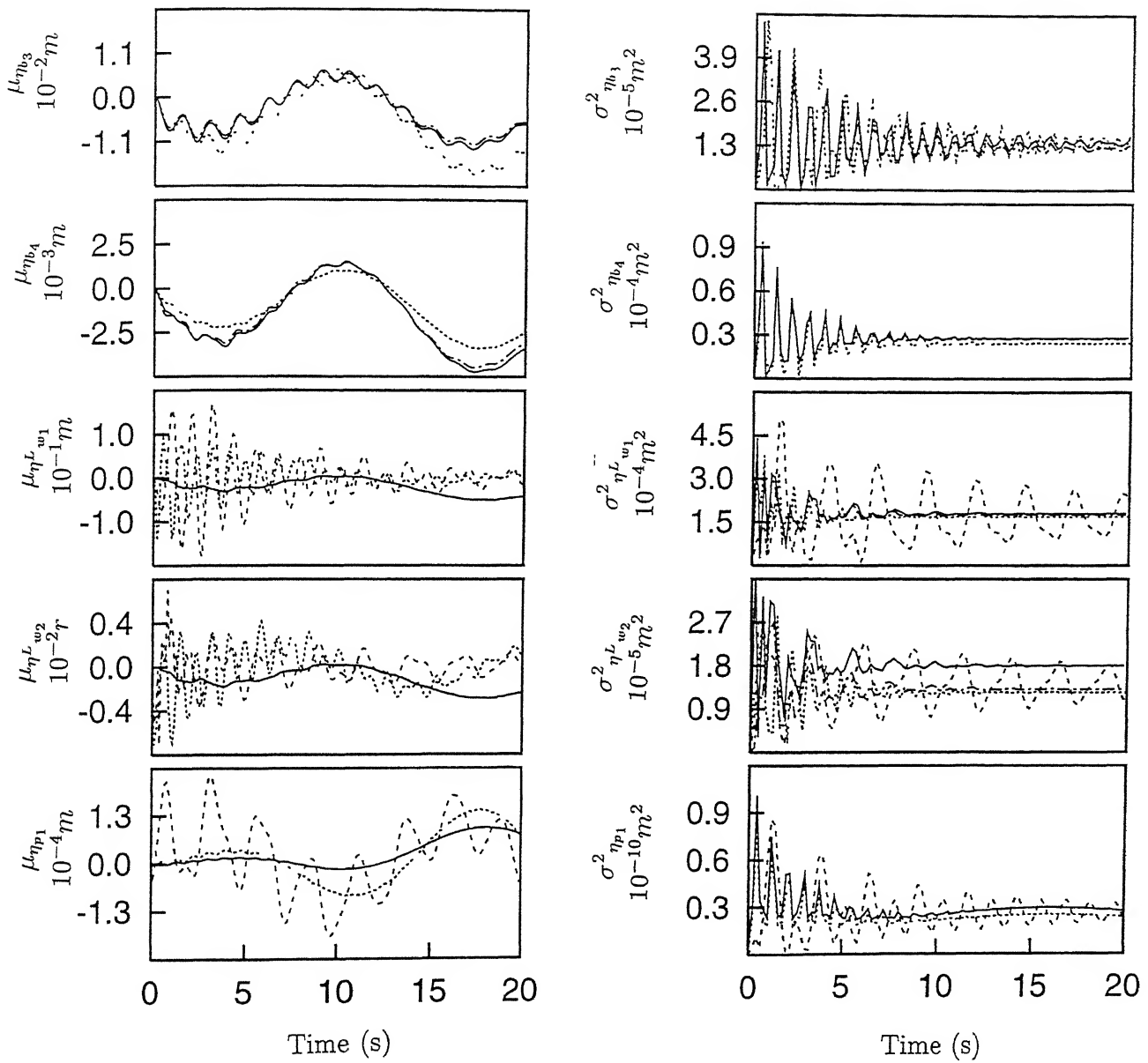


Fig.5.36(continued). Comparison of mean and variance of displacement in taxi run.
 Key: Model 1 — — — — —, model 2, model 3 — — — — —, model 4 — . — . — .

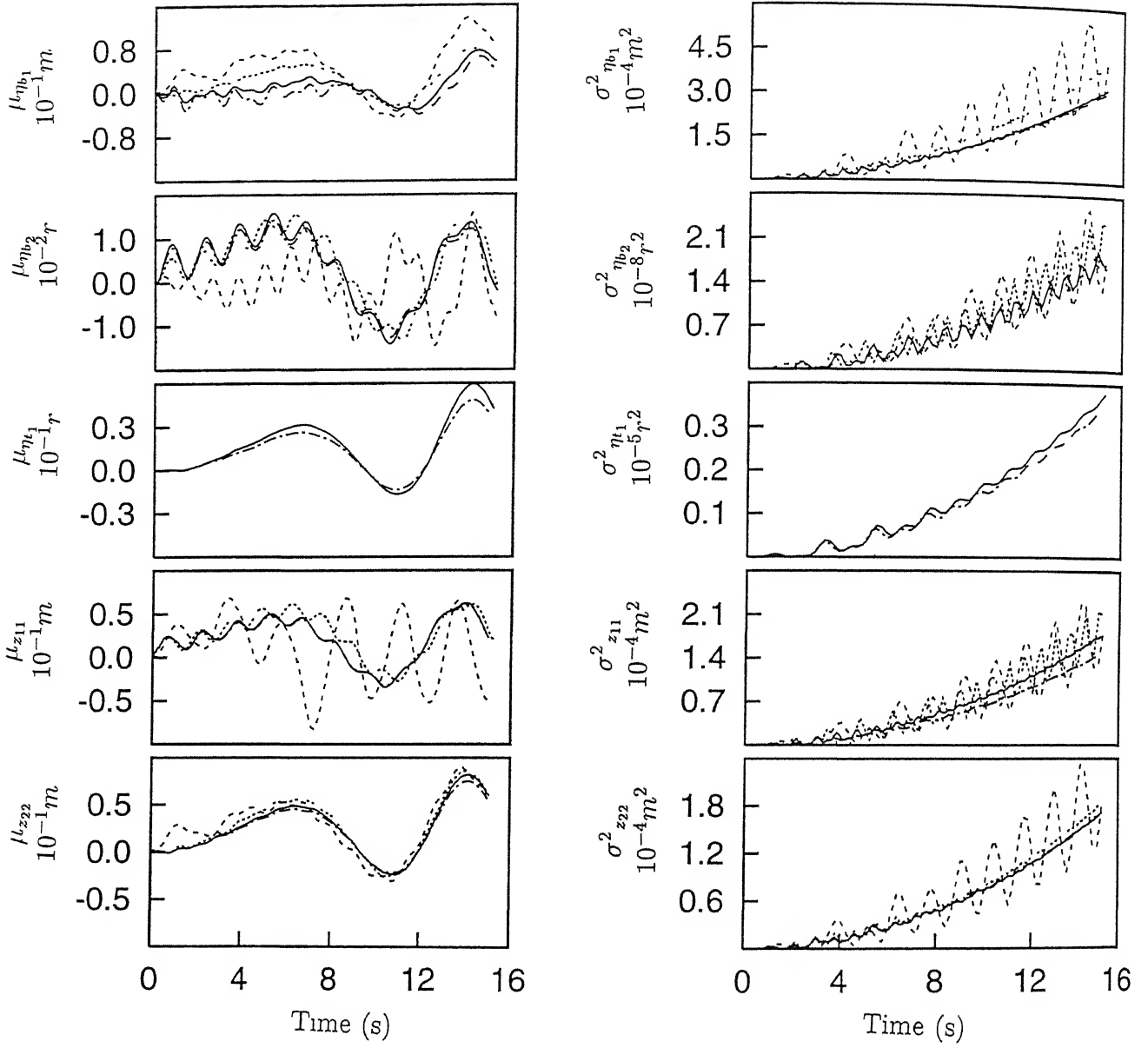


Fig.5.37. Comparison of mean and variance of displacement in takeoff run.
Key same as Fig.5.36

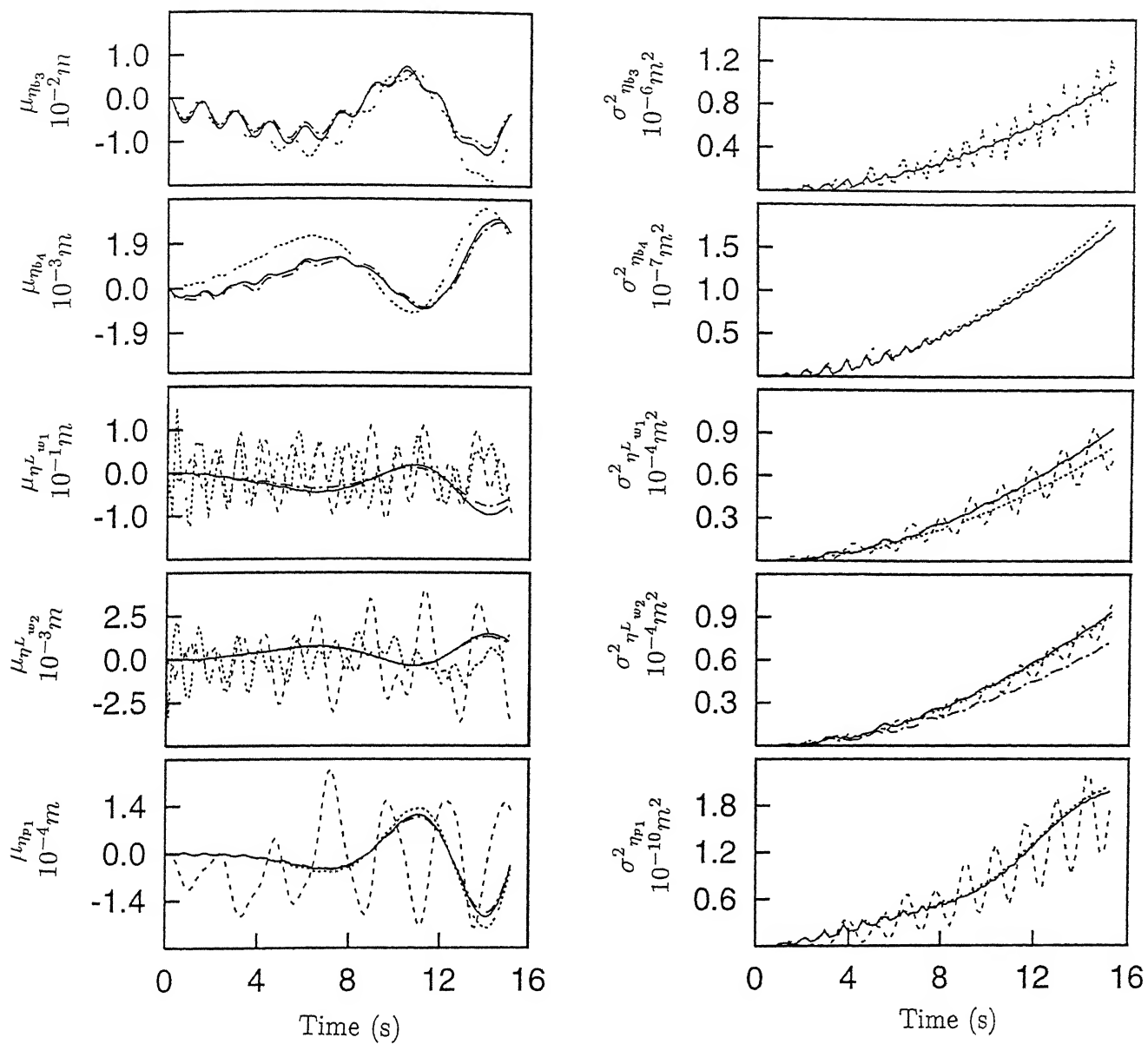


Fig.5.37(continued). Comparison of mean and variance of displacement in takeoff run.
Key same as Fig.5.36

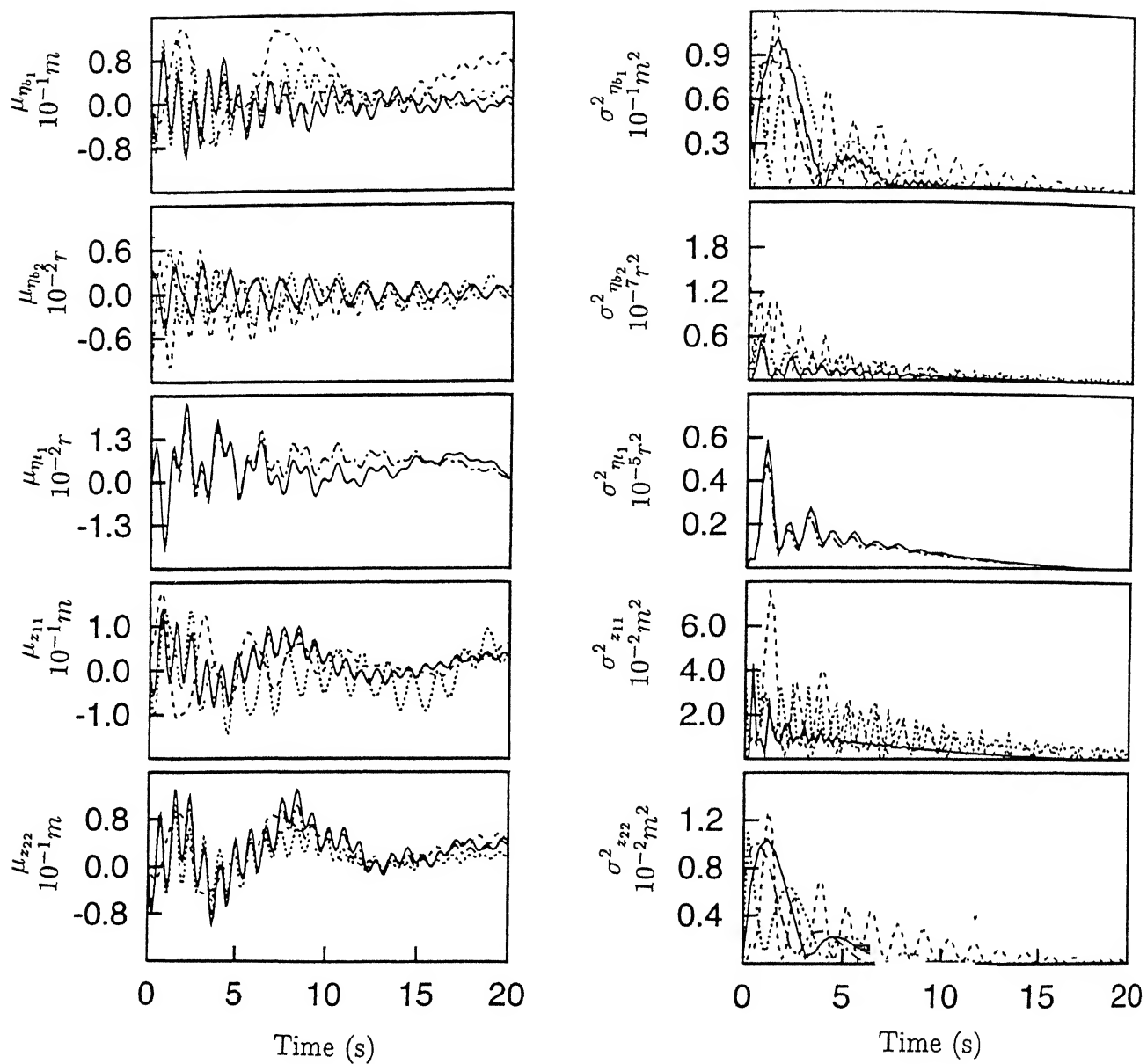


Fig.5.38. Comparison of mean and variance of displacement in landing run.
Key same as Fig.5.36

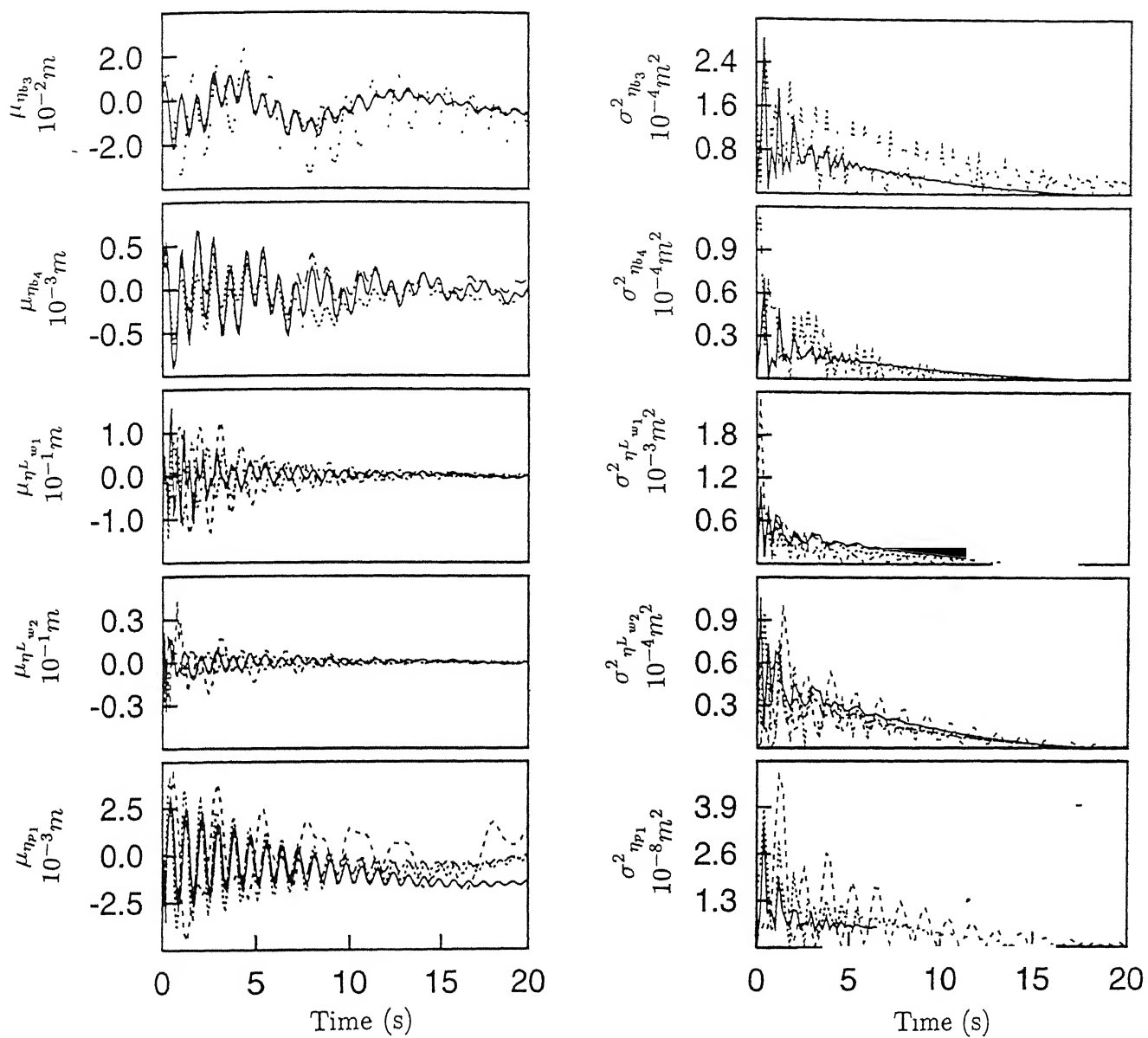


Fig.5.38(continued). Comparison of mean and variance of displacement in landing run.
Key same as Fig.5.36

density(ρ): 850 kg/m³, polytropic index (n): 1.4.

Response mean and variance are obtained for the system generalised coordinates in taxi, takeoff and landing run by two methods- instantaneous linear approach and Monte Carlo simulation.

5.3.1 Taxi Run

A constant vehicle forward velocity of 22.2 m/s has been assumed. Displacement, velocity and acceleration mean and variances are presented in Figs. 5.39, 5.40 and 5.41.

The displacement means of the two lumped masses show the characteristics of the track mean profile. The figures reveal similarity in response behaviour obtained by the two methods. The responses show the presence of high frequency components in the simulated results which are not always mimicked by the response of linearised model. However, the underlying low frequency pattern and the response in later stage of taxi run in the two cases are similar. The agreement in the variance is better than the mean between the two methods. The agreement improves with the progress of the motion. This is seen, in general, in all the three responses- displacement, velocity and acceleration.

5.3.2 Takeoff Run

Takeoff corresponds to an accelerated run at 2.0 m/s² starting from rest till liftoff velocity of 59.72 m/s is attained. Mean and variance of displacement are shown in Fig.5.42. The high

frequency component in the wing normal modes for the simulated response means are not fully reflected by the instantaneously linear model. Otherwise the two methods have a close match for the mean and the variance for the modes considered.

Displacement variances of sprung and unsprung mass show gradual building up of amplitude associated with the low frequency component. This may be due to effectiveness of ground input with increasing velocity. However, prior to takeoff, displacement variance indicate a decrease in magnitude. Wing response in both the models show growth of the amplitude at much faster rate in the initial period.

Velocity response mean and variance for takeoff run are shown in Fig.5.43. The lumped mass mean velocities show close agreement between the two methods except for a shift in the positions of the peaks. The continuous member mean velocities reveal high frequency components which are not reflected in the linearised model. However, the two solutions follow similar general trend. This is true for the variance response also.

Fig.5.44 presents the mean and variances of acceleration response. As for displacement and velocity response, the linearised model does not reflect the high frequency pattern of the simulated results completely. The low frequency behaviour in the two cases are similar.

5.3.3 Landing Run

Results have been obtained for the landing run of the

aircraft with sink velocity 1.2 m/s, glide velocity 60 m/s and constant deceleration of 1.5 m/s^2 . The results have been presented for the first 20 seconds of the run.

Mean and variances of displacement are shown in Fig.5.45. The linearised sprung and unsprung masses response again miss the high frequency oscillation during transience caused by the landing impact. The other response components also exhibit a similar general behaviour. During the later phase of the landing run, the agreement improves between the two approaches.

Displacement response variance have a better agreement between the two methods compared to the mean characteristics. Variance of the unsprung mass shows a slower dissipation of impact energy compared to variance of the sprung mass. Response variance of other degrees of freedom presented show the formation of peak caused by landing impact. In most of the cases, a single peak is seen. Peaks are found to have some differences in magnitude and position for the two models.

Mean and variance of velocity and acceleration response are presented in Figs. 5.46 and 5.47 respectively. The velocity and acceleration, in general, follow the pattern of the displacement response. However, dependence of mean response on the track roughness input reduces from displacement to velocity to acceleration. Results of the instantaneously linear model are found to be close to the simulated results when the vehicle loses a significant amount of its forward velocity.

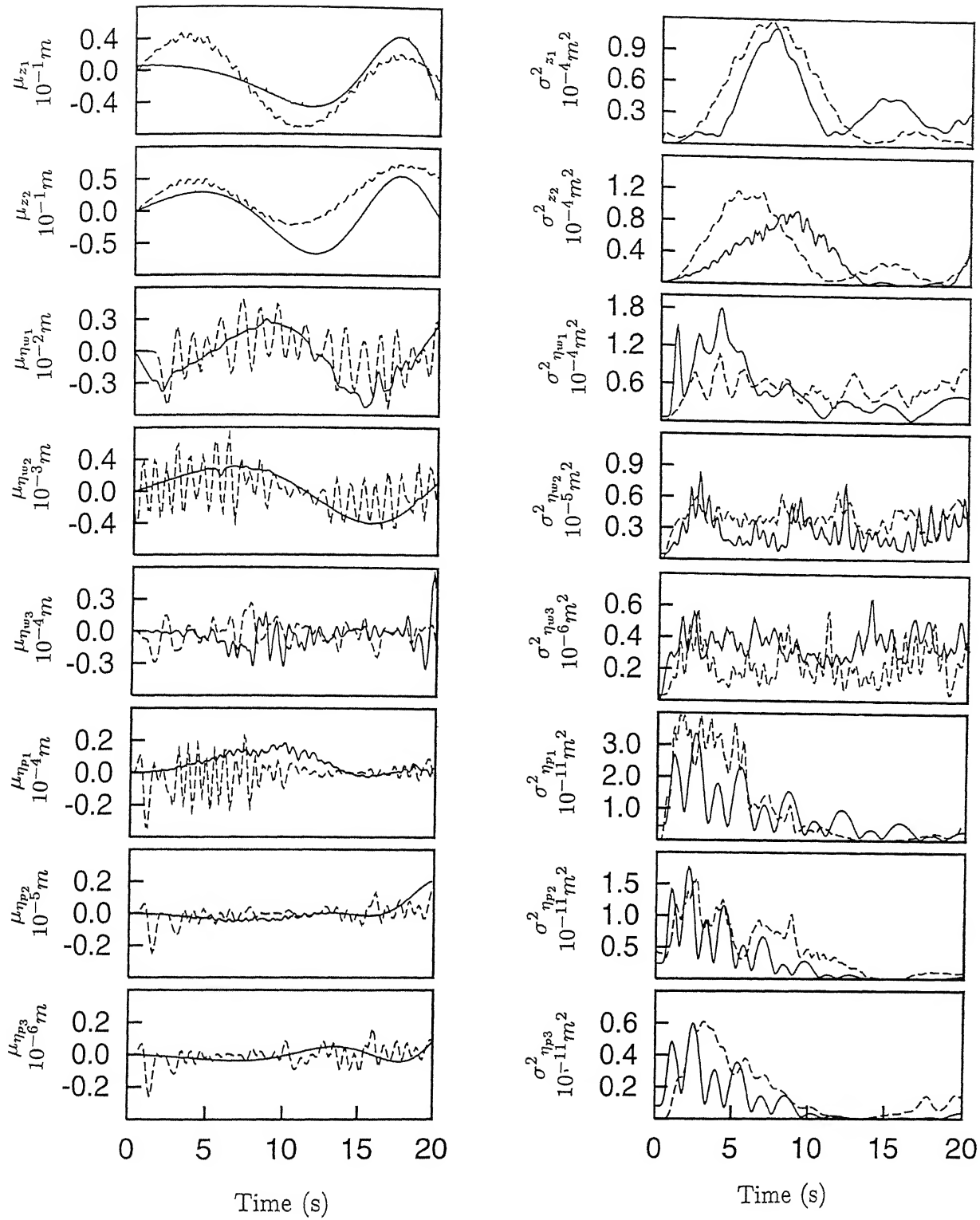


Fig.5.39. Nonlinear Aircraft Model-Mean and variance of displacement in taxi run.
Key: Linearised solution ———, simulation - - - - -

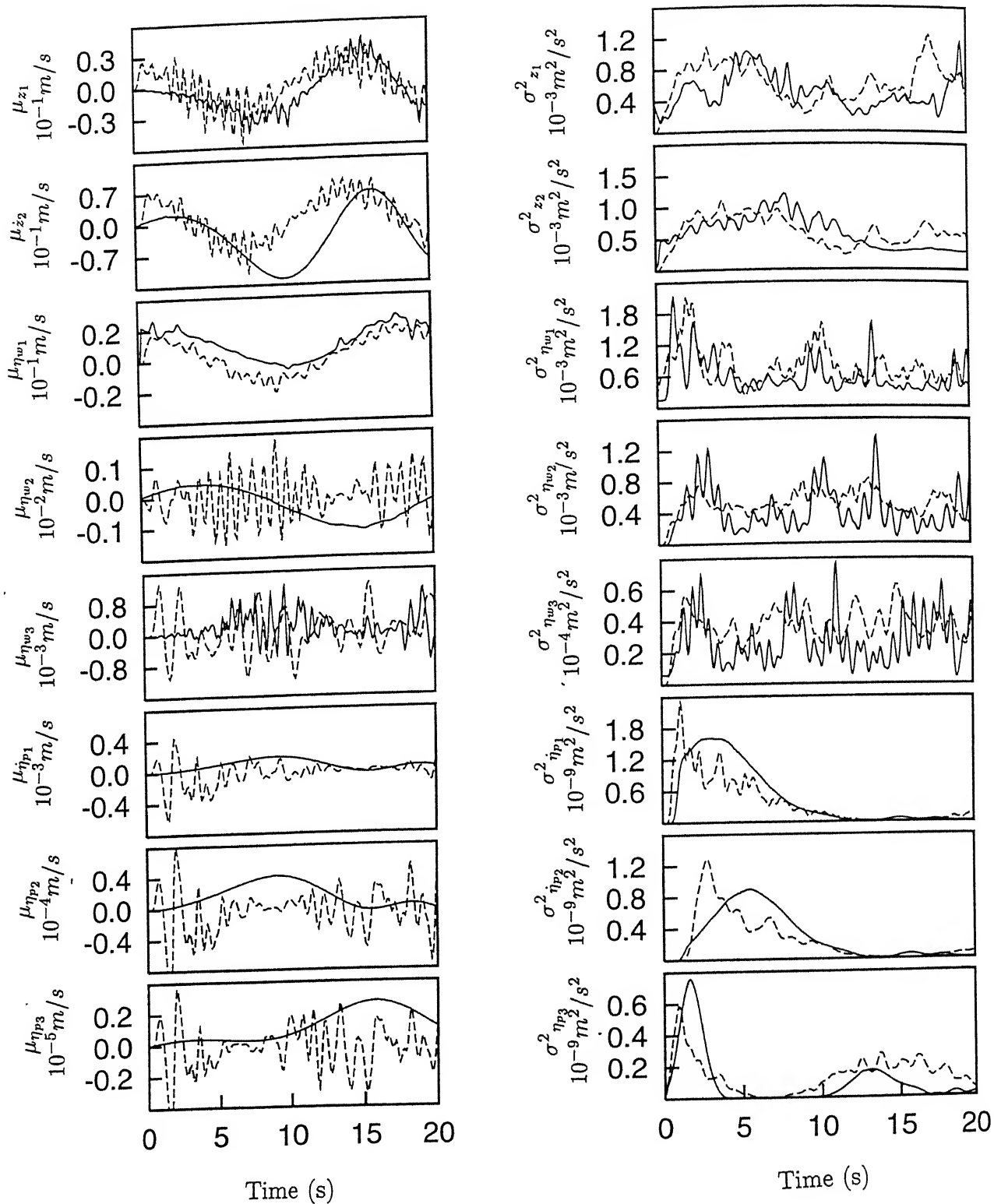


Fig.5.40. Nonlinear Aircraft Model-Mean and variance of velocity in taxi run.
Key same as Fig.5.39

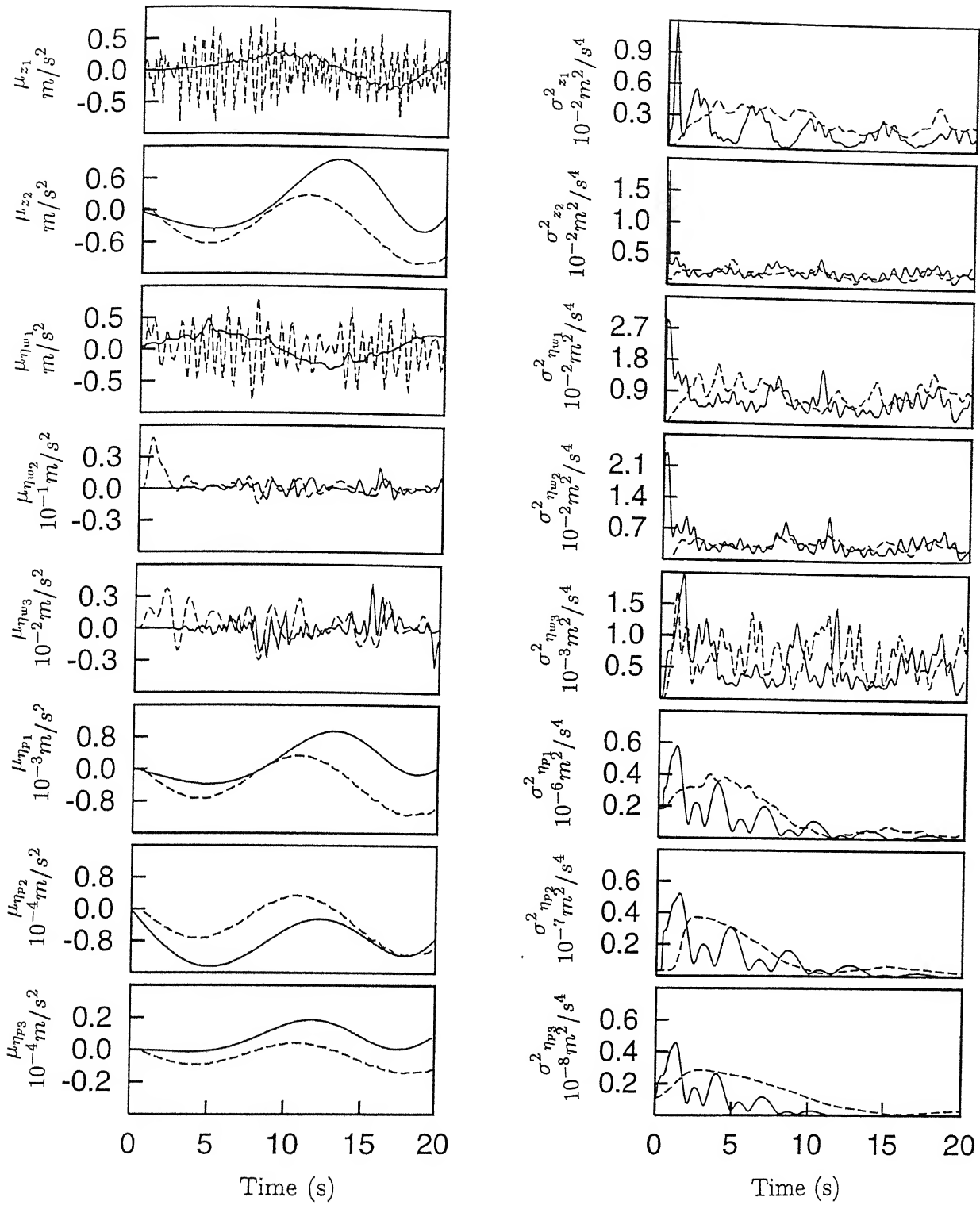


Fig.5.41. Nonlinear Aircraft Model-Mean and variance of acceleration in taxi run.
Key same as Fig.5.39

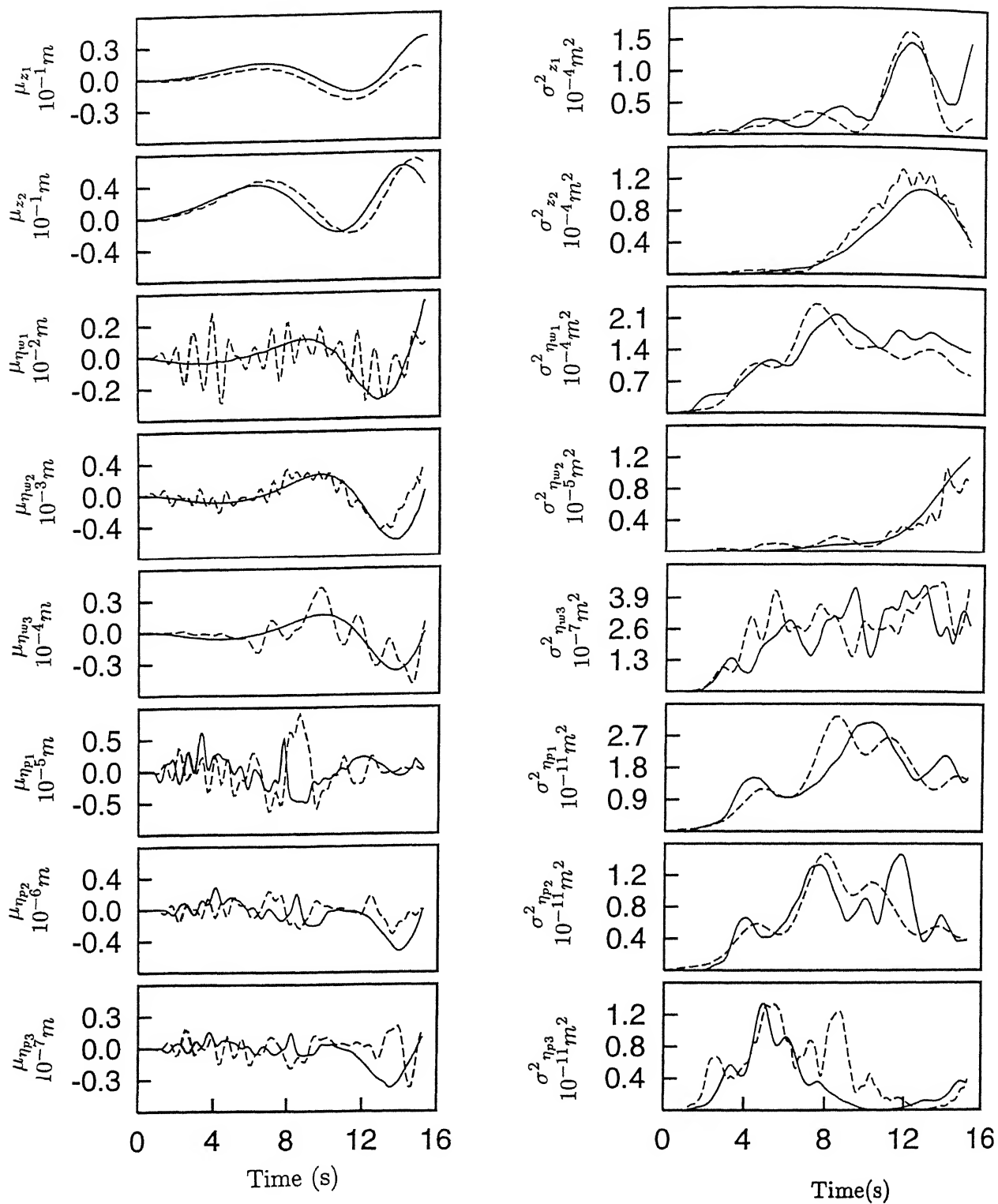


Fig.5.42. Nonlinear Aircraft Model-Mean and variance of displacement in takeoff run.
Key same as Fig.5.39

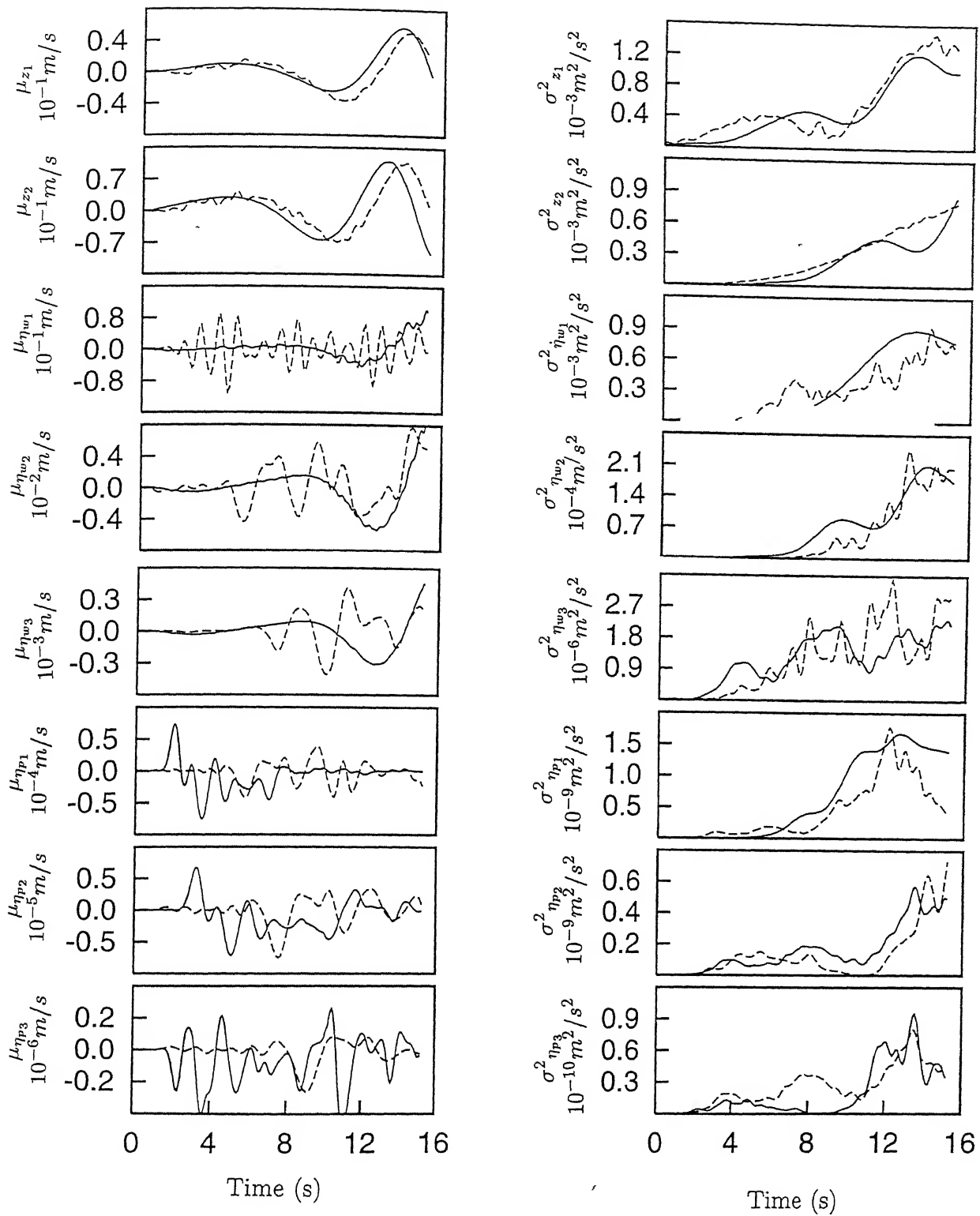


Fig.5.43. Nonlinear Aircraft Model-Mean and variance of velocity in takeoff run.
Key same as Fig.5.39

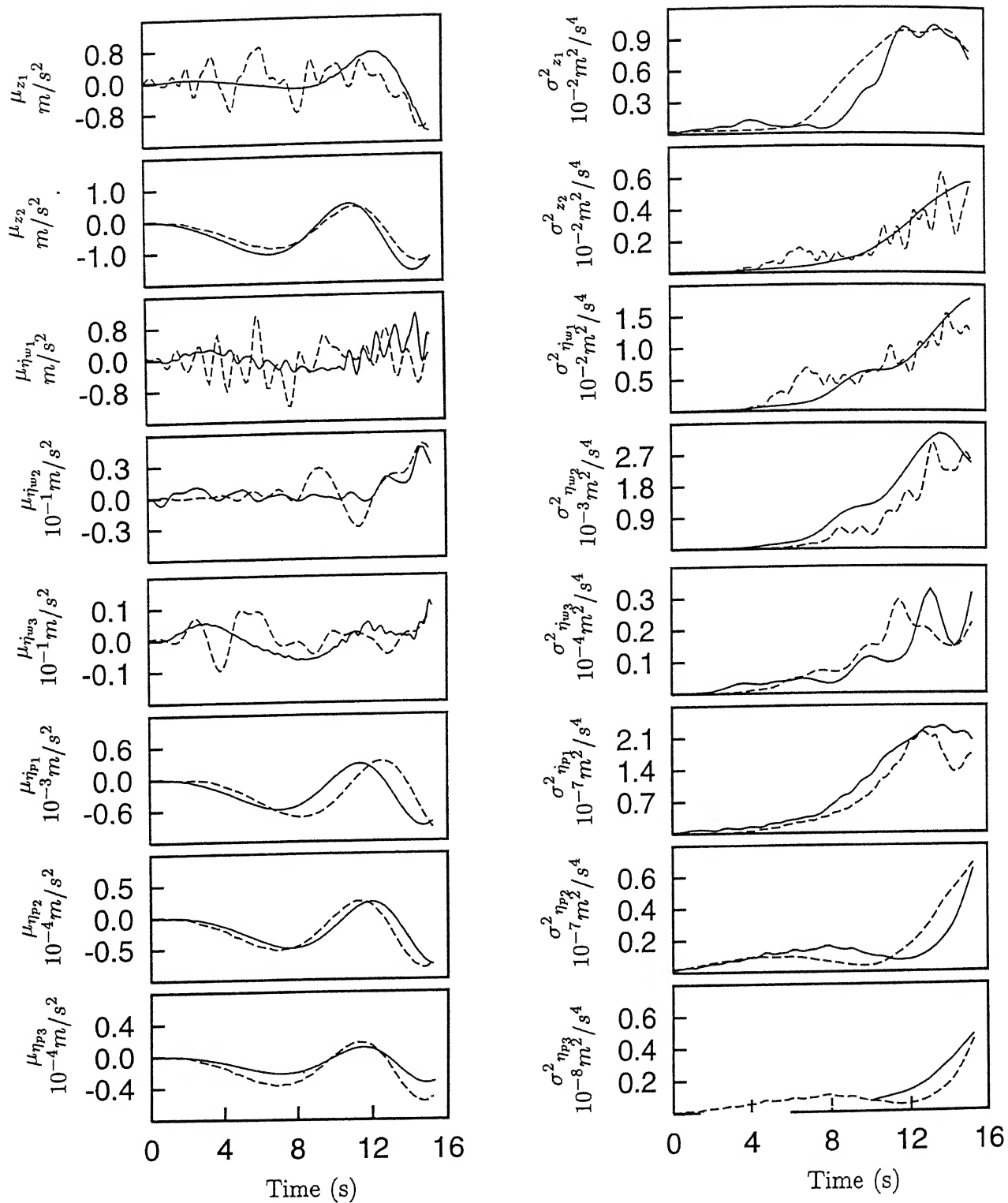


Fig.5.44. Nonlinear Aircraft Model-Mean and variance of acceleration in takeoff run.
Key same as Fig.5.39

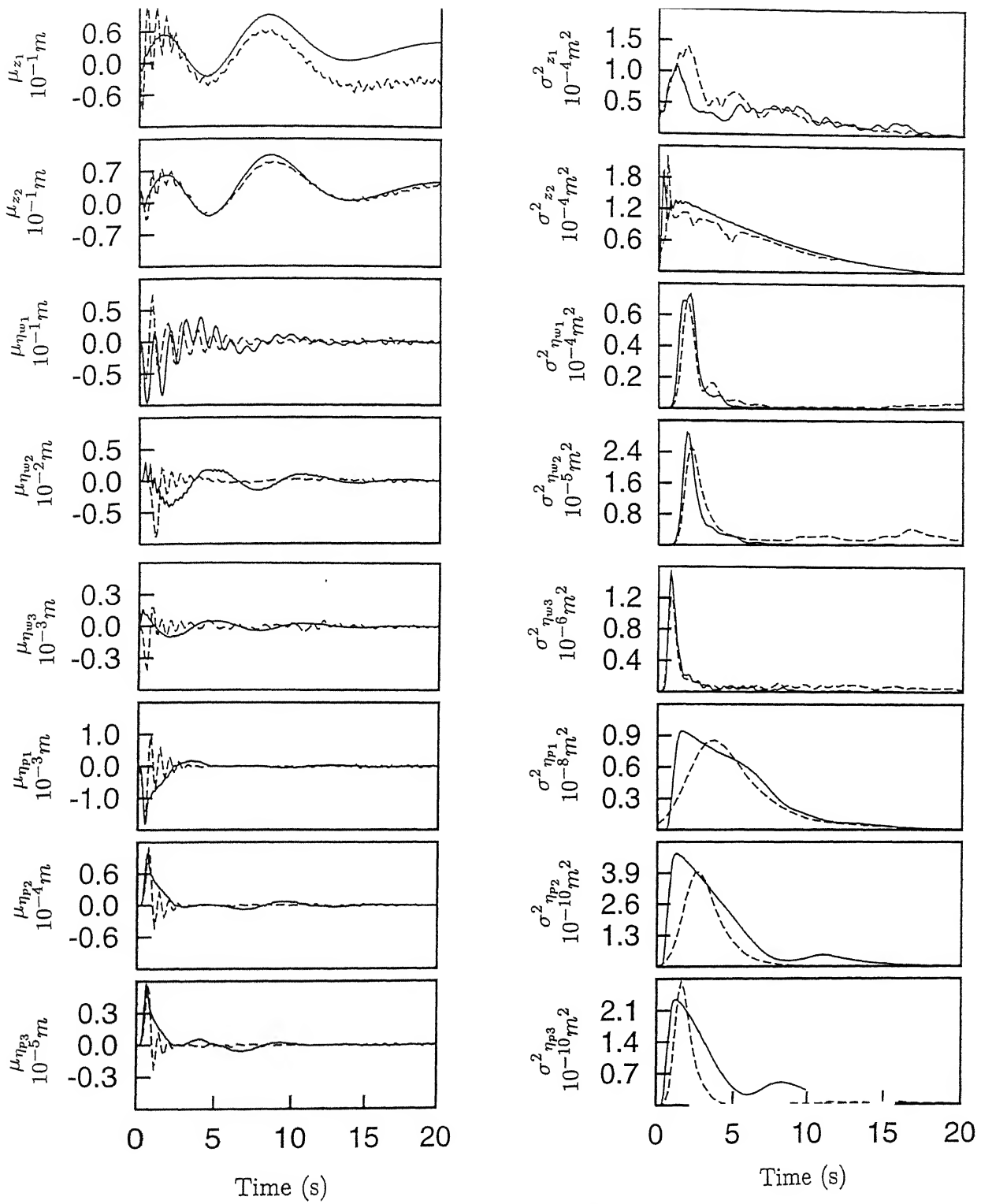


Fig.5.45. Nonlinear Aircraft Model-Mean and variance of displacement in landing run.
Key same as Fig.5.39

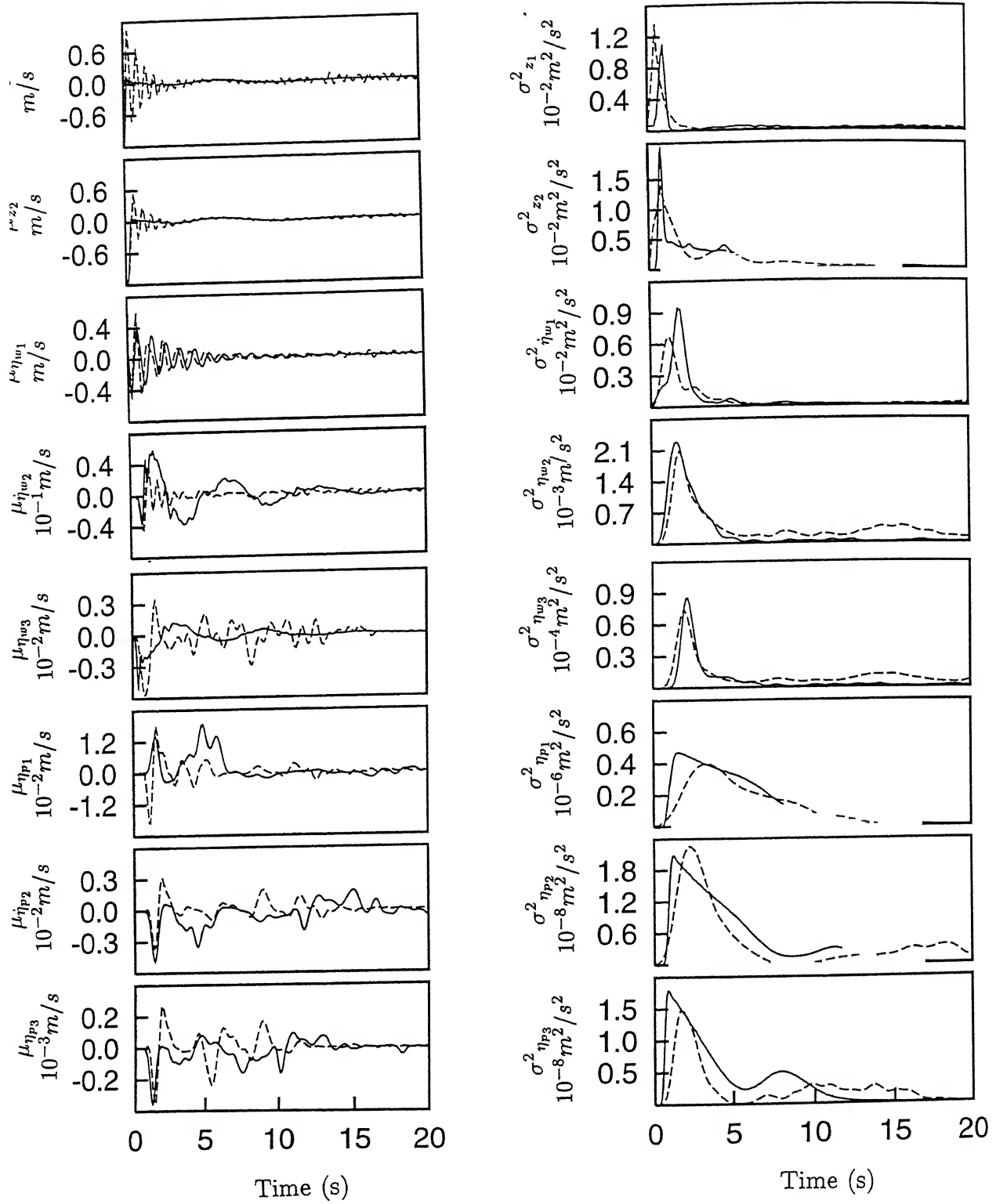


Fig.5.46. Nonlinear Aircraft Model-Mean and variance of velocity in landing run.
Key same as Fig.5.39

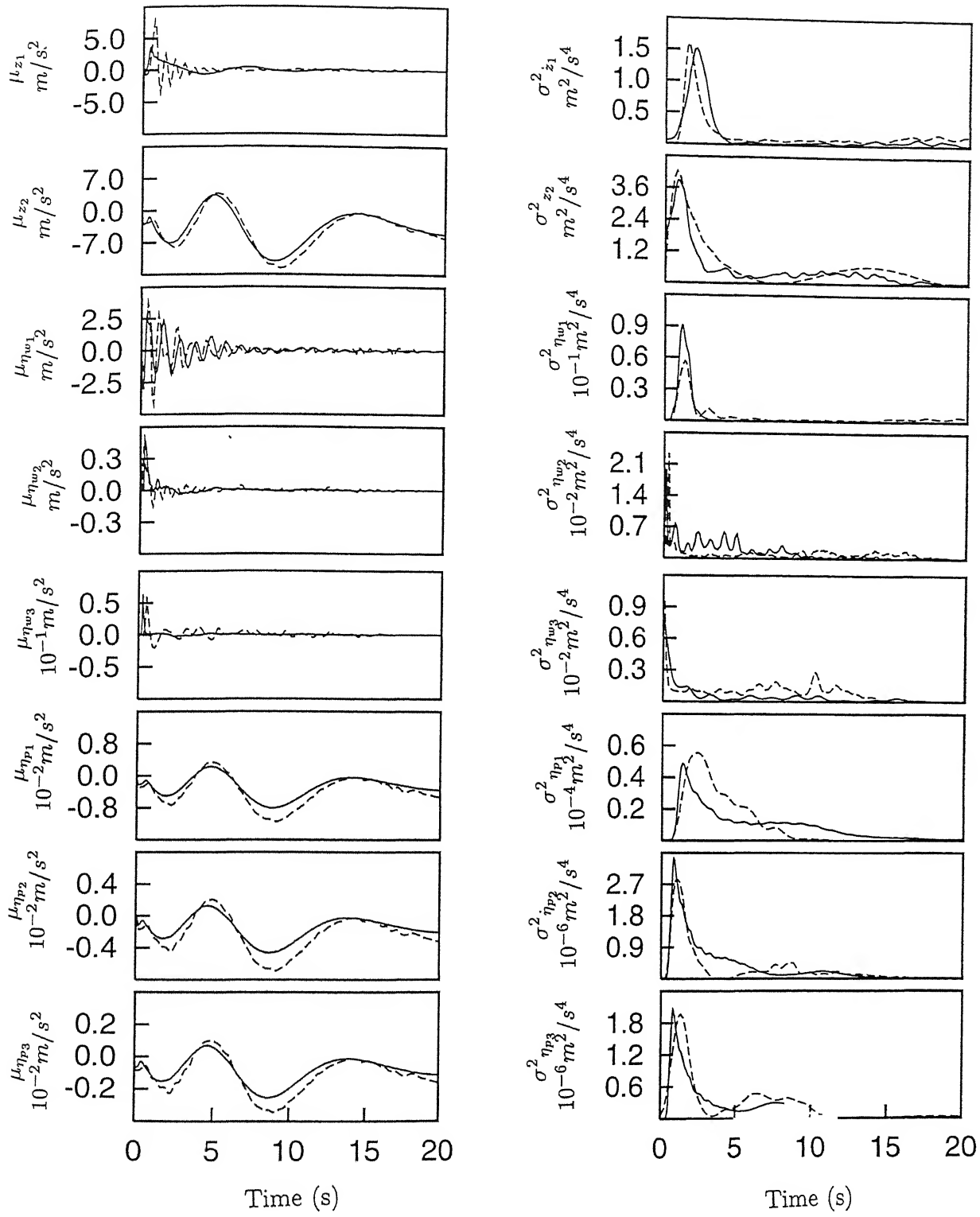


Fig.5.47. Nonlinear Aircraft Model-Mean and variance of acceleration in landing run.
Key same as Fig.5.39

CHAPTER 6

CONCLUSIONS

The conclusion based on the results obtained are being presented in this chapter. Following the preceeding chapter, the conclusions are also placed in three sections.

6.1 NONUNIFORM BEAM VIBRATION

An analytical approach has been outlined to study the free vibrational characteristics of a nonuniform beam. The beam mass and stiffness can be of general nature with distributed damping proportional to mass distributions. The approach is applicable for all types of boundary conditions. Some conclusions based on the study are:-

- (1) Natural frequency of a nonuniform beam is sensitive to the taper ratio and magnitude as well as location of the concentrated mass loading present in the beam.
- (2) The polynomial shape function derived may be useful to analyse nonuniform flexible structures modelled by finite beam elements. The use of the analytical nonuniform beam shape function instead of the traditional beam shape function is expected to bring out rapid convergence with less number of elements.

6.2 RESPONSE STATISTICS OF LINEAR VEHICLE MODELS

An approach has been outlined to analyse the flexible vehicle-track coupled dynamic behaviour for track irregularity in variable velocity run. The method uses linear suspension behaviour. A general pattern of vehicle forward motion and spatial nonhomogeneity of track roughness can be included in the analysis. Some major conclusions drawn from the study are:-

- (1) Mean response of the vehicle and track is primarily influenced by the mean track profile inducing mean input excitation.
- (2) Periodicity present in the mean track profile is reflected in the vehicle response. Response frequency is, however, modified by the vehicle forward velocity.
- (3) Variance characteristics of the vehicle response is influenced by track second order statistics.
- (4) Vehicle response is greatly dependent on the track roughness and vehicle speed. It is important to maintain track in proper condition to keep roughness low in high speed operation. This is expected to increase undercarriage and vehicle fatigue life.
- (5) System response is found to be higher during touch down impact compared to taxi and takeoff runs.
- (6) Flexible wings have strong transience set up at landing touch down and the system response suggests that inclusion of wing flexibility in the aircraft model is important for the analysis of possible metal fatigue damage as well as for catastrophic failure. Flexible wing has appreciable response in

taxi and takeoff runs also. Thus inclusion of slender members in the vehicle model is important from their design and performance considerations.

- (7) Increased speed of the vehicle is found to yield large response in the track bed. However, response magnitudes are smaller for the system parameters selected in the study. This low level of track deformation may not affect vehicle response significantly but its inclusion in system model may be important for track fatigue life and rehabilitation.
- (8) Unsymmetrical distribution of roughness across the track causes a significant system response not only in the roll mode but also in the heave and pitch modes due to strong coupling in the system.
- (9) The modelling predicts higher response magnitudes for rigid vehicles as compared to flexible vehicles.
- (10) Bending flexibility of aircraft type of vehicle is important for accurate description of the response behaviour. The low tread makes the torsional flexibility less significant for the prediction of vehicle response.
- (11) Consideration of rigid vehicle model may be adequate for preliminary design of undercarriages and vehicle structural components.

6.3 NONLINEAR AIRCRAFT MODEL

An instantaneously linearised approach for evaluation of the response statistics for nonlinear vehicle model has been presented for nonstationary track inputs. The method differs from other

linearisation techniques in the way that instead of finding equivalent set of linear parameters at one time, it introduces 'instantaneous' spring and damping coefficients evaluated from the response of the original nonlinear system at discrete time instants very close to each other. The method combines numerical technique with the linear random vibration theory. Accuracy of the method is tested with results obtained by Monte Carlo simulation of the nonlinear model. Some conclusions from the study are :-

- (1) The simulated response characteristics indicate high frequency components which are not always reflected by the linearised model. The simulation characteristics may contain digital noise introduced due to numerical integration and small sample size of 100. The noise is not present in the linearised solution leading to the above difference. This argument gains support from the presence of high frequencies in some linearised characteristics and absent in others.
- (2) Response characteristics show a good match between the two methods in the later stage of the vehicle run.
- (3) The variance matching is better compared to the mean between the two methods.
- (4) The present method can handle general combinations of nonlinearities found in vehicle suspension. It does not require a priori the probability density function of the response which is an essential feature of some other existing linearisation techniques.
- (5) The method proves cost effective as compared to digital simulation in terms of computer processing time and storage

space. Ratio of CPU time for the present linearised model and Monte Carlo simulation results per hundred samples is approximately 1 : 60.

- (6) The instantaneous linearisation approach has a potential for application to general nonlinear dynamics problems.

6.4 SUGGESTIONS FOR FUTURE WORKS

The present study has application to vehicle-track dynamics problems. The following scope exists for its extension:-

- (1) Vehicle forward motion and initial conditions may be treated as random variable.
- (2) Random variation of track subgrade properties with discontinuous jointed pavement can be included.
- (3) Effect of shear deformation, rotary inertia and warping deformation can be included in vibration of nonuniform beam element.
- (4) Vibration control studies can be carried out with the proposed models.
- (5) A procedure for fatigue life estimation can be developed for undercarriage and flexible vehicle components.
- (6) Instantaneous linearised approach for nonlinear models can be extended to multi wheeled input models including tyre nonlinearities.

REFERENCES

1. Houbolt, J. C., 'Runway roughness studies in the aeronautical field', *Proceedings of the American Society of Civil Engineers, Journal of Airtransport Division* 87, pp 11-31, 1961.
2. Wong, J. Y., 'Theory of ground vehicles', *John Willey and Sons*, 1978.
3. Walls, H., Houbolt, J. C. and Press, H., 'Some measurements and power spectra of runway roughness', *NACA TN-3305*, 1954.
4. Dodds, C. J. and Robson, J. D., 'The description of road surface roughness', *Journal of Sound and Vibration* 31, pp 175-183, 1973.
5. Sussmann, S., 'Statistical ground excitation models for highspeed vehicle dynamic analysis', *Highspeed Ground Transportation* 8, pp 145-154, 1974.
6. Kamesh, K. M. A. and Robson, J. D., 'The application of isotropy in road surface modelling', *Journal of Sound and Vibration* 57, pp 89-100, 1978.
7. Honda, H., Kajkawa, Y. and Kobori, T., 'Spectra of road surfaces on bridges', *Journal of Structural Engineering ASCE* 108, pp 1956-1966, 1982.
8. Heath, A. N., 'Application of the isotropic road roughness assumption', *Journal of Sound and Vibration* 115, pp 131-144, 1987.
9. Marcondes, J., Burgess, G. J., Harichandran, R. and Snyder, M. B., 'Spectral analysis of highway pavement roughness', *Journal of Transportation Engineering ASCE* 117, pp 540-549, 1991.

10. Marcondes, J., Synder, M. B. and Singh, S. P., 'Predicting vertical acceleration in vehicle through road roughness', *Journal of Transportation Engineering ASCE* **118**, pp 33-49, 1992.
11. Iyengar, R. N. and Jaiswal, O. R., 'Random field modelling of railway track irregularities', *Journal of Transportation Engineering ASCE* **121**, pp 303-308, 1995.
12. Silsby, N. S., 'An analytical study of effects of some airplanes and landing gear factors of the response to runway roughness with application to supersonic transport', *NASA TND-1492*, 1962.
13. Tung, C. C., Penzien, J. and Horonjeff, R., 'The effect of runway unevenness to the dynamic response of supersonic transports', *NASA CR-119*, 1964
14. Kirk, C. L and Perry, P. J., 'Analysis of taxiing induced vibration by power spectral density method', *Aeronautical Journal, Royal Aeronautical Society* **75**, pp 182-193, 1971.
15. Kirk, C. L., 'The random heave-pitch response of aircraft to runway roughness', *Aeronautical Journal, Royal Aeronautical Society* **75**, pp 476-483, 1971.
16. Virchis, V. J. and Robson, J. D., 'Response of an accelerating vehicle to random road undulations', *Journal of Sound and Vibrations* **18**, pp 423-427, 1971.
17. Sobczyk, K. and Macvean, D. B., 'Nonstationary random vibration of system travelling with variable velocity', *Stochastic Problems in Dynamics, University of Southampton*, Ed. Clarkson, B. L., pp 412-434, 1976.

18. Yadav, D. and Nigam, N. C., 'Ground induced nonstationary response of vehicles', *Journal of Sound and Vibration* 61, pp 117-126, 1978.
19. Kotb, M., Sankar, T. S. and Samaha, M., 'Suspension bounce response of Canadian MAGLEV vehicle under guideway excitation Part 2: Stochastic modelling and analysis', *Journal of Vibration, Accoustics, Stress and Reliability in Design ASME* 105, pp 261-266, 1983.
20. Hammond, J. K. and Harrison, R. F., 'Nonstationary response of vehicles on rough ground', *Journal of Dynamic Systems, Measurements and Control ASME* 103, pp 245-250, 1981.
21. Harrison, R. F. and Hammond, J. K., 'Approximate time domain nonstationary analysis of stochastically excited nonlinear system with particular reference to the motion of vehicles on rough ground', *Journal of Sound and Vibration* 105, pp 361-371, 1986.
22. Yadav, D., 'Vehicle response statistics to nonstationary track excitation - a direct formulation', *Mechanics Research Communication* 17, pp 65-74, 1990.
23. Yadav, D. and Kapadia, K. E., 'Nonhomogeneous track induced response of vehicles with nonlinear suspension during variable velocity run', *Journal of Sound and Vibration* 143, pp 51-64, 1990.
24. Yadav, D. and Ramamoorthy, R. P., 'Aircraft heave-pitch dynamics to track induced excitation', *Journal of Aeronautical Society of India* 43, pp 19-28, 1991.
25. Dahelberg, T., 'Parametric optimisation of 1 -DOF vehicle

- travelling on a randomly profiled road', *Journal of Sound and Vibration* 55, pp 245-253, 1977.
26. Dahelberg, T., 'An optimised speed-controlled suspension of a 2- DOF vehicle travelling on a randomly profiled road', *Journal of Sound and Vibration* 62, pp 541-546, 1979.
27. Narayanan, S. and Raju, G. V., 'Stochastic optimal control of nonstationary response of a single degree of freedom vehicle model', *Journal of Sound and Vibration* 141, pp 149-163, 1990.
28. Narayanan, S. and Raju, G. V., 'Optimal estimation and control of nonstationary response of a 2 D.O.F vehicle model', *Journal of Sound and Vibration* 149, pp 413-428, 1991.
29. Narayanan, S. and Raju, G. V., 'Active control of nonstationary response of vehicles with nonlinear suspensions', *Vehicle System Dynamics* 21, pp 73-87, 1992.
30. Venketeshan, C., 'Comparison of linear and nonlinear dampers for landing gear', *Journal of Aircraft* 15, pp 696-698, 1978.
31. Reddy, P. J., Nagaraj, V. T. and Ramamurthi, V., 'Analysis of articulated landing gear behaviour', *Sixth IFTOMM Congress on Theory of Machines and Mechanism, NewDelhi*, pp 391-394, 1983.
32. Reddy, P. J., Nagaraj, V. T. and Ramamurthi, V., 'Analysis of semi-levered suspension landing gear with some parametric study', *Journal of Dynamic Systems, Measurements and Control ASME* 106, pp 218-224, 1984.
33. Yadav, D. and Ramamoorthy, R. P., 'Nonlinear landing gear behaviour at touch down', *Journal of Dynamic Systems, Measurement and Control ASME* 113, pp 677-683, 1991.

34. Yadav, D. and Singh, C. V. K., 'Landing response of aircraft with optimal anti-skid braking', *Journal of Sound and Vibration* 181, pp 401-416, 1995.
35. Wilson, J. F. and Biggers, S. B., 'Dynamic interaction between long, high speed trains of air cushion vehicles and their guideways', *Journal of Dynamic Systems, Measurement and Control ASME* 93, pp 16-24, 1971.
36. Cherchas, D. B. 'A dynamic simulation for a high speed magnetically levitated guided ground vehicle', *Journal of Dynamic Systems, Measurement and Control ASME* 101, pp 223-229, 1979.
37. Hac, A., 'Stochastic optimal control of vehicles with elastic body and active suspension', *Journal of Dynamic Systems, Measurement and Control ASME* 108, pp 106-110, 1986.
38. Hac, A., Youn, L. and Chen, H. H., 'Control of suspensions for vehicles with flexible bodies-part I: Active suspension', *Journal of Dynamic Systems, Measurement and Control ASME* 118, pp 508-517, 1996.
39. Hac, A., Youn, L. and Chen, H. H., 'Control of suspensions for vehicles with flexible bodies-part II: Semi-active suspension', *Journal of Dynamic Systems, Measurement and Control ASME* 118, pp 518-525, 1996.
40. Conway, H. D. and Dubil, J. F., 'Vibration frequencies of truncated cone and wedge beam', *Journal of Applied Mechanics ASME* 32, pp 932-935, 1965.
41. Sanger, D. J., 'Transverse vibration of a class of nonuniform beam', *Journal of Mechanical Engineering Science* 10, pp

111-120, 1968.

42. Gorman, D. J., 'Free vibration analysis of beams and shafts', *John Willey and Sons*, 1975.
43. Wang, H. C., 'Generalised hypergeometric function solution on the transverse vibration of a class of tapered beam', *Journal of Applied Mechanics ASME* 34, pp 702-708, 1967.
44. Naguleswaran, S., 'Vibration of Euler Bernouli beam of constant depth and with linearly varying breadth', *Journal of Sound and Vibration* 153, pp 509-532, 1992.
45. Naguleswaran, S., 'A direct solution for the transverse vibration of Euler Bernouli wedge and cone beams', *Journal of Sound and Vibration* 172, pp 289-304, 1994.
46. Abrate, S., 'Vibration of nonuniform rods and beams', *Journal of Sound and Vibration* 185, pp 703-716, 1995.
47. To, C. W. S., 'Vibration of cantilever beam with base excitation and tip mass', *Journal of Sound and Vibration* 83, pp 445-460, 1982.
48. Chehil, D. S. and Jategaonkar, R., 'Determination of natural frequencies of a beam with varying section properties', *Journal of Sound and Vibration* 115, pp 423-436, 1987.
49. Bapat, C. N. and Bapat, C., 'Natural frequencies of beam with non classical boundary conditions and concentrated masses', *Journal of Sound and Vibration* 112, pp 177-182, 1987.
50. Kim, C. S. and Dickinson, S. M., 'On the analysis of laterally vibrating beams subject to various complicating effects', *Journal of Sound and Vibration* 122, pp 441-455, 1988.
51. Karabolis, D. L. and Beskos, D. E., 'Static, dynamic and

- stability analysis of structures composed of tapered beams', *Computers and Structures* 16, pp 731-748, 1983.
52. Beskos, D. E., 'Boundary element method in dynamic analysis', *Applied Mechanics Review* 40, pp 1-23, 1987.
53. Chu, F. H. and Pilkey, W. D., 'Transient analysis of structural members by CSDT Riccati transfer matrix method', *Computers and Structures* 10, pp 599-611, 1979.
54. Wu, J. S. and Lin, T. L., 'Free vibration analysis of a uniform cantilever beam with point masses by an analytical and numerical combined method', *Journal of Sound and Vibration* 136, pp 201-213, 1990.
55. Gibson, D. W., 'Flat car modelling technique and results', *Proceedings of conference on Train/track Dynamics and Design-Advanced Technique, Chicago 1977*, Eds. Moyar, G. J., Pilkey, W. D. and Pilkey, F., pp 125-148.
56. Khulief, Y. A. and Sun, S. P., 'Finite element modelling and semiactive control of vibrations in road vehicles', *Journal of Dynamic Systems, Measurement and Control ASME* 111, pp 521-527, 1989.
57. Apetaur, M. and Opicka, F., 'Small vibrations of nonlinear dynamic systems containing non rigid bodies excited by stationary stochastic process', *Vehicle System Dynamics* 20, pp 3-19, 1991.
58. Valk, R. V. and Pacejka, H. B., 'An analysis of a civil aircraft main gear shimmy failure', *Vehicle System Dynamics* 22, pp 97-121, 1993.
59. Goland, M., 'The flutter of a uniform cantilever wing',

Journal of Applied Mechanics ASME 12, pp A-197 - A-208, 1945.

60. Timoshenko, S. and Young, D. H., 'Vibration problems in engineering', *Von Nostrand NewYork*, 1955.
61. Dokumaci, E., 'An exact solution for the coupled bending and torsion vibrations of uniform beams having single cross sectional symmetry', *Journal of Sound and Vibration* 119, pp 443-449, 1987.
62. Bishop, R. E. D. and Price, W. G., 'Coupled bending and twisting of a Timoshenko beam', *Journal of Sound and Vibration* 50, pp 469-477, 1977.
63. Bishop, R. E. D., Cannon, S. and Miao, S., 'On the coupled bending and torsional vibration of uniform beam', *Journal of Sound and Vibration* 131, pp 457-464, 1989.
64. Anderson, R. A. and Houbolt, J. C., 'Determination of coupled and uncoupled modes and frequencies of natural vibration of swept and unswept wings from uniform cantilever modes', *NACA TN -1747*, 1948.
65. Rao, J. S. and Carnegie, W., 'Solution of the equation of motion of coupled bending torsion of turbine blades by the method of Ritz-Galerkin', *International Journal of Mechanical Science* 12, pp 875-882, 1970.
66. Mei, C., 'Coupled vibrations of thin walled beams of open section using finite element method', *International Journal of Mechanical Science* 12, pp 883-891, 1970.
67. Klausbruckner, M. J. and Pryputniewicz, R. J., 'Theoretical and experimental study of coupled vibrations of channel beam', *Journal of Sound and Vibration* 183, pp 239-252, 1995.

68. Hallauer, W. L. and Liu, R. Y. L., 'Beam bending torsion dynamic stiffness method for calculation of exact vibration modes', *Journal of Sound and Vibration* 85, pp 105-113, 1982.
69. Banerjee, J. R., 'Coupled bending-torsion dynamic stiffness matrix for beam elements', *International Journal of Numerical Methods in Engineering* 28, pp 1283-1298, 1989.
70. Eslimy-Isfahany, S. H. R., Banerjee, J. R. and Sobey, A. J., 'Response of a bending-torsion coupled beam to deterministic and random loads', *Journal of Sound and Vibration* 195, pp 267-283, 1996.
71. Blejwas, T. E., 'Dynamic interaction of moving vehicles and structures', *Journal of Sound and Vibration* 67, pp 513-521, 1979.
72. Duff, D. G., 'Response of an infinite rail road track to a moving vibratory mass', *Journal of Applied Mechanics ASME* 57, pp 66-73, 1990.
73. Yadav, D. and Upadhhay, H. C., 'Nonstationary dynamics of train and flexible track over inertial foundation during variable velocity run', *Journal of Sound and Vibration* 147, pp 57-71, 1991.
74. Yadav, D. and Upadhhay, H. C., 'Dynamics of vehicles in variable velocity runs over nonhomogeneous flexible track and foundation with two point input models', *Journal of Sound and Vibration* 156, pp 247-268, 1992.
75. Yadav, D. and Upadhhay, H. C., 'Heave-pitch-roll dynamics of a vehicle with a variable velocity over nonhomogeneously profiled track', *Journal of Sound and Vibration* 164, pp

- 337-348, 1993.
76. Hardy, M. S. and Cebon, D., 'Response of continuous pavements to moving dynamic load', *Journal of Engineering Mechanics ASCE*, **119**, pp 1762-1780, 1993.
 77. Hiltunen, R. D. and Bush, A. J., 'Measurement of airfield pavement response under moving aircraft loads', *Proceedings of symposium on Road and Airport Pavement Monitoring System, New Hampshire, W. Lebanon*, Eds. Janoo, V. C and Eaton, A. R., pp 336-351, 1991.
 78. Anant, R. K., Mohammed, R. T. and Ledesma, R. H., 'Dynamic analysis of a rigid aircraft pavement with discontinuities', *Journal of Transportation Engineering ASCE* **118**, pp 341-360, 1992.
 79. Cai, Y., Chen, S. S., Rote, D. M and Coffey, H. T., 'Vehicles/Guideway interaction for high speed vehicles on a flexible guideway', *Journal of Sound and Vibration* **175**, pp 625-646, 1994.
 80. Cai, Y., Chen, S. S., Rote, D. M and Coffey, H. T., 'Vehicle/Guideway dynamic interaction in maglev systems', *Journal of Dynamic Systems, Measurement and Control ASME* **118**, pp 526-530, 1996.
 81. Potter, T. E. C., Cebon, D., Cole, D. J. and Collop, A. C., 'An investigation of road damage due to measured dynamic tyre forces', *Proceedings of Institution of Mechanical Engineers Part D* **209**, pp 9-24, 1995.
 82. Laib, L., 'Analysis of the vibration excitation effect caused by deformable soil surface', *Journal of Terramechanics* **32**, pp

151-163, 1995.

83. Shinozuka, M., 'Simulation of multivariate and multidimensional random process', *Journal of Acoustical Society of America* 49, pp 357-367, 1971.
84. Gradshteyan, I. S. and Ryzhik, I. M., 'Tables of integrals, series and products', *Academic Press INC*, 1980.
85. Shevell, R. C., 'Fundamentals of Flight', *Prentice Hall, New Jersey*, 1989.
86. Meirovitch, L., 'Elements of vibration analysis', *Mc Graw Hill*, 1986.
87. Nigam, N. C., 'Introduction to random vibration', *MIT Press Cambridge*, 1983.
88. Kumar, R., 'Investigation of coupled flexural torsional vibration of aircraft wing', *M. Tech thesis*, 1997, Department of Aerospace Engineering, Indian Institute of Technology, Kanpur (India).
89. Roberts, J. B. and Spanos, P. D., 'Random vibration and statistical linearisation', *John Willey and Sons*, 1989.
90. Kreyszig, E. 'Advanced engineering mathematics', *Willey Eastern Limited*, 1983.